Vol. 295, No. 1–2, September 9, 1994 ISSN 0003-2670

ANALYTICA CHIMICA ACTA

An international journal devoted to all branches of analytical chemistry

ELSEVIER

ANALYTICA CHIMICA ACTA

Scope. *Analytica Chimica Acta* publishes original papers, rapid publication letters and reviews dealing with every aspect of modern analytical chemistry. Reviews are normally written by invitation of the editors, who welcome suggestions for subjects. Letters can be published within **four months** of submission. For information on the Letters section, see inside back cover.

Submission of Papers

Americas

Prof. Harry L. Pardue
Department of Chemistry
1393 BRWN Bldg, Purdue University
West Lafayette, IN 47907–1393
USA

Tel:(+1-317) 494 5320
Fax:(+1-317) 496 1200

Computer Techniques

Prof. J.T. Clerc
Universität Bern
Pharmazeutisches Institut
Baltzerstrasse 5, CH-3012 Bern
Switzerland

Tel:(+41-31) 6314191
Fax:(+41-31) 6314198

Prof. Sarah C. Rutan
Department of Chemistry
Virginia Commonwealth University
P.O. Box 2006
Richmond, VA 23284-2006
USA
Tel:(+1-804) 367 7517
Fax:(+1-804) 367 8599

Other Papers

Prof. Alan Townshend
Department of Chemistry
The University
Hull HU6 7RX
Great Britain

Tel:(+44-482) 465027
Fax:(+44-482) 466410

Prof. Willem E. van der Linden
Laboratory for Chemical Analysis
Department of Chemical Technology
Twente University of Technology
P.O. Box 217, 7500 AE Enschede
The Netherlands
Tel:(+31-53) 892629
Fax:(+31-53) 356024

Prof. Paul Worsfold
Dept. of Environmental Sciences
University of Plymouth
Plymouth PL4 8AA
Great Britain

Tel:(+44-752) 233006
Fax:(+44-752) 233009

Submission of an article is understood to imply that the article is original and unpublished and is not being considered for publication elsewhere. *Anal. Chim. Acta* accepts papers in English only. There are no page charges. Manuscripts should conform in layout and style to the papers published in this issue. See inside back cover for "Information for Authors".

Publication. *Analytica Chimica Acta* appears in 16 volumes in 1994 (Vols. 281–296). *Vibrational Spectroscopy* appears in 2 volumes in 1994 (Vols. 6 and 7). Subscriptions are accepted on a prepaid basis only, unless different terms have been previously agreed upon. It is possible to order a combined subscription (*Anal. Chim. Acta* **and** *Vib. Spectrosc.*).
Our p.p.h. (postage, packing and handling) charge includes surface delivery of all issues, except to subscribers in the U.S.A., Canada, Australia, New Zealand, China, India, Israel, South Africa, Malaysia, Thailand, Singapore, South Korea, Taiwan, Pakistan, Hong Kong, Brazil, Argentina and Mexico, who receive all issues by air delivery (S.A.L.–Surface Air Lifted) at no extra cost. For Japan, air delivery requires 25% additional charge of the normal postage and handling charge; for all other countries airmail and S.A.L. charges are available upon request.

Subscription orders. Subscription prices are available upon request from the publisher. Subscription orders can be entered only by calendar year and should be sent to: Elsevier Science B.V., Journals Department, P.O. Box 211, 1000 AE Amsterdam, The Netherlands. Tel: (+31-20) 5803 642, Telex: 18582, Telefax: (+31-20) 5803 598, to which requests for sample copies can also be sent. Claims for issues not received should be made within six months of publication of the issues. If not they cannot be honoured free of charge. Readers in the U.S.A. and Canada can contact the following address: Elsevier Science Inc., Journal Information Center, 655 Avenue of the Americas, New York, NY 10010, U.S.A. Tel: (+1-212) 633 3750, Telefax: (+1-212) 633 3990, for further information, or a free sample copy of this or any other Elsevier Science journal.
Advertisements. Advertisement rates are available from the publisher on request.

US mailing notice – Analytica Chimica Acta (ISSN 0003-2670) is published 3 times a month (total 48 issues) by Elsevier Science B.V. (Molenwerf 1, Postbus 211, 1000 AE Amsterdam). Annual subscription price in the USA US$ 3035.75 (valid in North, Central and South America), including air speed delivery. Second class postage paid at Jamaica, NY 11431. *USA Postmasters*: Send address changes to Anal. Chim. Acta, Publications Expediting, Inc., 200 Meacham Av., Elmont, NY 11003. Airfreight and mailing in the USA by Publication Expediting.

FOR ADVERTISING INFORMATION PLEASE CONTACT OUR ADVERTISING REPRESENTATIVES

USA/CANADA

Weston Media Associates

Mr. Daniel S. Lipner

P.O. Box 1110, GREENS FARMS, CT 06436-1110

Tel: (203) 261-2500, Fax: (203) 261-0101

GREAT BRITAIN

T.G. Scott & Son Ltd.

Tim Blake/Vanessa Bird

Portland House, 21 Narborough Road

COSBY, Leicestershire LE9 5TA

Tel: (0533) 753-333, Fax: (0533) 750-522

JAPAN

ESP - Tokyo Branch

Mr. S. Onoda

20-12 Yushima, 3 chome, Bunkyo-Ku

TOKYO 113

Tel: (03) 3836 0810, Fax: (03) 3839-4344

Telex: 02657617

REST OF WORLD

ELSEVIER SCIENCE

Ms. W. van Cattenburch

Advertising Department

P.O. Box 211, 1000 AE AMSTERDAM,

The Netherlands

Tel: (20) 515.3220/21/22, Telex: 16479 els vi nl

Fax: (20) 683.3041

Sampling of Heterogeneous and Dynamic Material Systems

Theories of Heterogeneity, Sampling and Homogenizing

by **P.M. Gy**, Sampling Consultant, Cannes, France

Data Handling in Science and Technology Volume 10

Although sampling errors inevitably lead to analytical errors, the importance of sampling is often overlooked. The main purpose of this book is to enable the reader to identify every possible source of sampling error in order to derive practical rules to (a) completely suppress avoidable errors, and (b) minimise and estimate the effect of unavoidable errors. In short, the degree of representativeness of the sample can be known by applying these rules.

The scope covers the derivation of theories of probabilistic sampling and of bed-blending from a complete theory of heterogeneity which is based on an original, very thorough, qualitative and quantitative analysis of the concepts of homogeneity and heterogeneity. All sampling errors result from the existence of one form or another of heterogeneity. Sampling theory is derived from the theory of heterogeneity by application of a probabilistic operator to a material whose heterogeneity has been characterized either by a simple scalar (a variance: zero-dimensional batches) or by a function (a variogram: one-dimensional batches). A theory of bed-blending (one-dimensional homogenizing) is then easily derived from the sampling theory.

The book should be of interest to all analysts and to those dealing with quality, process control and monitoring, either for technical or for commercial purposes, and mineral processing.

Although this book is primarily aimed at graduates, large portions of it are suitable for teaching sampling theory to undergraduates as it contains many practical examples provided by the author's 30-year experience as an international consultant. The book also contains useful source material for short courses in Industry.

ELSEVIER

SCIENCE

Contents:

Foreword. First Part: General Introduction. Second Part: Heterogeneity. Third Part: General Analysis of the Concept of Sampling. Fourth Part: Achievement of Sampling Correctness. Fifth Part: One-Dimensional Sampling Model. Sixth Part: Zero-Dimensional Sampling Model. Seventh Part: Sampling by Splitting. Ninth Part: Sampling for Commercial Purposes: Specific Problems. Tenth Part: Homogenizing. Useful References. Index.

1992 xxx + 654 pages
Price: Dfl. 425.00 / US$ 243.00
ISBN 0-444-89601-5

ORDER INFORMATION

For USA and Canada
ELSEVIER SCIENCE

Judy Weislogel
P.O. Box 945
Madison Square Station,
New York, NY 10160-0757
Tel: (212) 989 5800
Fax: (212) 633 3880

In all other countries
ELSEVIER SCIENCE

P.O. Box 211
1000 AE Amsterdam
The Netherlands
Tel: (+31-20) 5803 753
Fax: (+31-20) 5803 705

US$ prices are valid only for the USA & Canada and are subject to exchange fluctuations; in all other countries the Dutch guilder price (Dfl.) is definitive. Books are sent postfree if prepaid.

711/414\143\0001-00

ANALYTICA CHIMICA ACTA

An international journal devoted to all branches of analytical chemistry

(Full texts are incorporated in CJELSEVIER, a file in the Chemical Journals Online database available on STN International; Abstracted, indexed in: Aluminum Abstracts; Anal. Abstr.; Biol. Abstr.; BIOSIS; Chem. Abstr.; Curr. Contents Phys. Chem. Earth Sci.; Engineered Materials Abstracts; Excerpta Medica; Index Med.; Life Sci.; Mass Spectrom. Bull.; Material Business Alerts; Metals Abstracts; Sci. Citation Index)

VOL. 295 NO. 1–2 SEPTEMBER 9, 1994

CONTENTS

(Continued overleaf)

Contents (continued)

ANALYTICA CHIMICA ACTA
VOL. 295 (1994)

ANALYTICA CHIMICA ACTA

An international journal devoted to all branches of analytical chemistry
Revue internationale consacrée à tous les domaines de la chimie analytique
Internationale Zeitschrift für alle Gebiete der analytischen Chemie

Anal. Chim. Acta, Vol. 295 (1994)

ELSEVIER, Amsterdam – Lausanne – New York – Oxford – Shannon – Tokyo

0003-2670/94/$07.00

ELSEVIER

Analytica Chimica Acta 295 (1994) 1–26

ANALYTICA CHIMICA ACTA

Review

Assays for interferons and interleukins in biological matrices

A. Sparreboom [1], H.A.H. Rongen, W.P. van Bennekom *

Department of Pharmaceutical Analysis, Faculty of Pharmacy, Utrecht University, Sorbonnelaan 16, 3584 CA Utrecht, Netherlands

Received 17th November 1993; revised manuscript received 5th April 1994

Abstract

Recent advances in interferon and interleukin research entailed great interest upon specific and sensitive assays in biological media. Concurrently with the availability of (monoclonal) antibodies, a development in immunological assays originated, providing increased specificity over the conventional biological assays. However, most immunological assays, notwithstanding their sensitivity, cannot distinguish between biologically active and inactive interferons or interleukins. This drawback resulted in new assays, based on the use of receptors, which combine the advantages of both biological and immunological assays. In addition, quantitative chemical analysis of interferons and interleukins employing chromatographic, electrophoretic, mass spectrometric and surface plasmon resonance-based techniques, has emerged recently and appears to possess potentials for rapidity and specificity. So far, chemical assays lack the sensitivity for the determination of interferons and interleukins in biological matrices.

Key words: Interferons; Interleukins; Cytokines; Biological assays; Immunological assays; Receptor assays; Chemical assays; Review

Interferons and interleukins [2] are a group of low-molecular-weight (glyco)proteins variously called cytokines. They exert their biological effects by binding to a specific cell-surface receptor and act in a paracrine or autocrine manner. Interferons and interleukins play an important role in regulating immune responses [1] and have been implicated in the aetiology of several inflammatory and neoplastic diseases [2].

At present, the Nomenclature Committee of the U.S. National Centre on Interferon [3] and the WHO-IUIS Nomenclature Subcommittee on Interleukin Designation [4] have classified IFN-α, IFN-β and IFN-γ, and IL-1 up to IL-10, respectively (Table 1). However, further types are expected, as exemplified by recent molecular characterizations of IFN-δ [5], IL-11 [6], IL-12 [7] and IL-13 [8]. For a clear picture of biological effects of interferons and interleukins we refer to reviews dealing with activities of interferons and interleukins [9–12].

[1] Present address: Department of Clinical Chemistry, The Netherlands Cancer Institute, Antoni van Leeuwenhoekhuis, Plesmanlaan 121, 1066 CX Amsterdam (Netherlands).

* Corresponding author.

[2] Human interferon and human interleukin are meant when the species is not specified.

SSDI 0003-2670(94)00171-H

Table 1
Major classes of human interferons and human interleukins

Name	Former name(s)	MW (kDa)	Major cell source	Important biological properties		
				Immune response	in vivo effects	Hematopoiesis
IFN-αI [a], IFN-αII [a,b]	leukocyte IFN, acid-stable IFN, type I IFN	16–27	MO	antiproliferative effects, inhibition T cell proliferation, B cell proliferation and differentiation	anti-viral activity, pyrogenicity	
IFN-β	IFN-β I, fibroblast IFN, acid-stable IFN, type I IFN	20	Fb	antiproliferative effects, B cell proliferation	anti-viral activity, pyrogenicity	
IFN-γ	Immune IFN, acid-labile IFN, type II IFN, macrophage activating factor	20–25	T, NK	antiproliferative effects, macrophage activation, B cell proliferation and differentiation	anti-viral activity, pyrogenicity	
IL-1α, IL-1β	lymphocyte activating factor, haemopoietin-1, endogenous pyrogen	17.5	MO, Fb, a.o.	B and T cell proliferation	pyrogenicity, PGE release	
IL-2	T cell growth factor	15–17	T	T cell proliferation and differentiation, induction of B cell growth factors and IFN-γ	pyrogenicity	synergize with IL-3 and GM-CSF
IL-3	multi-colony stimulating factor, persisting cell-stimulating factor, mast cell growth factor	20–26	T	proliferation and differentiation of pluri-potent precursor cells in the bone marrow		mast cell growth factor
IL-4	B cell growth factor-1,B cell stimulating factor	20	T, MC	B and T cell proliferation, IgG and IgE secretion		mast cell growth synergy with G-CSF
IL-5	eosinophil differentiation factor, B cell growth factor-2	50–60	T, MC	B cell differentiation		eosinophil differentiation and function
IL-6	B cell stimulating factor-2, hybridoma-plastocytoma growth factor, 26 K protein, hepatocyte stimulating factor	26	MO, T, Fb, Ed	B cell proliferation and differentiation, T cell costimulation	stimulation of acute phase response by hepatocytes cells	growth promotion of hybridoma/plasmocytoma
IL-7	lymphopoietin-1	25	BSC	thymocyte and T cell proliferation		lymphocyte progenitors proliferation

Name	Former name(s)	MW (kDa)	Major cell source	Important biological properties		
				Immune response	Inflammation	Hematopoiesis
IL-8	monocyte-derived neutrophil activating protein, macrophage inflammatory protein, neutrophil activating factor	6–8	MO		neutrophil-specific activation of chemotaxis, lysosomal enzyme release	
IL-9	P 40	64	T	increased T cell survival		stimulation of erythroid burst-forming activity
IL-10	cytokine synthesis inhibitory factor	18.7	T, B1, MO	inhibition of IFN-γ and IL-2 synthesis by T cells		
IL-11	–	23	BSC	stimulation of T cell and B cell immunoglobulin secretion		megakaryocytopoiesis, growth of IL-6 dependent lines
IL-12	–	75		synergy with IL-2 for NK (LAK) cell activation, T cell proliferation		
IL-13	–	~10	T	monocyte differentiation, B cell proliferation and differentiation, IgM and IgG secretion		

[a] Subtypes of these species, based on specific amino acid sequence differences have been purified and characterized.
[b] IFN-αII also called IFN-ω.
B1 = B lymphoblastoid cells, BSC = bone marrow stromal cells, Ed = endothelial cells, Fb = fibroblasts, G-CSF = granulocyte colony stimulating factor, GM-CSF = granulocyte/macrophage colony stimulating factor, Ig = immunoglobulin, MC = mast cells, MO = macrophages/monocytes, NK = natural killer cells, T = T lymphocytes.

Sensitive and accurate interferon and interleukin assays are essential in many fields of immunological and biotechnological research, and for monitoring purification procedures [13]. There is a necessity for reliable and specific assay systems which are fast and easy to perform.

Assay methods for interferons and interleukins can be divided into different categories. When the cytokines are assayed by testing a particular cell function, the methods belong to the biological assays (or bioassays). Another category, that of the immunological assays (or immunoassays), involves the use of antibodies specific to an epitope, which are, ideally, exclusive to a particular interferon or interleukin.

In this review, the current status of interferon and interleukin assays is addressed. Beside the above mentioned methods some recently developed assays based on the use of receptors, liquid chromatography, mass spectrometry, (capillary) electrophoresis and surface plasmon resonance will be discussed.

1. Biological assays

Virtually all interferons and interleukins can nowadays be determined by a biological assay, which makes use of cell-culture methods. The effect of interleukins can be measured through proliferation of cells, cytotoxicity, or induction of antigens in cells. Determinations of interferon can be divided in non-viral and viral assays, the former representing the antiproliferative effect on cells or the effect on antigen expression, the latter representing the reduction of the cytopathic effect, reduction of plaque numbers after infection with a virus or inhibition of virus replication in cells (Fig. 1).

Apart from being sensitive, biological assays have the advantage of measuring only biological active interferons and interleukins, contrary to most other assays discussed. In general biological assays are laborious and not particularly specific, as may be exemplified by the IL-1 assays, which are influenced by other cytokines, including IL-2 and IL-6 [22,31]. Another major problem resides in the effects of biological constituents in the matrices, notably inhibitory factors and cytokine-binding molecules.

1.1. Proliferation and cytotoxicity assays

Proliferation or enhanced cell-survival assays are first choice for many cytokines, including interleukins. Cytotoxicity assays can use similar types of readout to proliferation assays, although in the most common systems the target cells are normally not highly proliferative.

There are many methods available for quantifying cell numbers, including direct cell counting by eye, indirect methods such as measurement of the uptake of radioactive nucleotides (^{3}H-TdR or ^{125}I-IDU) or dyes such as natural red [14], and the conversion of the tetrazolium salt MTT into the colored formazan product by mitochondrial enzymes [15] (Fig. 1).

In cytotoxicity assays simple vital stains such as crystal violet or methylene blue give adequate results. In measuring proliferation, the MTT colorimetric assay is often the method of choice due to the speed with which samples can be processed. Since the substrate does not interfere with the measurement of the product no removal or washing steps are required, increasing the speed of the assay and minimizing the variability between samples. Although the colorimetric assay is a measure for the energy metabolism of living cells, while ^{3}H-TdR incorporation measures the number of cells synthesizing DNA (including blastogenesis), there are usually no large differences between both proliferative profiles. Table 2 presents currently available proliferation and cytotoxicity assays for the determination of interleukins.

Conversion assays involve stimulation by IL-1 of certain cells, such as the LBRM33 line [17,23,24] or EL4 subclones [25], to produce IL-2 which is then detected by proliferation of a second cell line, usually CTLL.

Unwanted interleukin responses can be abrogated by performing assays in saturating concentrations of the interfering interleukin in question [18,19]. Lohoff et al. [48] devised a proliferation assay in the presence of antibodies to block unwanted activities.

Most biological fluids contain inhibitors of proliferation. A possible inhibitor is the secreted form of the 55-kDa IL-2R which is found in culture supernatants of activated T-cells and even in patients with rheumatoid arthritis [54]. Bell-shaped dose-response curves are normally observed when measuring interleukin levels, indicating the presence of inhibitors such as IL-1ra, TGF-β, PEG or non-specific binding proteins, e.g. α_2-macroglobulin. Chloroform extraction or PEG precipitation have been used as simple alternatives to chromatography to separate interleukins from inhibitory substances [55]. The effects of inhibitors and the problems of non-specificity indicate that proliferation and cytotoxicity assays are rarely unambiguous.

In general, proliferation assays are fast, sensitive and represent relatively simple test systems, since variables related to viruses are not included.

1.2. Antiproliferation assays

Beside their antiviral activities, interferons have also been shown to possess several non-antiviral effects such as inhibition of cell proliferation [56]. In interferon-antiproliferation assays the most sensitive cell lines are the continuous human Burkitt lymphoma cell line called 'Daudi' [56–58] and the murine lymphoma cells P388 [61].

Nederman et al. [59] determined the potent antiproliferative effect of IFN-α and IFN-β either by measuring ^{3}H-TdR incorporation or final cell density. Since determination of the latter response mostly gave more precise results with greater statistical weight, measurements of final

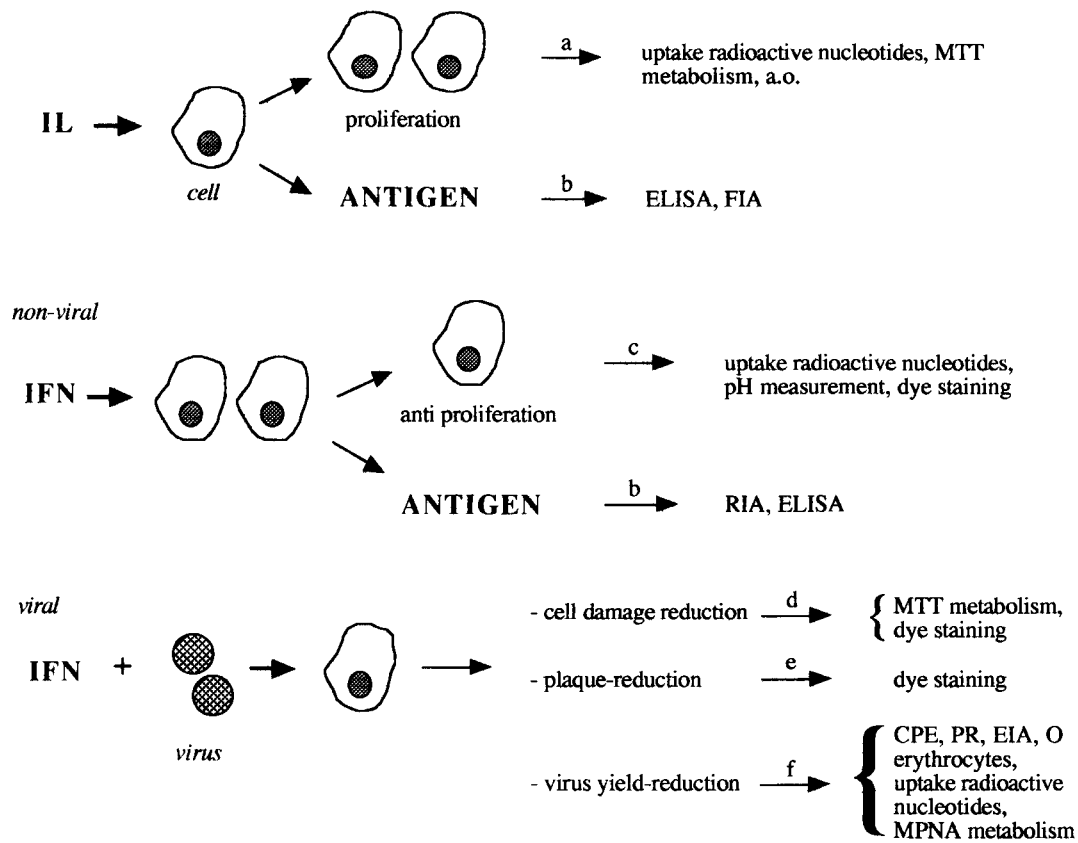

Fig. 1. Schematic representation of the major biological assays for the determination of interferons and interleukins. a = Proliferation assays; b = antigen induction assays; c = antiproliferation assays; d = cytopathic effect reduction assays; e = plaque-reduction assays; f = virus yield-reduction assays.

cell density was preferred for a routine assay. Furthermore, the ^{3}H-TdR method has been considered to be less adequate since it does not only reflect the rate of cell proliferation but also an interferon-induced inhibition of ^{3}H-TdR uptake into the cells [62–64].

Table 2
Proliferation and cytotoxicity assays for the determination of interleukins

Cytokine	Assay cell	Measurement	Sensitivity	Comments	Non-interference	Ref.
rIL-1	HT2A	cell counting	< 1 pg/ml	induction of IL-2 in LBRMTG6, silica extraction of plasma inhibitors	n.m.	[16]
rIL-1	RPMI 1788	^{3}H-TdR	1.5 pg/ml	–	mitogens, phorbol ester, calcium ionophore	[17]
rIL-1	D10.G4.1	^{3}H-TdR	n.m.	in presence of saturating IL-2/4	IL-6, TNF-α MuTNF-α	[18,19]
rIL-1	C3H/HeJ	^{3}H-TdR	10 pg/ml	–	n.m.	[20]
rIL-1	D10.G4.1	CFDA uptake	10 pg/ml	–	IL-6, TNF-α, MuTNF-α	[21]
rIL-1	HDF	^{3}H-TdR	< 10 pg/ml	–	IL-2, -6, TNF-α, GM-CSF	[22]
rIL-1	CTLL-2	^{3}H-TdR	< 10 pg/ml	induction of IL-2 in LBRM-33	n.m.	[23]
rIL-1	HT2	^{3}H-TdR	< 1 pg/ml	induction of IL-2 in LBRMFG6	n.m.	[24]
rIL-1	CTLL-20	^{3}H-TdR	0.8 pg/ml	induction of IL-2 in EL-4	n.m.	[25]
rIL-1	CTLL	^{3}H-TdR	1 pg/ml	induction of IL-2 in EL-4	TNF, IFN-γ ANF, LPS	[26,27]
nIL-1	C57BL/6	^{3}H-TdR	n.m.	–	n.m.	[28]
rIL-1α	C3H/HeJ	^{3}H-TdR	0.7 pg/ml	induction of IL-2R, in presence of saturating IL-2	n.m.	[29]
r/nIL-1α	A375	MB staining	n.m.	–	n.m.	[30]
rIL-1α	A375 S1	NR uptake	30 pg/ml	in presence of anti-IL-1β Ab	IL-2,-6, TNF, IFN-α,-γ, GM-CSF, M-CSF	[31]
rIL-1β	A375 S1	NR uptake	10 pg/ml	–	ibid	[31]
rIL-2	CD3^{+}	^{3}H-TdR	0.1 pg/ml	induction of IL-2R expression	IL-2,-6, TNF-α, IFN-α	[32]
rIL-2	CTLL	^{3}H-TdR	n.m.	–	n.m.	[33,34]
rIL-2	CTLL	CFDA uptake	3 pg/ml	–	IL-6, TNF-α, MuIFN-α	[21]
r/nIL-2	NKC3	MTT	n.m.	SDS–0.01 M HCl for dissolving	n.m.	[35]
rIL-2	CTLL	Giemsa staining	~ 5 pg/ml	–	n.m.	[36]
rIL-2	MNC	^{3}H-TdR	n.m.	–	n.m.	[37]
nIL-2	ATH8	^{125}I-IDU or FDU	n.m	–	n.m.	[38]
nIL-2	CTC	^{3}H-TdR	n.m.	–	n.m.	[39]
rIL-2	CTLL	MTT	n.m.	SDS–0.01 M HCl for dissolving	n.m.	[40]
rIL-2	CTLL-2	IL-2 IRMA	100 pg/ml	–	n.m.	[41]
rIL-2	CTLL	^{3}H-TdR	n.m.	–	n.m.	[42]
rIL-3	BMC	MTT	n.m.	SDS–0.01 M HCl for dissolving	n.m.	[43]
rIL-3	BMC	colony counting	n.m.	–	n.m.	[44,45]
rIL-4	PHA blast	^{3}H-TdR	200 pg/ml	in presence of saturating IL-2	IL-1,-2,-3,-6, IFN-α,-β, -γ, TNF, GM-CSF	[46]
rIL-4	TF-1	^{3}H-TdR	10 pg/ml	–	n.m.	[47]
rIL-4	MO-7	^{3}H-TdR	10 pg/ml	–	n.m.	[47]
rMuIL-5	BCL-1	^{3}H-TdR	25 pg/ml	in presence of anti-IFN-γ and anti-IL-4 Ab	IL-2,-3,-6, GM-CSF	[48]
rIL-6 or rMuIL-6	B9	^{3}H-TdR	0.5 pg/ml	–	n.m.	[49]
rIL-6	M1	MTT	0.5 ng/ml	isopropanol or SDS–0.01 M HCl for dissolving	IL-1α,-1β, G-CSF, M-CSF	[50]
rIL-6	B9	^{14}C-TdR	n.m.	–	IL-2,-4, IFN-γ, TNF-α	[51]
rIL-6	7TD1	MTT	0.5 ng/ml	–	n.m.	[52]
rIL-7	IxN/26	MTT	10 ng/ml	–	n.m.	[53]

In the antigrowth assay developed by Aebersold and Sample [60], the acidity of the medium due to the metabolism of the Daudi cells is measured. The acidity of the medium, as detected by phenol red, correlates with the number of cells.

In the P388-tryptan blue staining method presented by Tyring et al. [61], it was demonstrated that low concentrations of IFN-γ are mainly antiproliferative, while higher concentrations are clearly cytolytic.

Assays based on antiproliferative effects may have several advantages in comparison with conventional antiviral assays. The latter always represent more complex test systems, including variables related to both cells and viruses used. Antiproliferation assays provide sensitivities of about 500 pg/ml and *inter*assay coefficients of variation of 10% or less and can compete for reproducibility with the immunological assays [65]. The specificity of all assays was demonstrated by the lack of antiproliferative effects by other interferons.

1.3. Cytopathic effect reduction assays

Currently the most often used biological assays for interferons are variations of a method first described by Ho and Endres [66]. These assays depend upon a virus that causes damage to the cultured cells. The interferon is then determined by its ability to prevent a cytopathic effect (CPE) of cell lines such as L929 (mouse) or HEp2 (human) induced by, e.g. *Encephalomyocorditis* virus. Cells are cultured as monolayers in the presence of interferon samples for 24 h. Virus is added to microtiter plate-wells and the plates left for 24–48 h for optimal cell death to occur.

The CPE can be assessed either subjectively or objectively. In the former method, an estimate of CPE is scored usually by microscope observation of each infected culture. These CPE-inhibition assays have been used for most interferons [67,68]. The assay can be completed in 16 h if virus and interferon sample are added simultaneously. However, the assay is up to 30-fold more sensitive when interferon addition precedes virus challenge by 6 h or more [68]. Optionally, viral CPE can be determined spectrophotometrically by measuring the amount of a vital dye, such as natural red, that is taken up by living cells or by measuring the binding of crystal violet. Table 3 shows useful cell-virus combinations for CPE and 'dye-uptake' assays for interferons.

Both the subjective and objective CPE-inhibition assays can be carried out in microtiter plates so that large numbers of samples can be assayed simultaneously. Most CPE assays described for IFN-α and IFN-β also respond to IFN-γ. However, the cell-virus combination MDBK and VSV is not suitable for determination of IFN-β and IFN-γ [70,71,75]. Using MTT measurement, the lowest level of detection is around 10 pg/ml, in contrast to other CPE and dye-uptake assays, which can reliably detect 100–200 pg/ml. A reason for this difference in sensitivity is that in the MTT method no washing steps are required. These washings will often lead to unpredictable loss of cells which, in turn, will influence the final readings.

The CPE assay is straightforward and useful, but it has some disadvantages, notably the poor specificity and the short dilution range in which the end-point occurs.

Table 3
Cytopathic effect reduction and dye-uptake assays for the determination of interferons

Cytokine	Assay cell	Virus	Measurement	Non-interference	Ref.
nIFN-α	FL or L929	VSV or SFV	NR staining	n.m.	[69]
rIFN-α	MDBK	VSV	NR staining	IFN-β, IFN-γ	[70,71]
rIFN-α	SG-181 or HEp-2	VSV or EMCV	NR staining	n.m.	[72,73]
rIFN-α	HEp-2	SFV	CV staining	n.m.	[74]
rIFN-α	MDBK	VSV	MTT	IFN-β, IFN-γ	[75]
rIFN-α,-β,-γ	OCP or CSM	VSV or EMCV	microscope	nIFN-γ	[76]
rIFN-α,-β,-γ	WISH	EMCV	CV staining	n.m.	[77]
rRatIFN-α,-β,-γ	SD	VSV	CV staining	n.m.	[78]
rIFN-ω	HEp-2	VSV	NR staining	n.m.	[79]

1.4. Plaque-reduction assays

The plaque-reduction assay was developed in 1961 by Wagner [80] and is presently not in common use anymore. The procedure is essentially that of the CPE assay: after treating cells with interferon, cultures are inoculated with a dilution of virus that will give a sufficiently large number of countable plaques. After infection, the plaques can be enumerated by vital dyes, such as natural red or crystal violet. The most commonly used cells and viruses for plaque-reduction assays are identical to those used in the CPE assays. In addition, Ferreira et al. [81] reported poliovirus susceptibility to human interferon in monkey Vero cells.

Although plaque-reduction assays are relatively precise and reproducible, they are laborious, time consuming and not very sensitive (lowest limit of detection > 200 pg/ml) [82]. Campbell et al. [83] devised a microplaque-reduction assay for murine and human interferon that requires less sample, less time and fewer cells. The method is much less expensive than macroplaque assays, but the plaques must be counted visually using a microscope [84]. Green et al. [85] reported a rapid, quantitative, semi-automated microplaque-reduction assay for human interferon. Semi-automated equipment was used for dilution and distribution of interferon samples onto cell monolayers. This assay can be completed within 30 h from the time of addition of interferon, but it still requires visual counting of plaques.

Burleson and Herzog [78] conducted a study on the comparison of different bioassays for rat interferon, the sensitivity and precision of which are comparable to bioassays for interferon of other species [86]. The plaque-reduction assay exhibited the highest sensitivity, when compared to the CPE assay, and has equal or better precision.

1.5. Virus yield-reduction assays

In virus yield-reduction assays, the ability of interferon to reduce the yield of infectious virus, viral haemagglutinin (HA), viral enzymes, or viral nucleic acid is measured. Essentially, the procedure is that of the CPE assay. These assays, in some cases with detection limits as low as 25 pg/ml, shown in Table 4, generally use high multiplicities of infection and determine the extent of inhibition of the viral parameter after a single cycle of viral growth.

Assays based on reduction in infectious virus are usually time-consuming, but are still in use for the determination of international interferon standards [103].

HA yield-reduction assays are practical, sensitive, reproducible, objective and have been adopted to microtiter methods [94–96].

Retrovirus reverse transcriptase assays are reported to be simple, accurate and reproducible with sensitivities > 200 pg/ml [97,98].

The neuraminidase yield-reduction assay is rapid, simple and reproducible when using the synthetic substrate methoxyphenylneuraminic acid (MPNA) [99–102].

Table 4
Virus yield-reduction assays for the determination of interferons

Cytokine	Yield-reduction	Assay cell	Virus	Measurement	Comments	Ref.
IFN-α,-β,-γ	infectious virus	HEp2 a.o.	EMCV a.o.	CPE or PR	less sensitive to IFN-γ	[87–90]
IFN-α	infectious virus	MDBK	VSV	EIA	not suitable for IFN-β,-γ	[91]
IFN-α,-β,-γ	haemagglutinin	various	EMCV, Sindbis, GD-VII virus	human O erythrocytes	sensitivity increased by extraction of HA	[92–96]
IFN-α,-β,-γ	retrovirus reverse transcriptase	NIH/3T3	Moloney strain of murine leukemia virus or feline retrovirus	^{3}H-TdR	–	[97,98]
IFN-α,-β,-γ	neuraminidase	various	X7(F1)	MPNA a.o.	–	[99–102]

1.6. Antigen-induction assays

Various biological assays have been described for both interferons and interleukins, based on induction and/or enhancement of antigen expression in cells. These antigen induction assays are shown in Table 5.

Lleonart et al. [104] described a novel specific and quantitative assay for biologically active human IFN-α and IFN-β, called the MxR assay. Exposure of the Vero Mx13 line to IFN-α_2 or IFN-β for 12–48 h results in the production of hGH that is measured by a commercially available RIA. This assay displayed different dose response curves for IFN-α_2 and IFN-β at low concentrations, possibly caused by a higher affinity of the interferon receptors on the Vero cells for IFN-α_2 than for IFN-β.

A method developed by Gibson and Kramer [105] involves measurement of induction by IFN-γ of HLA-DR antigens on tumor cells. However, many cytokines can modulate the response to IFN-γ: TNF and IL-1 synergize, while IFN-α and G-CSF antagonize.

Recently, Agrewala et al. [106] described a new and specific method for measuring IFN-γ and IL-4, based on the estimation of IgG_1- and IgG_{2a}-isotype secretion from B-cells. An antagonizing effect of IFN-γ in the production of IgG_1 induced by IL-4 was neutralized by using IFN-γ specific antibodies. Similarly, the interference of IL-4 in the IFN-γ assay was blocked by anti-IL-4 antibodies. IgG levels were estimated by a standard sandwich ELISA procedure, with HRP-OPD detection [107]. Another assay for IL-4 measures the induction of CD23 (FcE receptor 2) on RAMOS B-cells by a fluorescence immunoassay [46].

Le Moal et al. [20] presented a new IL-1β titration method which takes advantage of the capacity of a thymoma line, EL4-6.1, to differentiate and express IL-2 receptors upon stimulation by IL-1β in the presence of phorbol ester. Membrane IL-2R measurement by flow cytometry or ELISA on this indicator cell line permits detection of 0.1 pg/ml IL-1β. IL-2 and TNF-α only exert a weak costimulation effect at very high doses. Due to their high sensitivity, this assay should permit reliable IL-1 determination in biological fluids such as IL-2-rich lymphocyte culture supernatants.

1.7. Proteinase-induced decomposition assays

Human interferon can be inactivated by proteinases such as trypsin and pepsin [108], and based on this fact methods for quantitative determination of IFN-α, IFN-β and IFN-γ were established [109,110].

It revealed that the decomposing substance of human interferon obtained by action of kallikrein or trypsin, under fixed conditions, hydrolyzed the fluorescent-peptide substrate MCA. Since kallikrein shows complicated changes in living body [111], the kallikrein-method is, contrary to the trypsin method, exclusively appropriate for determinations of interferon in pharmaceutical preparations.

Table 5
Antigen-induction assays for the determination of interferons and interleukins

Cytokine	Assay cell	Induced Ag	Measurement	Sensitivity	Ref.
rIFN-α/β	Vero Mx13	hGH	RIA	150 pg/ml	[104]
rIFN-γ	COLO203	HLA-DR	ELISA	250 pg/ml	[105]
rIFN-γ	B-cell	IgG_{2a}	ELISA	100 pg/ml	[106]
rIL-1β	E4-6.1	IL-2R	ELISA	0.1 pg/ml	[20]
rIL-4	B-cell	IgG_1	ELISA	300 pg/ml	[106]
rIL-4	RAMOS	CD23	FIA	500 pg/ml	[46]

It was reported that using the trypsin method, the IFN-α level in body fluids of rabbits could be assayed [112].

No information is given on the sensitivities of the assays.

2. Immunological assays

Specific antibodies for interferons and interleukins are available in large quantities and of good quality. Currently the availability of highly purified interferons and interleukins has resulted in the production of monoclonal antibodies (MAbs). Contrary to polyclonal antibodies (PAbs), MAbs can be produced in unlimited quantities and are identical with respect to affinity, avidity and specificity.

In immunological assays, interferon or interleukin is captured between two different (preferably monoclonal) antibodies simultaneously. For quantitation of the analyte, the second antibody has to be linked to a radiolabel (immunoradiometric assay), an enzyme (enzyme-linked immunosorbent assay), a Eu-complex (time-resolved fluoroimmunoassay) or a liposome (liposome immunosorbent assay). Alternatively, in a radioimmunoassay the antigen is linked to a radiolabel.

Despite their specificity, sensitivity, rapidity and ease of use, immunological assays have a major disadvantage compared to biological assays, viz. the detection of biologically inactive interferon and interleukin.

2.1. Radioimmunoassays

The most usual form of radioimmunoassay (RIA) is a competitive assay, which was developed in 1968 [113]. This type of assay requires pure antigen both for radiolabelling and to provide a standard, and a specific antibody. The most widely used nuclide for labelling is ^{125}I since it can readily be introduced in proteins by simple chemical methods [114]. RIA works on the principle that a given amount of antibody (Ab) will combine with radiolabelled antigen (Ag*), added in excess, to produce a radiolabelled complex (Ab:Ag*).

If unlabelled antigen is introduced into this system, the two forms of antigen compete for the limited number of antibody combining sites with the result that some radiolabelled antigen is displaced from the complex:

$$Ab + Ag + Ag^* \rightleftharpoons Ab{:}Ag + Ab{:}Ag^* + Ag^*$$

After separation of the complex from the free antigen, a standard curve can be set up, in which the amount of radiolabelled complex is ascertained in the presence of increasing amounts of unlabelled antigen. A summary of RIAs available

Table 6
Radioimmunoassays for the determination of interferons and interleukins

Cytokine	Antibody	Radiolabel	Sensitivity	Non cross-reactivity	Ref.
rIFN-α	anti-IFN-α rabbit IgG	^{125}I	60 pg/ml	IFN-β, IFN-γ, ACTH	[115]
rIFN-α_2	anti-IFN-α rabbit serum	^{125}I	200 pg/ml	n.m.	[116]
rIL-1α	anti-IL-1α rabbit serum	^{125}I	n.m.	IL-1β, TNF	[117]
rIL-1α	anti-IL-1α sheep serum	^{125}I	40 pg/ml	IL-1β porcine IL-1, MuIL-1	[118]
rRabbitIL-1α	anti-IL-1α goat IgG	^{125}I	20 pg/ml	rabbit IL-1β, IL-1α IL-1β, TNF-α	[119]
rIL-1β	anti-IL-1β rabbit serum	^{125}I	250 pg/ml	IL-1α, IL-2, TNF-α, IFN-γ	[120,121]
rIL-1β	anti-IL-1β rabbit serum	^{125}I	120 pg/ml	IL-1α, TNF	[117]
rIL-1β	anti-IL-1β sheep IgG	^{125}I	100 pg/ml	n.m.	[122]
rIL-1β	anti-IL-1β sheep serum	^{125}I	80 pg/ml	IL-1α, porcine IL-1, MuIL-1	[118]
rRatIL-1β	anti-IL-1β goat serum	^{125}I	100 pg/ml	IL-1α, IL-1β, IL-2, IL-6, IL-1ra, MuIFN-γ, TNF, bacterial LPS	[123]
rRabbitIL-1β	anti-IL-1β goat IgG	^{125}I	40 pg/ml	rabbit IL-1α, IL-1α, IL-1β, TNF-α	[119]
n/rIL-2	anti-IL-2 rabbit IgG	^{125}I	50 pg/ml	MuIL-2	[124]
rIL-6	LP-716	^{125}I	20 pg/ml	n.m.	[125]
rIL-8	A107	^{125}I	3 ng/ml	MCAF, PF4, βTG	[126]

Fig. 2. The basics of the sandwich immunoradiometric assay (IRMA).

for the determination of interferons and interleukins is given in Table 6.

RIAs have several distinct advantages over biological assays, being less complex and simpler to control. Competitive RIAs for several interferons and interleukins are now available from commercial sources, e.g. a kit for IL-1β (Cistron, Du Pont-NEN) [1], but are prohibitively expensive and have only been validated as research tools, often for cell culture supernatants [2]. In many cases, these assays lack the sensitivity for use in plasma, and some are subject to interference from rheumatoid factor or heterophilic antibodies. They are frequently imprecise and often do not demonstrate acceptable recovery profiles from a number of biological media, including plasma, cerebrospinal fluid and synovial fluid [127].

Normally, sensitivity can be obtained in the range down to 50–250 pg/ml. The specificity of the RIA depends on the affinity of the antibody and on the purity of the labelled interferon or interleukin [67,128]. A two- to fourfold increase in assay sensitivity may be obtained by delayed tracer addition [1].

Table 7
Immunoradiometric assays for the determination of interferons and interleukins

Cytokine	1st Antibody	2nd Antibody	Radiolabel	Sensitivity	Non cross-reactivity	Ref.
rIFN-α	anti-IFN-α sheep serum	anti-IFN-α sheep IgG	^{125}I	500 pg/ml	n.m.	[130]
nIFN-α	anti-IFN-α sheep IgG	NK2	^{125}I	> 5 ng/ml	IFN-β	[131]
nIFN-α	anti-IFN-α sheep IgG	NK2	^{125}I	500 pg/ml	n.m.	[132]
rIFN-α_2	anti-IFN-α_2 sheep IgG	NK2	^{125}I	500 pg/ml	IFN-α_1	[133]
rIFN-α_2	anti-IFN-α_2 rabbit IgG	anti-IFN-α_2 rabbit IgG	^{125}I	200 pg/ml	n.m.	[116]
rIFN-αA	LI-9	LI-1	^{125}I	10 pg/ml	IFN-γ	[134,135]
nIFN-β	anti-IFN-β rabbit IgG	anti-IFN-β rabbit IgG	^{125}I	500 pg/ml	n.m.	[136]
n/rIFN-β	4008	4020	^{125}I	3 ng/ml	IFN-α	[137]
nIFN-β	anti-IFN-β rabbit IgG	anti-IFN-β rabbit IgG	^{125}I	1 pg/ml	n.m.	[138,139]
nIFN-β	dinitrophilated (DNP) anti-IFN-β rabbit IgG	anti-DNP	^{125}I	500 pg/ml	n.m.	[140]
rIFN-γ	6008	3710	^{125}I	2 ng/ml	n.m.	[141]
rIFN-γ	M-Ab-γ-123	M-Ab-γ-127A	^{125}I	200 pg/ml	IFN-α, -β, MuIFN-γ	[142,143]
rIFN-γ	anti-IFN-γ mouse IgG	anti-IFN-γ mouse IgG	^{125}I	2 pg/ml	n.m.	[144,145]
rMuIFN-γ	AN-18	R4-6A2	^{125}I	1 pg/ml	IFN-γ, MuIFN-α, -β	[146]
rIL-1α	anti-IL-1α sheep IgG	anti-IL-1α sheep IgG	^{125}I	20 pg/ml	n.m.	[147]
rIL-1α	anti-IL-1α sheep IgG	anti-IL-1α sheep IgG	^{125}I	25 pg/ml	IL-1β	[148]
rMuIL-1β	anti-IL-1β rabbit IgG	anti-IL-1β rabbit Fab'	^{125}I	250 pg/ml	MuIL-1α, MuTNF, MuIL-6	[149]
rMuIL-1β	anti-IL-1β sheep IgG	anti-1β sheep IgG	^{125}I	10 pg/ml	RatIL-1β, IL-1β, -6	[150]
rRatIL-1β	anti-IL-1β sheep IgG	anti-IL-1β sheep IgG	^{125}I	10 pg/ml	MuIL-1β, L-1β, -6	[150]
rIL-2	35H10	RArIL-2	^{125}I	100 pg/ml	n.m.	[151]

2.2. Immunoradiometric assays

The immunoradiometric assay (IRMA) represents a technique in which an antibody is labelled with a radioisotope, usually ^{125}I. In IRMAs for interferons and interleukins, an antibody is typically immobilized on a solid support and exposed to the analyte-containing biological fluid [129]. This results in capture of the analyte in the form of a primary Ab:Ag complex which is subsequently exposed to a second specific antibody, directed towards another antigenic site on the analyte molecule (Fig. 2).

The particular advantages of this approach are that the antigen must be characterized by two geometrically separated and molecularly distinct binding sites. This imparts a much higher degree of specificity to the overall system. Table 7 lists antibody combinations used for sandwich IRMAs for interferons and interleukins.

Commercial versions of the IRMA are available as kits from Celltech, Boots-Celltech (IFN-α and IFN-β), Centocor (IFN-γ) and others [142,152]. These and other versions have sensitivities equivalent to or better than the conventional anti-viral assays, measuring down to 10 pg/ml. All IRMAs are relatively less accurate at the bottom and top ends of their sensitivity ranges where the *intra*-assay values for the coefficient of variation are greater than 10%.

IRMAs for interferons and interleukins currently described are essentially the one delineated by Secher [131] for IFN-α, utilizing a ^{125}I-labelled monoclonal antibody (NK2). In some IRMAs a pair of monoclonal antibodies is used and only those interferons or interleukins which are recognized by both antibodies are detected. The sensitivity of such assays approach that of the most sensitive biological assays.

Neurath et al. [140] described an aberrant IRMA in which IFN-β is adsorbed onto the surface of a solid support. The bound antigen forms a complex with a dinitrophenylated(DNP)-anti-IFN-β immunoglobulin (IgG), that can be detected in a second step in which radiolabelled anti-DNP IgG is added.

Overall, IRMAs are sensitive methods with low coefficients of variability compared with the biological assays, but they require extensively purified radiolabelled Ab elicited against pure interferon or interleukin [67,128].

2.3. Enzyme-linked immunosorbent assays

The most common type of enzyme immunoassay for interferons and interleukins is the sandwich enzyme-linked immunosorbent assay (ELISA), which closely resembles the IRMA. In an ELISA the first antibody is attached to a solid phase, antigen is incubated, and then detected by a second antibody linked to an enzyme, which converts an appropriate substrate into a detectable product (Fig. 3).

The demands on enzyme labels make only a limited number of enzymes admissible for ELISAs [153]. Basically, the enzyme should permit colorimetric, fluorimetric or luminometric measurement of the products formed. Horseradish peroxidase (HRP) and alkaline phosphatase (AP) can be used in conjunction with fluorescent and luminescent substrates with a higher sensitivity than colorimetry, and therefore permit a greater dilution of the product or a considerable reduction of the reaction volume. Nonetheless, colorimetric product measuring is the most frequently used detection method for interferon and interleukin ELISAs.

Since ELISAs do not depend on radiolabelled antibodies, which decay rapidly in terms of radioactivity, their increased shelf-life offers major

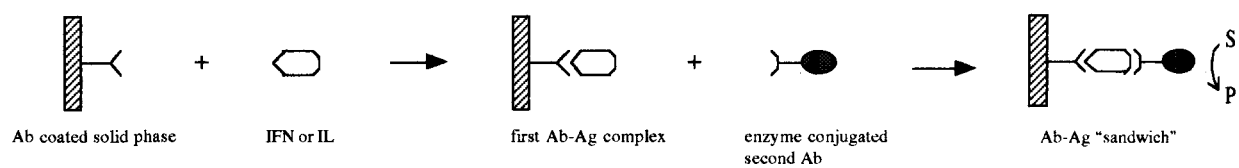

Fig. 3. The basics of the sandwich enzyme-linked immunosorbent assay (ELISA).

Table 8
Enzyme-linked immunosorbent assays for the determination of interferons and interleukins

Cytokine	1st Antibody	2nd Antibody	Enzyme	Substrate	Sensitivity	Non cross-reactivity	Ref.
nIFN-α	LI-9	LI-1	HRP	OPD	10 pg/ml	n.m.	[154]
rIFN-α_2	anti-IFN-α mouse IgG	anti-IFN-α mouse IgG	HRP	OPD	30 pg/ml	n.m.	[155]
rIFN-α_2	anti-IFN-α rabbit IgG	anti-IFN-α rabbit IgG	AP	PNPP	200 pg/ml	n.m.	[126]
rIFN-α_{2c}	OMG-2	OMG-7	HRP	OPD	10 pg/ml	rIFN-α_1, -β, -γ	[156,157]
rIFN-β_1	anti-IFN-β_1 rabbit IgG	YSB-1	HRP	OPD	50 pg/ml	n.m.	[158]
rIFN-γ	1-D1K	7-B6-1	AP	PNPP	25 pg/ml	n.m.	[159]
rIFN-γ	γ2-11.1	γ3-11.1	HRP	OPD	600 pg/ml	nIFN-γ	[160]
rIFN-γ	MD-2	MD-1	HRP	TMB	100 pg/ml	n.m.	[161]
rIFN-γ	MD-2	MD-1	AP	PNPP	100 pg/ml	n.m.	[162]
rIFN-γ	MD-2	MD-1	HRP	luminol	100 pg/ml	n.m.	[163]
rIFN-γ	MD-2	MD-1	AP	lumiphos	50 pg/ml	n.m.	[164,165]
rIFN-γ	HB170	XMG1.2	HRP	OPD	50 pg/ml	n.m.	[166]
rIFN-γ	D9D10	D1G2	HRP	OPD	1 ng/ml	n.m.	[167]
rIFN-γ	anti-IFN-γ mouse F(ab')$_2$	anti-IFN-α mouse IgG	HRP	OPD	80 pg/ml	n.m.	[168]
rMuIFN-γ	anti-IFN-α mouse IgG	anti-IFN-α mouse IgG	HRP	OPD	3 pg/ml	nMuIFN-α, -β, nIFN-γ, rTNF	[169]
rIL-1α	anti-IL-1α rabbit IgG	anti-IL-1α rabbit IgG	β-DGD	4-MU-G	10 pg/ml	rIL-1β, -2	[170]
rIL-1α	anti-IL-1α rabbit IgG	anti-IL-1α rabbit Fab'	HRP	OPD	10 pg/ml	rIL-1β, -2, rIFN-γ	[171]
rIL-1α	α185	α29	AChE	ER	1.5 pg/ml	rIL-1β, -2	[172,173]
rIL-1α	McAb 1190	McAb 964	HRP	OPD	n.m.	nIFN-α, -γ, rIL-1β, rTNF-α	[174]
rIL-1α	anti-IL-1α rabbit IgG	anti-IL-1α rabbit Fab'	HRP	HPPA	5 pg/ml	n.m.	[175]
rIL-1α	anti-IL-1α mouse IgG	anti-IL-1α mouse Fab'	HRP	HPPA	2 pg/ml	nIL-1β	[176–178]
rIL-1β	S77β	anti-IL-1β sheep Fab'	HRP	OPD	20 pg/ml	rIL-1α, -2, rIFN-γ	[171]
rIL-1β	β79	β36	AChE	ER	1 pg/ml	rIL-1α, -2	[172,173]
rIL-1β	anti-IL-1β mouse IgG	anti-IL-1β rabbit IgG	AP	PNPP	50 pg/ml	n.m.	[179–181]
rIL-1β	anti-IL-1β rabbit IgG	anti-IL-1α mouse Fab'	HRP	HPPA	25 pg/ml	nIL-1β	[176–178]
rIL-1β/ rMuIL-1β	DMS-1	DMS-5	AP	PNPP	150 pg/ml	denaturated IL-2	[182,183]
rMuIL-1β	anti-IL-1β rabbit serum	anti-IL-1β rabbit IgG	AP	PNPP	10 pg/ml	rIL-1α, -2, -3, IL-1ra, rTNF-α, GM-CSF, ETP	[184]
rIL-2	anti-IL-2 goat IgG	anti-IL-2 rabbit Fab'	HRP	OPD	30 pg/ml	n.m.	[185]
rIL-2	anti-IL-2 rabbit IgG	anti-IL-2 rabbit Fab'	HRP	OPD	40 pg/ml	n.m.	[186]
rIL-2	L23	L61	β-DGD	4-MU-G	0.3 pg/ml	rIL-1α, -1β, -4, -6, rMuIL-4, rTNF, M-CSF	[187]
nIL-2	DMS-1	EP-100	HRP	TMB	150 pg/ml	n.m.	[188]
rIL-2	anti-IL-2 mouse IgG	anti-IL-2 rabbit Fab'	HRP	PNPP	30 pg/ml	n.m.	[189]
rIL-2	anti-IL-2 mouse IgG	anti-IL-2 mouse IgG	AChE	ER	1.5 pg/ml	rIL-1α, -1β	[173]
rIL-2	9B11-1E5	R-135	AP	PNPP	10 ng/ml	n.m.	[190]
rIL-2	n.m.	anti-IL-2 mouse IgG	HRP	TMB	10 pg/ml	n.m.	[191]
rIL-3	F-14	F-15	AP	PNPP	20 pg/ml	cytokines n.s.	[192]
rIL-3	8F8.1	43D11	AP	PNPP	20 pg/ml	n.m.	[193]
rMuIL-3	anti-IL-3 peptide 1-29 rabbit IgG	anti-IL-3 peptide 1-140 sheep serum	HRP	OPD	60 pg/ml	n.m.	[194]
rIL-5	TRFK5	MAb 7 or 8	HRP	TMB	500 pg/ml	rMuIL-5	[195]
rIL-5	TRFK5	MAb 7 or 8	HRP	RPN-90 [a]	40 pg/ml	rMuIL-5	[195]

Table 8 (continued)

Cytokine	1st Antibody	2nd Antibody	Enzyme	Substrate	Sensitivity	Non cross-reactivity	Ref.
rIL-5	D171	C213	HRP	TMB	8 pg/ml	rGM-CSF, rIL-4, rTNF, rIFN-γ, rMuIL-5	[196,197]
nIL-5	39D10	5A10	HRP	ABTS	n.m.	n.m.	[198]
rIL-5	TRFK1 or 5	TRFK 2 or 4	HRP	TMB	20 pg/ml	n.m.	[199]
rIL-6	IG 61	IC 67	HRP	OPD	9.5 pg/ml	rGM-CSF, rG-CSF, rTNF, rIFN-α,-β,-γ, rMuIL-6	[200]
rIL-6	CLB.IL-6/8	anti-IL-6 sheep IgG	HRP	TMB	30 pg/ml	n.m.	[201]
rIL-6	MH166	αRV2	AP	lumiphos	0.1 pg/ml	n.m.	[202,203]
rIL-6	n.m.	anti-IL-6 goat IgG	HRP	TMB	2.6 pg/ml	cytokines n.s.	[204]
r/nIL-8	anti-IL-6 rabbit IgG	anti-IL-6 rabbit IgG	HRP	OPD	84 pg/ml	n.m.	[205]
nIL-10	9D7	1268	HRP	ABTS	n.m.	n.m.	[198]

[a] Enhanced chemiluminescence immunoassay signal reagent (Amersham).

advantages over IRMA [152]. In general, ELISAs are more sensitive than IRMAs. ELISAs for most interferons and interleukins are now commercially available from a number of companies [47], with sensitivities of tens to several hundreds pg/ml. Table 8 summarizes the sandwich ELISAs available for the determination of interferons and interleukins.

Detection limits, in some cases well below 1 pg/ml, and sensitivity ranges depend on the concentration and affinity of the second antibody added [152]. In some cases substitution of a PAb by a MAb, which binds to a different epitope than the second antibody, may also improve sensitivity. Further layers on the sandwich may be applied to increase assay sensitivity, for example Ag is detected by unlabelled Ab which is itself detected by an Ab linked to an enzyme, or by using the avidin–biotin system. Recent variations on the classical sandwich ELISA, using fluorescence and chemiluminescence detection, have been reported to increase sensitivity (Table 8).

Like all other immunological assays, ELISAs are reliable, rapid, specific, do not require cell cultures and can be sensitive, but depending on the specificity of their antibodies, can also detect biologically inactive precursors of interferon and interleukin or may not detect active but partly cleaved forms [206]. Careful selection of antibodies should prevent these problems. The specificity of ELISA may have some disadvantages when the biological activity of the cytokine is due to more than one closely related molecule. For example, IL-1 activity is composed of two related proteins which are antigenically distinct and yet bind to a shared receptor [207]. Measurement of total IL-1 activity therefore requires two different ELISAs. Furthermore, ELISAs for interferons and interleukins suffer like RIAs and IRMAs from interference by rheumatoid factor and immune complexes [207], which are found in serum and fluid samples in many disease states.

2.4. Time-resolved fluoroimmunoassays

In time-resolved fluoroimmunoassays (TR-FIAs) the difference between the fluorescence lifetimes (τ) of the specific signal and of the background is exploited to increase the signal-to-noise ratio and thus the sensitivity of the assay [208]. When the τ of the probe is sufficiently larger than the background, the specific signal can be integrated after the background signal has decayed [209]. The development of new long-lifetime probes, rare-earth metal chelates for which τ ranges from 10–1000 μs, provides the tools for increasing the sensitivity of immunoassays by reducing the background signal almost to zero [210].

Some lanthanides, especially Eu(III), form highly fluorescent chelates with some organic ligands. The ligand's absorption of light is followed by efficient energy transfer from its excited sin-

glet state through its triplet state to the resonance levels of the rare-earth ion.

The fluorescence of the chelate is characterized by broad excitation in the absorption region of the ligand, emission lines typical for the metal, and an exceptionally long fluorescence lifetime [211].

For a rapid determination of IFN-α_2, Schmidt et al. [212] used an ELISA with two different MAbs, one immobilized and the other labelled with HRP. To increase assay sensitivity they developed a TR-FIA [213], using the same monoclonals as in the ELISA but labelling the second antibody with Eu(III) (eight Eu(III) labels per molecule of antibody). Despite the fact that the sensitivity of the fluorimeter used is about 10^{-17} moles of Eu(III) per cuvette, the detection limit is only 20 pg/l (?) of IFN-α_2, the same as with the ELISA. Possibly, the complexing power of Eu(III) in the enhancement solution was not optimized.

The linear range of the TR-FIA for IFN-α_2 is superior to that of the ELISA, but the improved sensitivity, which in theory should be far better, could not be obtained experimentally.

2.5. *Liposome immunosorbent assays*

A liposome immunosorbent assay (LISA) is a relatively new immunological method, in which the detection antibody is labelled with a liposome. Recently, Rongen et al. [214,215] and Hugenholtz [216] described the development of a LISA for the determination of IFN-γ, in which carboxyfluorescein (CF) is used as a marker molecule.

In this assay an antibody MD-2 is coated to the wells of a microtiter plate. After capture of IFN-γ, a second antibody (MD-1) labelled with biotin is introduced, avidin is added, and finally a biotinylated liposome with encapsulated CF (Fig. 4). After lysis of the liposomes with Triton X-100, a large quantity of CF is released (proportional to the amount of IFN-γ present), and detected with a fluorescence detector.

The lower limit of detection is about 100 pg/ml, with a linear dynamic range to 40 ng/ml, hence the LISA is equivalent in sensitivity to the more common ELISA employing the same monoclonals [162], although in theory the sensitivity should be better. Like other immunological assays, this LISA is precise, specific, inexpensive, and compared to biological assays relatively fast.

3. Receptor assays

In receptor assays (RAs) an interleukin receptor, e.g. on a cell, is used together with a radiolabelled anti-cytokine-antibody or cytokine. Analogously to the radiolabelled-immunological assays, RAs can be divided into receptor radiometric assays and radioreceptor assays, employing labelled antibody or antigen, respectively.

Contrary to biological assays, RAs possess a relatively high specificity and hence extraction procedures can be avoided. Moreover, RAs represent rapid techniques that will only detect cytokines with the ability to bind to the receptor used, and thus RAs are (theoretically) preferable to immunological assays.

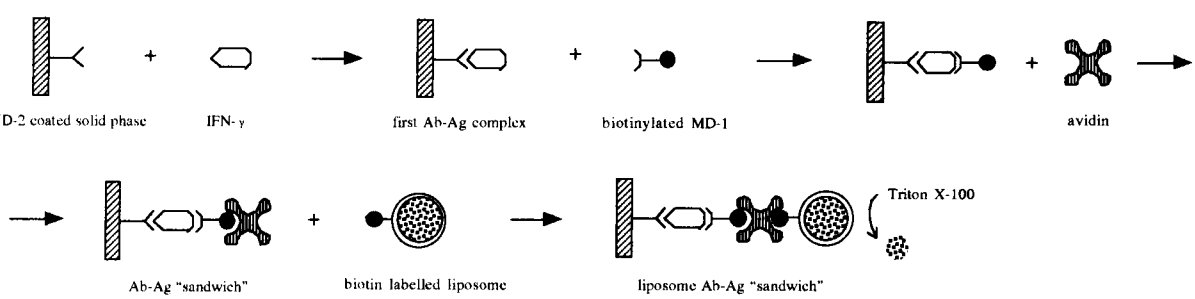

Fig. 4. Liposome immunosorbent assay (LISA) for the determination of IFN-γ (as described by Rongen et al. [215]).

3.1. Receptor radiometric assays

Recently, Ohiki et al. [217] described the development of a method to determine IL-2, which makes use of one of the antigenic determinants and the ability of the cytokine to bind to the receptor on hematopoietic cell lines [218]. A monoclonal antibody was obtained directed against an epitope of IL-2 that was not masked after IL-2 had bound to the receptor. The MAb against IL-2 (anti-IL-2 mouse IgG; no. 6512) was labelled with ^{125}I and applied to detect IL-2 that had been captured on cells with the receptor. For the purpose of catching IL-2 in the test samples, a hematopoietic cell line infected with human T-cell leukemia virus Type I (MT-1) [219] was employed; the virus is known to augment the expression of IL-2 receptors on human leukemic T-cells [220,221].

The receptor radiometric assay (Fig. 5), in which IL-2 is sandwiched between the receptor and a MAb, could detect r/nIL-2 in concentrations as low as 5 ng/ml, with a linear dynamic range up to 100 ng/ml.

3.2. Radioreceptor assays

An alternative approach to measuring cytokine levels that does not require antibodies, is to use the cytokine receptors on cells to capture labelled cytokines [222]. Displacement of labelled cytokine by unlabelled cytokines in a sample can be used to quantify levels. Scapigliati et al. [223] reported a rapid, solid-phase radioreceptor assay based on the adsorption onto nitrocellulose of detergent-extracted preparations of plasma membranes from an IL-$1R_{II}$-hyperexpressing subclone of Raji cells [224]. Non-specific binding was determined by adding a 500-fold molar excess of unlabelled IL-1β. Unbound radioactivity was separated from receptor-associated reactivity by centrifugation in an oil gradient.

This assay is suitable for specific and quantitative determinations of IL-1 both in physiological buffers and in human plasma without the need for prior extraction protocols. The assay can detect IL-1α and IL-1β levels separately as low as 65 ng/ml and 175 pg/ml, respectively.

The application of solubilized IL-$1R_I$ in a radioreceptor assay for the determination of IL-1α and IL-1β has been reported recently by Riske et al. [225]. The lower limit of detection of this assay is about 30 ng/ml for IL-1α and 580 ng/ml for IL-1β.

4. Chemical assays

At present, also instrumental methods are available to assay peptides and proteins, including interleukins and interferons, without using biologically- or immunologically-based tools. Various separation methods including liquid chromatography and capillary electrophoresis are providing selectivity and when equipped with a sensitive on-line detector (e.g. mass spectrometer or fluorimeter), rather low detection limits can be achieved. Currently, with these instrumental methods it is still not possible to assay (very) low levels of peptides and proteins in biological fluids, so the biological and immunochemical methods described before are still preferred. However, large progress is being made in various areas of instrumental analysis as demonstrated in some recent reviews [226–228].

4.1. Chromatographic assays

Liquid chromatography is an analytical method that is extensively used for the separation and

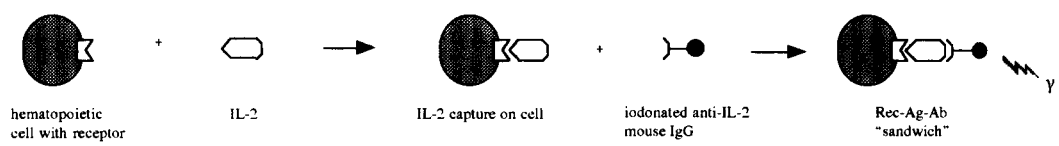

Fig. 5. Receptor radiometric assay for the determination of IL-2 (as described by Ohiki et al. [217]).

identification of interferons and interleukins in biological samples, but is less widely used for their determination. Nonetheless, a few chromatographic assays for interferons have been described and are summarized in Table 9.

Rybacek et al. [229] described a rapid dual-column chromatographic assay for determining rIFN-α_2 in complex mixtures. The assay relies on the use of a high-performance immuno-affinity column (IAC) connected in tandem with a reversed-phase column. These columns permit the quantitation of subcomponent species, such as interferon oligomers that may be present in the assay samples. The assay has a limit of sensitivity of 1 μg/ml and a range of only 1–20 μg/ml. The precision of the assay was estimated to be about 5%. A similar procedure was described by Roy et al. [230,231] for rIFN-αA, which measured the total interferon concentration at a sensitivity limit of about 30 μg/ml.

In a method presented by Rubinstein [232], interferon samples were analysed by treatment with the proteolytic enzyme trypsin followed by fractionation of the peptide mixture by chromatography. The column effluent was then monitored with an automated fluorescamine system [233]. The reagent fluorescamine, dissolved in acetone, is added to the effluent at pH 9 (the samples are hydrolysed in order to increase sensitivity). The fluorogenic reaction is complete within 1 min. Since both the reagent and its hydrolysis by-products are non-fluorescent, the fluorescence may be measured without further manipulations. With this methodology interferon detection at the microgram level is possible.

Compared to biological and immunological assays the chromatographic methods described above have higher limits of sensitivity, but are relatively fast to perform. In addition, the IAC assays can be used to determine the relative abundances of the interferon subcomponents in samples, while the immunological assays cannot.

4.2. Mass spectrometric assays

Mass spectrometry is concerned with the electron ionisation and subsequent fragmentation of molecules, with the determination of the mass to the charge ratios (m/z) and the relative abundances of the ions which are produced [234]. Quantitative measurements can be carried out at the picogram or even femtogram levels.

Padron et al. [235] used mass spectrometry for the analysis of rIFN-α_2. After purification by IAC chromatography, rIFN-α_2 was digested with trypsin and *Staphylococcus aureus* protease V8, separately or in tandem. Then the peptide mixture was analysed by fast atom bombardment mass spectrometry (FAB-MS). No information is given on the sensitivity of this interferon assay.

In a study by Tsarbopoulos et al. [236] rIFN-α_{2a} and rIL-4 were determined by ^{252}Cf plasma desorption mass spectrometry (PDMS) and Cs^+ liquid secondary ion mass spectrometry (LSIMS). In the PDMS method the cytokines were dissolved in an ethanol -0.1% aqueous trifluoroacetic acid (TFAA) mixture and applied to a nitrocellulose-coated aluminium foil, thoroughly rinsed with 0.1% TFAA to remove salt contaminants and analysed using a BIOION20 ^{252}Cf plasma desorption time-of-flight mass spectrometer. In the LSIMS method, the cytokines were dissolved di-

Table 9
Chromatographic assays for the determination of interferons

Cytokine	Column	Eluent	Detect.	Sensitivity	Non-interference	Ref.
rIFN-α_2	LIT-1 IA and Chromegabond C-4	0.1% TFAA in ACN	UV	1 μg/ml	matrix proteins	[229]
rIFN-αA	LI-8 IA	25 mM NH_4Ac	UV	30 μg/ml	n.m.	[230,231]
rIFN-α_1,-β,-γ	Ultrasphere C_8	n-propanol in 30 mM pyridine/0.1 M formic acid	F	< 90 μg/ml	n.m.	[232,233]

rectly in *m*-nitrobenzyl alcohol or glycerol–thioglycerol, followed by the addition of neat TFAA and analysis using a VG ZAB-SE double-sector mass spectrometer.

In both PDMS and LSIMS experiments, the observed sensitivity was dependent on the complexicity of the cytokine sample. Some of the strengths and limitations of these MS techniques are attributed to the inherent characteristics of the analyzers. The LSIMS technique can readily be adapted to existing sector mass spectrometers and, compared to PDMS, is requiring a shorter analysis time. However, the relatively non-destructive nature of PDMS allows additional chemical and/or enzymatic reactions to be carried out on the nitrocellulose-bound cytokine sample with direct and rapid analysis of the products. The sensitivity of the assays was in the μg/ml range.

4.3. Capillary electrophoretic assays

In CE, a high-voltage electric field introduced along a small fused-silica capillary provides the driving force needed to separate the components of the assay sample [237,238].

Guzman et al. [239] evaluated CE as a complementary technique for the analysis of IFN-α and IL-1α in pharmaceutical formulations. Separations were performed using a 50 mM sodium tetraborate buffer at pH 8.3 containing 25 mM LiCl. The experiments described demonstrate that CE has the sensitivity and degree of resolution for the determination of these cytokines in typical formulation mixtures. Both cytokines were well-separated from their excipients in a relatively short time and with a minimum of sample required. The resulting electropherograms generated with either a simple CE apparatus, operating under ambient temperature conditions, or with a more sophisticated CE unit, using temperature control of the capillary column, show excellent reproducibility at isothermal conditions. Capillary column temperature was observed to have an important influence on the electrophoretic results. Higher temperatures resulted in an increased degree of degradation of the cytokine, presumably through a deamidation pathway. Despite the enhanced degradation of the protein in the capillary column, the detection signal appears to be linear up to a cytokine concentration of 100 μg/ml. The lower limit of detection is not mentioned.

Analysis of commercial samples containing rIL-3 by CE have been reported by Hecht et al. [240,241]. Untreated fused-silica capillaries were used, and the electrophoretic buffer employed was 20 mM cyclohexylethane sulfonic acid (cHES) at pH 9.0 containing 10 mM KCl.

Recently Bullock [242] applied CE to the analysis of rIL-4, attaining an estimated lower limit of detection of 18 pg rIL-4.

For quantification of proteins such as interferons and interleukins, which might be subject to degradation during the assay, the running conditions must be optimized in order to minimize degradation and appropriate standards developed. When the additional work has been completed, CE should complement existing methodology for the determination of interferons and interleukins in, especially, pharmaceutical dosage forms.

4.4. Surface plasmon resonance assays

In surface plasmon resonance (SPR) spectrometry small changes of the refractive index of a solution in close proximity to a gold surface are detected [243]. The antibody or antigen is immobilized onto a metal surface, either by direct adsorption, by indirect coupling through a bifunctional thiol or a (strept)avidin–biotin bridge, or through a dextran hydrogel [244,245]. When an unlabelled analyte interacts with an unlabelled immobilized species, the refractive index of the metal–solution interface will change.

SPR can be used to monitor protein–protein or protein–ligand interactions in real-time and allows quantification of the interacting species [243,246]. The detection limit of SPR, however, is about 10^{-8} M for 20-kDa proteins (i.e. interleukins and interferons), so application of SPR for assaying cytokines in biological fluids is restricted to higher concentrations, e.g. in the supernatant of cytokine-producing cells.

In our laboratory research has been initiated to improve the detection limit of SPR largely. In

these studies IFN-γ is used as the model antigen. Signal enhancement is achieved by application of liposomes. Detection limits are in the picomolar range (to be published).

Recently, Ward et al. [247] used SPR detection for studying the binding of IL-6 and a series of anti-IL-6 MAbs. The binding sites on IL-6 could be mapped using several synthetic peptides (15-20 residues) spanning the IL-6 sequence. Recombinant IL-6-glutathione-S-transferase (rIL-6-GST) was immobilized onto a dextran matrix, and inhibition of the binding of an anti-IL-6 MAb, preincubated with one of the synthetic peptides, to rIL-6-GST could be established. In the study binding sites could be localized and association equilibrium constants be determined.

5. Other assays

5.1. Enzyme-linked immunospot assays

In an enzyme-linked immunospot assay (ELISPOT), the ELISA principle is employed to quantify interferons and interleukins produced by cells. For the enumeration of cytokine-producing cells, microtiterplate coated anti-cytokine-antibodies are incubated with the cytokine producing cells. After thorough washings, the cytokines are sandwiched by a second (enzyme conjugated) antibody, and detected using an appropriate substrate. Using this assay system, sensitive and specific assays have been reported for cells secreting IFN-γ [248,249], MuIL-2 or MuIL-4 [250], IL-5 or MuIL-6 [249].

5.2. Western blot analysis

The (semi)quantitative detection of specific cytokines in complex mixtures can be performed by western blot analysis, by which proteins are electrophoretically transferred from sodium dodecylsulphate polyacrylamide gels to nitrocellulose and then detected by enzyme- or radiolabelled cytokine-specific antibodies. This technique has been described for rIFN-α_1, rIFN-α_2, nIFN-γ [251,252] and for IL-1 [253], and allows cytokine determination at the nanogram level.

5.3. Indirect immunofluorescence assays

In indirect immunofluorescence assays cytokine-producing cells are fixated and permeabilized, after which fluorescent dyes, such as fluorescein or rhodamine, coupled to an anti-cytokine-antibody can penetrate the cell membrane and intracellular located cytokines can be measured. Employing this method Sander et al. [254] recently reported intracellular detection of several cytokines, including Hu/MuIFN-γ, IL-1α, IL-1β, IL-2, Hu/MuIL-4, MuIL-5, and IL-6.

5.4. Ribonucleic acid measurement assays

Cytokine expression can be evaluated by quantitating the ribonucleic acid (RNA) by in situ hybridization (IL-5) [255,256], northern blot analysis (IL-3, IL-5) [257,258] and polymerase chain reaction (PCR) assays (IL-5) [259].

6. Conclusions

Interferons and interleukins are proteins which belong to a group of (glyco)proteins variously called cytokines. Methods for the determination of interferons and interleukins currently available are based upon biological, immunological, receptor or chemical procedures.

In biological assays the effect of interferon or interleukin is being measured upon proliferation or cytotoxicity of cells, antiproliferation of cells, reduction of the viral cytopathic effect, reduction of viral plaque numbers, inhibition of virus replication or induction and/or enhancement of antigen expression in cells.

Proliferation and cytotoxicity assays can only be used for the determination of interleukins and can be extremely sensitive. A major drawback of these assays is their low specificity.

Determinations based on antiproliferative effects of interferon represent relatively simple test systems, since variables related to viruses are not included. These assays are sensitive and specific.

Cytopathic effect reduction assays can be used to measure interferon bioactivity. These methods are straightforward, sensitive but have an unde-

sirable feature in that they do not discriminate between different interferon subtypes.

Plaque-reduction assays and virus yield-reduction assays for interferons are relatively precise and reproducible, but they are laborious, time-consuming and not very sensitive.

Antigen induction assays, described for both interferon and interleukin, and proteinase induced decomposition assays for interferon usually exhibit a poor sensitivity.

In immunological assays interferon or interleukin is captured between two antibodies, one of which is linked to a solid phase, the other conjugated to a radiolabel (IRMA), an enzyme (ELISA), a Eu-complex (TR-FIA) or a liposome (LISA). In RIAs the antigen is linked to a radiolabel. Immunological assays are precise, specific, inexpensive, relatively fast and the sensitivity approaches that of the most sensitive biological assays. Properly validated two-site immunological assays are at present the assay systems in common use, although they may be inhibited by the same binding proteins or soluble receptors which also interfere in biological assays. Immunological assays for interferon and interleukin offer advantages over biological assays in terms of rapidity and reproducibility. However, immunological assays will also detect biologically inactive interferons and interleukins, while bioassays will not.

In receptorassays an interleukin receptor on a cell is used together with a radiolabelled antibody or antigen. Receptor displacement or binding assays are an area for assay development with potential for sensitivity, specificity, speed and biological relevance, since they combine the advantages of both biological and immunological assays.

Chemical assays available for the determination of interferons and interleukins include liquid chromatography, mass spectrometry, capillary zone electrophoresis and surface plasmon resonance-based assays. These methods are relatively fast, specific and inexpensive, but generally they lack the sensitivity required for the analysis of biological samples. Furthermore, chemical assays do not differentiate between biological active and inactive interferons and interleukins.

The determination of interferons and interleukins in biological matrices is hampered by the presence of interfering substances, such as other active cytokines with overlapping biological activities or substances that synergize with or inhibit the activity of the cytokine of interest. First choice assay formats are sensitive biological assays in which interfering cytokines are blocked with specific antibodies, and employing extraction procedures to eliminate deranging substances. Alternatively, many problems related to quantifying interferon and interleukin levels in tissue fluids can be overcome by using two different independent methods in conjunction, i.e. a specific biological assay and a sensitive immunological assay.

7. List of abbreviations

4-MU-G	4-Methylumbelliferyl-D-galactoside
Ab	Antibody
Ab*	Radiolabelled antibody
ABTS	2,2′-Azino-bis-(2-ethylbenzthiazoline-6-sulfonic)acid
AChE	Acetylcholinesterase
Ag	Antigen
Ag*	Radiolabelled antigen
AIDS	Acquired immunodeficiency syndrome
ANF	Human atrial naturietic factor 99-126
AP	Alkaline phosphatase
β-DGD	β-D-Galactosidase
Bl	B Lymphoblastoid cell
BSC	Bone marrow stromal cell
βTG	β-Thromboglobulin
CE	Capillary electrophoresis
CF(DA)	Carboxyfluorescein (diacetate)
CPE	Cytopathic effect
^{14}C-TdR	^{14}C-Labelled thymidine
CV	Crystal violet
DNA	Desoxyribonucleic acid
Ed	Endothelial cell
EIA	Enzyme immunoassay
ELISA	Enzyme-linked immunosorbent assay
EMCV	Encephalomycarditis virus
ER	Ellman's reagent
ETP	Erythropoietin
F	Fluorescence
Fb	Fibroblast
FDU	Fluorodeoxyuridine

FIA	Fluorescence immunoassay
G-CSF	Granulocyte colony stimulating factor
GM-CSF	Granulocyte/macrophage colony stimulating factor
HA	Haemagglutinin
hGH	Human growth hormone
HPLC	High-performance liquid chromatography
HPPA	3-(4-Hydroxyphenyl)propionic acid
HRP	Horseradish peroxidase
^{3}H-TdR	^{3}H-Labelled thymidine
IAC	Immuno affinity column
IFN	Interferon(s)
Ig	Immunoglobulin
^{125}I-IDU	^{125}I-Labelled iododeoxyuridine
IL	Interleukin(s)
IL-1R$_{II}$	Interleukin-1 receptor Type II
IL-1ra	Interleukin-1 receptor antagonist
IL-2R	Interleukin-2 receptor
IRMA	Immunoradiometric assay
LISA	Liposome immunosorbent assay
LPS	Lipopolysaccharide
MAb	Monoclonal antibody
MB	Methylene blue
MC	Mast cell
MCA	4-Methylcoumaryl-7-amide
MCAF	Monocyte chemotactic and activating factor
M-CSF	Macrophage colony stimulating factor
MO	Macrophage/monocyte
MTT	3-(4,5-Dimethyl-thiazol-2-yl)-2,5-diphenyltetrazolium bromide
Mu	Murine
n	Natural
NK	Natural killer cell
n.m.	Not mentioned
NR	Natural red
n.s.	Not specified
OPD	*o*-Phenylenediamine
PAb	Polyclonal antibody
PEG	Polyethylene glycol
PF4	Platelet factor 4
PNPP	*p*-Nitrophenyl phosphate
PR	Plaque reduction
r	Recombinant
RA	Receptor assay
RIA	Radioimmunoassay
SDS	Sodiumdodecyl sulphate
SFV	Semliki forest virus
SPR	Surface plasmon resonance
T	T-Lymphocyte
TB	Tryptan blue
TGF	Transforming growth factor
TMB	3,3′,5,5′-Tetramethylbenzidine
TNF	Tumor necrosis factor
TR-FIA	Time-resolved fluoroimmunoassay(s)
UV	Ultraviolet
VSV	Vesicular stomatitis virus

References

[1] R.C. Newton and J. Uhl, in J.Y. Chang and A.J. Lewis (Eds.), Pharmacological Methods in the Control of Inflammation, Alan R. Liss, New York, 1989, p. 83.
[2] J.T. Whicher and S.W. Evans, Clin. Chem., 36 (1990) 1269.
[3] W.E. Stewart II, Nature, 286 (1980) 110.
[4] W.E. Paul, J. Immunol. Methods, 147 (1992) 149.
[5] M.F. Wilkinson and A.G. Morris, Methods Enzymol., 119 (1986) 96.
[6] S.C. Clark, Serono Symp. Publ. Raven Press, 92 (1992) 23.
[7] F.J. Podlaski, V.B. Nanduri, J.B. Hulmes, Y-C.E. Pan, W. Levin, W. Danho, R. Chiazonite, M.K. Gately and A.S. Stern, Arch. Biochem. Biophys., 294 (1992) 230.
[8] S.M. Zurawski, F. Vega Jr., B. Huyghe and G. Zurawski, EMBO J., 12 (1993) 2663.
[9] F.R. Balkwill and F. Burke, Immunol. Today, 10 (1989) 299.
[10] P.H. Krammer, H. Kirchner and A. Schumpl, Immunol. Today, 10 (1989) 529.
[11] G. Günther and B. Otto, Arzneim. Forsch., 43 (1993) 182.
[12] V. Bocci, Immunology, 64 (1988) 1.
[13] W.E. Stewart II, The Interferon System, Springer Verlag, Vienna, 1981, p. 13.
[14] E. Borenfreud, H. Babisch and N. Martin-Alguacil, Toxicol. In Vitro, 2 (1988) 1.
[15] T. Mosman, J. Immunol. Methods, 65 (1983) 55.
[16] J.J. Series, D. Shapiro, I. Cameron, J. Smith, W.D. Fraser, O.J. Garden and A. Shenkin, J. Immunol. Methods, 108 (1988) 33.
[17] P. Vandenabeele, W. Declerq, C. Libert and W. Fiers, J. Immunol. Methods, 135 (1990) 25.
[18] S.J. Hopkins and M. Humphreys, J. Immunol. Methods, 120 (1989) 271.
[19] S.J. Hopkins and M. Humphreys, J. Immunol. Methods, 133 (1989) 127.
[20] M.A. Le Moal, M. Stoeck, J-M. Cavaillon, H.O. Robson MacDonald and P. Truffa-Bachi, J. Immunol. Methods, 107 (1988) 23.

[21] Y. Hansson, E. Jacobson, J. Oertlund, S. Paulie and P. Perlmann, J. Immunol. Methods, 100 (1987) 261.
[22] H. Loppnow, H-D. Flad, I. Duerrbaum, J. Musehold, R. Fletting, A.J. Ulmer, H. Herzbeck and E. Brandt, Immunobiol., 179 (1989) 283.
[23] P.J. Conlon, J. Immunol., 131 (1983) 1280.
[24] J.W. Larrick, L. Brindley and M.V. Doyle, J. Immunol. Methods, 79 (1985) 39.
[25] P.L. Simon, J.T. Laydon and J.C. Lee, J. Immunol. Methods, 84 (1985) 85.
[26] A.H.J. Gearing, C.R. Bird, A. Bristow, S. Poole and R. Thorpe, J. Immunol. Methods, 99 (1987) 7.
[27] L. Remvig, J. Vibe-Petersen, M. Svenson, C. Enk and K. Bendtzen, Allergy, 46 (1991) 59.
[28] C. de Vos and W. Libert, J. Immunol. Methods, 74 (1984) 375.
[29] W. Falk, P.H. Krammer and D.N. Maennel, J. Immunol. Methods, 99 (1987) 47.
[30] K. Nakano, K. Okugawa, H. Hayashi, S. Abe, Y. Sohmura and T. Tsuboi, Develop. Biol. Standard, 69 (1988) 93.
[31] S. Nakai, K. Mizuno, M. Kaneta and Y. Hirai, Biochem. Biophys. Res. Commun., 154 (1988) 1189.
[32] T. Leivestad, G. Gaudernack, R. Halvorsen and E. Thorsby, J. Immunol. Methods, 114 (1988) 95.
[33] G. Hewlett, K.G. Stuenkel and H.D. Schlumberger, J. Immunol. Methods, 117 (1989) 243.
[34] B. White Needleman, F.M. Wigley and R.W. Stair, Arthritis and Rheumatism, 35 (1992) 67.
[35] H. Tada, O. Shiho, K.-I. Kuroshima, M. Koyama and K. Tsukamoto, J. Immunol. Methods, 93 (1986) 157.
[36] W. Schreier and E. Kroemer, Develop. Biol. Standard, 55 (1984) 131.
[37] R. Patel, H. Hajarian and D.R. Patel, J. Immunol. Methods, 112 (1988) 285.
[38] J. Antoonen, H. Mitsuya and K. Krohn, J. Immunol. Methods, 99 (1987) 271.
[39] M. Gramatzki, D.M. Strong, S.B. Grove and G.D. Bonnard, J. Immunol. Methods, 53 (1982) 209.
[40] U. Hammerling, A-C. Henningsson and L. Sjoedin, J. Pharm. Biomed. Anal., 10 (1992) 547.
[41] R.W. Nadeau, N.F. Oldfield, W.A. Garland and D.J. Liberato, Anal. Chem., 61 (1989) 1732.
[42] H. Martensen, K. Haslov, B. Mansua and M.W. Bentzon, J. Immunol. Methods, 104 (1987) 209.
[43] V. Kotnik and W.R. Fleischmann Jr., J. Immunol. Methods, 129 (1990) 23.
[44] T.R. Bradley and D. Metcalf, Aust. J. Exp. Biol. Med. Sci., 44 (1966) 287.
[45] D. Metcalf, in The Hemopoietic Colony Stimulating Factors, Elsevier, Amsterdam, 1984, p. 55.
[46] M.C. Custer and M.T. Lotze, J. Immunol. Methods, 128 (1990) 109.
[47] A.J.H. Gearing, J.E. Cartwright and M. Wadhwa, in A.W. Thomson (Ed.), The Cytokine Handbook, Academic Press, 1991, p. 339.
[48] M. Lohoff, F. Sommer and M. Roellinghoff, Eur. J. Immunol., 19 (1989) 1327.
[49] M. Helle, L. Boeije and L.A. Aarden, Eur. J. Immunol., 18 (1988) 1535.
[50] M. Ohno and T. Abe, J. Immunol. Methods, 145 (1991) 199.
[51] N. Chirmule, N. Oyaizu, V.S. Kalyanaraman and S. Pahwa, J. Immunol. Methods, 137 (1991) 141.
[52] J. van Snick, S. Cayphas, A. Vink, C. Uyttenhove, P.G. Coulie, M.R. Rubira and R.J. Simpson, Proc. Natl. Acad. Sci. U.S.A., 83 (1986) 9679.
[53] L.S. Park, D.J. Friend, A.E. Schmierer, S.K. Dover and A.E. Namen, J. Exp. Med., 171 (1990) 1073.
[54] J.A. Eastgeate, J.A. Symmons, N.C. Wood, F.M. Grinlington, F.S. Di Giovine and G.W. Duff, Lancet, 2 (1988) 706.
[55] J.G. Cannon, J.W.M. van der Meer, D. Kwiatkowski, S. Endres, G. Lonneman, J.F. Buirke and C.A. Dinarello, Lymphokine Res., 7 (1988) 457.
[56] M. Shearer and J. Taylor-Papadimitriou, Cancer Metast. Rev., 6 (1987) 199.
[57] A. Adams, H. Strander and K. Cantrell, J. Gen. Virol., 28 (1975) 207.
[58] N. Hirai, N. Hattori, N.O. Hill and K. Osther, J. Exp. Med., 151 (1987) 309.
[59] T. Nederman, E. Karlstroem and L. Sjoedin, Biologicals, 18 (1990) 29.
[60] P. Aebersold and S. Sample, Methods Enzymol., 119 (1986) 579.
[61] S. Tyring, W.R. Fleischmann Jr. and S. Baron, Methods Enzymol., 119 (1986) 574.
[62] D. Brouty-Boye and M.G. Tovey, Intervirology, 9 (1978) 243.
[63] D.R. Gewert, S. Shah and M.J. Clemens, Eur. J. Biochem., 116 (1981) 487.
[64] L.M. Pfeffer and I. Tamm, J. Cell. Physiol., 121 (1984) 431.
[65] Anonymous, WHO Tech. Rep. Ser. 771 (Annese 1) (1988) 37.
[66] M. Ho and J.F. Endres, Proc. Natl. Acad. Sci. U.S.A., 45 (1959) 385.
[67] S.E. Grossberg, P.M. Jameson and J.J. Sedmak, Handb. Exp. Pharmacol., 71 (1984) 23.
[68] P.C. Familletti, S. Rubinstein and S. Pestka, Methods Enzymol., 78 (1981) 387.
[69] J. Imanishi, S. Hoshino, A. Hoshino, T. Oku, M. Kita and T. Kishida, Biken J., 24 (1981) 103.
[70] M. Cappelier, R. Levy-Benezra and P. Poindron, Ann. Pharm. Fr., 44 (1986) 217.
[71] M. Cappelier, R. Levy-Benezra and P. Poindron, Ann. Pharm. Fr., 44 (1986) 285.
[72] R.L. Forti, R.A. Moldovan, W.M. Mitchell, P. Collicoat, S.S. Schuffman, H.A. Davies and D.M. Smith Jr., J. Clin. Microbiol., 21 (1985) 689.
[73] R.L. Forti, S.S. Schuffman, H.A. Davies and W.M. Mitchell, Methods Enzymol., 119 (1986) 533.

[74] G.M. Scott, J.A. Robinson, D.S. Secher, C.M. Ashburner and S.R. Abbott, J. Gen. Virol., 66 (1985) 1621.
[75] K. Berg, M.B. Hansen and S.E. Nielsen, APMIS, 98 (1990) 156.
[76] T. Yilma, Methods Enzymol., 119 (1986) 551.
[77] T-J. Yeh, P.T. McBride, J.C. Overll Jr. and J.A. Green, J. Clin. Microbiol., 16 (1982) 413.
[78] G.R. Burleson and D.P. Herzog, J. Virol. Methods, 9 (1984) 163.
[79] R.H.L. Pang, Belg. BE 902,663 (Cl. C12G), 30 Sep 1985, US Appl. 628,612, 06 Jul 1984, 16 pp.
[80] R.R. Wagner, Virology, 13 (1961) 111.
[81] P.C.P. Ferreira, M.L.P. Peixoto, M.A.V. Silva and R.R. Golgher, J. Clin. Microbiol., 9 (1979) 471.
[82] H.K. Oie, Tex. Rep. Biol. Med., 35 (1977) 154.
[83] J.B. Campbell, T. Grunberger, M.A. Kochman and S.L. White, Can. J. Microbiol., 21 (1975) 1247.
[84] M.P. Langford, D.A. Weigert, G.J. Stanton and S. Baron, Methods Enzymol., 78 (1981) 339.
[85] J.A. Green, T-J. Yeh and J.C. Overall Jr., J. Clin. Microbiol., 12 (1980) 433.
[86] S.E. Grossberg, P. Jameson and J.J. Sedmak, in The Production and Use of Interferon for the Prevention of Human Virus Infections, Tissue Culture Association, Rockville, 1974, p. 26.
[87] F. Fournier, S. Rousset and C. Chang, Proc. Soc. Exp. Biol. Med., 132 (1969) 943.
[88] W.E. Stewart II and R.Z. Lockart Jr., J. Virol., 6 (1970) 795.
[89] J.G. Gallagher and N. Khobyarian, Proc. Soc. Exp. Biol. Med., 136 (1971) 920.
[90] Y. Ito and L. Montaigner, Infect. Immunol., 18 (1970) 13.
[91] R. Salonen and A. Salmi, J. Virol. Methods, 5 (1982) 143.
[92] A. Isaacs and J. Lindenmann, Proc. R. Soc. London Ser. B., 147 (1957) 258.
[93] H.K. Oie, C.E. Buckler, C.P. Uhlendorf, D.A. Hill and S. Baron, Proc. Soc. Exp. Biol. Med., 140 (1972) 1178.
[94] G.J. Stanton, M.P. Langford and F. Dianzani, Methods Enzymol., 78 (1981) 351.
[95] J.J. Sedmak, M. Dixon, C. Schoenherr, J.L. Sabron and S.E. Grossberg, J. Virol. Methods, 6 (1983) 99.
[96] P. Jameson and S.E. Grossberg, Methods Enzymol., 78 (1981) 357.
[97] M. Aboud, O. Weiss and S. Salzburg, Infect. Immunol., 13 (1976) 1626.
[98] S. Salzburg, A. Heller, D. Gurari-Rotman and M. Revel, Virology, 93 (1979) 209.
[99] J.J. Sedmak and S.E. Grossberg, J. Gen. Virol., 21 (1973) 1.
[100] J.J. Sedmak, S.E. Grossberg and P. Jameson, Proc. Soc. Exp. Biol. Med., 149 (1975) 433.
[101] J.J. Sedmak and S.E. Grossberg, Methods Enzymol., 78 (1981) 369.
[102] J.J. Sedmak and S.E. Grossberg, Virology, 56 (1973) 658.
[103] S.E. Grossberg, J. Biol. Standards, 7 (1979) 383.
[104] R. Lleonart, D. Naef, H. Browning and C. Weissmann, Bio/Technology, 8 (1990) 1263.
[105] U.E.M. Gibson and S.M. Kramer, J. Immunol. Methods, 125 (1989) 105.
[106] J.N. Agrewala, G.P.S. Raghava and G.C. Mishra, J. Immunoassay, 14 (1993) 83.
[107] A.S.K. Schneegans, C. Gaveriaux, P. Fonteneau and F. Loor, J. Immunol. Methods, 119 (1989) 117.
[108] R.Z. Lockart Jr. in Interferon and Interferon Inducers, Elsevier, Amsterdam, 1979, p. 11.
[109] S.-I. Naito, S. Tanaka, M. Mizuno and H. Kawashima, Int. J. Pharm., 17 (1983) 109.
[110] S.-I. Naito and H. Tominaga, Int. J. Pharm., 26 (1985) 1.
[111] S.-I. Naito, H. Tanaka, S. Tanaka and K. Oshima, Arch. Int. Pharmacodyn. Ther., 252 (1981) 162.
[112] S-I. Naito, S. Tanaka, M. Mizuno and H. Kawashima, Int. J. Pharm., 18 (1984) 117.
[113] G.C. Oliver, B.M. Parker, D.L. Brasfield and C.W. Parker, J. Clin. Invest., 47 (1968) 1035.
[114] A.E. Bolton, in A. Voller, A. Bartlett and D. Bidwell (Eds.), Immunoassays for the 80s, MTP Press, Lancester, 1981, p. 69.
[115] S. Shiozawa, K. Chihara, K. Shiozawa, T. Fujita, H. Ikegami, S. Koyama and M. Kurimoto, Clin. Exp. Immunol., 66 (1986) 77.
[116] O. Horovitz, D. Novick, M. Rubinstein and M. Revel, in S. Avrameas, P. Druet, R. Masseyeff and G. Feldmann (Eds.), Developments in Immunology, Vol. 18, Immunoenzymatic Techniques, Elsevier, Amsterdam, 1983, p. 193.
[117] J.C. Cornette and S.K. Sharma, J. Immunoassay, 10 (1989) 107.
[118] S. Poole, A.F. Bristow, S. Selkirk and B. Rafferty, J. Immunol. Methods, 116 (1989) 259.
[119] B.D. Clark, I. Bedrosian, R. Schindler, F. Cominelli, J.G. Cannon, A.R. Shaw and C.A. Dinarello, J. Appl. Physiol., 71 (1991) 2412.
[120] P.J. Lisi, C.W. Chu, G.A. Koch, S. Endres and G. Lonnemann, C.A. Dinarello, Lymphokine Res., 6 (1987) 229.
[121] J.G. Cannon, J.W.M. van der Meer, S. Endres, G. Lonnemann and C.A. Dinarello, in M.C. Powanda, J.J. Oppenheim, M.J. Kluger and C.A. Dinarello (Eds.), Monokines and Other Non-Lymphocytic Cytokines, Alan R. Liss, New York, 1988, p. 373.
[122] A.F. Bristow, B. Rafferty, S. Selkirk and S. Poole, Develop. Biol. Standards, 69 (1988) 103.
[123] R. Derijk and F. Berkenbosch, Am. J. Physiol., 263 (1992) E1092.
[124] T.P. Lee, B.K. Mookerjee and J.L. Pauly, J. Immunoassay, 9 (1988) 193.
[125] A.-M. Teppo, K. Metsaerinne and F. Fyhrquist, Clin. Chem., 37 (1991) 1691.
[126] Y.-C. Ko, N. Mukaida, A. Panyutich, N.N. Voitenok, K. Matsushima, T. Kawai and T. Kasahara, J. Immunol. Methods, 149 (1992) 227.

[127] C.I. Westcacott, J.T. Whicher, A.C. Barnes, D. Thompson, A.J. Swan and D.A. Dieppe, Ann. Rheum. Dis., 17 (1990) 489.
[128] S.E. Grossberg and J.J. Sedmak, in Interferon, Vol. 1, General and Applied Aspects, Elsevier, Amsterdam, 1984, p. 189.
[129] R. Ekins, in A. Voller, A. Bartlett and D. Bidwell (Eds.), Immunoassays for the 80s, MTP Press, Lancester, 1981, p. 69.
[130] V. Valwa, F. Noll, E. Eichmann, M. Gerestel and F. Schneider, Ger. (East) DD 241,788 (Cl.G01N33/543), 24 Dec 1986, Appl. 281,753, 15 Oct 1985, 3 pp.
[131] D.S. Secher, Nature, 290 (1981) 501.
[132] J.R. Walker, J. Nagington, G.M. Scott and D.S. Secher, J. Gen. Virol., 62 (1982) 181.
[133] W.P. Protzman, M. Minnicozzi, S.L. Jacobs, D.I. Surprenant, J. Schwartz and E.M. Oden, J. Clin. Microbiol., 22 (1985) 596.
[134] T. Staehelin, C. Staehli, D.S. Hobbs and S. Pestka, Methods Enzymol., 79 (1981) 589.
[135] S. Pestka and H.F. Kung, in Interferon, Vol. 2, Interferons and the Immune System, Elsevier, Amsterdam, 1984, p. 259.
[136] M. Inoue and Y.H. Tan, Infect. Immunol., 33 (1981) 763.
[137] T. Sano, Y. Yanase, E. Tanaka, S. Usuda, K. Tachibana, M. Imai, T. Nakamura, Y. Miyakawa and M. Mayumi, J. Immunol. Methods, 64 (1983) 31.
[138] M. Inoue, H. Ehrlich, L. Nyari, B. Colby and Y.H. Tan, in The Biology of the Interferon System, Elsevier, Amsterdam, 1981, p. 73.
[139] M. Inoue and Y.H. Tan, Tex. Rep. Biol. Med., 41 (1982) 287.
[140] A.R. Neurath, N. Strick, N.B.K. Raj and P.M. Pitha, J. Interferon Res., 2 (1982) 51.
[141] E. Tanaka, M. Imai, S. Usuda, K. Tanibana, H. Okamoto, Y. Ohiki, T. Nakamura, Y. Miyakawa and M. Mayumi, J. Immunol. Methods, 77 (1983) 275.
[142] T.-W. Chang, S. McKinney, V. Liu, P.C. Kung, J. Vilcek and J. Le, Proc. Natl. Acad. Sci., 81 (1984) 5219.
[143] B. Kelder, A. Rashidbaigi and S. Pestka, Methods Enzymol., 119 (1986) 582.
[144] W. Woluszczuk, Clin. Chem., 31 (1985) 1090.
[145] A.D. DiAndrea, S.A. Plotkin, S.D. Douglas and R.A. Polin, J. Clin. Microbiol., 23 (1986) 911.
[146] P.M. Taylor, A. Maeger and B.M. Askonas, J. Gen. Virol., 70 (1989) 975.
[147] R. Thorpe, M. Wadhwa, A. Gearing, B. Mahon and S. Poole, Lymphokine Res., 7 (1988) 119.
[148] G. Lonnemann, S. Endres, J.W.M. van der Meer, J.G. Cannon and C.A. Dinarello, Lymphokine Res., 7 (1988) 75.
[149] P. Gnocchi, Lymphokine Cytokine Res., 11 (1992) 257.
[150] A.F. Bristow, K. Mosley and S. Poole, J. Mol. Endocrin., 7 (1991) 1.
[151] J.M. Cardenas, P. Marshall, B. Henderson and A. Altman, J. Immunol. Methods, 89 (1986) 181.
[152] A. Meager, in M.J. Clemens, A.G. Morris and A.J.H. Gearing (Eds.), Lymphokines and Interferons, a Practical Approach, IRL Press, Oxford, 1987, p. 105.
[153] T. Porstmann and S.T. Kiessig, J. Immunol. Methods, 150 (1992) 5.
[154] H. Gallati, J. Clin. Chem. Clin. Biochem., 20 (1982) 907.
[155] W. Berthold, Arzneim. Forsch., 35 (1985) 364.
[156] G.R. Adolf, Virology, 175 (1990) 410.
[157] G.R. Adolf, Ger. Offen. DE 3,3633,323 (Cl. C12H5/00), 07 Apr 1988, Appl. 01 Oct 1986, 13 pp.
[158] S. Yamazaki, K. Kuramoto, E. Matsuo, K. Hosoi, M. Hara and H. Shimizu, J. Immunoassay, 10 (1989) 57.
[159] G. Andersson, H-P.T. Ekre, G. Alm and P. Perlmann, J. Immunol. Methods, 125 (1989) 89.
[160] Y. Ishimori, T. Kurokawa, S. Honda, N. Suzuki, M. Wakimasu and K. Tsukamoto, J. Immunol. Methods, 80 (1985) 55.
[161] A. Sparreboom, Verslag Differentiatiepakket Bioanalyse II, Utrecht University, 1992.
[162] P.H. van der Meide, M. Dubbeld and H. Schellekens, J. Immunol. Methods, 79 (1985) 293.
[163] A. Sparreboom, Bijvakverslag, Utrecht University, 1992.
[164] R.M.W. Hoetelmans, Verslag Differentiatiepakket Bioanalyse II, Utrecht University, 1992.
[165] R.M.W. Hoetelmans, Bijvakverslag, Utrecht University, 1992.
[166] H.C. Cherwinski, J.H. Schumacher, K.D. Brown and T.R. Mosmann, J. Exp. Med., 166 (1987) 1229.
[167] T. Jitsukuwa, S. Nakajima, I. Sugawara, S. Mori and M. De Ley, Microbiol. Immunol., 31 (1987) 809.
[168] S.L. Jones, J.C. Cose, J.M. Shepherd, J.S. Rother, P.R. Wood and A.J. Radford, J. Immunol. Methods, 155 (1992) 233.
[169] R.C. Curry, P.A. Kiener and G.L. Spitalny, J. Immunol. Methods, 104 (1987) 137.
[170] N. Mukaida, T. Kasahara, Y. Ko and T. Kawai, J. Immunol. Methods, 107 (1988) 41.
[171] B. Ferrua, P. Becker, L. Schaffer, A. Shaw and M. Fehlmann, J. Immunol. Methods, 114 (1988) 41.
[172] J. Grassi, Y. Frobert, P. Pradelles, F. Chercuitte, D. Gruaz, J.-M. Drayer and P.E. Poubelle, J. Immunol. Methods, 123 (1989) 193.
[173] J. Grassi, C.J. Roberge, Y. Frobert, P. Pradelles and P.E. Poubelle, J. Immunol. Methods, 119 (1989) 125.
[174] N. Sunahara, S. Kawata, K. Kaibe, R. Furuta, M. Yamayoshi, M. Yamada and S. Kuruoka, J. Immunol. Methods, 119 (1989) 75.
[175] K. Tanaka, E. Ishikawa, Y. Ohmoto and Y. Hirai, Clin. Chim. Acta, 166 (1987) 237.
[176] K. Tanaka, E. Ishikawa, Y. Ohmoto and Y. Hirai, Eur. J. Immunol., 17 (1987) 1527.
[177] K. Tanaka, E. Ishikawa, Y. Ohmoto, Y. Hirai, H. Madokoro, S. Ohdo and K. Hayakawa, Anal. Lett., 21 (1988) 169.
[178] K. Tanaka, E. Ishikawa, Y. Ohmoto and Y. Hirai, Clin. Chim. Acta, 170 (1987) 97.

[179] E.V. Gaffney, G.A. Koch, S-C.J. Tsai, S.E. Lingenfelter and J. Piscitelli, J. Immunol. Methods, 101 (1987) 271.
[180] E.V. Gaffney, A.E. Andersson, Y.T. Pfanenstiel and G.A. Koch, Immunol. Rev., 119 (1991) 181.
[181] E.V. Gaffney, C.W. Chu, S.E. Lingenfelter, P.J. Lisi and G.A. Koch, Bio/Techniques, 5 (1987) 652.
[182] R.C. Budd, Serono Symp. Publ. Raven Press, 30 (1986) 275.
[183] R.C. Budd and K.A. Smith, Bio/Techniques, 4 (1986) 983.
[184] R.C. Newton, R. Dowling, A.J. Daulerio and S. Culp, J. Immunol. Methods, 161 (1993) 257.
[185] N. Moriya, K. Kato, N. Suzuki, T. Yamada and O. Nishimura, J. Immunoassay, 8 (1987) 131.
[186] B. Ferrua, C. Aussch and M. Fehlmann, J. Immunol. Methods, 97 (1987) 215.
[187] K. Kitamura, K. Matsuda, M. Ide, T. Tokunaga and M. Honda, J. Immunol. Methods, 121 (1989) 281.
[188] M.K. Sharief, R. Hentges and E.J. Thompson, J. Immunol. Methods, 147 (1992) 51.
[189] S. Hashida, E. Ishikawa, H. Umehara, S. Kumagai, H. Imura, Y. Ohmoto and Y. Hirai, Anal. Lett., 20 (1987) 1083.
[190] L.O. Gehman and R.J. Robb, J. Immunol. Methods, 74 (1984) 39.
[191] M. Fukui, Jpn. Kokai Tokkyo Koho JP. 61,213,672 [86,213,672] (Cl. G01N33/543), 18 Nov 1986, Appl. 85/102,390, 14 May 1985, 4 pp.
[192] R. Papoian, F. Duffy, M. Sanner and E. Wilt, J. Immunol. Methods, 145 (1991) 161.
[193] J.S. Abrams and M.K. Pearce, J. Immunol., 140 (1988) 131.
[194] H.J. Zittener, Cytokine (Philadelphia), 1 (1989) 56.
[195] L.A. McNamee, D.I. Fattah, T.J. Baker, S.K. Brains and P.H. Hissey, J. Immunol. Methods, 141 (1991) 81.
[196] Y. Fukuda, J. Hanshino, M. Haruyama, N. Tsuruoka, H. Nakarato and T. Nakanishi, J. Immunol. Methods, 143 (1991) 89.
[197] Y. Fukuda, Jpn. Kokai Tokkyo Koho JP. 04,271,795 [92,271,795] (Cl. C12P21/08), 28 Sep 1992, Appl. 91/32,829, 27 Feb 1991, 6 pp.
[198] J.S. Abrams, M.G. Roncarolo, H. Yssel, U. Andersson, G.J. Gleich and J.E. Silver, Immunol. Rev., 127 (1992) 5.
[199] J.H. Schumacher, A. O'Garra, B. Shrader, A. von Kimmenade, M.W. Bond, T.R. Mosmann and R.L. Loffmann, J. Immunol., 141 (1988) 1576.
[200] N. Ida, S. Sakurai, T. Hosaka, K. Hosoi, T. Kunimoto, Y. Matsuura and M. Kohase, J. Immunol. Methods, 133 (1990) 279.
[201] M. Helle, L. Boeije, E. de Groot, A. de Vos and L. Aarden, J. Immunol. Methods, 138 (1991) 47.
[202] M. Honda, K. Kitamura, Y. Mizutani, M. Oschi, M. Arai, T. Okura, K. Igarahi, T. Hirano, T. Kishimoto, R. Mitsuyasu, J.C. Chermann and T. Tokunaga, J. Immunol., 145 (1990) 4059.
[203] T. Matsuda, T. Hirano and T. Kishimoto, Eur. J. Immunol., 18 (1989) 1834.
[204] K.A. Corcoran, M. Gallagher, C.V. Asmus, H. Gaylord, B.J. Tall, K.J. Callahan, P.G. Will, J.E. Humphrey and W.A. Lidinsky, Clin. Chem., 37 (1991) 1046.
[205] L.E. DeForge, Immunol. Invest., 20 (1991) 89.
[206] E.N. Dotsika, Curr. Opin. Immunol., 2 (1989-1990) 932.
[207] P. Loux-Rombard and G. Stainer, Clin. Exp. Rheumatol., 10 (1992) 515.
[208] I. Hemmilae, Clin. Chem., 31 (1985) 359.
[209] E. Soini and I. Hemmilae, Clin. Chem., 25 (1979) 353.
[210] I. Wieder, in W. Knapp, K. Holubar, G. Wick (Eds.), Immunofluorescence and Related Staining Techniques, Elsevier, Amsterdam, 1978, p. 67.
[211] A.P.B. Sinka, Spectrosc. Inorg. Chem., 2 (1971) 255.
[212] B. Schmidt and G. Steimetz, Clin. Chem., 33 (1987) 1070.
[213] W. Berthold, W. Merk and G.R. Adolf, Arzneim. Forsch., 35 (1985) 364.
[214] H.A.H. Rongen, personal communication.
[215] H.A.H. Rongen, H.M. van der Horst, G.W.K. Hugenholtz, A. Bult, W.P. van Bennekom and P.H. van der Meide, Anal. Chim. Acta, 287 (1994) 191.
[216] G.W.K. Hugenholtz, Bijvakverslag, Utrecht University, 1991.
[217] Y. Ohiki, M. Imai, E. Tanaka, N. Mukaida, T. Kasahara, K. Tachibana, Y. Miyakawa and M. Mayumi, J. Immunol. Methods, 87 (1986) 245.
[218] R.J. Robb, A. Munck and K.A. Smith, J. Exp. Med., 154 (1981) 1455.
[219] T. Miyoshi, T. Kubonishi, M. Sumida, S. Hiraki, T. Tsubota, I. Kimura and K. Mijamoto, J. Sato, Gann, 71 (1980) 155.
[220] J.M. Depper, W.J. Leonard, M. Kronke, T.A. Waldmann and W.C. Greene, J. Immunol., 133 (1984) 1691.
[221] R.J. Robb, W.C. Greene and C.M. Rusk, J. Exp. Med., 160 (1984) 1126.
[222] L.S. Park, D. Friend, H.M. Sassenfeld and D.L. Urdal, J. Exp. Med., 166 (1987) 476.
[223] G. Scapigliati, P. Bossu, S. Censini, A. Tagliabue, D. Boraschi and P. Ghiara, J. Immunol. Methods, 138 (1991) 31.
[224] G. Scapigliati, P. Ghiara, M. Bartalini, A. Tagliabue and D. Boraschi, FEBS Lett., 243 (1989) 394.
[225] F. Riske, R. Chizzonite, P. Nunes and A.S. Stern, Anal. Biochem., 185 (1990) 206.
[226] C. Schoeneich, S.K. Kwolk, G.S. Wilson, S.R. Rabel, J.F. Stobaugh, T.D. Williams and D.G. Vander Velde, Anal. Chem., 65 (1993) 67R.
[227] Y. Xu, Anal. Chem., 65 (1993) 425R.
[228] R. Caprioli and A.H.B. Wu, Anal. Chem., 65 (1993) 470R.
[229] L. Rybacek, M. D'Andrea and S.J. Tarnowski, J. Chromatogr., 397 (1987) 355.
[230] S.K. Roy, D.V. Weber and W.C. McGregor, J. Chromatogr., 303 (1984) 225.

[231] S.K. Roy and W.C. McGregor, J. Chromatogr., 327 (1985) 189.
[232] M. Rubinstein, Methods Enzymol., 79 (1981) 16.
[233] S. Steina and J. Moschera, Methods Enzymol., 79 (1981) 7.
[234] R.E. Ardrey, in A.C. Moffat, J.V. Jackson, M.S. Moss and B. Widdop (Eds.), Clarke's Isolation and Identification of Drugs, The Pharmaceutical Press, London, 1986, p. 251.
[235] G. Padron, V. Besada, A. Agraz, Y. Quinones, L. Herrera, Y. Shimonishi and T. Takao, Anal. Chim. Acta, 223 (1989) 361.
[236] A. Tsarbopoulos, B.N. Pramanik, T.L. Nagabhushan, P.P. Trotta, M.M. Siegel, R. Tsao and V.W. Doelling, Anal. Chim. Acta, 241 (1990) 315.
[237] N.A. Guzman, L. Hernandez and B.G. Hoebel, BioPharm., 2 (1989) 22.
[238] D.M. Goodall, D.K. Lloyd and S.J. Williams, LC–GC, 8 (1990) 788.
[239] N.A. Guzman, H.A.J. Moschera, K. Iqbal and A.W. Malick, J. Chromatogr., 559 (1991) 307.
[240] R.I. Hecht, J. Morris, G.D. Seark, F. Stover, L. Fossey and C. Demerest, Prep. Biochem., 19 (1989) 201.
[241] R.I. Hecht, J.C. Coleman, J.C. Morris, F. Stover and C. Demerest, Prep. Biochem., 19 (1989) 362.
[242] J. Bullock, J. Chromatogr., 633 (1993) 235.
[243] L.G. Fagerstam, A. Frostell, R. Karlsson, M. Kullmann, A. Larsson, M. Malmquist and H. Butt, J. Mol. Recogn., 3 (1990) 208.
[244] H. Morgan and D.M. Taylor, Biosensors Bioelectron., 7 (1992) 405.
[245] C.D. Bain, E.B. Troughton, Y.-T. Tao, J. Evall, G.M. Whitesides and R.G. Nuzzo, J. Am. Chem. Soc., 111 (1989) 321.
[246] M. Malmquist, Curr. Opin. Immunol., 5 (1993) 282.
[247] L.D. Ward, P. Shi and R.J. Simpson, Biochem. Int., 26 (1992) 559.
[248] J.M.T. Versteegen, T. Logtenberg and R.E. Ballieux, J. Immunol. Methods, 111 (1988) 25.
[249] T. Taguchi, J.R. McGhee, R.L. Coffman, K.W. Beagley, J.H. Eldridge, K. Takatsu and H. Kiyono, J. Immunol. Methods, 128 (1990) 65.
[250] K. Fujihashi, J.R. McGhee, K.W. Beagley, D.T. McPherson, S.A. McPherson, C.-M. Huang and H. Kiyono, J. Immunol. Methods, 160 (1993) 181.
[251] N. Lee, J. Yang and D. Testa, Anal. Biochem., 175 (1988) 30.
[252] N. Lee, J. Yang and D. Testa, J. Immunol. Methods, 106 (1988) 27.
[253] J. Uhl and R.C. Newton, J. Immunol. Methods, 110 (1988) 79.
[254] B. Sander, J. Andersson and U. Andersson, Immunol. Rev., 119 (1991) 65.
[255] M. Samoszuk and L. Nansen, Blood, 45 (1990) 13.
[256] Q. Hamid, M. Azzawi, S. Ying, R. Moqbel, A.J. Wardlaw, P.K. Corrigan, B. Bradley, S.R. Durham, J.V. Collins, P.K. Jeffrey, D.J. Quint and A.B. Kay, J. Clin. Invest., 87 (1991) 1541.
[257] A.P. Limaye, J.S. Abrams, J.E. Silver, E.A. Ottensen and T.B. Nutman, J. Exp. Med., 172 (1990) 399.
[258] C. Inoue, A. Ichikawa, T. Holta and H. Saito, Br. J. Haematol., 76 (1990) 554.
[259] A. Guiffre, K. Atkinson and P. Kearney, Anal. Biochem., 212 (1993) 50.

ELSEVIER

Analytica Chimica Acta 295 (1994) 27–35

ANALYTICA CHIMICA ACTA

Novel labelling agents for immunoassay by time-resolved electrogenerated chemiluminescence

J. Kankare [a,*], A. Karppi [a], H. Takalo [1,b]

[a] *Department of Chemistry, University of Turku, 20500 Turku, Finland*
[b] *Centre for Biotechnology, P.O.Box 123, 20521 Turku, Finland*

Received 13th January 1994; revised manuscript received 22nd March 1994

Abstract

In order to develop more efficient labelling agents for the binding assays based on time-resolved electrogenerated chemiluminescence, thirteen derivatives of (1-hydroxybenzene-2,6-diyl)bis(methylenenitrilo)tetrakis(acetic acid) were synthesized. The aim was to study the influence of different substituents on the intensity of electrogenerated chemiluminescence (ECL) of their terbium(III) chelates. For comparison, also photoluminescent intensities of these chelates were recorded at the terbium emission line corresponding to the transition $^5D_4 \rightarrow {}^7F_5$ (546 nm). The highest ECL intensities were recorded for the parent compound and its 4-methyl derivative, whereas the photoluminescent intensity was highest for the 4-cyano and 4-phenyl derivatives. There was no statistically significant correlation of the ECL intensity with the Hammett substituent constants.

Key words: Chemiluminescence; Immunoassay; Time-resolved electrogenerated chemiluminescence

1. Introduction

Electrogenerated chemiluminescence (ECL) as an analytical tool is gradually gaining importance especially in connection with the samples of biological origin. Analytical systems based on ECL have already been commercialized for immunoassay and PCR (polymerase chain reaction). The role of ECL is to provide an alternative method in labelling bioactive molecules. The older and still more commonly used photoluminescent labels have the drawback in demanding a more complicated instrumentation with the excitation optics, whereas the instrumentation for the ECL labels involves only an inexpensive electronic excitation system. The main advantage of the ECL method of labelling is, however, the confinement of the phenomenon on the surfaces. This makes, e.g., a homogeneous immunoassay feasible with the consequent simplification of the assay procedure.

In principle, purely organic compounds could be used as ECL labels. In fact, the well-known

* Corresponding author.
[1] Present address: Wallac Oy, P.O.Box 10, FIN-20101 Turku, Finland.

SSDI 0003-2670(94)00154-E

examples of ECL are purely organic luminophores such as polycyclic aromatic hydrocarbons which produce light emission in radical annihilation reactions. These radicals are highly reactive towards water and oxygen which limits their utilization in practical analyses. The cathodic electroluminescence of oxide-covered electrodes is inherently an aqueous process [1] and consequently suitable for the determination of analytes of biological origin. We have previously shown that various organic fluorescent compounds can be excited on an oxide-covered aluminium electrode by using electric pulses [2]. This method seems to be rather generally applicable as an alternative excitation for fluorescent compounds. For the immunoassay purposes fluorescent organic probe molecules could be attached to antibodies or antigens and the immunocomplexation followed at the surface of an oxide-covered electrode by electroluminescence of the probe. However, this approach would suffer from the same drawback as the conventional photoluminescence, namely the background luminescence of the "natural" fluorophores of proteins. The remedy is analogous to the time-resolved fluorometry [3], i.e., the use of a short electric pulse for excitation and subsequent time-resolved follow-up of emission. In order to get separation from the signal of fast-decaying natural fluorophores, a slow decay of the probe emission is necessary, and one way to reach this goal is to use lanthanide chelates as labels.

A large number of chelating agents for lanthanides and having feasible luminescent properties as terbium(III) and europium(III) chelates for photoluminescent labelling of biomolecules have been synthesized and recently reported by us [4]. As previously mentioned, it seems that nearly any organic compound exhibiting photoluminescence, is also excitable by an electric pulse at an aluminium electrode [2]. However, this generalization cannot be fully extended to the lanthanide chelates. First of all, only the chelates of terbium(III) seem to show appreciable electroluminescence of any practical use, at least with the chelates studied so far, although low level ECL is observed even from the non-complexed ions Tb(III), Eu(III) and Sm(III) [1]. Secondly, according to our unpublished observations, even among the brightly photoluminescent Tb(III) complexes, chelates showing intense electrogenerated chemiluminescence are relatively rare. The first ligand whose Tb(III) complex showed reasonably intense ECL on an aluminium electrode was Tiron (4,5-dihydroxy-1,3-benzenedisulfonic acid) [5]. Using this ligand Tb(III) could be determined in solution down to the nanomolar level. However, the stability constant of the Tb(III)–Tiron complex is not high enough to allow its use as a labelling compound for biomolecules. The first ligand which showed both sufficient stability and high ECL intensity of the Tb(III) complex was 2,2′,2″,2‴-[(4-benzoyl-1-hydroxybenzene-2,6-diyl)-bis(methylenenitrilo)]tetrakis(acetic acid) (**25**) [1]. In the time-resolved mode this ligand allows the detection of Tb(III) at less than picomolar level. By adding an isothiocyanato group this chelate could be used as a label in the immunoassay as we showed in our previous paper [6]. However, search for more efficient luminophores has been going on and the purpose of this paper is to report on the results of this systematic study of varying substituents in the phenolic backbone of the ligand structure.

2. Experimental

2.1. General

Flash chromatography is abbreviated as FC. IR Spectra were recorded with a Perkin-Elmer 1600 Fourier transform infrared spectrometer; ν is in cm^{-1}. ^1H NMR spectra: 400-MHz Jeol GX-400. Tetramethylsilane was used as internal standard. Chemical shifts, δ, are in ppm and coupling constants J in Hz.

2.2. Dimethyl iminobis(acetate)

$SOCl_2$ (275 g, 2.31 mol) was added dropwise slowly to cooled MeOH (700 ml). After stirring at r.t. for 0.5 h, iminobis(acetic acid) (77.0 g, 0.58 mol) was added and the mixture was refluxed overnight. The solution was evaporated, $CHCl_3$ (500 ml) and H_2O (200 ml) added, and the cooled mixture neutralized with solid $NaHCO_3$. The

aqueous phase was extracted with $CHCl_3$ (3 × 100 ml), the combined organic phase dried with Na_2SO_4 and evaporated. The residue was distilled under reduced pressure: 63 g (67%). IR (film): 3354 (N–H), 1744, 1438, 1203 (C=O, C–O). ^{1}H NMR ($CDCl_3$): 2.06 (s, 1 H); 3.49 (s, 4 H); 3.74 (s, 6 H).

2.3. Synthesis of 1–11: general procedure

Dimethyl iminobis(acetate) (1.23 g, 8.00 mmol) was added to a solution of 37% aqueous formaldehyde (0.65 g, 8.0 mmol) and MeOH (12 ml). After evaporation another portion of MeOH (12 ml) was added, and the solution was evaporated. A phenol derivative (4.00 mmol) was added, and the mixture was stirred at 110° for 20 h. The residue was purified by FC (silica gel, petroleum ether (b.p. 40–60°C)/AcOEt): viscous tetraesters.

Tetramethyl 2,2',2'',2'''-[(4-chloro-1-hydroxybenzene-2,6-diyl)bis(methylenenitrilo)]tetrakis(acetate) (**1**). FC: 3/5. Yield: 25%. IR (film): 1746, 1436, 1204 (C=O, C–O). ^{1}H NMR ($CDCl_3$): 3.57 (s, 8 H); 3.74 (s, 12 H); 3.93 (s, 4 H); 7.13 (s, 2 H).

Tetramethyl 2,2',2'',2'''-[(4-bromo-1-hydroxybenzene-2,6-diyl)bis(methylenenitrilo)]tetrakis(acetate) (**2**). FC: first 5/1, then 5/3. Yield: 29%. IR (film): 1742, 1436, 1206 (C=O, C–O). ^{1}H NMR ($CDCl_3$): 3.56 (s, 8 H); 3.72 (s, 12 H); 3.93 (s, 4 H); 7.26 (s, 2 H).

Tetramethyl 2,2',2'',2'''-[(1-hydroxy-4-methylbenzene-2,6-diyl)bis(methylenenitrilo)]tetrakis(acetate) (**3**). FC: first 3/5, then 1/1. Yield: 23%. IR (film): 1742, 1435, 1203 (C=O, C–O). ^{1}H NMR ($CDCl_3$): 2.22 (s, 3 H); 3.58 (s, 8 H); 3.72 (s, 12 H); 3.94 (s, 4 H), 6.93 (s, 2 H).

Tetramethyl 2,2',2'',2'''-[(4-tert-butyl-1-hydroxybenzene-2,6-diyl)bis(methylenenitrilo)]tetrakis(acetate) (**4**). FC: first 5/1, then 5/3. Yield: 30%. IR (film): 1743, 1436, 1204 (C=O, C–O). ^{1}H NMR ($CDCl_3$): 1.27 (s, 9 H); 3.57 (s, 8 H); 3.72 (s, 12 H), 3.96 (s, 4 H); 7.09 (s, 2 H).

Tetramethyl 2,2',2'',2'''-[(1-hydroxy-4-phenylbenzene-2,6-diyl)bis(methylenenitrilo)]tetrakis(acetate) (**5**). FC: first 5/1, then 1/1. Yield: 40%. IR (film): 1743, 1436, 1205 (C=O, C–O). ^{1}H NMR ($CDCl_3$): 3.62 (s, 8 H); 3.72 (s, 12 H), 4.04 (s, 4 H), 7.26 (t, J = 8.2, 1 H); 7.38 (s, 2 H), 7.39 (t, J = 8.2, 2 H); 7.53 (d, J = 8.2, 2 H).

Tetramethyl 2,2',2'',2'''-[(1-hydroxy-4-methoxybenzene-2,6-diyl)bis(methylenenitrilo)]tetrakis(acetate) (**6**). FC: first 5/3, then 1/1. Yield: 27%. IR (film): 1746, 1437, 1206 (C=O, C–O). ^{1}H NMR ($CDCl_3$): 3.57 (s, 8 H); 3.72 (s, 15 H); 3.95 (s, 4 H); 6.73 (s, 2 H).

Tetramethyl 2,2',2'',2'''-[(1-hydroxy-3,4,5-trimethoxybenzene-2,6-diyl)bis(methylenenitrilo)]tetrakis(acetate) (**7**). FC: petroleum ether (40–60°C)/EtOAc/Et_3N, 70:29:1. Yield: 39%. IR (film): 1747, 1436, 1204 (C=O, C–O). ^{1}H NMR ($CDCl_3$): 3.57 (s, 8 H); 3.72 (s, 12 H); 3.82 (s, 9 H); 3.97 (s, 4 H).

Tetramethyl 2,2',2'',2'''-[(1-hydroxy-4-phenoxybenzene-2,6-diyl)bis(methylenenitrilo)]tetrakis(acetate) (**8**). FC: first 5/3, then 1/1. Yield: 25%. IR (film): 1743, 1435, 1212 (C=O, C–O). ^{1}H NMR ($CDCl_3$): 3.57 (s, 8 H); 3.70 (s, 12 H), 3.94 (s, 4 H); 6.86 (s, 2 H); 6.90 (d, J = 7.3, 2 H); 7.02 (t, J = 7.3, 1 H); 7.27 (t, J = 7.3, 2 H).

Tetramethyl 2,2',2'',2'''-[(4-cyano-1-hydroxybenzene-2,6-diyl)bis(methylenenitrilo)]tetrakis(acetate) (**9**). FC: first 10/3, then 1/1. Yield: 34%. IR (film): 2221 (C≡N), 1743, 1436, 1206 (C=O, C–O). ^{1}H NMR ($CDCl_3$): 3.57 (s, 8 H); 3.74 (s, 12 H); 3.97 (s, 4 H); 7.49 (s, 2 H).

Tetramethyl 2,2',2'',2'''-[(4-aminocarbonyl-1-hydroxybenzene-2,6-diyl)bis(methylenenitrilo)]tetrakis(acetate) (**10**). FC: first EtOAc, then MeOH/$CHCl_3$, 1:9. Yield: 16%. IR (film): 1740, 1660, 1436, 1207 (C=O, C–O). ^{1}H NMR ($CDCl_3$): 3.56 (s, 8 H); 3.76 (s, 12 H); 4.00 (s, 4 H); 7.79 (s, 2 H).

Tetramethyl 2,2',2'',2'''-[(4-acetamido-1-hydroxybenzene-2,6-diyl)bis(methylenenitrilo)]tetrakis(acetate) (**11**). FC: first 1/2, then 0/1. Yield: 32%. IR (film): 1739, 1667, 1436, 1206 (C=O, C–O). ^{1}H NMR ($CDCl_3$): 2.12 (s, 3 H); 3.55 (s, 8 H); 3.72 (s, 12 H); 3.92 (s, 4 H); 7.32 (s, 2 H); 7.44 (s, 1 H).

Tetramethyl 2,2',2'',2'''-[(1-hydroxybenzene-2,6-diyl)bis(methylenenitrilo)]tetrakis(acetate) (**12**). A mixture of compound **2** (0.50 g, 0.96 mmol), 10% Pd/C (78 mg), Et_3N (0.19 g, 1.92 mmol) and MeOH (30 ml) was stirred in a hydrogen atmosphere (0.69 MPa) for 3h. After filtration, the

filtrate was evaporated and the residue purified by FC: first 5/3, then 1/1. Yield: 0.29 g (68%). IR (film): 1742, 1436, 1205 (C=O, C–O). ^{1}H NMR ($CDCl_3$): 3.57 (s, 8 H); 3.72 (s, 12 H); 3.97 (s, 4 H); 6.77 (t, J = 7.3, 1 H); 7.11 (d, J = 7.3, 2 H).

2.4. Synthesis of **13–24**: general procedure

A mixture of a tetraester (0.84 mmol) and 0.5 M KOH in EtOH (30 ml) was stirred at r.t. for 2 h. Some H_2O (2–4 ml) was added and the stirring was continued for 2 h. After evaporation, the residue was dissolved in H_2O (10 ml), the solution was acidified with 2M HCl (pH ca. 2) and extracted with phenol (3 × 2.3 g). The combined phenol phase was treated with water (6 ml) and diethyl ether (8 ml). The aqueous phase was washed with diethyl ether (3 × 8 ml) and evaporated to dryness.

2,2′,2″,2‴-[(4-Chloro-1-hydroxybenzene-2,6-diyl)bis(methylenenitrilo)]tetrakis-(acetic Acid) (**13**). Yield: 82%. IR (KBr): 1727, 1631, 1490, 1239 (C=O, C–O). ^{1}H NMR ((D_6)DMSO): 3.38 (s, 8 H); 3.80 (s, 4 H); 7.11 (s, 2 H).

2,2′,2″,2‴-[(4-Bromo-1-hydroxybenzene-2,6-diyl)bis(methylenenitrilo)]tetrakis-(acetic Acid) (**14**). Yield: 99%. IR (KBr): 1725, 1634, 1396, 1236 (C=O, C–O). ^{1}H NMR ((D_6)DMSO): 3.36 (s, 8 H); 3.80 (s, 4 H); 7.22 (s 2 H).

2,2′,2″,2‴-[(1-Hydroxy-4-methylbenzene-2,6-diyl)bis(methylenenitrilo)]tetrakis-(acetic Acid) (**15**). Yield: 100%. IR (KBr): 1729, 1630, 1400, 1237 (C=O, C–O). ^{1}H NMR ((D_6)DMSO): 2.17 (s, 3 H); 3.43 (s, 8 H); 3.81 (s, 4 H); 6.89 (s, 2 H).

2,2′,2″,2‴-[(4-tert-Butyl-1-hydroxybenzene-2,6-diyl)bis(methylenenitrilo)]tetrakis(acetic Acid) (**16**). Yield: 37%. IR (KBr): 1636, 1399, 1222 (C=O, C–O). ^{1}H NMR ((D_6)DMSO): 1.21 (s, 9 H); 3.45 (s, 8 H); 3.86 (s, 4 H); 7.11 (s, 2 H).

2,2′,2″,2‴-[(1-Hydroxy-4-phenylbenzene-2,6-diyl)bis(methylenenitrilo)]tetrakis-(acetic Acid) (**17**). Yield: 62%. IR (KBr): 1728, 1621, 1399, 1248 (C=O, C–O). ^{1}H NMR ((D_6)DMSO): 3.46 (s, 8 H); 3.91 (s, 4 H); 7.26 (t, J = 7.8, 1 H); 7.41 (t, J = 7.8, 2 H); 7.42 (s, 2 H); 7.55 (d, J = 7.8, 2 H).

2,2′,2″,2‴-[(1-Hydroxy-4-methoxybenzene-2,6-diyl)bis(methylenenitrilo)]tetrakis(acetic Acid) (**18**). Yield: 36%. IR (KBr): 1731, 1633, 1399, 1236 (C=O, C–O). ^{1}H NMR ((D_6)DMSO): 3.42 (s, 8 H); 3.64 (s, 3 H); 3.81 (s, 4 H); 6.70 (s, 2 H).

2,2′,2″,2‴-[(1-Hydroxy-3,4,5-trimethoxybenzene-2,6-diyl)bis(methylenenitrilo)]tetrakis(acetic Acid) (**19**). Yield: 46%. IR (KBr): 1735, 1629, 1367, 1190 (C=O, C–O). ^{1}H NMR ((D_6)DMSO): 3.42 (s, 8 H); 3.75 (s, 9 H); 3.83 (s, 4 H).

2,2′,2″,2‴-[(1-Hydroxy-4-phenoxybenzene-2,6-diyl)bis(methylenenitrilo)]tetrakis(acetic Acid) (**20**). Yield: 39%. IR (KBr): 1730, 1630, 1398, 1219 (C=O, C–O). ^{1}H NMR ((D_6)DMSO): 3.42 (s, 8 H); 3.83 (s, 4 H); 6.85 (s, 2 H); 6.88 (d, J = 7.3, 2 H); 7.03 (t, J = 7.3, 1 H); 7.31 (t, J = 7.3, 2 H).

2,2′,2″,2‴-[(4-Cyano-1-hydroxybenzene-2,6-diyl)bis(methylenenitrilo)]tetrakis(acetic Acid) (**21**). Yield: 69%. IR (KBr): 2228 (C≡N), 1712, 1677, 1385, 1244 (C=O, C–O). ^{1}H NMR ((D_6)DMSO): 3.44 (s, 8 H); 3.87 (s, 4 H); 7.58 (s, 2 H).

2,2′,2″,2‴-[(4-1-hydroxybenzene-2,6-diyl)bis (methylen enitrilo)]tetrakis(acetic Acid) (**22**). Yield: 65%. IR (KBr): 1720, 1634, 1399, 1248 (C=O, C–O). ^{1}H NMR ((D_6)DMSO): 3.42 (s, 8 H); 3.87 (s, 4 H); 7.64 (s, 2 H).

2,2′,2″,2‴-[(4-Acetamido-1-hydroxybenzene-2,6-diyl)bis(methylenenitrilo)]tetrakis(acetic Acid) (**23**). Yield: 75%. IR (KBr): 1731, 1643, 1398, 1240 (C=O, C–O). ^{1}H NMR ((D_6)DMSO): 1.96 (s, 3 H); 3.42 (s, 8 H); 3.80 (s, 4 H), 7.30 (s, 2 H).

2,2′,2″,2‴-[(1-Hydroxybenzene-2,6-diyl)bis (methylenenitrilo)]tetrakis(acetic Acid) (**24**). Yield: 96%. IR (KBr): 1732, 1633, 1393, 1238 (C=O, C–O). ^{1}H NMR ((D_6)DMSO): 3.41 (s, 8 H); 3.84 (s, 4 H); 6.73 (t, J = 7.3, 1 H); 7.06 (d, J = 7.3, 2 H).

2,2′,2″,2‴-[(4-Benzoyl-1-hydroxybenzene-2,6-diyl)bis(methylenenitrilo)]tetrakis-(acetic Acid) (**25**). 4-Hydroxybenzophenone (9.91 g, 50.0 mmol), iminobis(acetic acid) (13.3 g, 100 mmol), and NaOH (9.00 g, 230 mmol) were dissolved in H_2O (60 ml). After addition of 37% aqueous formaldehyde (8.9 g, 110 mmol), the mixture was refluxed for 5 h. The cold solution was acidified with 6 M HCl (pH ca. 2), filtered and the product was washed with cold H_2O and crystallized from EtOH/H_2O. Yield: 9.76 g (40%). IR (KBr): 1730, 1640, 1395, 1225 (C=O, C–O). ^{1}H NMR

((D_6)DMSO): 3.48 (s, 8 H); 3.92 (s, 4 H); 7.53–7.56 (m, 2 H); 7.62 (s, 2 H); 7.64–7.68 (m, 1 H); 7.69–7.71 (m, 2 H).

2.5. Photoluminescence measurements

The excitation spectra and decay times of terbium chelates were measured on a Perkin Elmer LS5 spectrofluorometer using the 545 nm emission peak of Tb(III). The solutions were 1.0×10^{-5} M for both Tb(III) and ligand in borate buffer, pH 8.5, except in the case of ligands **17** and **21** when the concentration of 1.0×10^{-6} M was used.

2.6. ECL measurements

The ECL measurements were done in disposable aluminium cups using the apparatus described in Ref. [1]. The solutions were 1.0×10^{-7} M both for Tb(III) and ligand in borate buffer, pH 9.1. The coulostatic cathodic pulse used for the excitation was 50 V in amplitude and the injected charge was adjusted to 120 μC/pulse. Emission after the falling edge of the pulse was followed for 8 ms using a gated photon counter (Stanford Research SR400). Totally 50 excitation pulses were applied at 20 ms time intervals and the number of photons summed to give the final result.

3. Results and discussion

3.1. Syntheses

A number of different pathways was used in the preparation of ligands **13–25** (see Fig. 1). Most of the ligands (**13–23**) were prepared through the tetramethyl esters **1–11**, which were made from corresponding phenols, 37% aqueous formaldehyde and dimethyl iminobis(acetate) using the Mannich reaction without any solvent in the reaction mixture. The main product of the synthesis, dimethyl ester (60–84%), was formed quite easily while the formation of the desired tetramethyl ester required longer heating and gave lower yields (16–40%). The electronegativity of the substituents did not have any effect on the yields of the syntheses. Compound **12** (R = H) was prepared from the 4-bromo derivative **2** using H_2 and Pd/C as a catalyst in a mixture of Et_3N and MeOH.

Finally, the tetramethyl esters **1–12** were hydrolyzed with KOH in EtOH to the target tetraacetic acids **13–24**. The crude products were precipitated by acid treatment, and purified from inorganic salts using phenol extraction. Although the yields of the procedure were variable (36–100%), the purification method was easy, simple and fast.

Only in the synthesis of ligand **25** a one-step procedure could be used without the difficulties in the separation of tetraacetic acid from diacetic acid.

3.2. Luminescence

The procedure employed for measuring the ECL intensity was essentially the same as applied in our previous paper [1]. The concentrations of the ligand and Tb(III) were both kept at the level of 10^{-7} M which demands a rather high stability constant for the complex. The chelating moiety is the same in all the compounds and one cannot expect any large variations in the stability constants. The stability constants of the 1:1 and 1:2 complexes of Tb(III) with the heptadentate ligand **25** are $\log \beta_{11} = 23.6$ and $\log \beta_{12} = 29.8$, respectively [1]. Any variation in the ECL intensity between the different ligands cannot be addressed to the different stabilities and consequent variation in the composition of the solutions.

For the purpose of comparison, the emission intensities of the photoluminescence of these Tb(III) complexes were recorded. The terbium emission line corresponding to the transition $^5D_4 \rightarrow {}^7F_5$ (546 nm) was employed and excitation occurred at the peak value depending on the ligand. In most cases the decay curves of emission could not be interpreted as single exponentials but as a sum of two exponential decays:

$$I = Ae^{-t/\tau_1} + Be^{-t/\tau_2}$$

In order to get the total emission intensity this

expression is integrated with respect to time from 0 to ∞ giving

$$I_{tot} = A\tau_1 + B\tau_2$$

The results for ECL together with photoluminescence are reported in Table 1. The intensities are normalized with respect to the ECL and photoluminescence intensities of the Tb(III) chelates of the unsubstituted parent compound **24**. The intensities are also shown as bar graphs in Fig. 2.

As can be seen from Table 1 and Fig. 2, there is hardly any correlation between the ECL and photoluminescence intensities. It is rather obvious that the factors which have the main influence on the emission intensity of photoluminescence, such as molar absorptivity, the rates of nonradiative transition, intersystem crossing and energy transfer to the resonance levels of terbium, play only minor roles in ECL and its intensity. In fact, the mechanism of the cathodically generated luminescence on an aluminium electrode is not yet clear, although it has been a subject of research for a long time; initially by us [7] and more recently by Meulenkamp et al. [8]. It is most probable that a number of electrochemical processes are simultaneously occurring; important factors are the production of energetic radicals from dissolved oxygen or other com-

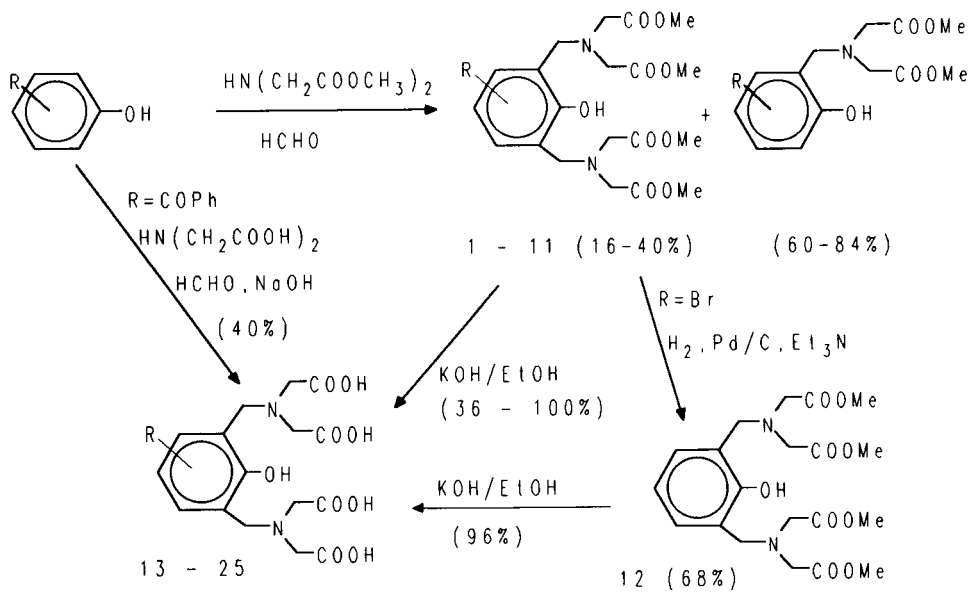

1, 13: R=4-Cl
2, 14: R=4-Br
3, 15: R=4-Me
4, 16: R=4-t-Bu
5, 17: R=4-Ph
6, 18: R=4-MeO
7, 19: R=3,4,5-tri-MeO
8, 20: R=4-PhO
9, 21: R=4-CN
10, 22: R=4-$CONH_2$
11, 23: R=4-$NHCOCH_3$
12, 24: R=H
25: R=COPh

Fig. 1. Ligands and synthetic pathways.

pounds intentionally added to the solution. With oxygen the following mechanism can be proposed:

$$O_2 + e^- + H^+ \rightarrow HOO^{\cdot}$$

$$L - Tb + e^- \rightarrow L - Tb^{\cdot -}$$

$$L - Tb^{\cdot -} + HOO^{\cdot} \rightarrow L - Tb^* + HOO^-$$

$$L - Tb^* \rightarrow L - Tb + h\nu$$

The cathodic processes lead to the formation of a radical as the reduction product from the chelate L–Tb, and a reactive hydroperoxide radical from dissolved oxygen. These radicals react together in an energetic reaction whereupon the neutral chelate is formed back, but in the excited state. Apparently the factors which determine the efficiency of these processes are the facility of one-electron reduction of the chelate, the stability of the resulting radical, its energetics, and finally the efficiency of the radiative transition of the excited species down to the ground state. A reasonably long lifetime of the radical is needed to have time to encounter the reactive hydroperoxide radical. On the other hand, too high stability means often low energy of the radical and this would mean a low reaction rate and possibly insufficient enthalpy of the radical–radical reaction to raise the product to the excited state. If the efficiency of the radiative deactivation is a determining step, a clear correlation should prevail between the intensities of ECL and photoluminescence, which is obviously against the experimental results as seen from Fig. 2.

Assuming that the hypothesis on the mechanism shown above is acceptable, the intensity of the ECL emission is influenced by a number of rate processes. If these rates are governed by the resonance and inductive effects of the substituents in the aromatic ring, one can expect a linear correlation of the logarithms of the rate constants with the Hammett substituent constants. The first process is the charge transfer from the electrode to the chelate molecule. It is not easy to find a precedent in the literature dealing with the correlation of the charge transfer rates with the substituent parameters. However, correlations of the polarographic half-wave potentials of aromatic compounds with the Hammett substituent constants have been well documented in the literature [9]. The half-wave potential bears a linear relationship with the redox potential and consequently with the standard Gibbs free energy of the redox equilibrium. On the other hand, with closely similar compounds the activation energy of the rate process and the

Table 1
Electrochemiluminescence intensities (ECL), excitation maxima (λ_{exc}), integrated photoluminescence intensities and decay times (τ) of the terbium(III) chelates of substituted (1-hydroxybenzene-2,6-diyl)bis(methylenenitrilo)tetrakis(acetic acids)

Compound	ECL intensity [a.u.]	Photoluminescence			
		λ_{exc} (nm)	Emission intensity (a.u.)	Decay times (ms)	
				τ_1	τ_2
Parent compound (**24**)	100 (def)	282	100 (def)	2.58	0.066
4-Cl (**13**)	18	308	108	2.46	-
4-Br (**14**)	43	307	196	3.19	-
4-Me (**15**)	153	290	124	2.76	0.097
4-*tert.*-Bu (**16**)	58	286	163	2.49	0.099
4-Ph (**17**)	61	272	900	1.59	0.20
4-OMe (**18**)	94	304	93	2.54	0.15
3,4,5-Tri-OMe (**19**)	11	330	86	3.05	0.61
4-OPh (**20**)	39	292	200	2.27	0.041
4-CN (**21**)	40	284	1070	2.43	-
4-$CONH_2$ (**22**)	27	272	154	2.38	-
4-$NHCOCH_3$ (**23**)	39	300	15	2.13	-
4-COPh (**25**)	41	324	4	-	0.055

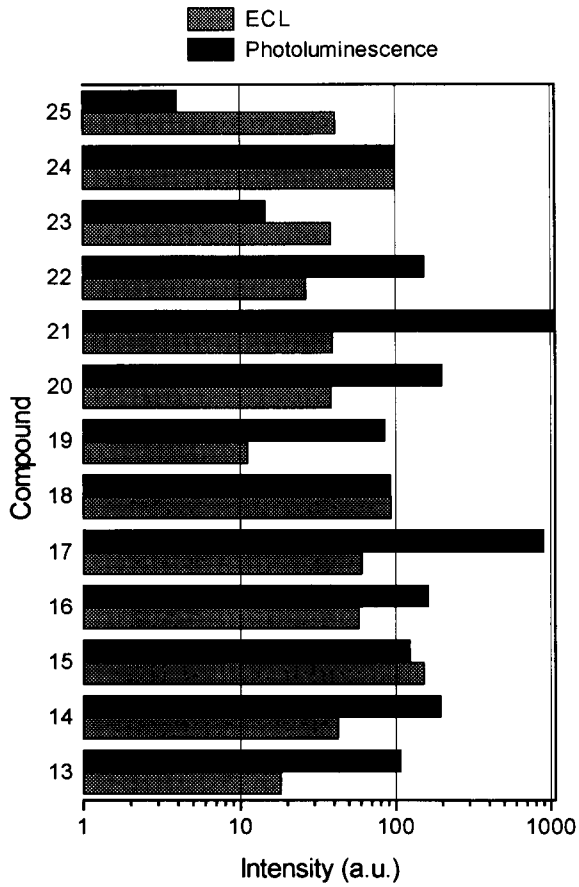

Fig. 2. ECL and photoluminescence emission intensities of 13 terbium chelates of substituted (1-hydroxybenzene-2,6-diyl)-bis(methylenenitrilo)tetrakis(acetic acids). The intensities are normalized with respect to the parent compound **24**.

Gibbs free energy of the equilibrium state of the same or closely related process have in most cases a linear correlation. This is best manifested in the Brønsted relation of the proton transfer processes, but actually the Butler-Vollmer equation has been derived basically on the similar argumentation. Hence we have reasons to expect that logarithms of the rate constants for the charge transfer of our chelates bear a linear relationship with the Hammett substituent constants. In the same way, the rate of the homogeneous charge transfer between the reduced chelate molecule and hydroperoxide radical is expected to correlate with the same substituent parameters. The third important rate process is the radiative deactivation process of the excited state. However, the emission intensity does not depend only on the rate of this process but also on the rates of intersystem crossing and various unknown nonradiative processes. No simple relationship between substituent parameters and rate coefficients of these processes can be expected to prevail. We assume now that the emission intensity can be roughly presented as proportional to the product of various rate coefficients, i.e.

$$I_{ECL} \propto k_{het} k_{hom} k_{flu} k_x$$

where k_{het} and k_{hom} refer to the heterogeneous and homogeneous charge transfers, respectively, k_{flu} to the lumped rate constants of luminescence processes and k_x to the various unspecified rate constants which are hopefully constant or linearly dependent on the Hammett parameters within the group of compounds. Assuming that k_{flu} is roughly proportional to the measured intensity of photoluminescence, we can cancel its influence on the correlation by correlating log I_{ECL} − log I_{flu} against the Hammett parameters. Fig. 3a shows the correlation of this difference with the Hammett σ_X parameters and Fig. 3b shows log I_{ECL} correlated with the same parameters. The obvious outliers, compound **25** in the former case and compound **19** in the latter case, are removed, but still the correlations are hardly statistically significant, the correlation coefficient being 0.56 in Fig. 3a and 0.52 in Fig. 3b. Presumably there are still factors which are not influenced by the inductive and resonance effects generally so well predicted by the Hammett substituent constants. If one dares to draw any conclusions on the basis of Fig. 3, there is a slight tendency to a higher ECL intensity at lower values of the Hammett substituent constants.

Although no clear-cut correlation could be found, the experimental results of this work do provide some basis on the choice of the synthetic targets in developing efficient ECL luminophors. Apparently efficient photoluminescence does not guarantee highly efficient ECL as shown by compound **21**. The main result of this work is that the simple 4-methyl derivative **15** gives the highest intensity, although the differences between the

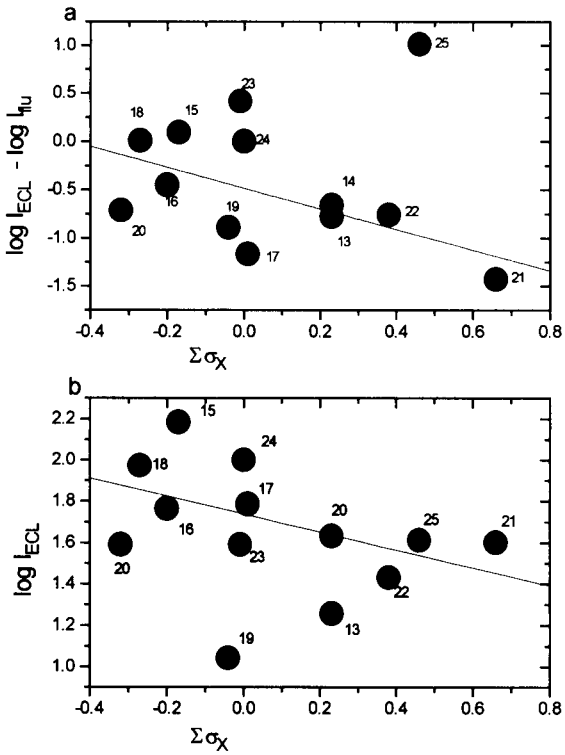

Fig. 3. Correlation of the ECL intensities of 13 terbium chelates of substituted (1-hydroxybenzene-2,6-diyl)bis(methylenenitrilo)tetrakis(acetic acids) with the Hammett substituent constants (from Ref. 9): (a) corrected for photoluminescence, (b) uncorrected for photoluminescence.

compounds tested are not too high to prevent any of them to be used as a label in biomolecules.

Acknowledgments

The authors wish to acknowledge Mr. Sakari Kulmala, M.Sc., Mr. Martti Latva, M.Sc., and Miss Marjatta Kuisma for their skilful technical assistance in recording ECL and fluorescence spectra, and the University Foundation of Turku (Turun Yliopistosäätiö) for financial aid.

References

[1] J. Kankare, K. Fälden, S. Kulmala and K. Haapakka, Anal. Chim. Acta, 256 (1992) 17.

[2] K. Haapakka, J. Kankare and O. Puhakka, Anal. Chim. Acta, 207 (1988) 195; K. Haapakka, J. Kankare and K. Lipiäinen, Anal. Chim. Acta, 215 (1988) 341.

[3] E. Soini and T. Lövgren, CRC Crit. Rev. Anal. Chem., 18 (1987) 105.

[4] V.-M. Mukkala and J. Kankare, Helv. Chim. Acta, 75 (1992) 1578; V.-M. Mukkala, C. Sund, M. Kwiatkowski, P. Pasanen, M. Högberg, J. Kankare and H. Takalo, Helv. Chim. Acta, 75 (1992) 1621; H. Takalo, E. Hänninen, J. Kankare, Helv. Chim. Acta, 76 (1993) 877; V.-M. Mukkala, M. Kwiatkowski, J. Kankare and H. Takalo, Helv. Chim. Acta, 76 (1993) 893; V.-M. Mukkala, M. Helenius, I. Hemmilä, J. Kankare and H. Takalo, Helv. Chim. Acta, 76 (1993) 1361.

[5] J. Kankare, K. Haapakka, O. Puhakka and S. Kulmala, The 36th Meeting of the International Society of Electrochemistry, Salamanca, September 1985, Extended Abstracts, p. 7010.

[6] J. Kankare, K. Haapakka, S. Kulmala, V. Näntö, J. Eskola and H. Takalo, Anal. Chim. Acta, 266 (1992) 205.

[7] J. Kankare, D.E. Ryan and B.J. Fürst, Can. J. Chem., 55 (1977) 1193.

[8] E.A. Meulenkamp, J.J. Kelly and G. Blasse, J. Electrochem. Soc., 140 (1993) 84.

[9] P. Zuman, Substituent effects in Organic Polarography, Plenum Press, New York, 1967.

ELSEVIER

Analytica Chimica Acta 295 (1994) 37–46

ANALYTICA CHIMICA ACTA

An amperometric bi-enzyme sensor for glycolic acid determination based on spinach tissue and ferrocene-mediation

W. Oungpipat, P.W. Alexander *

Department of Analytical Chemistry, University of New South Wales, P.O. Box 1 Kensington, NSW 2033 Australia

Received 29th November 1993; revised manuscript received 15th March 1994

Abstract

A new amperometric plant tissue biosensor based on the co-immobilisation of ground spinach leaves and ferrocene in a carbon paste matrix is described for the determination of glycolic acid. The spinach tissue acts as a source of glycolate oxidase and peroxidase. Ferrocene is employed as a mediator which facilitates electron transfer between the electrode surface and hydrogen peroxide. The glycolic acid assay is based on the amperometric measurement of a reduction current corresponding to the reduction at the electrode surface of ferricinium ion generated from the enzymatic reaction at 0.00 mV vs. Ag/AgCl. The effect of various experimental parameters such as pH, working buffer, applied potential and paste composition is explored for optimum analytical performance. The bioelectrode exhibits linear response up to 5×10^{-4} M glycolic acid with a relative standard deviation of 1.50% ($n = 30$) and a detection limit of 1×10^{-6} M. The bioelectrode responds rapidly to glycolic acid, with steady state current responses achieved in less than 1 min. The sensitivity of the bioelectrode decreased to 50% of the original value after 12 days of continuous use.

Key words: Amperometry; Biosensors; Plant-tissue electrodes; Glycolic acid

1. Introduction

Glycolic acid is used in numerous areas of technology, for example in adhesives, metal cleaning, electroplating, dairy cleaning, biodegradable polymers, dyeing, water-well cleaning, masonry, textiles and detergents [1]. The measurement of glycolic acid concentration for such applications is therefore of great interest. Moreover, the concentration of glycolic acid in biological fluids has been used as an index for differential diagnosis of the hyperoxaluria syndromes [2]. All these have prompted attempts to develop a reliable, rapid and economical method for its assay.

Numerous methodologies have been applied for the measurement of glycolic acid. These include colorimetric [3,4], isotope dilution [5], chromatographic [6–8] and enzymatic methods [9,10]. These methods have inherent problems. The colorimetric methods are non-specific. The isotope dilution methods are used in combination with colorimetric methods which are unreliable. Gas chromatographic (GC) and liquid chromato-

* Corresponding author.

SSDI 0003-2670(94)00155-F

graphic (LC) methods require complex isolation and derivatisation steps as well as involve the use of expensive apparatus. Enzymatic methods appear to be the most widely used but suffer from instability and high cost of the commercially purified enzyme glycolate oxidase.

This paper describes a new amperometric plant tissue-based electrode for monitoring glycolic acid. Plant tissues have received considerable interest in recent years as alternative biocatalysts for replacing isolated enzymes to construct biosensors [11]. Plant tissue-based biosensors offer advantages which include high activity, high stability, ease of preparation and low cost. The spinach leaves (*Spinacia oleracea*) used in the present work have been reported to be rich in glycolate oxidase [12–14] and peroxidase [15–17]. This enables the use of both enzymatic activities in a series of reactions for a sensitive measurement scheme for determining glycolic acid. In the first reaction, glycolate oxidase converts glycolic acid to glyoxylate and hydrogen peroxide. Hydrogen peroxide is then used as the substrate for the second reaction that involves the utilisation of the second enzyme, peroxidase. The peroxidase (reduced form) reduces hydrogen peroxide to water, forming the oxidised form which then oxidises the ferrocene used as a mediator to the ferricinium ion. The ferricinium is subsequently reduced back to ferrocene by accepting an electron from the electrode. The latter reduction current which is quantitatively related to the concentration of hydrogen peroxide and hence glycolic acid is monitored amperometrically. The methods for bioelectrode construction and characterisation are reported in the following sections.

2. Experimental

2.1. Apparatus

A three-electrode assembly incorporating a spinach tissue-based and ferrocene-mediated working electrode, a Ag/AgCl reference electrode and a platinum auxiliary electrode was used in the batch measurements. The electrodes were connected to a BAS Model CV-1b cyclic voltammograph and digital multimeter (Mironta). The output was displayed on a Graphtec *X–Y* recorder (Model WX 4425) and Omniscribe strip-chart recorder for cyclic voltammetric and amperometric measurements, respectively. A magnetic stirrer and a stirring bar provided the convective transport for the amperometric experiments.

2.2. Materials

Mineral oil, ferrocene, chloroform and graphite powder were obtained from Aldrich. Glycolic acid was purchased from Sigma. Chemicals for interference studies were all obtained from Unilab except glucose which was purchased from Sigma. All chemicals were of analytical grade and were used as received. All solutions were prepared with deionised water prepared by passing distilled water through a Milli-Q system (Millipore). Spinach (*Spinacia oleracea*) was obtained from a local supermarket and stored at 4°C until used.

2.3. Electrode construction

The bioelectrode was made by firstly preparing a 6% ferrocene modified graphite powder. This can be done by mixing 0.94 g graphite powder with 0.06 g ferrocene dissolved in 20 ml of chloroform. The solvent was subsequently evaporated. Finally, 0.6 g of this ferrocene-modified graphite powder was mixed with 0.4 g of mineral oil to produce ferrocene-modified carbon paste. This paste (0.88 g) was then thoroughly mixed with 0.12 g of ground tissue from Spinach leaves. Subsequently, the resulting mixture which contained 3.2% ferrocene and 12% tissue was packed firmly into the electrode body made from glass with a geometric surface area of 3.14 mm^2 and the surface was smoothed with a piece of weighing paper. The electrode connection to the carbon paste was established via a copper wire. When not in use, the bioelectrode was stored in a refrigerator at 4°C.

In some experiments, tissue-modified plain carbon paste was utilised. This was prepared by the same procedure as mentioned above except that a plain carbon paste (60% graphite powder

and 40% mineral oil) was substituted for ferrocene-modified carbon paste.

2.4. Procedures

Cyclic voltammetry was performed in an unstirred 0.05 M NaH_2PO_4–NaOH buffer of pH 7.5. The test solutions were not deaerated. The voltammograms were recorded using a cyclic potential sweep between 700 and −200 mV with an initial value of 0.00 mV. The scan rate was 30 mV s^{-1}.

The amperometric measurements were performed either by single or successive injections of aliquot(s) of stock glycolic acid solution. In both cases, the electrodes are immersed into an electrochemical glass cell containing 10 ml of NaH_2PO_4–NaOH buffer, pH 7.5 (except stated otherwise). After a constant potential of 0.00 mV had been applied to the working electrode, the background current was allowed to decay to a steady-state. Following this initial stabilisation step, aliquots of stock glycolic acid solution were added into the cell while the current–time data were recorded. All experiments were performed at room temperature.

The pH dependence of the bioelectrode response was monitored using a single injection of 2.5×10^{-4} M glycolic acid in a 0.05 M phosphate buffer of varying pH ranging from 4.0 to 9.0. The potential was set at 0.00 mV vs. Ag/AgCl. The effect of working buffers on the bioelectrode response was investigated using a single injection of 2.5×10^{-4} M glycolic acid in 0.05 M concentration of five different buffer systems (pH 7.5), namely NaH_2PO_4–NaOH, Na_2HPO_4–NaH_2PO_4, H_3BO_3–NaH_2PO_4, $C_4H_6O_6$–NaOH and Tris–HCl. The potential was kept constant at 0.00 mV vs. Ag/AgCl. Similarly, the dependence of the bioelectrode response on the applied potential was studied in the potential ranging from −200 to 100 mV vs. Ag/AgCl in NaH_2PO_4–NaOH buffer (pH 7.5) using a single injection of 2.5×10^{-4} M of glycolic acid.

The effect of spinach tissue composition was studied at 3, 6, 9, 12 and 24% (w/w) of spinach tissue with ferrocene loading held constant at 3.2%. Likewise, the effect of ferrocene loading on sensor response was investigated at four different loadings of 0.8, 1.6, 3.2 and 6.4% (w/w) at 12% tissue composition. The studies of both effects were pursued using successive injections of glycolic acid.

Calibration graphs for the bioelectrode response were measured over the concentration range 5×10^{-5}–1.5×10^{-3} M in NaH_2PO_4–NaOH buffer (pH 7.5) at 0.00 mV vs. Ag/AgCl.

3. Results and discussion

3.1. Cyclic voltammetry

Fig. 1 shows cyclic voltammograms obtained with a plain carbon paste electrode (A) and a ferrocene-modified carbon paste electrode (B) in an unstirred 0.05 M phosphate buffer. It can be seen that whereas no redox wave was observed for a plain carbon paste electrode, well-defined cathodic and anodic waves appeared at ferrocene-modified carbon paste. Accordingly, the waves appearing at the ferrocene-modified electrode were ascribed to the electrochemical redox reaction of ferrocene molecules that had been mixed in the carbon paste electrode. Addition of ground spinach leaves in the ferrocene-modified paste showed no effect on the redox wave peak

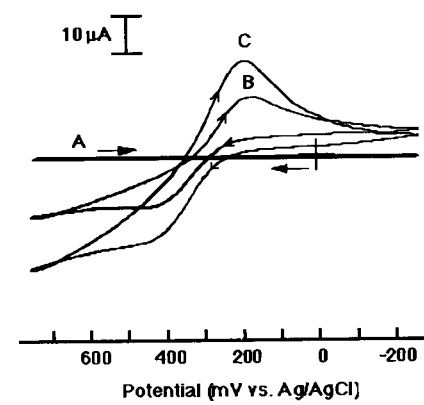

Fig. 1. Cyclic voltammograms in 0.05 M NaH_2PO_4–NaOH buffer solution (pH 7.5) for: (A) plain carbon paste electrode, (B) ferrocene (3.2%, w/w)-modified carbon paste electrode, (C) spinach tissue (6%, w/w) and ferrocene (3.2%, w/w)-modified carbon paste bioelectrode. Scan rate, 30 mV s^{-1}.

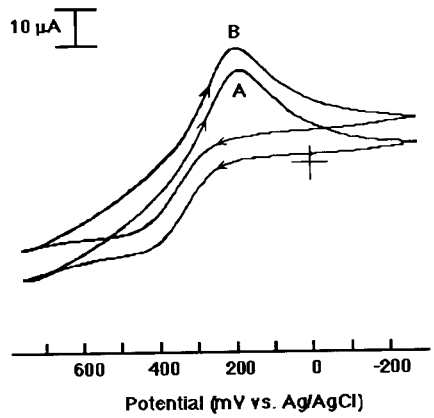

Fig. 2. Cyclic voltammograms of the spinach tissue (6%, w/w) and ferrocene (3.2%, w/w)-modified carbon paste bioelectrode in 0.05 M NaH_2PO_4–NaOH buffer solution (pH 7.5) in the absence (A) and in the presence of 9×10^{-3} M glycolic acid (B). Scan rate, 30 mV s^{-1}.

potentials except that a larger current was experimentally observed, indicating an enhanced diffusional flux (Fig. 1C). The larger currents obtained for the tissue modified carbon paste compared with those of the ferrocene-modified carbon paste indicate that the former electrode is much more hydrophobic, thus allowing a large surface exposure. This results in a larger faradic current for ferrocene response.

Upon addition of glycolic acid, the voltammetry of the bioelectrode clearly changes with an increase in the reduction current and a decrease in the oxidation current (Fig. 2B). The fact that the oxidation current does not increase along with the reduction current is indicative of an enzyme-dependent catalytic oxidation of the ferrocene produced at reducing potential values.

The results obtained above show the absence of an anodic wave in the region from 0.7 to 0.8 V which may be due to direct oxidation of hydrogen peroxide formed in the reaction. The existing peroxidase in oxidised and reduced forms in spinach tissue therefore acts as a reaction intermediate. Two electrons for the ferrocene equivalents are therefore required from the surface of the electrode to the redox centre of the peroxidase. During the catalytic cycle, ferrocene reacts with oxidised peroxidase and then undergoes

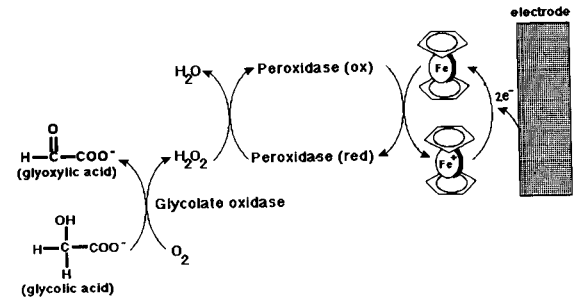

Fig. 3. Reaction sequence within the spinach tissue-based and ferrocene-mediated bioelectrode; for further details see text.

rapid reaction accepting the two electrons from the electrode as shown in Fig. 3.

3.2. Constant potential experiments

Optimisation of experimental variables

The pH dependence of the bioelectrode was studied at 2.5×10^{-4} M glycolic acid over the pH range from 4.0 to 9.0. The resulting peak-shaped pH profile illustrated in Fig. 4 reveals that the bioelectrode showed good sensitivity of response within the pH range value of 7.0–8.0. An optimum pH value of 8.3 has been reported for the spinach glycolate oxidase [12]. This indicates that

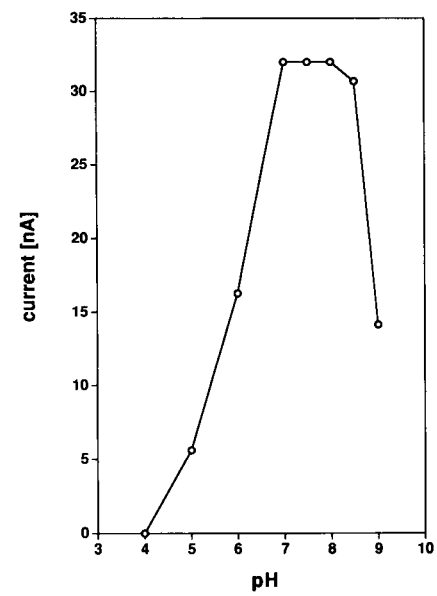

Fig. 4. Effect of pH on the response of the bioelectrode with composition of 6% (w/w) spinach tissue and 3.2% (w/w) ferrocene to 2.5×10^{-4} M glycolic acid in 0.05 M NaH_2PO_4–NaOH buffer solution (pH 7.5) at 0.00 mV (vs. Ag/AgCl).

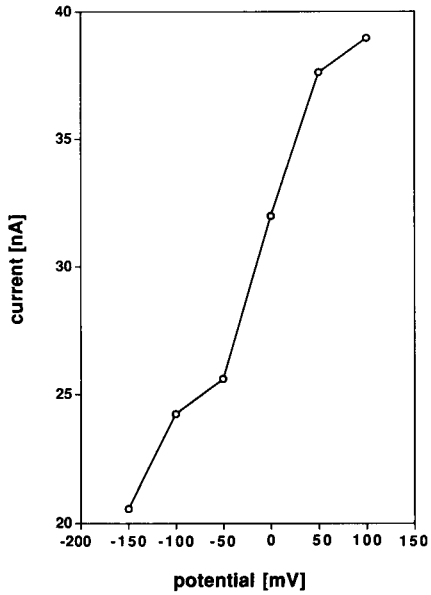

Fig. 5. Effect of operating potential on the bioelectrode response to 2.5×10^{-4} M glycolic acid. Conditions as in Fig. 4.

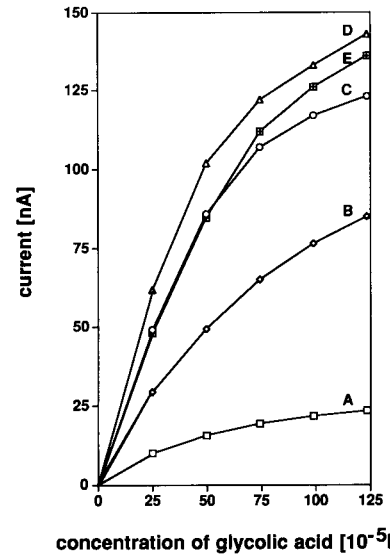

Fig. 6. Effect of spinach tissue composition on the bioelectrode response to glycolic acid at: (A) 3%, (B) 6%, (C) 9%, (D) 12% and (E) 24% spinach tissue with ferrocene loading held constant at 3.2%.

the pH profile is governed by the enzymatic activity. Based on the results obtained, the phosphate buffer solution of pH 7.5 was selected for subsequent study.

The influence of five types of working buffers on the response of the bioelectrode to glycolic acid (2.5×10^{-4} M) was investigated. Table 1 summarises the data obtained in terms of the resulting current response. It can be seen that the NaH_2PO_4–NaOH buffer was the most efficient working buffer giving the highest response among the five types of buffers studied. Hence It was employed for further study.

The effect of applied potential on the bioelectrode response to 2.5×10^{-4} M glycolic acid is shown in Fig. 5. It was found that the reduction current increased from 13.6 to 39.0 nA on changing the potential from −200 to 100 mV (vs. Ag/AgCl). An increase in the applied potential towards a positive value resulted in a high noise level especially when it reaches 150 mV. This behaviour is ascribed to the electrochemical oxidation of the ferrocene contained in the paste occurring in this potential range. The potential of 0.00 mV was selected for the remainder of the experiments as the best compromise between the resulting signal and the noise level. Moreover, this low potential is expected to minimise possible interferences, as shown later in interference studies.

The graphite composition shows a profound effect upon the bioelectrode response to glycolic acid. As would be expected, increasing the tissue composition of the bioelectrode from 3–12% resulted in an increase in the bioelectrode response (Fig. 6), reflecting the increase in the biocatalytic activity. On the other hand, the noise level also gradually increased with the increase in tissue composition. Increasing the tissue composition

Table 1
Effect of working buffer

Buffer system	NaH_2PO_4–NaOH	Na_2HPO_4–NaH_2PO_4	H_3BO_3–NaH_2PO_4	$C_4H_6O_6$–NaOH	Tris–HCl
Current (nA)	31.2	25.6	19.5	19.5	23.2

beyond 12% caused lower response. This behaviour could be attributed to the increased resistance of the carbon paste [18]. A similar trend was observed for the influence of mediator loading on the response of the bioelectrode. Fig. 7 illustrates signals increasing substantially with increase in mediator loading from 0.8 to 1.6%. Further increase in mediator loading above 1.6% resulted in a decrease in the bioelectrode response, while the linear range is gradually extended. Such a decrease in response of the bioelectrode when a larger amount of mediator is used is a typical behaviour of a mediator-based sensor [19]. Again this behaviour is ascribed to the lowering of the electrical conductivity due to the reduction in graphite loading [20]. Based on these results, the bioelectrode with a composition of 12% tissue and 3.2% ferrocene was employed throughout the study as the best compromise for highest sensitivity, lowest noise level and widest linear range.

It is interesting to note that whereas no response to glycolic acid was observed with the ferrocene-modified carbon paste electrode, an amperometric response to glycolic acid was obtained at the spinach tissue-modified carbon paste electrode as shown in Fig. 8C. The fact that plasma membranes of plant cells contain several constituents that can carry electrons such as NAD(P)H dehydrogenase, flavins, quinones and cytochromes [21,22], suggests that the small bioelectrode response in the absence of ferrocene may thus be attributed to the endogenous mediators contained in the tissue in limited concentrations. In addition, it was recently found that electrocatalytic reduction of hydrogen peroxide by horseradish peroxidase immobilised on graphite electrodes could occur without the addition of an electron mediator [23–25]. Therefore it is also possible that the current for glycolic acid in the absence of ferrocene can be ascribed to this phenomenon.

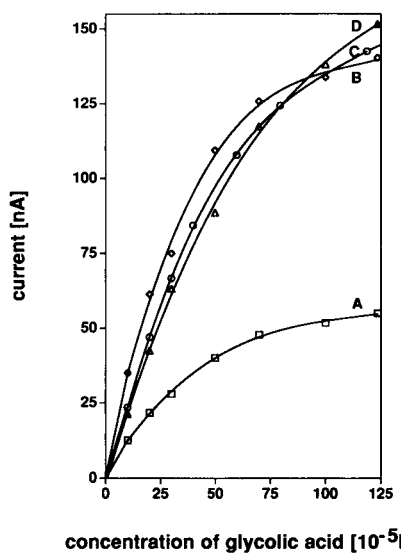

Fig. 7. Effect of mediator loading on the bioelectrode response to glycolic acid at: (A) 0.8%, (B) 1.6%, (C) 3.2% and (D) 6.4% ferrocene with spinach tissue composition held constant at 12%.

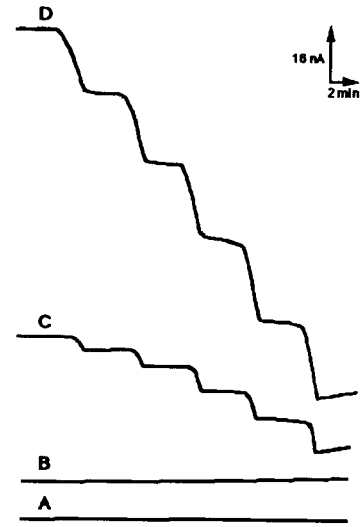

Fig. 8. Typical current–time recordings obtained at: (A) the plain carbon paste electrode, (B) the ferrocene (3.2%, w/w)-modified carbon paste electrode, (C) the spinach tissue (12%w/w) - modified carbon paste electrode and (D) the spinach tissue (12% w/w) and ferrocene (3.2% w/w)-modified carbon paste bioelectrode with stepwise additions of 1×10^{-4} M glycolic acid for (A), (B), (D) and 5×10^{-5} for (C). Electrolyte, 0.05 M NaH_2PO_4–NaOH buffer solution (pH 7.5) and operating potential 0.00 mV (vs. Ag/AgCl).

3.3. Bioelectrode characterisation

Fig. 8 displays typical current vs. time responses obtained using the bioelectrodes under

the optimised experimental conditions. The resulting calibration for glycolic acid over the concentration range of 5×10^{-5}–1.5×10^{-3} M is presented in Fig. 9. The bioelectrode exhibits linearity of calibration up to 5×10^{-4} M with curvature at higher concentrations. The slope of the initial linear range is 2.38×10^{2} μA M^{-1} with a correlation coefficient of 1.000. A detection limit of 1×10^{-6} M was experimentally obtained by measuring the standard deviation of six replicate sample peaks. Replicate measurements of 1 x10^{-4} M glycolic acid for the same bioelectrodes yielded 1.50% ($n = 30$) relative standard deviation from the mean. Five independently made bioelectrodes showed acceptable bioelectrode reproducibility with a relative standard deviation of 3.75%.

The apparent Michaelis-Menten constant, K_m^{app}, and the maximum current density can be determined from the electrochemical Eadie-Hofstee form of the Michaelis-Menten equation [26,27]:

$$j = j_{max} - K_m^{app}(j/C)$$

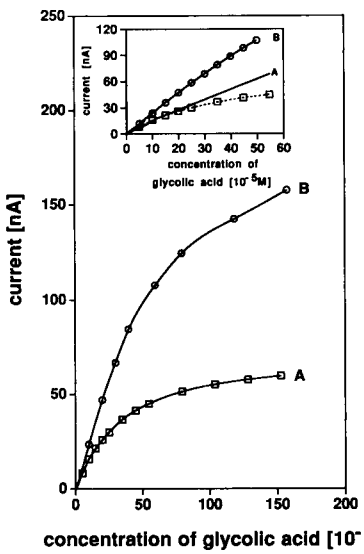

Fig. 9. Glycolic acid calibration graphs for: (A) spinach tissue (12% w/w)-modified carbon paste and (B) spinach tissue (12%, w/w) and ferrocene (3.2%)-modified carbon paste bioelectrodes at 0.00 mV. Conditions are as Fig. 8. Inset shows the initial linear ranges of the bioelectrodes (A) and (B).

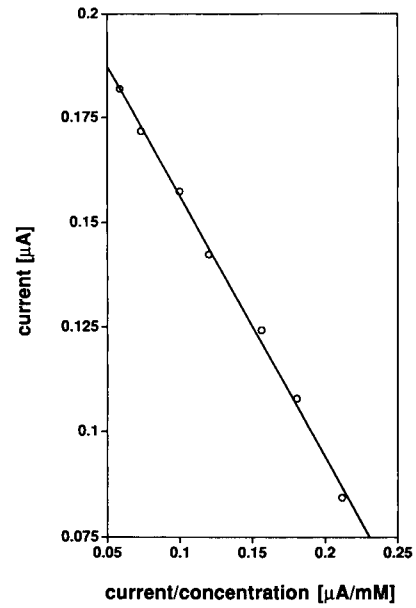

Fig. 10. Eadie-Hofstee plot for the bioelectrode at an applied potential of 0.00 mV (vs. Ag/AgCl).

where j is the steady-state current, j_{max} is the maximum current measured under conditions of enzyme saturation, and C is the glycolic acid concentration. The plot is graphically illustrated in Fig. 10. It is seen that the system produced a straight line over the entire range examined. The K_m^{app} and j_{max} values for the bioelectrode were found to be 0.62 mM and 218 nA, respectively. This K_m^{app} value is higher than found for the enzyme in solution ($K_m = 0.38$ mM for pH 8.3 with 2,6-dichlorophenol indophenol as the electron acceptor [28]). This result indicates that the immobilisation process employed generated a loss of affinity to the substrate. The higher K_m^{app} value obtained for the bioelectrode might be attributed to the mass transfer limitation. In comparison with previously reported glycolate biosensors [29,30], the K_m^{app} of the proposed bioelectrode is lower than that reported [29] for a carbon paste containing siloxane polymer covalently attached to ferrocene and 1,1'-dimethylferrocene (2.2 mM) and that obtained [30] for a carbon paste electrode containing monomeric 1,1'-dimethylferrocene as the mediator (13 mM). The higher K_m^{app} value obtained from the polymer-based electrode

is probably due to the use of the polycarbonate membrane covering in the previous work [30] which produces an additional resistance to the diffusion of substrate to the active enzyme layer.

The steady-state response time (t_{90}) of the present bioelectrode was estimated to be less than 1 min whereas a response time of 2 min was obtained with the previously reported glycolic acid biosensor [30]. The rapid response of the present bioelectrode could be attributed to the intimate contact between biocatalytic and sensing sites.

The stability of the bioelectrode under the proposed storage conditions in this study was evaluated. It was found that the response of the bioelectrode decreased with time. Thus, after 12 days the bioelectrode sensitivity decreased to 50% of the original value. It is experimentally observed that the cathodic and anodic waves in the cyclic voltammograph of ferrocene-modified carbon paste become smaller and eventually the cathodic wave disappears after several scans. As well, a decrease in the amperometric response of spinach-modified carbon paste occurs as a function of the age of bioelectrode. The loss of bioelectrode sensitivity is, therefore, ascribed to the leaching of ferrocene from the electrode and loss of enzyme activity.

The effect of oxygen interference on the response of the bioelectrode to glycolic acid and hydrogen peroxide was also evaluated. The results obtained are shown in Fig. 11. In the absence of oxygen, the bioelectrode showed a sluggish response to glycolic acid. This behaviour indicates that oxygen acts as an essential co-substrate for glycolate oxidase. In fact, curve A should show no response in the absence of oxygen. However, in practice, it is possible that oxygen from the surrounding air redissolves into the deaerated buffer thus allowing some reaction to take place, which results in the small signal response observed in curve A. In the second step of the reaction, it was found that the bioelectrode response to hydrogen peroxide was independent of the presence of oxygen.

Twelve substances were used to evaluate the selectivity of the bioelectrode. The current obtained for each interfering substance (4×10^{-4} M) in the presence of glycolic acid at a concentration of 1×10^{-4} M was used as an indicator for the bioelectrode selectivity in comparison with the glycolic acid reading alone. The results are listed in Table 2, showing that the bioelectrode is quite selective for glycolic acid. Of the interferences studied, only ascorbic acid at a concentra-

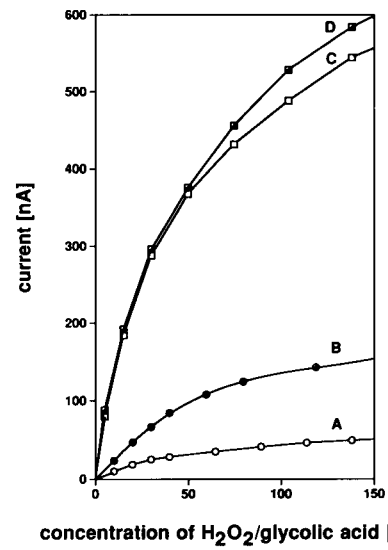

Fig. 11. Glycolic acid calibration graph for the bioelectrode under nitrogen (A), and under air saturated solution (B) and that for hydrogen peroxide under nitrogen, (C) and under air saturated solution (D) at 0.00 mV (vs. Ag/AgCl).

Table 2
Possible interferences tested with the bioelectrode

Substance	Current Ratios [a]
Citric acid, malonic acid, tartaric acid oxalic acid, acetic acid, glutamic acid, fructose, formic acid	1.00
Glucose	0.96
Maleic acid	0.97
Succinic acid	0.94
Lactic acid	1.10
Ascorbic acid	1.00 [b], 1.44 [c]

[a] Ratio of currents for mixtures of 4×10^{-4} M substance and 1×10^{-4} M glycolic acid compared with 1×10^{-4} M glycolic acid alone. [b] Ratio of current for mixture of 1×10^{-6} M ascorbic acid and 1×10^{-4} M glycolic acid compared with 1×10^{-4} M glycolic acid alone. [c] Ratio of current for mixture of 1×10^{-5} M ascorbic acid and 1×10^{-4} M glycolic acid compared with 1×10^{-4} M glycolic acid alone.

tion of 1×10^{-5} M interfered to any large extent. Lactic acid at 4×10^{-4} M shows only a small effect on the bioelectrode response to glycolic acid. As for most amperometric sensors, electroactive species such as ascorbic acid can easily oxidise directly on the electrode surface, thus changing the enzyme-mediated current. This effect clearly occurs in the present work. However, in the presence of a lower concentration of ascorbic acid (1×10^{-6} M), it was found that no interference effect on the glycolic acid response was observed. The small bioelectrode response to lactic acid implies some cross-reactivity of the enzyme glycolate oxidase towards lactic acid. This result is consistent with previous works [12–14] regarding the ability of glycolic acid oxidase to oxidise lactic acid.

The accuracy of the bioelectrode was evaluated by determining the recoveries of glycolic acid after concentrations ranging from 5×10^{-5} to 4.0×10^{-4} M were added to a 10-fold dilution of charcoal pretreated urine. Other compounds may interfere by reacting with hydrogen peroxide, ferrocene or by direct electrochemical activity at the operating voltage. The pretreatment step of urine sample with charcoal is essential and recommended in order to eliminate any ascorbic acid and other electro-active compounds contained in the sample. The samples were mixed with 200 mg of activated charcoal and the charcoal was removed by centrifugation. A 10 fold-dilution of the supernatant was then used for the glycolic acid assay [9]. The results obtained are given in Table 3. The bioelectrode shows satisfactory results with an average recovery of 100.9%.

Table 3
Recovery of glycolic acid added to 10-fold dilution of pretreated urine sample

Glycolic acid concentration ($\times 10^{-5}$ M)		
Added	Found	Recovery (%)
5.0	5.0	100.0
10.0	10.2	102.0
20.0	20.2	101.0
30.0	30.8	102.7
40.0	39.6	99.0

4. Conclusions

This work has demonstrated the feasibility of utilising the available bi-enzyme system in spinach leaf for construction of a new plant tissue-based biosensor for glycolic acid determination. The bioelectrode offers favourable analytical features for use as a biosensor. It is typical of amperometric sensors based on mixed tissue carbon paste electrodes to have high sensitivity and rapid response. Additionally, the use of a low operating potential together with the specific enzymatic reaction resulted in minimal interference effects. The simple design and low cost of the bioelectrode construction are further distinctive features of the proposed bioelectrode. To achieve bioelectrode accuracy, however, pretreatment of samples containing ascorbic acid with activated charcoal is required. For applications apart from the quantitation of glycolic acid, the present bioelectrode may be used in the area of plant biology where it could be used as a rapid screening test to monitor the glycolate oxidase activity in plants.

Acknowledgments

The authors are grateful to the Australian International Development Assistance Bureau and Thai Authorities especially DTEC and Rajamangala Institute of Technology for the training award granted to W. Oungpipat.

References

[1] Kirk-Othmer, Encyclopedia of Chemical Technology, Vol. 13, Wiley, New York, 1981, p. 92.
[2] H.E. Williams, Kidney Int., 13 (1978) 410.
[3] J.P. Viccaro and E.L. Ambye, Microchem. J., 17 (1972) 710.
[4] A. Niederwieser, A. Matasovic and E.P. Leumann, Clin. Chim. Acta, 89 (1978) 13.
[5] T.D.R. Hockaday, E.W. Frederick, J.E. Clayton and L.H. Smith, J. Lab. Clin. Med., 65 (1965) 677.
[6] M. Petrarulo, S. Pellegrino, O. Bianco, M. Marangella, F. Linari and E. Mentasti, J. Chromatogr., 405 (1989) 87.
[7] M. Petrarulo, O. Bianco, D. Cosseddu, M. Marangella, S. Pellegrino and F. Linari, J. Chromatogr., 532 (1990) 130.
[8] T.R. Wandzilak, L.E. Hagen, H. Hughes, R.A.L. Sutton,

L.H. Smith and H.E. Williams, Kidney Int., 39 (1991) 765.
[9] G.P. Kasidas and G.A. Rose, Clin. Chim. Acta, 96 (1979) 25.
[10] R. Bais, J.M. Nairn, N. Potezny, A.M. Rofe, R.A.J. Conyers and A. Bar, Clin. Chem., 31 (1985) 710.
[11] J. Wang, Electroanalysis, 3 (1991) 255.
[12] I. Zelitch and S. Ochoa, J. Biol. Chem., 201 (1953) 707.
[13] I. Zelitch, J. Biol. Chem., 201 (1953) 719.
[14] N.A. Frigerio and H.A. Harbury, J. Biol. Chem., 231 (1958) 135.
[15] K. Herrmann, Z. Lebensmitt-Untersuch., 106 (1957) 451.
[16] N.M. Sisakyan and A.M. Kobyakova, Biokhimiya, 14 (1949) 86.
[17] S.G. Wildman and J. Bonner, Arch. Biochem., 14 (1947) 413.
[18] L. Zhihong, Q. Wenjian and W. Meng, Anal. Lett., 25 (1992) 1175.
[19] P.D. Hale, L.I. Boguslavsky, H.I. Karan, H.L. Lan, H.S. Lee, Y. Okamoto and T.A. Skotheim, Anal. Chim. Acta, 248 (1991) 155.
[20] H. Gunasingham and C.H. Tan, Analyst, 115 (1990) 35.
[21] H.F. Bienfait, J. Bioenerg. Biomembr., 17 (1985) 73.
[22] F. Bienfait and U. Luttge, Plant Physiol. Biochem., 67 (1988) 665.
[23] G. Jönsson-Pettersson, Electroanalysis, 3 (1991) 741.
[24] L. Gorton, G. Jönsson-Pettersson, E. Csöregi, K. Johansson, E. Dominguez and G. Marko-Varga, Analyst, 117 (1992) 1235.
[25] E. Csöregi, G. Jönsson-Pettersson and L. Gorton, J. Biotechnol., 30 (1993) 315.
[26] R.A. Kamin and G.S. Wilson, Anal. Chem., 52 (1980) 1198.
[27] B.A. Gregg and A. Heller, Anal. Chem., 62 (1990) 258-263.
[28] T.F. Barman, Enzyme Handbook, Vol. 1, Springer, New York, 1969, p. 101.
[29] P. Hale, T. Inagaki, H.S. Lee, H.I. Karan, Y. Okamoto and T.A. Skotheim, Anal. Chim. Acta, 228 (1990) 31.
[30] J.M. Dicks, W.J. Aston, G. Davis and A.P.F. Turner, Anal. Chim. Acta, 182 (1986) 103.

ELSEVIER

Analytica Chimica Acta 295 (1994) 47–57

ANALYTICA CHIMICA ACTA

Amperometric NADH determination via both direct and mediated electron transfer by NADH oxidase from *Thermus aquaticus* YT-1

Mithran Somasundrum [a,*], Jennifer Hall [a], Joe V. Bannister [a,b]

[a] *Biotechnology Centre, Cranfield University, Cranfield, Beds., MK43 0AL UK*
[b] *Department of Biomedical Sciences, University of Malta, Msida, Malta*

Received 15th February 1994; revised manuscript received 11th April 1994

Abstract

Using NADH oxidase extracted from *Thermus aquaticus* YT-1, the determination of NADH by the direct oxidation of labile $FADH_2$ and by mediated electron transfer using the Ru(III/IV) redox couple is described. A scheme for enzyme amplification is outlined using alcohol dehydrogenase (ADH) and NADH oxidase in solution, and enables 1–10 μM NADH to be determined. Detection is performed at +150 mV using the $RuCl_6^{2-}/RuCl_6^{3-}$ couple. Additionally, an electrode is modified by an ADH/NADH oxidase bilayer, enabling ethanol determination (20–200 μM) at 0 mV via the oxidation of ruthenium red.

Key words: Amperometry; NADH oxidase; Ruthenium

1. Introduction

The existence of over 250 dehydrogenases utilizing the NAD^+/NADH redox couple has made the detection of NADH an attractive goal for biosensor research [1]. The oxidation of NADH involves the removal of two electrons and the cleavage of a carbon–hydrogen bond and at bare carbon [2] and platinum [3] electrodes, appears as a single, irreversible peak. However, this direct oxidation requires a high overpotential (from 1.1 to 1.3 V [2,3]) and at NADH concentrations of above 0.5 mM, involves the formation of dimeric products which lead to electrode poisoning [4]. Hence, the oxidation of NADH by electron-transfer mediators has received considerable interest [5–7].

Mediators which have been examined include quinones [8], catechols [9], redox dyes [10,11], ferrocene derivatives [12], inorganic metal complexes [13], conducting organic salts [14] and conducting polymers which are either inherently electrocatalytic [15–19], or which entrap a redox active group [20]. The drawback to this approach has occasionally been found to be poor stability. For example, quinone-modified electrodes have been found to lose activity, due to side reactions in which NAD radicals form covalent bonds with the mediator [4]. Another problem often associ-

* Corresponding author; present address: School of Bioresources and Technology, King Mongkuts Institute of Technology, Thonburi, Bangkok 10140, Thailand.

SSDI 0003-2670(94)00178-O

ated with this form of electrocatalysis, is that of poor selectivity to the analyte. If the half-wave potential of the mediator is not sufficiently low, an electrocatalytic response can be observed to other substances present in real samples (e.g., ascorbic acid, uric acid, glutathione, etc. [10,16,21,22]).

Another route to NADH determination is the utilization of an NADH oxidizing enzyme, such as diaphorase [23,24], or an NADH oxidase [25,26]. Diaphorase catalyses the oxidation of NADH in the presence of an electron acceptor such as methylene green, while the NADH oxidases function via the reduction of oxygen to either water [27] or hydrogen peroxide [28–30]. NADH oxidases have previously been isolated from *Bacillus megaterium* [28–30], *Streptococus faecalis* [27], *Thermus aquaticus* YT-1 [29] and *Thermus thermophilus* HB8 [30].

When selecting an enzyme for biosensor development, an important consideration is that of stability. The high stability of proteins isolated from thermophilic organisms [31,32], makes them ideal components for biosensor construction. The enzymes from both *T. aquaticus* and *T. thermophilus* show activity at elevated temperatures (80 and 95°C, respectively). However, the oxidase from *T. thermophilus* shows peak activity at pH 5.0 [30], whilst the activity of the *T. aquaticus* oxidase is pH independent from pH 5.5–9.5 [25]. This would enable it to be coupled with a wider range of dehydrogenases.

Although the oxidation of enzyme-generated hydrogen peroxide provides one route to NADH determination, it is not the most preferable, since the overpotential required (+650 mV vs. SCE) would leave the sensor response open to interference. A more selective, enzyme-based NADH determination could be provided by obtaining either direct or mediated electron transfer at lower potentials.

Direct electron transfer from the NADH oxidase of *T. aquaticus* has not so far been examined. Mediated electron transfer from the enzyme has previously been attempted using ferrocene derivatives and 1',3-dimethylferrocene-ethanolamine ($E_{1/2}$ = 155 mV vs. SCE) has been shown to couple with the enzyme [25]. However, the second order rate constant for the mediated reaction (8.10×10^4 M^{-1} s^{-1}) was significantly lower than that for oxygen (3×10^6 M^{-1} s^{-1}). Although applications for NADH determination were also illustrated, they involved hydrogen peroxide detection and did not progress to mediated systems. This was due to concern about the possible interactions between the ferrocene derivative and the coupled dehydrogenase. Also, these studies did not include enzyme immobilisation. The NADH oxidase from *B. megaterium* has been immobilised for L-malate and L-lactate determination [26], but again only using oxygen as the electron acceptor.

The aims of this study were therefore as follows: Firstly to examine both direct and mediated electron transfer from NADH oxidase, with a view to producing a detection system exhibiting low electrocatalytic activity to NADH and to interferents such as ascorbate; secondly to examine immobilisation of NADH oxidase and to illustrate some of the possible applications for enzyme based NADH detection.

2. Experimental

2.1. Reagents

NADH oxidase was purified from *Thermus aquaticus* YT-1 as previously described [29]. NADH (disodium salt, grade I), NAD^+ (grade I), alcohol dehydrogenase (ADH) from baker's yeast (alcohol:NAD^+ oxidoreductase, EC 1.1.1.1), FAD (disodium salt), glutaraldehyde (grade I) and ammonium hexachlororuthenate (IV) were purchased from Sigma (Poole). Ruthenium red was purchased from Aldrich (Poole). Hexaamine ruthenium(III) chloride was purchased from Johnson Matthey (Royston). The ADH used was specified as being suitable for micro-recycling of NADH and contained < 0.005 moles of β-NAD^+ and β-NADH per mol of ADH. All solutions were prepared using de-ionized water. 1-Cyclohexyl-3-(2-morpholino-ethyl) carbodiimide metho-*p*-toluene sulphonate (Sigma) was used in 100 mM citric acid–sodium citrate, pH 5.5. For electrochemical experiments involving ADH, the

buffer used was 50 mM Tris–HCl, pH 8.8 containing 50 mM KCl as supporting electrolyte. For all other electrochemical studies this buffer and electrolyte were used at pH 7.0. All reagents were freshly prepared in the working buffer and were stored on ice during the course of each experiment.

2.2. Apparatus

A 10-ml volume single compartment three-electrode cell was used for all experiments. The working electrode was a glassy carbon disc of 3 mm diameter. The reference and counter electrodes were a saturated calomel electrode (SCE) and a piece of platinum wire, respectively. Potentials are quoted here relative to SCE. Before recording each voltammogram or amperometric trace, the working electrode was polished by cotton wool containing an alumina–water slurry (particle size 0.3 μm), sonicated in deionized water for 3 min, rinsed with acetone and then left to air-dry.

Cyclic voltammetry experiments were performed using an Autolab Electrochemical Analyser (Windsor Scientific, Windsor), interfaced to a DSL personal computer. Amperometric experiments were performed using a Ministat potentiostat (Thompson, Newcastle-upon-Tyne), with current–time curves recorded on a BBC Goerz chart recorder, via a JJ Junior resistance bridge. Where required, anaerobic conditions were created by passing nitrogen through the cell for 20 min and then maintaining a nitrogen blanket over the solution during the electrochemical measurement.

For amperometric NADH determinations, FAD was added to the cell to a final concentration of 0.2 mM, in order to ensure that the enzyme was fully active. When used in solution, NADH oxidase was present at a concentration of 4 μg/ml, unless otherwise stated. Enzyme amplification experiments used ADH and ethanol at final cell concentrations of 9 U/ml and 2% (v/v), respectively. When required, mediators were present at a final concentration of 0.4 mM unless otherwise stated. All experiments were performed at room temperature.

2.3. Enzyme immobilisation

Covalent immobilisation of NADH oxidase was based on the carbodiimide method of Bourdillon et al. [33]. Carboxylic acid groups were generated on the electrode surface by exposure to a solution of 10% HNO_3 and 2.5% $K_2Cr_2O_7$ for 30 s at a potential of 1.1 V. These were then activated by incubation in a 20 mg/ml carbodiimide solution for 90 min at room temperature. Following rinsing with deionized water, a 40-μl aliquot of enzyme solution (56 μg of enzyme) was then transferred to the electrode and left for 90 min at room temperature to allow amide bonds to form. The electrode was then washed with deionized water and stored in the working buffer at < 4°C.

Immobilisation was also performed by crosslinking the enzyme to the electrode using glutaraldehyde. The same mass of enzyme as above was transferred to the electrode and was left to stand (approx. 1 h) to allow partial evaporation of the buffer solution. A 10-μl aliquot of glutaraldehyde (2.5%) was then deposited onto the electrode surface and the mixture was left (0.5 h) to allow crosslinking to occur. The electrode was washed and stored in the working buffer at < 4°C.

Immobilisation of an ADH/NADH oxidase bilayer was also performed using glutaraldehyde. NADH oxidase was immobilised as described above and, following amperometric confirmation of enzyme activity, a 10-μl aliquot of ADH (19 U) was deposited on the electrode and was crosslinked with glutaraldehyde as described above. The deposition of the enzymes as separate layers was made with consideration to the possible instability of ADH, since prior immobilisation of the oxidase alone meant that its activity could be measured (and if necessary, additional enzyme immobilized) before exposure of ADH.

3. Results and discussion

3.1. Electrochemistry of FAD

The electrochemistry of a 2 mM FAD solution was examined in buffer solution (pH 7.0) by cyclic

voltammetry. Two-electron transfer from the molecule was observed as a single set of redox peaks ($E_{1/2} = -515$ mV), with the cathodic wave exhibiting a slight shoulder at slow scan rates (< 5 mV/s), as shown in Fig. 1. This is likely to be due to the presence on the electrode surface of strongly adsorbed FAD, which would possess a slightly different pK_a to the freely dissolved component and would thus exhibit a different $E_{1/2}$ value around the pH used here. The electrochemistry of FAD can be considered overall to be quasi-reversible, with a value of ΔE_P (54 mV) greater than the predicted Nernstian value ($59/n$ mV) and which (above values of 15 mV/s) increases with increasing scan rate.

3.2. Lability of FAD

The lability of FAD was examined by slow scan rate cyclic voltammetry. Fig. 2A shows the voltammogram of 0.2 mM FAD in the presence of 3.3 mM NADH, following purging of the electrochemical cell by N_2. It should be noted that the anodic peak shape is somewhat distorted. This perhaps reflects the presence in the buffer solution of trace amounts of molecular oxygen, since at the relatively low FAD concentration used here, the electrocatalytic reduction of oxygen by $FADH_2$:

$$FADH_2 + O_2 \rightarrow FAD + H_2O_2$$

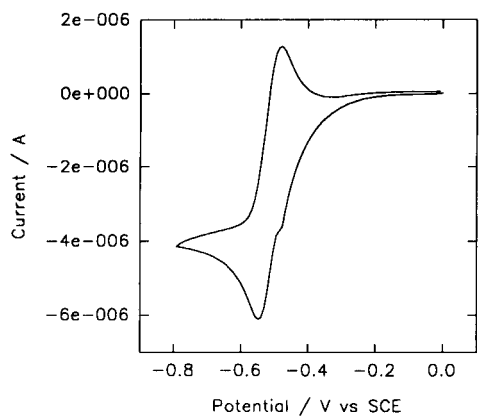

Fig. 1. Cyclic voltammogram of 2 mM FAD in Tris–HCl buffer solution (pH 7.0). Scan rate = 5 mV/s.

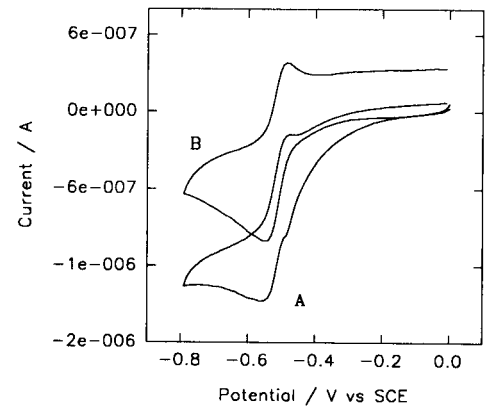

Fig. 2. (A) Cyclic voltammogram of FAD (0.2 mM) in the presence of NADH (3.3 mM). (B) As for (A) but following the addition of 28 μg of NADH oxidase. In both cases scan rate = 2 mV/s.

could be noticeable. Fig. 2B shows the effect of adding NADH oxidase (28 μg) and suggests that the enzymatically catalysed oxidation of NADH has been coupled to the electrochemical re-oxidation of $FADH_2$, following diffusion of the prosthetic group from the active site of the enzyme. Also to be noted is the straightening of the background current, which would agree with the remaining oxygen being consumed by the NADH oxidase.

Amperometric determination of NADH was attempted at 0 mV, using the re-oxidation of $FADH_2$ as the analytical signal. However, a major drawback to this approach was found to be electrode passivation, presumably due to the flavin moiety undergoing side reactions at the electrode surface. Amperometric traces gave a peaked, rather than steady-state response, while the NADH calibrations given in Fig. 3 reflected the occurrence of this passivation, with the initial NADH response (at the bare electrode) considerably higher than that for subsequent additions. Removal of oxygen from the cell caused the gradient of the linear portion of the calibration to almost double (from 0.17 to 0.42 nA μM^{-1}), again suggesting that to a large extent $FADH_2$ is re-oxidised by ambient oxygen before it can reach the electrode. These drawbacks made NADH determination by this method unrealistic and we

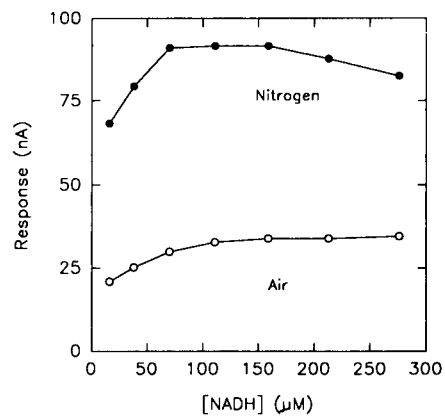

Fig. 3. Amperometric determination of NADH via the re-oxidation of $FADH_2$ at 0 mV vs. SCE, with or without deaeration with nitrogen.

therefore examined mediated electron transfer as an alternative.

3.3. Mediated electron transfer criteria

As noted in the Introduction, the direct oxidation of NADH causes poisoning of the electrode surface and would thus need to be kept to a minimum for a sensor to function effectively. Therefore when choosing possible mediators, the resulting operating potential of the electrode should be considered. We determined the oxidation potential for NADH at bare glassy carbon to be approximately +560 mV and hence the use of mediators which could be re-oxidised at below +200 mV was regarded as being unlikely to cause electrode fouling. Also to be considered is the possible electrocatalytic effect of the mediator to NADH. A mediator directly oxidising NADH, at a lower rate than the oxidase, would cause a decrease in the total analyte signal.

3.4. Electrochemistry of mediators

The electrochemistry of three quasi-reversible, water-soluble ruthenium complexes exhibiting acceptably low oxidation potentials was examined. These were hexammineruthenium(III) trichloride ($[Ru(NH_3)_6]Cl_3$), ruthenium red ($[(NH_3)_5Ru-O-Ru(NH_3)_4-O-Ru(NH_3)_5]Cl_6$) and ammonium hexachlororuthenate(IV) ($(NH_4)_2[RuCl_6]$).

$Ru(NH_3)_6^{3+}$ and $RuCl_6^{2-}$ both exhibit a single set of redox peaks, corresponding to the Ru(II/III) and Ru(III/IV) couples respectively (for Ru(II/III): $E_{1/2} = -175$ mV, $\Delta E_P = 80$ mV at 50 mV/s; for Ru(III/IV): $E_{1/2} = -80$ mV, $\Delta E_P = 155$ mV at 50 mV/s). It should be noted that once formed, $RuCl_6^{3-}$ will undergo aquation over a period of time, with substitution of the first Cl^- taking place in a few seconds [34]. Hence, the structure of the actual mediating species is unclear and for the timescale of these experiments, would probably be $[RuCl_5H_2O]^{2-}$.

Ruthenium red is a trinuclear ammine complex of the form ($Ru^{III}-Ru^{IV}-Ru^{III}$). It has been shown to undergo a series of one-electron-transfer reactions, leading eventually to the formation of ($Ru^{V}-Ru^{V}-Ru^{V}$) [35] and has been used in its higher oxidation states for water splitting [36]. Here we chose to examine the first redox couple of the molecule ($E_{1/2} = -190$ mV, $\Delta E_P = 60$ mV at 50 mV/s) corresponding to the formation of ruthenium brown ($Ru^{IV}-Ru^{III}-Ru^{IV}$).

3.5. Electrocatalytic oxidation of NADH

The possible electrocatalytic activity to NADH of each mediator and of unbound FAD was examined using amperometry. Determinations were made at the foreseen working potential of the sensor. Thus, FAD and both ruthenium ammine complexes were used at 0 mV, while for $RuCl_6^{2-}$ the electrode was poised at +150 mV. To record the maximum electrocatalytic activity expected, solution concentrations of the components were set at slightly higher values than would be used for the working sensor. Hence, mediators were present at 0.61 mM and FAD at 0.41 mM. The response to 0.82 mM NADH was measured. All determinations were made in duplicate.

As shown in Table 1, none of the components when used alone gave an increase in the rate of NADH oxidation. However, when combined with FAD, all three mediators showed some degree of electrocatalysis. Miyawaki and Wingard [37] have previously reported that when immobilised on glassy carbon, FAD lowered the overpotential for NADH oxidation by 195 mV. Hence, the electrocatalysis reported here is likely to be a solution

form of this electron-transfer, facilitated by the metal complex's interaction with the electrode:

$$NADH + FAD \rightleftharpoons NAD^+ + FADH_2$$

$$FADH_2 + 2RuL_{ox} \rightleftharpoons FAD + 2RuL_{red}$$

$$2RuL_{red} \rightleftharpoons 2RuL_{ox} + 2e^- \text{ (at the electrode)}$$

This reaction sequence is supported by the fact that steady-state rather than peaked responses were obtained. As seen earlier, this would not be the case if $FADH_2$ was directly re-oxidised at the electrode.

The electrocatalytic current produced by $FAD/Ru(NH_3)_6^{3+}$ (220 nA) was considerably greater than the uncatalysed, background value for direct NADH oxidation (18 nA) and $Ru(NH_3)_6^{3+}$ was therefore considered unsuitable for use with the enzyme. Ruthenium red and $RuCl_6^{2-}$, while both increasing the response to NADH, did so to a much lesser extent than $Ru(NH_3)_6^{3+}$ (from 18 to 40 nA and from 79 to 108 nA, respectively) and hence, both compounds were examined for coupling with NADH oxidase.

3.6. Mediated electron transfer from NADH oxidase

Coupling with the enzyme in the presence of ambient oxygen was examined using amperometry; the working electrode was poised positive of the oxidation potential of each mediator (+150 mV for $RuCl_6^{2-}$, 0 mV for ruthenium red). The final cell concentrations of enzyme, mediator and FAD are those given in the Experimental section.

Table 1
Steady-state current produced by the oxidation of 0.82 mM NADH. Electrocatalytic oxidation used mediators and extraneous FAD at 0.61 and 0.41 mM, respectively. Enzymatic oxidation used mediators FAD and NADH oxidase at 0.4 mM, 0.2 mM and 4 μg/ml respectively

Potential (mV)	Oxidant	Current (nA)
0	none	18
0	FAD	–
0	RR	–
0	$Ru(NH_3)_6^{3+}$	–
0	RR/FAD	40
0	$Ru(NH_3)_6^{3+}$/FAD	220
0	RR/FAD/Enz.	432
150	none	79
150	FAD	–
150	$RuCl_6^{2-}$	–
150	$RuCl_6^{2-}$/FAD	108
150	$RuCl_6^{2-}$/FAD/Enz.	437

– = No current increase.

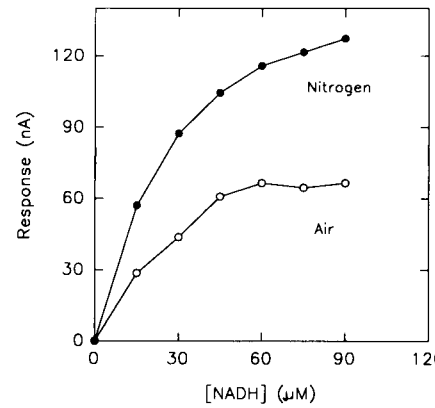

Fig. 4. Amperometric determination of NADH using the ruthenium red/ruthenium brown redox couple. Electrode poised at 0 mV vs. SCE, with or without deaeration with nitrogen.

NADH (final concentration 0.82 mM) was added to a cell containing mediator and FAD. After the electrocatalytic oxidation current had reached a steady-state, NADH oxidase was added. As seen in Table 1, for both mediators, this produced a significant current increase (up to 432 and 437 nA for ruthenium red and $RuCl_6^{2-}$ respectively). The same concentrations of mediator and FAD gave no response to approx. 770 mM H_2O_2. This suggests that these current increases were not due to electrocatalysis of H_2O_2 oxidation, but instead to the ruthenium complexes replacing oxygen as oxidant of the reduced form of NADH oxidase.

Using each mediator, the response to NADH was calibrated under both anaerobic and ambient conditions. As can be seen in Fig. 4 and Fig. 5, the removal of oxygen from the cell caused an increase in sensitivity, suggesting that neither mediator had fully replaced oxygen as electron acceptor to the enzyme.

3.7. Mediated electron transfer from interferents

When coupling an enzyme to an electron transfer mediator, it is important to consider the

effect of that mediator on other species present in the sample matrix. Hence, the possible electrocatalytic oxidation of ascorbate and urate by the ruthenium red (RR)/FAD and $RuCl_6^{2-}$/FAD systems was examined by amperometry. The extent of electrocatalysis was compared to that observed when using mediators previously reported as electrocatalytic to NADH. Theses were potassium hexacyanoferrate(III) [13], Meldola blue (MB) [4] and phenazine methosulphate (PMS) [10].

Amperometric determinations were made at 0 mV for MB, PMS and RR; at +150 mV for $RuCl_6^{2-}$ and at +300 mV for $Fe(CN)_6^{3-}$. At each potential, the response to ascorbate (0.044 mM) and urate (0.088 mM) was recorded in mediator-free buffer solution (pH 7.0) and in a buffer solution containing 0.67 mM mediator. When it was used, FAD was present at a final cell concentration of 0.44 mM. All measurements were made in duplicate.

The results are shown in Table 2. As can be seen, urate is less of an interference than ascorbate and at the concentrations used here, is only oxidised at the operating potential for $Fe(CN)_6^{3-}$ (+300 mV). When present in the cell, $Fe(CN)_6^{3-}$ caused a slight increase in the urate response (9.1%) and a far greater increase in the ascorbate response (80.4%).

The other four mediator systems only gave responses to ascorbate. The least electrocatalytic

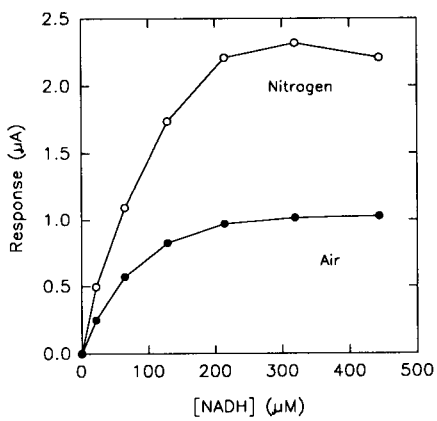

Fig. 5. Amperometric determination of NADH using the $RuCl_6^{2-}/RuCl_6^{3-}$ redox couple. Electrode poised at +150 mV vs. SCE, with or without deaeration with nitrogen.

Table 2
The effect of some mediator systems on the oxidation of 0.044 mM ascorbate and 0.088 mM urate. Mediators were present at 0.67 mM, FAD at 0.44 mM. Bracketed values give the percentage increase in oxidative current, with respect to the uncatalysed reaction

Potential (mV)	Oxidant	Current (nA)	
		Ascorbate	Urate
0	none	83	-
150	none	679	-
300	none	726	801
0	RR/FAD	173 (109%)	-
0	MB	356 (330%)	-
0	PMS	310 (275%)	-
150	$RuCl_6^{2-}$/FAD	713 (0.14%)	-
300	$Fe(CN)_6^{3-}$	1310 (80.4%)	874 (9.1%)

of these was $RuCl_6^{2-}$/FAD, which left the oxidative current virtually unchanged (0.14% difference). However, it should be noted that the unmediated current at +150 mV was itself still relatively high (679 nA). The direct oxidation current at 0 mV was considerably lower (83 nA), although the three mediators working at this potential showed a greater electrocatalytic effect. Of these, the mediator system to exhibit least ascorbate interference was RR/FAD (i_c increased to 173 nA compared with 356 and 310 nA for MB and PMS, respectively).

Two conclusions can be drawn from this experiment: Firstly, if we note the unmediated ascorbate response at +300 mV (726 nA), it is clear that the use of either RR or $RuCl_6^{2-}$ with NADH oxidase would give less interference than hydrogen peroxide detection at +650 mV. Secondly, if determining NADH via solution phase mediators, the use of NADH oxidase with RR/FAD would provide a more selective response than electroctalytic NADH oxidation by either $Fe(CN)_6^{3-}$, MB or PMS. (However, it is important to note that the adsorption of PMS and MB can significantly lower their observed oxidation potentials; in the case of MB, to −175 mV vs. SCE [38].)

3.8. Use of NADH oxidase in enzyme amplification

Enzyme amplification has been used successfully to improve the sensitivity of enzyme immunoasssays [13,39,40]. The principle, as de-

scribed by Stanley et al. [38–40], is to increase the apparent activity of the enzyme label (the "pre-amplifier"), by coupling to a "power-amplifier" stage. Previous methods of amplification have included the use of alkaline phosphatase as the label; the catalytic dephosphorylation of $NADP^+$ allowing NAD^+ to enter the regenerative cycle. The NAD^+ response has been increased by using diaphorase with ADH and hexacyanoferrate(III), via either spectrophotometric [39] or electrochemical transduction [13]. However, this approach can lack sensitivity due to a difference of 3.0 pH units between the optima of the two enzymes. A previous study has suggested that NAD^+ exhibited adequate stability at the pH optima of ADH, for a bi-enzyme response to be measured [25] and therefore the broad pH insensitivity exhibited by NADH oxidase makes it a better choice for such an amplification scheme. Here we report the construction of an NADH oxidase-based amplification system, operating by mediating electron transfer through the $RuCl_6^{2-}$/$RuCl_6^{3-}$ redox couple.

The intended reaction scheme is shown in Fig. 6. The viability of the amplification sequence was tested in the absence of alkaline phosphatase, using NADH as the trigger molecule. This was to demonstrate the scale of any possible electrocatalytic effects. At the relatively low NADH concentrations used ($< 12\ \mu M$), no current was observed for the oxidation of NADH by either direct means or via its interaction with $RuCl_6^{2-}$/FAD; nor did $RuCl_6^{2-}$/FAD show any electrocatalytic activity toward the oxidation of ethanol. Hence, in the absence of the oxidase no current was observed. As shown in the inset to Fig. 7, in the absence of ADH, an NADH calibration gave a sensitivity of 8.7 nA μM^{-1}. This compares with a value of 350 nA μM^{-1} (Fig. 6 main graph) when the same mass of oxidase was used in the presence of the other amplifier components. This increase can therefore be attributed to the regenerative sequence outlined.

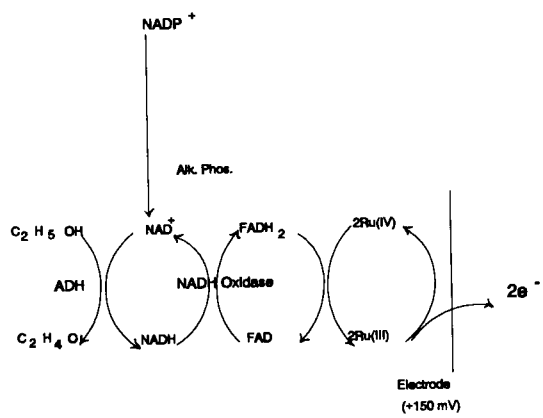

Fig. 6. Schematic diagram of enzyme amplification system. NAD^+ is produced by the enzyme label and is regenerated in the presence of excess ethanol. $RuCl_6^{3-}$ is oxidised at the electrode. ADH = Alcohol dehydrogenase; Alk.Phos. = alkaline phosphatase.

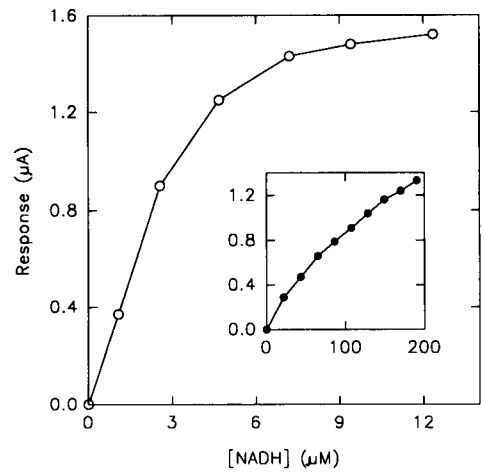

Fig. 7. Calibration of NADH at +150 mV vs. SCE using enzyme amplification. The signal is provided by the $RuCl_6^{2-}/RuCl_6^{3-}$ couple present in bulk solution. Inset: An unamplified NADH response using the same enzyme/mediator combination. Axes are the same as those given in the main figure.

3.9. Ethanol determination using an ADH / NADH oxidase bilayer

A second possible use for NADH oxidase is in the detection of the substrate of a coupled NAD^+-dependent dehydrogenase. This was illustrated by producing an enzyme bilayer responsive to ethanol.

The immobilisation of NADH oxidase was examined using both carbodiimide activation of glassy carbon and physical adsorption following

crosslinking with glutaraldehyde. Lineweaver-Burk plots were made for each electrode treatment, using $RuCl_6^{2-}$ in bulk solution to provide the analytical signal. The values for the apparent K_m and $V_m$ax were 172 μM, 0.77 μA and 66 μM, 0.22 μA, for glutaraldehyde and carbodiimide, respectively.

Michaelis-Menten experiments have previously been performed for soluble NADH oxidase, using its natural electron acceptor, oxygen [25]. Spectrophotometric and oxygen consumption data gave K'_m values of 40 and 43 μM, respectively, while H_2O_2 oxidation produced a K'_m value of 90 μM. This last value was thought to be higher due to the presence over the electrode, of a membrane to exclude direct NADH oxidation. Hence, the K'_m values reported here for the immobilised enzyme can be seen to be considerably higher than the solution value. This is as expected and can be attributed to the unstirred Nernst diffusion layer at the electrode, the possible diffusion barrier presented by any immobilised, inactive enzyme and the lower rate constant for enzyme oxidation by the mediator. Comparison between the two immobilisation procedures suggests that the glutaraldehyde method lead to a greater mass of enzyme present on the electrode, both in the active state (leading to a greater V_{max}) and inactive state (producing a greater diffusion barrier, leading to a higher K'_m).

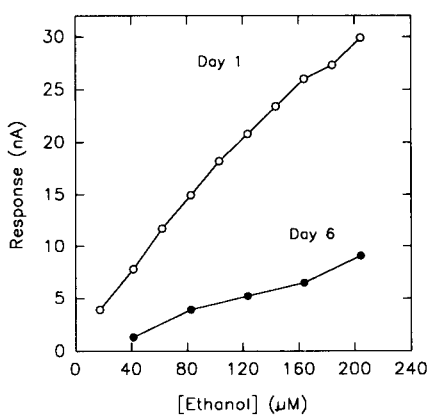

Fig. 8. Amperometric response to ethanol at 0 mV vs. SCE, using an ADH/NADH oxidase bilayer with ruthenium red present in bulk solution. Calibrations were performed once a day.

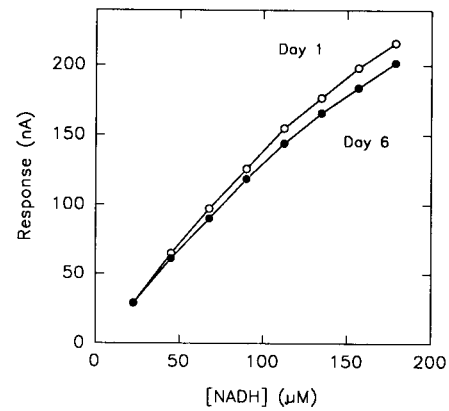

Fig. 9. Change in activity of NADH oxidase in enzyme bilayer. Monitored at 0 mV using ruthenium red in solution. Calibrations were performed once a day.

For the construction of a functioning enzyme bilayer, it is important that the activity toward NADH is higher than that toward ADH. Otherwise, changes in ethanol concentration would not be reflected in an increased response. Crosslinking was therefore chosen as the preferred form of immobilisation. To illustrate the use of the ruthenium red/brown redox couple, determinations were made at 0 mV with this mediator present in bulk solution.

After confirming the activity of an NADH oxidase layer, ADH was deposited and crosslinked. As shown in Fig. 8, ethanol responses were recorded across the range 20–200 μM. The electrode was stored in the working buffer at < 4°C and was calibrated for ethanol once a day for six days. Over the same period of time, the activity of the oxidase alone was monitored by adding NADH directly to the cell. The results, given in Fig. 9, show very little change in the NADH response over this time period, suggesting that the drop in ethanol sensitivity was due chiefly to the decrease in ADH activity.

4. Conclusions

Various methods of electrical communication with NADH oxidase, using both direct and mediated electron transfer were examined. Cyclic voltammetry indicated the lability of FAD from

this enzyme and thus the oxidation of $FADH_2$ was used as the basis for NADH measurement. However, electrode passivation made this technique impractical.

Electrochemical coupling has been observed between the enzyme and the complexes ruthenium red and $RuCl_6^{2-}$. It is interesting to note that while the Ru(II/III) couple has been used previously to mediate with enzymes such as glucose oxidase [41], sulphite oxidase [42] and horseradish peroxidase [43], this is, to the best of our knowledge, the first reported use of the Ru(III/IV) couple with an enzyme. The first redox peak exhibited by ruthenium red was very similar to the $Ru(NH_3)_6^{3+/2+}$ couple and previous work in our laboratory (unpublished results) has shown that ruthenium red can also oxidise the reduced form of glucose oxidase. However, $RuCl_6^{2-}$ showed no coupling with glucose oxidase. It should be noted that ruthenium red is the larger molecule and therefore the failure of $RuCl_6^{2-}$ to mediate cannot be attributed to steric hindrance and is more likely to be due to the difference in charge between the two complexes, since it has previously been shown that oxidases in general couple more efficiently with positively charged derivatives [44]. The coupling of $RuCl_6^{2-}$ with NADH oxidase probably reflects the greater accessibility of FAD in this enzyme, owing to its lability.

A comparison of aerobic and anaerobic calibrations for NADH, suggests that the rate constant for the reaction between reduced NADH oxidase and either mediator was significantly less than that for the reaction of the enzyme with oxygen. Clearly, one factor affecting the rate of the mediated reaction is the thermodynamic driving force provided by the electrode, that is, the difference between the redox potentials of enzyme-bound $FAD/FADH_2$ and the electron acceptor couple. In this instance, the use of a relatively high electrode potential was precluded by the need to prevent direct NADH oxidation. Thus, the main advantage of mediation here is in the lowering of the electrode response to possible interferents, rather than the removal of O_2-dependency.

NADH oxidase has previously been reported to couple with ferrocene derivatives exhibiting $E_{1/2}$ values from 70 to 280 mV vs. SCE [45]. However, its use with dehydrogenase enzymes has so far only involved hydrogen peroxide detection. Here we describe electron transfer from the enzyme to mediators of notably lower half-wave potentials ($E_{1/2} = -80$ and -190 mV vs. SCE) and report for the first time the use of a dehydrogenase/NADH oxidase system functioning by mediated electron transfer. Applications to both enzyme amplification and the stoichiometric determination of a dehydrogenase substrate, have been outlined. When immobilised with ADH, the dehydrogenase proved to be the limiting factor in sensor stability, thus emphasising the utility of thermostable enzymes for immobilisation.

Acknowledgments

The authors would like to thank the referee for helpful comments during the preparation of this manuscript; especially concerning FAD electrochemistry. We acknowledge funding from the S.E.R.C and from a European Community BRIDGE Programme [Contract No. BIOT-CR 91-0279 (RZJE)].

References

[1] H.K. Chenault and G.M. Whitesides, Appl. Biochem. Biotechnol., 14 (1987) 147.
[2] P.J. Elving, W.T. Bresnahn, J. Moiroux and Z. Samec, Bioelectrochem. Bioenerg., 9 (1982) 365.
[3] H. Jaegfelt, J. Electroanal. Chem., 110 (1983) 295.
[4] L. Gorton, J. Chem. Soc. Faraday Trans., 86 (1986) 1245.
[5] P.N. Bartlett, P. Tebbutt and R.G. Whitaker, Prog. Reaction Kinetics, 16 (1991) 55.
[6] L. Gorton, B. Persson, P.D. Hale, L.I. Boguslavsky, H.I. Karan, H.S. Lee, T. Skotheim, H.L. Lan and Y. Okamoto, in P.G. Edelman and J. Wang (Eds.), Electrocatalytic Oxidation of Nicotinamide Adenine Dinucleotide Cofactor at Chemically Modified Electrodes, Biosensors and Chemical Sensors, ACS Symp. Ser. Vol. 487, ACS, Washington, DC, 1992, pp. 56–83.
[7] W. Schuhmann and H.-L. Schmidt, in A.P.F. Turner (Ed.), Amperometric Biosensors for Substrates of Oxidases and Dehydrogenases, Advances in Biosensors, JAI Press, London, 1992, pp. 79–130.
[8] L.L. Miller and J.R. Valentine, J. Am. Chem. Soc., 110 (1988) 3982.

[9] D.C-S. Tse and T. Kuwana, Anal. Chem., 50 (1978) 1315.
[10] A. Torstensson and L. Gorton, J. Electroanal. Chem., 130 (1981) 199.
[11] K. Hajizadeh, H.T. Tang, H.B. Halsall and W.R. Heineman, Anal. Lett., 24 (1991) 1453.
[12] T. Matsue, M. Suda, I. Uchida, T. Kato, U. Akibi and T. Osa, J. Electroanal. Chem., 234 (1987) 163.
[13] M.F. Cardosi, C.J. Stanley, R.B. Cox and A.P.F. Turner, J. Immunol. Methods, 112 (1988) 153.
[14] J.J. Kulys, Biosensors, 2 (1986) 3.
[15] N.F. Atta, A. Galal, A.E. Karagozler, H. Zimmer, J.F. Rubinson and J. Mark Jr., J. Chem. Soc., Chem. Commun., (1990) 1347.
[16] M. Somasundrum and J.V. Bannister, J. Chem. Soc., Chem. Commun., (1993) 1629.
[17] E. Dominguez, H.L. Lan, Y. Okamoto, P.D. Hale, T.A. Skotheim and L. Gorton, Biosensors Bioelectron., 8 (1993) 167.
[18] E. Dominguez, H.L. Lan, Y. Okamoto, P.D. Hale, T.A. Skotheim, B. Hahn-Hagerdal and L. Gorton, Biosensors Bioelectron., 8 (1993) 229.
[19] B. Persson, H.L. Lan, L. Gorton, Y. Okamoto, P.D. Hale, L.I. Boguslavsky and T. Skotheim, Biosensors Bioelectron., 8 (1993) 81.
[20] W. Schuhmann, R. Lammert, M. Hammerle and H.-L. Schmidt, Biosensors Bioelectron., 6 (1991) 689.
[21] J.J. Kulys and E.J. D'Costa, Anal. Chim. Acta, 243 (1991) 173.
[22] J. Wang and R.L. Li, Anal. Chem., 61 (1989) 2809.
[23] J. Kulys, G. Gleixner, W. Schuhmann and H.-L. Schmidt, Electroanalysis, 5 (1993) 201.
[24] T. Ikeda, Bull. Electrochem., 8 (1992) 145.
[25] C.J. McNeil, J.A. Spoors, D. Cocco, J.M. Cooper and J.V. Bannister, Anal. Chem., 61 (1989) 25.
[26] F. Mizutani, S. Yabuki and T. Katsura, Anal. Sci., 7 (1991) 871.
[27] D.D. Hoskins, H.R. Whiteley and B. Mackler, J. Biol. Chem., 237 (1962) 2647.
[28] Y. Saeki, M. Nozaki and K. Matsumoto, J. Biochem., 98 (1985) 1433.
[29] D. Cocco, A. Rinaldi, I. Savini, J.M. Cooper and J.V. Bannister, Eur. J. Biochem., 174 (1988) 267.
[30] H-J. Park, C.O.A. Reiser, S. Kondruweit, H. Erdmann, R.D. Schmid and M. Sprinzl, Eur. J. Biochem., 205 (1992) 881.
[31] R.E. Amelunxen and A.L. Murdock, CRC Crit. Rev. Microbiol., 6 (1978) 343.
[32] R.M. Daniel, D.A.C. Cowan, H.W. Morgan and M.P. Curran, Biochem. J., 207 (1982) 641.
[33] C. Bourdillon, J.P. Bourgeois and D. Thomas, J. Am. Chem. Soc., 102 (1980) 4231.
[34] F.A. Cotton and G. Wilkinson, Advanced Inorganic Chemistry, 4th edn., Wiley, New York, 1980, pp. 917–919.
[35] R. Ramaraj, A. Kira and M. Kaneko, J. Chem. Soc. Faraday Trans. 1, 83 (1987) 1539.
[36] R. Ramaraj and M. Kaneko, J. Mol. Catal., 81 (1993) 319.
[37] O. Miyawaki and L.M. Wingard, Biochim. Biophys. Acta, 838 (1985) 60.
[38] R. Appelqvist, G. Marko-Varga, L. Gorton, A. Torstensson and G. Johansson, Anal. Chim. Acta, 169 (1985) 237.
[39] C.J. Stanley, A. Johannsson and C.H. Self, J. Immunol. Methods, 83 (1985) 89.
[40] R. Renneberg, F. Schubert and F. Scheller, Trends Biochem. Sci., (1986) 216.
[41] N.A. Morris, M.F. Cardosi, B.J. Birch and A.P.F. Turner, Electroanalysis, 4 (1992) 1.
[42] L.A. Coury, B.N. Oliver, J.O. Egekeze, C.S. Sosnoff, J.C. Brumfield, R.P. Buck and R.W. Murray, Anal. Chem., 62 (1990) 452.
[43] J.E. Frew, M.A. Harmer, H.A.O. Hill and S.I. Libor, J. Electroanal. Chem. Interface Electrochem., 201 (1986) 1.
[44] M.J. Green and H.A.O. Hill, J. Chem. Soc., Faraday Trans., 182 (1986) 1237.
[45] J.M. Cooper, PhD Thesis, Cranfield Institute of Technology, 1989.

ELSEVIER

Analytica Chimica Acta 295 (1994) 59–65

ANALYTICA CHIMICA ACTA

Fluorimetric flow-through sensor for aluminium speciation

P. Cañizares [1], M.D. Luque de Castro *

Department of Analytical Chemistry, Faculty of Sciences, University of Córdoba, 14004 Córdoba, Spain

Received 7th December 1993; revised manuscript received 25th March 1994

Abstract

A fluorimetric flow-through integrated sensor for aluminium based on C_{18} packed in a flow-cell located in a conventional spectrofluorimeter is reported. The sensor is suitable for aluminium speciation thanks to the aid of an appropriate flow-injection manifold where a modification of the Driscoll methodology based on the use of a fluorimetric reagent is accomplished in an automatic way. Three forms of aluminium (i.e., acid reactive aluminium, total monomeric aluminium, and non-labile monomeric aluminium) can be determined and two other forms (i.e., acid soluble and labile monomeric) can be calculated as the difference by injecting three sample aliquots into the continuous system and making use of an in-line ion-exchange microcolumn. The overall system is applied to aluminium speciation in different types of water.

Key words: Fluorimetry; Sensors; Flow system; Flow-through sensor; Aluminium; Speciation; Complex formation; Driscoll method

1. Introduction

Sensors allowing two or more analytes to be determined by a simple procedure are one of the challenges at present. They are technically more complex than single-parameter sensors, but also more advantageous, which justifies the endeavours devoted to them. Few multi-parameter sensors have so far been developed, however, and even fewer are actually operative, of which some are commercially available. Progress in this area is therefore highly needed. Multi-determinations based on flow-through sensors have been accomplished by: (a) using a detector capable of distinguishing the signal produced by each analyte [1,2]. This is the case for the determination of primary aromatic amines with the use of a sensor included in a diode array detector (DAD) by measuring the intrinsic absorbance of the analytes [3], or on subjecting the analyte to a chemical reaction with a sensor proposed for the determination of carbamate pesticides [4] using a DAD, or a sensor for B_6 vitamins based on derivative synchronous fluorimetry [5]. (b) By separating the analytes using an on-line coupled chromatograph. This is the case for the determination of carbaryl and its hydrolysis product [6]. Also possible is a non-chromatographic separation technique (reported here), which in turn can be preceded by a chemi-

* Corresponding author.

[1] Permanent address: Department of Analytical Chemistry, Faculty of Chemistry, UNAM, México, DF (México)

SSDI 0003-2670(94)00157-H

cal reaction. Depending on the particular approach used, multi-determinations can be performed simultaneous (which, in flow-injection analysis terms, means that two or more analytes are determined in a single injection operation [7]) or sequential (each analyte requires one injection).

The sensor reported here derives its multi-determination character from the prior discrimination carried out in the flow-injection (FI) system to which the sensor is coupled and then integrated in a conventional spectrofluorimeter. The different forms of the analyte are separated in the previous manifold, where the derivatizing reaction is also developed, and the species to be monitored reach the flow-cell where a suitable support retains the product during the time necessary to acquire the transient signal; afterwards the product is removed and sent to the waste by a suitable solution.

The significance of aluminium toxicity is now universally recognized, also by the fact that the actual toxicity depends on the chemical form in which the metal appears both in the environment and in different living organisms (plants and animals). A series of both manual and automatic methods have been published in recent years which deal with aluminium speciation [8,9]. Flow-injection analysis has hardly been described in the development of these methods. Sanz-Medel et al. [10] have reported on two FI methods for the determination of aluminium species before separation by liquid chromatography, and by using the Driscoll method [11]. Both methods are based on the reaction of the analytes with 8-hydroxyquinoline-5-sulphonic acid in micellar media to yield a strongly fluorescent compound. A FI photometric method for aluminium speciation in waters based on the Driscoll–pyrocatechol violet chelation/ion-exchange method has also been reported recently [12]. There are no flow-through sensors for aluminium speciation, but only two such devices have been reported for the determination of total aluminium. One of them is based on the use of a 8-hydroxyquinoline derivative (Kelex-100) immobilised on Amberlite XAD-7 packed in a flow-cell connected to a light source and photodetector by optical fibres [13]. The other more recent approach on which the sensor described here is based, consists of an integrated flow-through sensor in which the Al–salicylaldehyde picolinoylhydrazone fluorescent complex is retained on a support packed in the flow-cell located in a conventional spectrofluorimeter [14]. The method here proposed takes advantage of the separation model described by Driscoll to discriminate between the different forms of aluminium. The use of both a fluorimetric reagent and retention of the reaction product, which constitute the proposed innovation, were aimed to improve sensitivity.

1.1. Principle of speciation

Among the number of fractionation procedures developed over the last decade to operationally distinguish between the various aqueous forms of aluminium the most popular procedure is the so-called "Driscoll methodology" [13]. This fractionation scheme directly measures three aluminium fractions in waters: acid reactive aluminium (Al_r), total monomeric aluminium (Al_{Tm}) and non-labile monomeric aluminium (Al_n). From these measurements, two more fractions can be calculated: "acid soluble" aluminium (Al_a), from $Al_r - Al_{Tm}$, and "labile monomeric" aluminium (Al_l), from $Al_{Tm} - Al_n$.

2. Experimental

2.1. Instruments and apparatus

A Perkin-Elmer 150 MPF-44A spectrofluorimeter, equipped with a Knauer recorder and a Hellma 178.12QS flow-cell (18 μl inner volume) was used. A Gilson Minipuls-2 4-channel peristaltic pump, four Rheodyne 5041 injection valves, one of them acting as selecting valve, and 0.5 mm i.d. PTFE tubing were used to construct the flow manifold.

The ion-exchange microcolumn was made using a 3 mm i.d. PTFE tube packed with Amberlite IR-120 plus from Sigma. The ends of the microcolumn were filled with glass-wool and small

fragments of Technicon filter to avoid the loss of resin from the PTFE tube.

2.2. Reagents

The salicylaldehyde picolinoylhydrazone (SAPH) was synthesized according to the procedure proposed in Refs. [16–18] and 40% ethanol–water solutions were prepared at the required concentration. Stock aqueous solution of aluminium(III) (1.000 mg ml^{-1}) was prepared from $Al(NO_3)_3 \cdot 9H_2O$ (Merck). 1.0 M acetic acid–sodium acetate buffer (Merck) of different pH values was used. SP-Sephadex, Amberlite IR-120 plus, Dowex-50W (50 × 4-100), CM-Sephadex (Sigma) and XAD-2 and XAD-7 (Serva) ion-exchange materials and C_{18} 60–100 μm (Waters Sep-Pak) were also used. All chemicals were analytical reagent grade and deionized water was used throughout this study.

2.3. Material and cleaning

Sample collection, storage and preparation of sample and reagent solutions were done in polyethylene containers (Aldrich), which are widely used to store environmental and trace component samples. All vessels were decontaminated by soaking in 10% HNO_3 for 48 h followed by rinsing five times with Ultrapure water and filling with Ultrapure water until further use [19].

2.4. Manifold and procedure

The manifold shown in Fig. 1 was used for sequential speciation of aluminium, which was implemented as follows:

For total monomeric aluminium (Al_{Tm}), 500 μl of sample was injected into a 0.1 M NaCl carrier solution which merged with the SAPH stream and the fluorescent complex was formed along reactor r_3. After monitoring (λ_{ex} = 382 nm, λ_{em} = 468 nm) the signal provided by the complex retained on the C_{18} material packed in the flow-cell, the product was removed from the support by 200 μl 2 M HCl which was injected in the continuous system via injection valve IV_3.

The non-labile monomeric aluminium (Al_n)

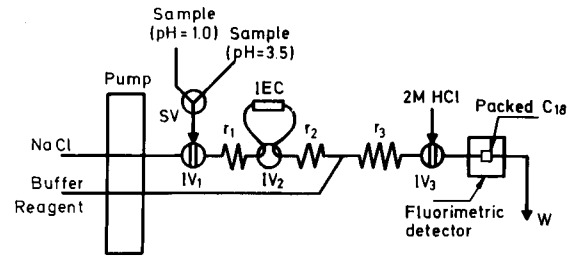

Fig. 1. Manifold for aluminium speciation by use of the Driscoll method and a flow-through sensor. SV = Switching valve; IV = injection valve; r = reactor; IEC = ion-exchange column; W = waste.

was determined by injecting 500 μl of sample as above but keeping injection valve IV_2 in the load position; the sample passed through the ion-exchange microcolumn where positively-charged species were retained. Only negative and neutral species reached reactor r_2 and merged with the reagent to yield the complex as above. After retention and once the non-retained forms had passed through the column, IV_2 was switched and a 0.5 M acetic acid–sodium acetate stream eluted the retained species in the opposite direction and sent them to waste. Increased compactness of the ion-exchange material in the microcolumn was thus avoided. IV_2 remained in the filling position until the next determination of Al_n.

Determination of acid reactive aluminium (Al_r) requires prior adjustment of the sample at pH 1 and leaving it for 1 h. The pH was subsequently changed to 6 by adding NaOH and the procedure for total monomeric aluminium was followed.

The other two forms of aluminium are calculated as the difference.

3. Results and discussion

Preliminary studies were aimed to complete the information contained in Ref. 14. These studies showed that the fluorimetric derivatization reagent is capable to react with any form of monomeric aluminium except with hydroxy species, as the analytical signal provided for a given amount of analyte remained unchanged in

the presence of sulphate, fluoride, cyanide, chloride, etc. [14–16] at pH < 4 and > 9, but decreased for free aluminium between these values.

The performance of the overall system was optimized by grouping the variables affecting the results into four groups: (a) chemical variables characteristic for the derivatizing reaction (type, pH and concentration of the buffer solution, sample pH, and concentration of the reagent); (b) FI variables such as flow-rate, coil length and injected volume; (c) characteristics of the flow-through sensor (type and level of the support packed in the flow-cell, sensor regeneration and focusing lenses to increase the sensitivity); (d) in-line ion-exchange separation (cleaning and conditioning, column length, flow-rate and type of eluent).

According to the literature, the use of an acetic acid–sodium acetate buffer provided the maximal formation of the Al–SAPH complex. Variation of the concentration (between 0.2 and 1.0 M) and pH (between 4 and 8) of the buffer showed that a 0.5 M solution of pH 5.0–5.5 provided the highest signal. The sample was conditioned by using this buffer in order to prevent the presence of a parasitic signal owing to changes in the sensor support compactness.

The concentration of hydrazone was studied in the range 0.0125 to 0.0350% (w/v) in 20, 40 and 60% ethanol–water mixtures. The highest signal obtained without appearance of a double peak was provided by a 0.0250% (w/v) solution of SAPH in 40% ethanol.

The function of reactors r_1 and r_2 was only to stabilize the plug profile before and after passage through the microcolumn in order to achieve a reproducible retention and mixing with the reagent stream, respectively. Afterwards the derivatizing reaction took place. The lengths of r_1 and r_2 were 30 and 40 cm, respectively, whereas r_3 was 400 cm long in order to achieve an optimum reaction using a flow-rate of 1 ml min^{-1}. This last variable was assayed between 0.8 and 1.6 ml min^{-1}.

An increase of the volume of injected sample did increase the analytical signal but decreased the sampling frequency. A volume of 500 μl was chosen as a compromise between sensitivity and sample throughput.

The different supports assayed in the preliminary study which yielded some retention of the Al–SAPH complex were exhaustively checked in order to select the support that provides both a suitable retention and a fast elution. Some anionic ion-exchange materials such as Dowex and Sephadex provided partial retention, but further removal was very slow. C_{18} bonded silica beads with a suitable mesh size (60–100 μm) were the best support to avoid overpressure shortcomings. This material provided an acceptable fluorescence baseline, and a transient signal which was at least twice higher than that obtained by use of the ion-exchange materials.

The level of C_{18} in the flow-cell was a critical variable, with an optimum value of 9 mm, corresponding to the height at which the light beam passes through the cell. When the packed material bed was higher, the complex was retained in the resin lying above the light beam; with lower levels the light beam passed through the solution only.

The pH and ionic strength of the regenerating solution was optimized after checking the use of chloric acid solutions as the best eluting agent. The presence of an electrolyte (NaCl and K_2SO_4) was checked in order to achieve minimal change in compactness of the packed material in the measurements/regeneration steps. A 2 M HCl + 1 M K_2SO_4 solution was selected as the best eluting solution to achieve quantitative removal of the complex on passage of the solution through the cell without changes in the compactness of the packing. A volume of 200 μl was sufficient for this quantitative removal.

The use of a lens to focus the excitation radiation to the packed cell increased the signal obtained by avoiding loss of light from the lamp. Two types of lenses, a concave and a biconcave one, were located at different distances from the source. The maximal gain of sensitivity (36% higher signal than without a lens) was obtained by locating a concave lens at 4 cm from the source.

Amberlite IR-120 plus cation-exchange resin was used for preparing the microcolumns by packing it in PTFE tubes of 3 mm i.d. and differ-

ent lengths. The resin, in its sodium form, was washed with 3 ml of 1 M HCl, then with 1 M NaCl until the pH of the effluent was 5.5, and finally conditioned by passing a NaCl solution with the same conductivity and pH as the sample to be treated until the pH of the effluent was equal (± 0.2) to that of the sample.

A 5-cm microcolumn was in its optimum form when it enabled a suitable Al exchange at low flow-rate (1 ml min^{-1}). This was also the optimum flow-rate for the Al–SAPH complex formation in the continuous manifold.

3.1. Features of the method

Aluminium standard solutions with concentrations between 10 and 200 ng ml^{-1} were prepared and injected in triplicate in order to establish the features of the method for both the total monomeric and acid-reactive aluminium. Table 1 summarises the results obtained and also those of the repeatability study which was carried out using 11 samples of 35 ng ml^{-1}, injected in triplicate, for both forms of aluminium.

The study was performed by determining the total monomeric aluminium first and then the non-labile monomeric aluminium by passage of the injected sample through the column. The labile monomeric aluminium was calculated as the difference.

3.2. Performance of the ion-exchange column

The repeatability of the ion-exchange process was evaluated by using 11 aqueous aluminium samples of 100 ng ml^{-1} in the presence of 4000 ng ml^{-1} oxalate. The average value of total monomeric aluminium was 69.3 ng ml^{-1} and that of non-labile monomeric aluminium was 37.0 (6.7% R.S.D.).

Table 1
Features of the calibration curves

Parameter	Total monomeric aluminium	Acid reactive aluminium
Intercept (RF) [a]	0.58	0.65
Slope (RF ng^{-1} ml)	0.1	0.1
Correlation coefficient	0.9995	0.9995
Linear range (ng ml^{-1}) [b]	0–200	0–50
R.S.D. (%)	6.7	5.8

[a] Relative fluorescence.
[b] Detection limit (3σ): 3 ng ml^{-1}.

Table 2
Influence of the concentration and type of the organic ligand

Ligand (ng ml^{-1})	Al_{tm} (ng ml^{-1})	Al_n (ng ml^{-1})	Al_l (ng ml^{-1})
Oxalate			
50	97	4	93
100	99	4	95
200	100	5	95
300	98	4	94
600	104	8	95
2000	72	24	48
4000	67	46	22
Citrate			
50	100	5	95
100	97	4	92
300	89	4	85
600	85	8	77
2000	15	6	9
4000	10	5	5
Acetylacetone			
100	99	4	95
300	84	5	79
600	80	4	76
4000	79	4	75

3.3. Non-labile monomeric aluminium

The presence of organic compounds able to form neutral or anionic complexes with aluminium was evaluated by passage of the sample through the exchange column. The equilibrium of the complex formation was reached in less than 30 min at pH 6.0. Longer analyte–ligand contact time yielded similar results. A study was accomplished by use of 100 ng ml^{-1} aluminium and different organic ligands (oxalate, citrate and acetyl acetonate) at several concentrations. Table 2 shows the results found. When the complexed aluminium passed through the column it merged with SAPH. The displacement reaction took place to a different extent depending on the Al to organic ligand ratio and the stability constant of the complex when compared with the Al–SAPH complex. When the organic compound to aluminium ratio and/or the formation constant were

Table 3
Comparison of the speciation of aluminium in waters by the proposed method with the overall determination by atomic absorption spectrometry (AAS)

Water	pH	AAS	Al_{tm}	Al_r	Al_a	Al_n	Al_l
Bottled							
Rosal	7.6	2	1	2	0	-	-
Mandariz	6.7	10	6	7	0	-	-
Tap							
Córdoba	7.1	9	8	11	2	-	-
Alcolea	7.4	20	10	17	7	-	-
Spring							
Valencia	7.5	7	5	6	0	-	-
Well							
Alcolea	7.7	34	28	30	2	-	-
River							
Casariche	7.9	80	90	95	5	-	-
River + 1 $\mu g\ ml^{-1}[Ox^{2-}]$			66			12	55
River + 1 $\mu g\ ml^{-1}[Cit^{3-}]$			57			8	49
River + 1 $\mu g\ ml^{-1}[Ox^{2-}]$ + 1 $\mu g\ ml^{-1}[Cit^{3-}]$			28			16	12

The concentration of the analyte is expressed in ng ml^{-1} in all instances.

high, part of the aluminium did not undergo the derivatizing reaction. Due to the fact that the derivatizing reagent was unable to displace these organic ligands. Therefore, it was not included in the analytical result.

3.4. Analysis of water samples

The method was applied to the speciation of aluminium in bottled, tap, well, fresh and river water. The results obtained by the proposed flow-through sensor are given in Table 3, which also shows the values obtained by atomic absorption (Perkin-Elmer Model 1100B spectrometer with an HGA-700 graphite furnace and an AS-70 autosampler). Table 3 shows that there is no non-labile monomeric aluminium in the sample, and the results obtained by the proposed and the atomic absorption method agree within ca. 10%. When organic ligands are added to the sample, a decrease in aluminium is found, as was predicted by the data in Table 2.

4. Final remarks

The method reported here is an example of sample manipulation in an automatic continuous way prior to the use of a flow-through sensor. A series of chemical steps is developed before the sample reaches the sensing device: pH change, ion-exchange separation and derivatization which enable the analytes to have the suitable form for detection. In addition the sensor is automatically regenerated by switching an injection valve; and the ion-exchange microcolumn is also regenerated automatically by use of the most appropriate way to avoid changes in compactness. An alternative to the difficult task of designing specific sensors and/or multisensors is therefore the sample manipulation before the analytes are transported to the sensor in the form that provides an unequivocal response.

Acknowledgments

Dirección General de Investigación Científica y Técnica (DGICyT) is thanked for financial support. One of the authors (P.C.) expresses her gratitude to Dirección General de Asuntos del Personal Académico, DGAPA, of UNAM (México). This work was done under the Agreement between UNAM and Córdoba University.

References

[1] M. Valcárcel and M.D. Luque de Castro, Flow-Through (Bio)chemical Sensors, Elsevier, Amsterdam, 1994.
[2] M.D. Luque de Castro and M. Valcárcel, Flow-through (Bio)Chemical Sensors in Environmental Analysis, in Quality Assurance of Environmental Analysis, Elsevier, Amsterdam, 1994.
[3] B. Fernández-Band, F. Lázaro, M.D. Luque de Castro and M. Valcárcel, Anal. Chim. Acta, 229 (1990) 177.
[4] B. Fernández-Band, M.D. Luque de Castro and M. Valcárcel, Anal. Chem., 63 (1991) 1672.
[5] D. Chen, M.D. Luque de Castro and M. Valcárcel, Anal. Chim. Acta, 261 (1992) 269.
[6] M.T. Tena, M.D. Luque de Castro and M. Valcárcel, J. Chromatogr. Sci., 30 (1992) 276.
[7] M.D. Luque de Castro and M. Valcárcel, Trends Anal. Chem., 5 (1986) 71.
[8] P.G.C. Campbell, M. Bisson, R. Bougie, A. Tessier and J.P. Villeneuve, Anal. Chem., 55 (1983) 2246.
[9] P.M. Bertsche and M.A. Anderson, Anal. Chem., 61 (1989) 535.
[10] J.I. García Alonso, A. López García, A. Sanz-Medel, E. Blanco González, L. Ebdon and P. Jone, Anal. Chim. Acta, 225 (1989) 339.
[11] B. Fairman and A. Sanz-Medel, Int. J. Environ. Anal. Chem., 50 (1993) 161.
[12] J.M. Quintela, M. Gallego and M. Valcárcel, Analyst, 118 (1993).
[13] M.R. Pereiro, M.E. Diaz-García and A. Sanz-Medel, Analyst, 115 (1990) 575.
[14] P. Cañizares, M.D. Luque de Castro and M. Valcárcel, Anal. Lett., 27 (1993) 247.
[15] C.T. Driscoll, J.P. Baker, J.J. Bisogni and C.L. Schofield, Nature, 284 (1980) 161.
[16] M. Gallego, M. García-Vargas and M. Valcárcel, Analyst, 108 (1983) 92.
[17] M. Gallego, M. García-Vargas and M. Valcárcel, Microchem. J., 24 (1979) 143.
[18] M. Gallego, M. García-Vargas and M. Valcárcel, Analyst, 104 (1979) 613.
[19] M. Wilhelm and F.K. Ohnesorge, J. Anal. Toxicol., 14 (1990) 206.

ELSEVIER

Analytica Chimica Acta 295 (1994) 67–72

ANALYTICA CHIMICA ACTA

Detection of cadmium ion using the fluorescence probe Indo-1

T. Vo-Dinh [a,*], P. Viallet [b], L. Ramirez [a], A. Pal [a], J. Vigo [b]

[a] *Advanced Monitoring Development Group, Health and Safety Research Division, Oak Ridge National Laboratory, Oak Ridge, TN 37831-6101, USA*

[b] *Physical Chemistry Laboratory, University of Perpignan, Perpignan 66860, France*

Received 15th November 1993; revised manuscript received 14th March 1994

Abstract

Fluorescence probes for biosensors used for the determination of intracellular concentration of metal ions have been synthesized in order to bind selectively with a specific cation. Since certain ions exhibit similar chemical properties, binding selectivity with the probes is difficult. In this paper we describe for the first time the interaction between Indo-1, a fluorescence probe representative of a family of "specific chelating compounds" (mainly used for calcium) with the cadmium ion. The fluorescence properties of the cadmium complex are described and a method is proposed to determine the concentrations of both calcium and cadmium ions in aqueous solutions.

Key words: Biosensors; Fluorimetry; Cadmium; Indo-1

1. Introduction

Fluorescence calcium-sensitive probes for biosensors seem particularly well adapted to monitor intracellular calcium levels, which is one of the challenges of modern cell biology. In previous studies, the chemical structure of ethyleneglycol-bis(β-aminoethyl ether)-*N*,*N*,*N*′,*N*′-tetraacetic acid (EGTA), a non-fluorescent calcium chelator was used as a basis for the synthesis of some fluorescent analogues. The first fluorescence calcium indicator was 2-{[2-(bis-(carboxymethyl)amino)-5-methylphenoxyl]methyl}-6-methoxy-8-[bis-(carboxymethyl)amino]quinoline (Quin 2) designed by Tsien [1]. Calcium binding leads to an increase in fluorescence intensity of this compound but its use in living cells remains limited. Other types of fluorescent calcium indicators [2] include 1*H*-indole-6-carboxylic acid, 2-[4-bis-(carboxymethyl) amino]-3{2-[2-(bis-carboxymethyl)amino-5-methylphenoxy]ethoxy}phenyl (Indo-1) and 1-[2-(5-carboxyazol-2-yl)-6-amino]-benzofuran-5-oxyl-2(2′-amino-5′-methylphenoxy)-ethane-*N*,*N*,*N*′,*N*′-tetraacetic acid (Fura 2). Some of the spectral characteristics of these new calcium probes were examined and their calcium

* Corresponding author.

SSDI 0003-2670(94)00164-H

binding constants at pH 7.0–7.2 were determined using EGTA as a calcium buffer.

The physicochemical properties of Indo-1 and Fura 2 have been recently reviewed [3–5]. It has been clearly demonstrated that the respective fluorescence spectrum of these compounds exhibits characteristic spectral shifts when the pH values of the sample solution changes. Such shifts have been interpreted in terms of deprotonation of the carboxylic groups of Indo-1 and Fura 2. Two acidity constants have been evaluated for these compounds.

Since the latter pK_a value is in the range of biological pH values, it has been suggested that a practical use of the Indo-1 spectroscopic properties would allow the simultaneous determination of pH and Ca^{2+} in biological fluids [3–5].

Moreover it has also been demonstrated that both Indo-1 and Fura 2 are able to bind to proteins, resulting in a shift of their respective fluorescence spectrum. A detailed analysis of the results leads to the conclusion that the interactions of Indo-1 respectively with Ca^{2+}, H^+ and proteins are mutually exclusive so that they can be modeled as indicated in the inset of Fig. 1.

As it is shown in Fig. 1, the fluorescence spectra of L (ligand), LH (ligand and hydrogen), LCa (ligand and calcium), and LP (ligand and protein) are structureless and strongly overlap each other. With such spectra, a powerful computational method developed for spectral resolution [6] was successfully used to allow a quantitative resolution of a complex experimental spectrum of Indo-1 into the above mentioned components. Unfortunately such a technique cannot be used with the excitation spectra of the different forms of Fura 2 because the excitation spectrum of LP is practically identical to the one of L [5]. Such a result explains why we have concentrated our work on Indo-1 only. Moreover, other metal ions could also form complexes with Indo-1, thus limiting the use of this agent as a selective probe for calcium ions.

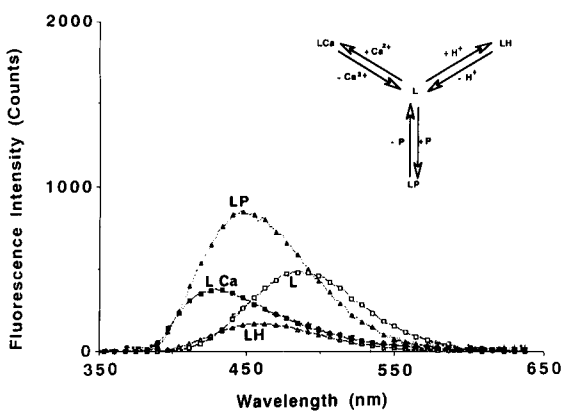

Fig. 1. Respective fluorescence spectrum of L (ligand, viz., Indo-1), LH (ligand + hydrogen), LCa (ligand + calcium), LP (ligand + protein). See text for further discussion. $\lambda_{exc} = 340$ nm.

All these problem areas contribute to make intracellular determination of the ion calcium using Indo-1 a challenging goal. The concentrations of the transition elements inside living cells are generally so low that they are not expected to affect the measurements significantly. Unfortunately, this might not be the case for people exposed to polluted environments containing large concentrations of these elements such as workers in some metal processing plants or paint production plants. In these cases, even relatively low levels of these elements in the working atmosphere may result in intracellular accumulation in specific organs due to the long term exposure.

As a first contribution to the problem of exposure to multiple chemical agents, a study of the complexation of cadmium ion with Indo-1 in the presence of calcium ion has been conducted. Cadmium ion is of specific importance since in vitro studies have shown that it was able to link with biological molecules such as calmodulin [7,8]. Moreover, it has been demonstrated on living cells that cadmium chloride is a mutagenic compound which may act as an inducer of the heme oxygenase messenger RNA [9–11] or can increase the synthesis of a protein suspected to be one of the heat shock proteins [12]. The shape of the fluorescence spectrum of the Cd–Indo-1 complex has been compared with that of the Ca–Indo-1 complex and a method is proposed for simultaneous determination of calcium and cadmium concentrations in samples using the Indo-1 probe. This is, to the best of our knowledge, the first report on the use of the Indo-1 probe for the detection of cadmium ions.

2. Materials and methods

2.1. Chemicals

Indo-1 (pentapotassium salt) was purchased from Molecular Probes. Stock solutions (10^{-3} M) were prepared by adding 1.0 ml of water to 1 mg of the probe. The mixture was stirred in the dark for 45 min to achieve complete solubilization. Stock solutions were kept at −5°C in the dark and stirred in the dark for 5–10 min at room temperature before each use in order to minimize the self-aggregation process of Indo molecules in the solution stored at low temperature.

Ethylenediaminetetraacetic acid (EDTA) disodium salt was purchased from Fisher Scientific (purity ≈ 100%) and was used at a concentration of 2×10^{-3} M.

Calcium chloride and cadmium chloride were purchased from MC and Alfred Chemicals, respectively. Although great care was exercised to use purified water, an average background (residual) calcium concentration in the range of 10^{-6} M was observed in the water (Millipore, Milli-Q) used in all experiments.

2.2. Procedure

Fluorescence measurements were performed at Oak Ridge National Laboratory using a Perkin-Elmer fluorimeter, Model LS-50. All fluorescence spectra were recorded between 350 and 600 nm using an excitation wavelength of 325 nm except when differently specified. All calculations for the numerical resolution of fluorescence spectra were performed using a Victor 386 AT computer and software programs developed at the University of Perpignan.

3. Results and discussion

3.1. Fluorescence spectrum of the Cd–Indo-1 complex

In order to avoid any complication resulting from a partial protonation of Indo-1, the characteristic fluorescence spectrum of the Cd–Indo-1 complex was recorded under the following experimental conditions. A large excess of cadmium chloride was progressively added to a solution having 2.38×10^{-6} M of Indo-1 at pH 8. After verification that no variation in the pH value occurred, the fluorescence spectrum was recorded and the process was repeated until any other addition of cadmium ion did not modify the shape and the intensity of the fluorescence spectrum. This fluorescence spectrum is shown in Fig. 2, curve 1. It can be compared with the characteristic fluorescence spectrum of the Ca–Indo-1 complex recorded under the same experimental conditions (Fig. 2, curve 2). Although both spectra exhibit peak maxima approximately at the same wavelength, they differ sufficiently in shape so that one can use these spectra to differentiate the complexes in a mixture. The spectra profile of LCa is far less symmetric than that of LCd. As the result the mathematical expression of these spectra are sufficiently different to be successfully used for mathematical differentiation. It is note-

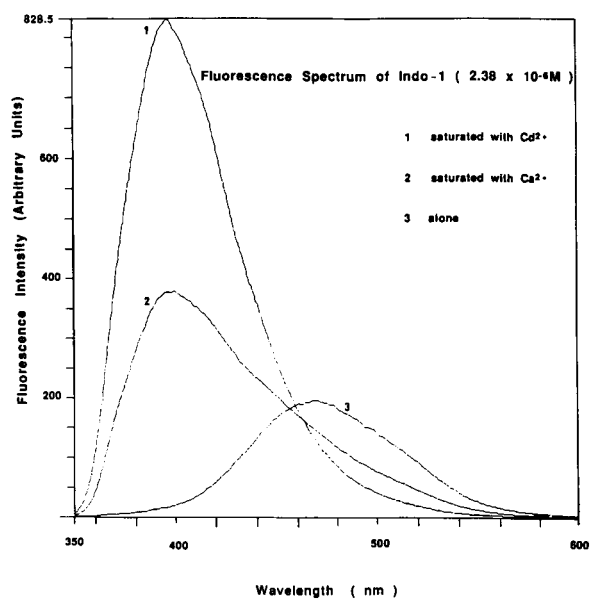

Fig. 2. Fluorescence spectrum of (1) Cd–Indo-1 complex (LCd), (2) Ca–Indo-1 complex (LCa), (3) free Indo-1. Experimental conditions: pH 8; $\lambda_{exc} = 325$ nm.

worthy that the quantum yield of the Cd–Indo-1 complex (LCd) is larger than that of the Ca–Indo-1 (LCa). The ratio of the intensities at 400 nm shown in Fig. 2 (curve 1 for LCd; curve 2 for LCa) indicates that the quantum yield of LCa is 2.25 fold larger than that of LCa. For comparison the fluorescence spectrum of a solution containing the same concentration of Indo-1 with no cation is also depicted in Fig. 2, curve 3. In order to avoid any distortion of this spectrum due to possible residual Ca ion in the water used for the experiments, an excess of EDTA was added to the Indo-1 solution. It is of interest to point out that the fluorescence intensity of this spectrum (Indo-1 alone) is negligible around 400 nm where the other two spectra (of Ca–Indo-1; Cd–Indo-1) exhibit maximum intensity at this wavelength.

3.2. Calibration graphs

In accordance with the previous results, the wavelength at 400 nm was used to monitor the variation of the fluorescence intensity with the cadmium ion concentration in a solution containing an excess of Indo-1. Curve B of Fig. 3 shows

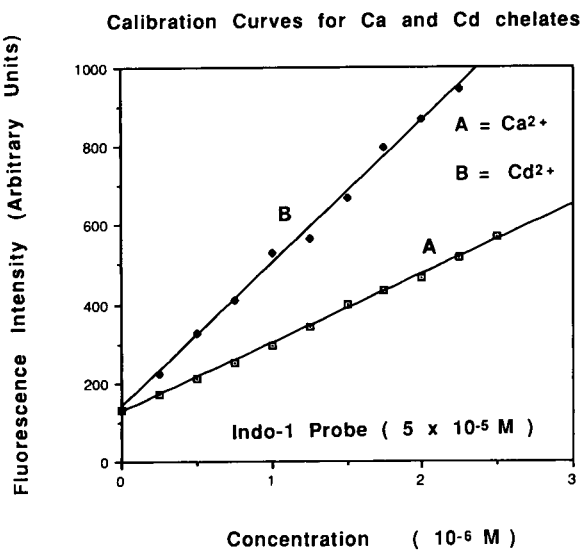

Fig. 3. Calibration curves for calcium (curve A) and cadmium (curve B) chelates. Experimental conditions: pH 8; $\lambda_{exc} = 325$ nm; $\lambda_{em} = 400$ nm. Curve A: $y = 174.38x + 126.40$, $r^2 = 0.998$. Curve B: $y = 362.48x + 138.89$, $r^2 = 0.996$.

that this variation is linearly related to cadmium ion concentration. It is noteworthy that the background fluorescence intensity (recorded at zero concentration of cadmium ion) is not negligible.

This background fluorescence was assumed to be due to Ca–Indo-1 complexes resulting from the presence of calcium ion in the water used for the experiments. Fluorescence intensity measurements at 400 nm (i.e., at the same wavelength when calcium chloride was added to a separate sample) result in plot A, which assumes by extrapolation that the initial value of the calcium ion concentration (originally present in water) is around 1×10^{-6} M. The linearity of both plots A and B indicates that the Cd–Indo-1 complex is a 1:1 complex as with the Ca–Indo-1 complex.

3.3. Competitive binding between calcium and cadmium ions with Indo-1

Due to the high affinity of Indo-1 for calcium and to the high sensitivity of fluorescence techniques, it is quite difficult to obtain water having such a purity that Indo-1 does not react to the presence of residual traces of calcium in it. So taking into account the fact that the dissociation constant of the Ca–Indo-1 complex has been recently reevaluated, the complexation of cadmium ion by Indo-1 was determined as follows. Small amounts of a solution of cadmium chloride (10^{-4} M) were successively added to a solution containing 2.38×10^{-6} M of Indo-1 and the fluorescence spectrum was recorded after each addition (Fig. 4).

Taking into account that free Indo-1 does not significantly contribute to the emission of fluorescence at 400 nm, a plot of the fluorescence intensity at 400 nm versus the concentration of cadmium ion will illustrate the competition between the ions calcium and cadmium. Such a "quantitative analytical curve" (Fig. 5) can then be used to evaluate the cadmium concentration in a solution prepared with water containing the same initial concentration in calcium. The data show that concentrations in cadmium ion lower than 10^{-7} M can be detected even in presence of 10^{-6} M of calcium. It is noteworthy that the level of calcium in cells is generally lower than 10^{-6} M. Analysis

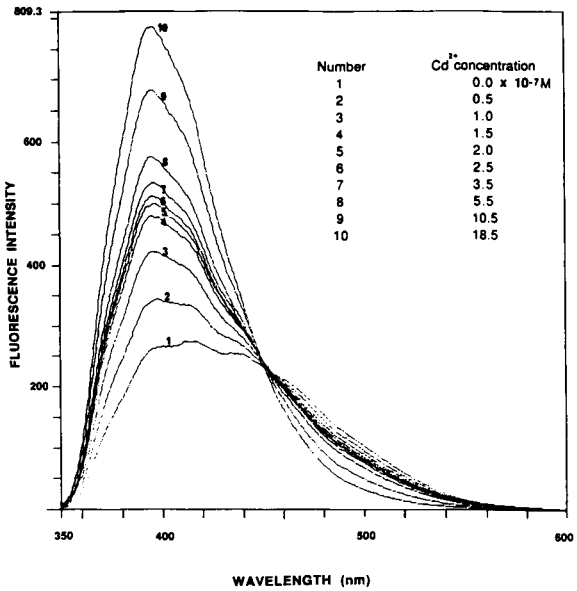

Fig. 4. Variation of the fluorescence spectrum of a solution of Indo-1 (2.38×10^{-6} M) upon addition of Cd^{2+}.

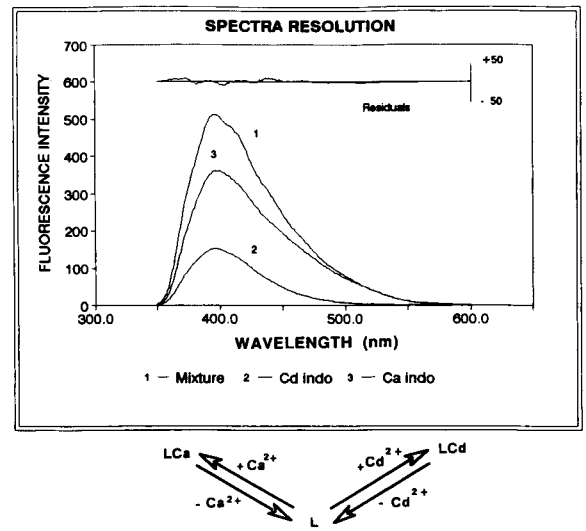

Fig. 6. Example of resolution of the fluorescence spectra displayed on Fig. 4. Curve 1 = curve 7 from Fig. 4; curve 2: contribution of Cd–Indo-1 to the whole fluorescence spectrum (30.6%); curve 3: contribution of Ca–Indo-1 to the whole fluorescence spectrum (69.8%).

of the "raw" data cannot determine the difference in the quantum yield of these complexes. Nevertheless, this "first-order" direct treatment of the data will be useful only for these specific experimental conditions; it is far better to use a more sophisticated treatment of the data.

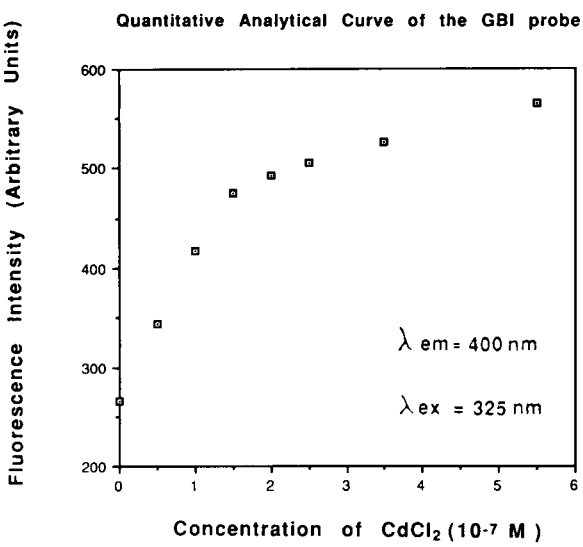

Fig. 5. Quantitative analytical curve of the gel-based Indo (GBI) probe for cadmium Experimental conditions: pH 8; $\lambda_{exc} = 325$ nm; $\lambda_{em} = 400$ nm.

Improved data treatment can be achieved using an original method of resolution of complex fluorescence spectra into their components. This method, which was described previously [6] is capable of resolving the spectra of various mixtures displayed in Fig. 4 using the spectra of individual components (in Fig. 2) in order to provide the relative amount of free Indo-1, Ca–Indo-1 and Cd–Indo-1 complexes in the mixture. An example of the capability of the mathematical procedure for the spectral resolution is presented in Fig. 6. The efficiency of the spectral resolution is assessed by different statistical tests such as chi square, weighted residuals and matrix conditioning [6]. In this example the fluorescence of a mixture containing Ca and Cd ions in an Indo-1 solution (Fig. 6, curve 1) can be decomposed into the two fluorescence spectra of Cd–Indo-1 (curve 2) and Ca–Indo-1 (curve 5). In this example the contribution of free Indo-1 to the whole fluorescence spectrum has been found negligible, especially for cadmium concentrations higher than 1.5×10^{-7} M.

4. Conclusions

The development of chelating agents used as probes specific to metal ions with close physicochemical properties is an important but challenging goal. This is particularly true for ions that belong to the same row of the transition elements as well as for ions that possess the same net charge and the same coordination index. In general, the value of the dissociation constants of these chelates are in the same range of magnitude and the specificity comes from other properties such as the absorption or emission spectra. So it is not surprising that the behavior of cadmium with Indo-1 is similar to that of calcium. Since these ions are diamagnetic, it can be also expected that both form fluorescent complexes with Indo-1 and that these spectra are not very different. Our experiments have verified the above hypothesis. In spite of the similarity of the spectra of Cd–Indo-1 and Ca–Indo-1 complexes, using our numerical resolution of complex fluorescence spectra, we have been able to evaluate both the concentrations of calcium and cadmium of an aqueous solution, even for relatively low cation concentrations.

Acknowledgments

This research was sponsored by the U.S. Department of Energy, Office of Health and Environmental Research under Contract DE-AC05-84OR21400 with Martin Marietta Energy Systems, Inc. and the ORNL Laboratory Directed Research and Development Fund. L. Ramirez acknowledges the support of a post-doctoral fellowship from the Oak Ridge Associated Universities. P. Viallet and J. Vigo acknowledge the financial support from the French CNRS Foundation.

References

[1] R.Y. Tsien, Biochemistry, 19 (1980) 2396.
[2] G. Grynkiewicz, M. Poenie and R. Tsien, J. Biol. Chem., 260 (1985) 3440.
[3] F. Bancel, J. Vigo, J.M. Salmon and P. Viallet, J. Photochem. Photobiol. A, Chemistry, 53 (1990) 397.
[4] F. Bancel, J.M. Salmon, J. Vigo and P. Viallet, Cell Calcium, 13 (1992) 59.
[5] F. Bancel, J.M. Salmon, J. Vigo, T. Vo-Dinh and P. Viallet, Anal. Biochem., 231 (1992) 204.
[6] J.M. Salmon, J. Vigo and P. Viallet, Cytometry, 9 (1988) 25.
[7] S.H. Chao, Y. Suzuki, J.R. Zyst and W.Y. Cheung, Mol. Pharmacol., 75 (1984) 26.
[8] W.Y. Cheung, in Calcium Antagonists; Pharmacology and Clinical Research; Ann. of the New York Acad. of Sciences, Vol. 522, 1988, p.74.
[9] J. Alam, S. Shibahara and A. Smith, J. Biol. Chem, 264 (1989) 6371.
[10] S.M. Keyse and R.M. Tyrrell, Proc. Natl. Acad. Sci. USA, 99 (1989) 86.
[11] K. Mitani, H. Fujita, S. Sassa and A. Kappas, Biochem. Biophys. Res. Commun., 1429 (1990) 166.
[12] T. Hiwasa and S. Sakiyama, Cancer Res., 2474 (1986) 46.

ELSEVIER

Analytica Chimica Acta 295 (1994) 73–83

ANALYTICA CHIMICA ACTA

Fractionation of surface active substances on the XAD-8 resin Part I. Mixtures of model substances

Vjeročka Vojvodić *, Božena Ćosović, Vladimira Mirić

Ruđer Bošković Institute, Center for Marine Research Zagreb, Zagreb, Croatia

Received 14th December 1993; revised manuscript received 5th April 1994

Abstract

Sorption properties on the XAD-8 resin and adsorption behaviour at the mercury electrode surface of different model surface active substances (SAS), Triton-X-100, oleic acid, fulvic acid, and polysaccharides Dextran T-500 and xanthan, were studied. Fractionation of the mixtures of model SAS into hydrophobic neutral, hydrophobic acid and hydrophilic components by sorption on the XAD-8 resin was followed by dissolved organic carbon (DOC) analysis and by adsorption measurements at the mercury electrode surface in influent and effluent solutions. A good separation of the components of the mixture containing Triton-X-100, fulvic acid and Dextran T-500 was proved to be possible by electrochemical analysis of different fractions. In the case of a mixture containing very reactive components such as oleic acid and fulvic acid, it was concluded on the basis of adsorption measurements at the mercury electrode and from DOC analysis of different fractions, that a new material is formed which is more adsorbable at the XAD-8 resin and at the electrode surface. It is shown in this work that, in different mixtures of SAS, without exception, small amounts of hydrophobic neutral material, like non-ionic Triton-X-100 and oleic acid, have a dominant role in adsorption at the mercury electrode surface in the presence of larger quantities of less adsorbable macromolecular compounds, such as hydrophilic polysaccharides and amphiphilic fulvic acid.

Key words: Surface active substances; XAD-8

1. Introduction

The complex mixture of dissolved organic matter in natural aquatic systems comprises different types of hydrophobic and hydrophilic substances. Most of them are surface active, and show a tendency to be concentrated by adsorption processes at the natural phase boundaries of water with atmosphere and living and non-living particles, as well as with the sediment [1–3]. These substances are involved in many physico-chemical processes occurring at the natural phase boundaries, either at the molecular level or as a group of compounds of similar properties. Surface active substances (SAS) may complex metal ions and other organic molecules, influencing thus their bioavailability in natural waters [4,5].

There are numerous methods for separation and determination of dissolved organic compounds in natural aquatic systems recognized on the molecular level, such as for example hydrophobic fatty acids and hydrophilic sugars,

* Corresponding author.

Elsevier Science B.V.
SSDI 0003-2670(94)00174-K

while a large number of uncharacterised organic substances have been analysed by fractionation into groups of homologous compounds based on the size, charge and hydrophobicity of the compounds. The fractionation of dissolved organic matter in natural waters based on their hydrophobic and hydrophilic properties was introduced by Leenheer and Huffman [6]. The analytical procedure of the dissolved organic carbon (DOC) fractionation provided percentages of dissolved organic carbon of the fractions separated from the mixture by sorption on the XAD-8 resin at the controlled polarity. The advancement of the method into a preparative procedure gave the possibility for characterization of separated fractions by determination of their average structural and functional groups [7–9].

Organic substances with surface active properties in natural waters have been widely investigated by using the electrochemical methods based on the measurement of the adsorption phenomena at the mercury electrode surface [10–17]. The main advantage of these methods is a simple and direct determination of the total concentration of surface active substances in natural waters and a rough characterization of predominant adsorbable groups of substances by comparison with various model substances and their mixtures. The adsorption effects at the mercury electrode surface are influenced by the qualitative and quantitative composition of the complex mixture of adsorbable compounds in natural water samples. The adsorption processes can be described by competitive adsorption in which small amounts of strongly adsorbable substances are mostly responsible for the adsorption effect measured at the mercury electrode surface even in the presence of larger amounts of less adsorbable compounds [18]. In this work the adsorption properties of different hydrophobic and hydrophilic model surface active substances and their mixtures fractionated on the XAD-8 resin will be discussed, with the aim of determining the participation of different fractions in the total adsorption effect at the mercury electrode surface compared to their organic carbon content. The model SAS used in this work were oleic and fulvic acid and polysaccharides Dextran T-500 and xanthan as representative substances for natural aquatic systems. The non-ionic synthetic surfactant Triton X-100 was used as well.

2. Experimental

2.1. Fractionation of surface active substances by sorption on the XAD-8 resin

The modified procedure for fractionation of organic matter into hydrophobic and hydrophilic fractions by sorption on the XAD-8 resin, described by Leenheer and Huffman [6] and Leenheer [7], was used. Hydrophobic and hydrophilic fractions obtained on the XAD-8 resin are operationally defined as follows. The hydrophobic basic and neutral organic substances are sorbed on the resin at pH 7–8, the hydrophobic acids are sorbed at pH 2, while hydrophilic organic solutes are non-sorbable and remain in the final effluent.

The fractionation procedure of a mixture of hydrophobic neutral, hydrophobic acid and hydrophilic SAS is illustrated in Fig. 1. Hydrophobic neutral and basic compounds (fraction 1) were separated from the mixture by sorption on the resin at pH 7–8 (1st column). The solution remained after sorption (fraction 2 + 3) was acidified to pH 2 and run through the 2nd XAD-8 column, in order to separate the hydrophobic acid compounds (fraction 2). The hydrophilic compounds (fraction 3) which are not sorbed on the resin at all at both pH values, remained in the final effluent. The calculation of different fractions was based on the measurement of adsorption effects at the mercury electrode surface and determination of DOC values, as shown in Fig. 1.

2.2. Measurements of adsorption effects of surface active substances at the mercury electrode / solution interface

For the characterization of SAS, the electrochemical method phase sensitive alternating current (a.c.) polarography was used in the manner described elsewhere [14–17]. Briefly, the phase sensitive a.c. polarography method, measuring the out of phase signal of the capacitive current, is

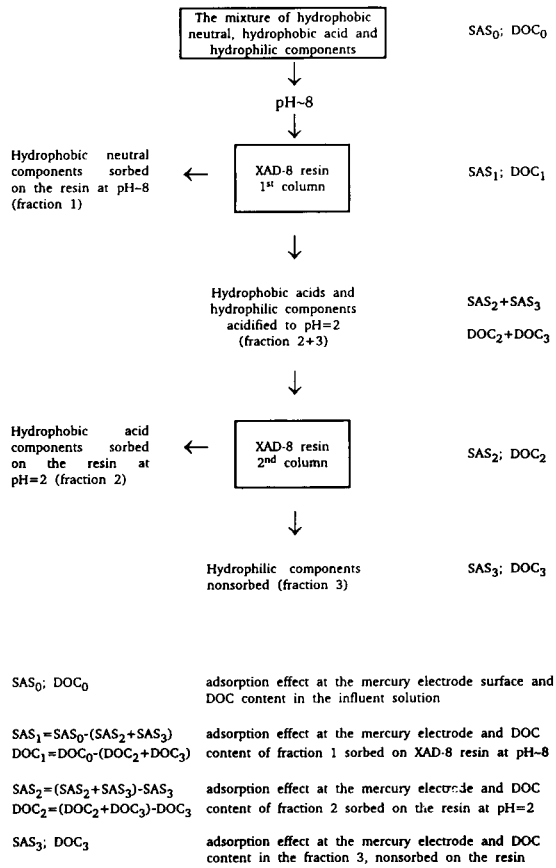

Fig. 1. Analytical scheme of fractionation of the mixture of model surface active substances by sorption on the XAD-8 resin.

based on the study of adsorption effects of SAS in 0.55 M NaCl solution at the mercury electrode surface at selected conditions of potential (−0.6 V vs. Ag/AgCl electrode), time of adsorption (15, 60 and 120 s) and transport mode controlled by diffusion or accumulation by stirring the solution. Adsorption effects at the electrode, i.e., the decrease of the capacity current ΔI (μA), depend on the concentration of all dissolved and/or dispersed SAS, their adsorbability at the electrode, the kinetics of adsorption and on the structure and dielectric properties of the adsorbed layer [19]. The total adsorption effect at an electrode surface completely covered with different surface active organic substances gives a characteristic and constant ΔI_{max} value which can be used for differentiation of surface active substances. Adsorption effects, together with the shape of polarographic curves, which are characteristic for different types of SAS, serve as a convenient tool for a rough characterization of the predominant adsorbable substance of the mixture. For a quantitative determination of adsorption effects of a mixture of different model SAS, the calibration curve prepared with an arbitrary model SAS, Triton X-100, was used.

Additional information of the adsorption behaviour and structure of the adsorbed layer of different SAS and their mixtures at the electrode surface can be obtained by investigation of the influence of adsorbed layer on the electrode processes of 10^{-5} M Cd(II) ions used as a probe [19]. Phase sensitive a.c. polarography, which measures in phase signal of Faradaic current of the oxidation or reduction processes that occur at the electrode surface, was applied. The normalized peak current i/i_0 is determined, where i_0 is the peak current of cadmium in the absence of SAS and i the peak current in the presence of adsorbed layer at the electrode surface. Electrochemical measurements were performed with a Metrohm E-506 polarecord (Metrohm) using a hanging mercury drop electrode.

2.3. Determination of dissolved organic carbon concentration

The dissolved organic carbon concentration (DOC) was determined by using a sensitive high temperature catalytic oxidation (HTCO) technique proposed by Sugimura and Suzuki [20]. A Model TOC-500 system (Shimadzu) with high sensitive Pt catalyst and a non-dispersive infrared (NDIR) detector for CO_2 measurements was used.

2.4. Materials

Amberlite XAD-8 (20–50 mesh beads), obtained from Rohm and Haas (Milan), was purified according to the procedure proposed by Leenheer [7]. Before application of the sample, the resin was rinsed with deionized carbon free water until the blank of the column measured by a.c. polarography was less than 0.02 mg Triton X-100/l and organic carbon content less than 0.8

mg/l. The flow rate of organic solutes controlled by the peristaltic pump was 2 ml/min, while the volume of organic solutes was calculated according to the resin capacity and the expected concentration of organic carbon present in the solution [7].

Fulvic acid was isolated from the lagoon sediment (Canet-Saint-Nazaire en Roussillon, France). The stock solution of fulvic acid was prepared in 3×10^{-2} M $NaHCO_3$. Stock solution of oleic acid (Fluka, Buchs) (17.8 mg/l in 3×10^{-2} M $NaHCO_3$) was prepared by shaking the solution for 4 h. The water soluble non-ionic surface active substance polyethoxylene *tert.*-octylphenol, Triton X-100 (average mol.wt. 600), was a product of Rohm and Haas (Milan). The polysaccharides, Dextran T-500 (average mol.wt. 5×10^5) obtained from Pharmacia (Uppsala), and xanthan, produced by the bacterium *Xanthomonas campestris* (average mol.wt. 2×10^6) formed a commercial substance (Sigma, St. Louis, CA), used without further purification.

3. Results and discussion

3.1. Adsorption effects of model SAS and their mixtures at the mercury electrode surface

Adsorption characteristics of model SAS at the mercury electrode surface in neutral and acidic media are illustrated in Table 1 presenting the concentration range of adsorption (C_1 in mg/l), the ΔI_{max} value (μA), which represents the total adsorption effect at the completely covered electrode surface, and the concentration of SAS (C_2 in mg/l), which produces adsorption effect at the mercury electrode of $\Delta I = 1$ μA, arbitrarily used for comparison of surface active substances. The results presented in Table 1 also include the percentage values of DOC concentrations (in mg/l) of model SAS investigated. According to the C_1, C_2 and ΔI_{max} values, the model SAS can be divided into two groups of substances. On one side oleic acid and Triton X-100, with organic carbon contents higher than 65%, show lower C_1 and C_2 values, and their ΔI_{max} values are greater than 2 μA. They belong to strongly adsorbable substances at the mercury electrode. In contrast, under the same experimental conditions, less adsorbable macromolecular substances, such as fulvic acid, Dextran T-500 and xanthan, are characterized with higher C_1 and C_2 values and ΔI_{max} values smaller than 2 μA. Numerous experiments have shown that there exists a simple relationship between the structure of the adsorbed layer and the ΔI_{max} value. Higher ΔI_{max} values indicate formation of a more dense layer, usually accompanied with a strong inhibition effect upon oxidation–reduction processes of other substances at the electrode

Table 1
Adsorption characteristics of model SAS at the mercury electrode surface

Model surface active substance	pH	Concentration range of adsorption C_1 (mg/l)	ΔI_{max} (μA)	C_2 [a] (mg/l)	DOC [b] (%)
Triton X-100	8	0.02–1.0	2.10	0.108	66
	2	0.02–1.0	2.10	0.108	
Oleic acid	8	0.02–1.0	2.70	0.057	72
	2	0.02–0.4	2.25	0.060	
Fulvic acid	8	0.1 –10.0	1.35	2.00	32
	2	0.1 –7.0	1.94	0.56	
Dextran T-500	8	0.1 –10.0	1.80	1.12	47
	2	0.1 –10.0	1.80	1.12	
Xanthan	8	0.5 –100.0	1.55	9.6	32
	2	0.5 –100.0	1.62	7.5	

[a] Concentrations of SAS which produce adsorption effect at the mercury electrode of $\Delta I = 1$ μA arbitrary used for comparison of SAS.
[b] The DOC values were not corrected for ash and/or moisture.

surface. On the contrary very low ΔI_{max} values correspond to more porous structures permeable for other substances. This was confirmed also by measurements of the oxidation–reduction peaks of 10^{-5} Cd(II) ions in the presence of SAS. At the completely covered electrode surface, adsorbed molecules of oleic acid and Triton X-100 create a compact layer which inhibits the reduction processes of cadmium ions, resulting in the suppression of the polarographic peak of Cd(II) ions [19,21,22]. However, adsorbed molecules of fulvic acid at the electrode surface in neutral and basic media create a very porous layer without any influence on the reduction of cadmium [21–23]. The macromolecular compound Dextran T-500, with chains of helix structure, which are stable to acid and alkaline hydrolysis, shows a higher ΔI_{max} value compared to fulvic acid in neutral solution, indicating the formation of less porous adsorbed layers. This is in good agreement with the observed inhibition effect of Dextran T-500 upon the reduction processes of Cd(II) ions in neutral and acidic solutions. The influence of pH on the adsorption behaviour of surface active substances at the mercury electrode surface was observed only in the cases of fulvic acid, oleic acids and xanthan, while there was no effect of pH on the adsorption of Triton X-100 and Dextran T-500. Increased adsorption effect of fulvic acid at pH 2 is noticed in Table 1 with a lower C_2 value compared to those obtained in neutral medium. The ΔI_{max} value of fulvic acid increased upon acidification from 1.35 μA to 1.94 μA, indicating the formation of a more dense adsorbed layer at the electrode surface in acidic solution. This effect can be explained by conformational changes of the fulvic acid molecules possessing polyelectrolyte properties, caused by protonation of negatively charged carboxylic groups [4,24–26]. In acidic solution, molecules of fulvic acid become more hydrophobic and thus more adsorbable at the electrode surface. This is accompanied also with the inhibition effect upon the reduction processes of Cd(II) ions [21,23]. Adsorption behaviour of polysaccharide xanthan, which also possesses polyelectrolyte properties [27], is similar to that obtained for fulvic acid, but less pronounced (the ΔI_{max} value for xanthan increased in acidic media from 1.55 μA to 1.62 μA). Slightly higher adsorbability at the electrode surface at pH 2 is accompanied with the suppression of the polarographic peak of Cd(II) ions in contrast to neutral media, without any influence on the reduction of cadmium.

3.2. Sorption of model SAS on the XAD-8 resin

Results of the sorption analysis of individual model SAS on the XAD-8 resin are presented in Table 2. Oleic acid and Triton X-100 were completely sorbed on the resin in neutral medium, while the major part of fulvic acid, as expected, was sorbed in acidic medium. No affinity of polysaccharide Dextran T-500 on the resin was detected at either pH value. Macromolecular polysaccharide xanthan is predominantly hydrophilic. In neutral solution of xanthan, only 3.3% of the total organic carbon was sorbed on the XAD-8 resin. In acidic medium, 18.4% of the surface active xanthan (its hydrophobic acid fraction), corresponding to 13.8% of total organic carbon content, was sorbed on the XAD-8 resin. 81.6% of the surface active xanthan, i.e., 82.9%

Table 2
Sorption characteristics of model SAS on XAD-8 resin

Surface active substance	Influent concentration (mg/l)	Fraction (%)		
		Hydrohobic neutral pH ~ 8	Hydrophobic acid pH ~ 2	Hydrophilic (nonsorbed)
Triton X-100	0.20	98	–	2
Oleic acid	0.15	100 (100)	–	–
Fulvic acid	3.00	–	96.4	3.6
Dextran T-500	1.40	–	–	100
Xanthan	10.80	(3.3)	18.4 (13.8)	81.6 (82.9)

Values in brackets are obtained from DOC analysis.

of the total organic carbon content of xanthan, possesses hydrophilic character and remained in final effluent. According to the operational definition of the sorption affinity to the XAD-8 resin given by Leenheer [7], Triton X-100 and oleic acid possess hydrophobic neutral properties, fulvic acid is hydrophobic acid just like a minor part of xanthan, while Dextran T-500 and major parts of xanthan are hydrophilic surface active substances.

3.3. Fractionation of mixtures of model SAS by sorption on the XAD-8 resin

The investigated mixtures of model SAS had the following compositions: Triton X-100, Dextran T-500 and fulvic acid (Mixture I), oleic acid and fulvic acid (Mixture II), and oleic acid and xanthan (Mixture III). The concentrations of the components were chosen so that each of them contributed approximately by 1/3 (Mixture I) or 1/2 (Mixtures II and III) in the total adsorption effect of the mixture at the mercury electrode surface. Concentrations of the components, given in mg/l, and their concentration ratios and DOC ratios (percentage values) in the mixtures are presented in Table 3.

3.4. Mixture I

The mixture of model SAS described in Table 3 was fractionated on the XAD-8 resin according

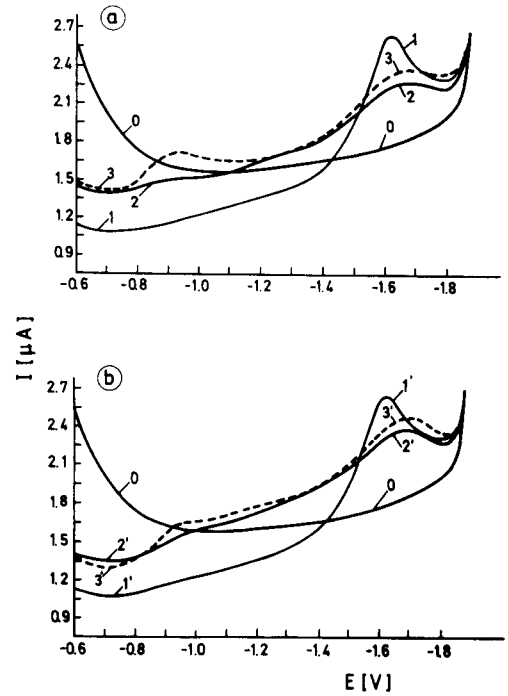

Fig. 2. Capacity current–potential curves of Mixture I and its components. (a) Fractionation on XAD-8 resin: (1) influent solution, (2) effluent solution remained after sorption on the resin in neutral medium, (3) effluent solution remained after sorption on the resin at pH 2, neutralized to pH 8. All solutions were diluted before measurement (1:5). (b) Parallel experiment: (1) initial three-component mixture ($C = 2.1$ mg/l), (2) 1 mg/l fulvic acid + 1 mg/l Dextran T-500, (3) 1 mg/l Dextran T-500. Accumulation time: 120 s with stirring solution. Curve 0 is the basic line of 0.55 M NaCl without surfactants.

Table 3
Concentration (mg/l), concentration ratio and DOC ratio (percentage values of components) of the mixtures fractionated on the XAD-8 resin

Composition of mixture	Concentration of components (mg/l)	Concentration ratio (%)	Organic carbon ratio (%)
Mixture I	(10.51)		
Triton X-100	0.46	4.4	7.2
Dextran T-500	5.02	47.8	55.2
Fulvic acid	5.03	47.8	37.6
Mixture II	(2.65)		
Oleic acid	0.15	5.7	11.9
Fulvic acid	2.50	94.3	88.1
Mixture III	(9.14)		
Oleic acid	0.14	1.5	3.4
Xanthan	9.00	98.5	96.6

to the procedure illustrated in Fig. 1 with the only exception that DOC recoveries of the fractions were not determined for this mixture. The different fractions were analyzed by adsorption effect measurements at the mercury electrode surface. The efficiency of the fractionation procedure was tested by comparing electrochemical responses, i.e. capacity–current potential curves of different fractions with those of the components of the mixtures as given in Fig. 2a and b. The influent solution of the Mixture I is represented by curves 1 and 1'. Taking into consideration the affinity of individual components for the XAD-8 resin it is reasonable to assume that only hydrophobic neutral Triton X-100 will be sorbed

on the resin in neutral medium while fulvic acid and Dextran T-500 will remain in the effluent solution. Curve 2, which represents the effluent solution, after sorption of the mixture in neutral medium, corresponds to curve 2′ obtained by measurement of the mixture composed from fulvic acid and Dextran T-500 in a parallel experiment. Hydrophobic neutral fraction sorbed on the resin in neutral medium participates with 30.1% in the total adsorption effect of Mixture I at the mercury electrode surface. The hydrophobic acid fraction, which participates in the adsorption effect of the mixture with 53.4%, was sorbed on the resin at pH 2, while hydrophilic Dextran T-500, presented by curve 3, remained in the final effluent. The hydrophilic fraction (16.5%) produced the same adsorption effect at the electrode surface as the T-500 in the parallel experiment, which is illustrated by polarographic curve 3′. As shown in Table 4 the percentages of different fractions obtained by using the fractionation procedure of Mixture I on the XAD-8 resin are in a good agreement with the calculated values on the basis of the adsorption effects of the components of the mixture.

Table 4
Mixture I fractionated on XAD-8 resin

	Fraction (%)	
	I	II
Hydrophobic neutral	30.1	27.8
Hydrophobic acid	53.4	53.8
Hydrophilic	16.5	18.4

I = Fractions obtained by separation procedure on the XAD-8 resin.
II = Fractions calculated from surfactant activity values of components as obtained in the parallel experiment

Influence of different fractions in Mixture I on reduction processes of 10^{-5} Cd(II) ions obtained with accumulation periods of 15, 60 and 120 s at the mercury electrode surface

Sample	pH	i/i_0		
		15 s	60 s	120 s
Mixture I	8	0.25	0.13	0.07
	2	0.23	0.08	0.06
Fraction 2 + 3	8	1.21	1.03	1.06
	2	0.45	0.12	0.08
Fraction 3	8	1.04	0.43	0.37
	2	0.93	0.40	0.38

Further inspection of the efficiency of fractionation procedure was made by using the Cd(II) reduction process as a probe. The results are also presented in Table 4. In the three-component mixture, the adsorbed layer formed at the mercury electrode exhibits a strong inhibition effect on the cadmium reduction processes in neutral and acidic medium, which corresponds mainly to the influence of Triton X-100 in the adsorbed layer. In the mixture of fulvic acid and dextran, the organic coating formed is permeable for Cd(II) ions at neutral pH; even a small accumulation of Cd(II) ions in the adsorbed layer is observed at short adsorption times (normalized peak current > 1). In acidic medium, a strong inhibition effect is observed as it is expected for the adsorption of fulvic acid. The hydrophilic fraction (Dextran T-500), shows an inhibition effect at both pH values. In conclusion, it can be summarized that different hydrophobic and hydrophilic surface active substances of Mixture I are quantitatively separated on the XAD-8 resin. With regard to the adsorption behaviour of organic substances at the hydrophobic mercury surface the contributions of the individual components in the adsorption of the mixture depend more on their adsorbabilities at the electrode surface then on their weight percentages in the mixture. The percentage values of the fractions presented in Table 4 are in good agreement with the general idea of a competitive adsorption process, in which small amounts (0.46 mg/l) of strongly adsorbable Triton X-100 is responsible for a significant adsorption effect of hydrophobic neutral fraction compared to the effect produced by high contents of less adsorbable fulvic acid (5.03 mg/l) like the hydrophobic acid fraction and Dextran T-500 (5.02 mg/l) like the hydrophilic component.

3.5. Mixture II

The results of fractionation of the Mixture II, composed of a small amount (0.15 mg/l) of hydrophobic neutral oleic acid and a higher content of fulvic acid (2.5 mg/l) as hydrophobic acid material, are presented in Table 5. The fractions

Table 5
Mixture II fractionated on XAD-8 resin

Fraction (%)		
Hydrophobic neutral	Hydrophobic acid	Hydrophilic
79.6	18.1	2.3
(22.8)	(77.2)	(0)

Values in brackets are obtained from DOC analysis.

were analysed by a.c. polarography and DOC measurements. On the basis of the electrochemical measurement, this mixture comprises most of the hydrophobic neutral material, and significantly lower contents of hydrophobic acids. In contrast, the distribution of fractions is quite different as calculated from DOC measurement, i.e., the hydrophobic neutral fraction contains lower amounts of DOC in comparison with hydrophobic acid fractions with higher amounts of total DOC. The electrochemical analysis of the mixture and the fractions are illustrated in Fig. 3. The shape of the capacity current–potential curves 1, 2 and 3 of Mixture II compared to the curves 1′, 2′ and 3′ of pure oleic acid with the same concentration as used in the mixture given in Fig. 3a, shows mutual influence of the components on their adsorption behaviour at the mercury electrode surface. A good separation of oleic acid and fulvic acid by sorption on XAD-8 resin is visible from the electrochemical response of the effluent solution remained after sorption on the XAD-8 resin in neutral medium represented by curves 1, 2 and 3 in Fig. 3b. These curves are practically the same as those obtained with the pure fulvic acid, given in Fig 3c. The interaction which occurred between oleic acid and fulvic acid in the mixture is indicated from the higher percentage value obtained of the organic carbon content of hydrophobic neutral fraction (i.e., 22.8%) compared to the expected 11.9%, which is the oleic acid participation in the mixture (see Table 3). Interaction between macromolecular fulvic acid and the very hydrophobic oleic acid is explained by the amphiphilic structure of fulvic acid in which non-polar groups of the molecules offered the environment into which hydrophobic molecules of oleic acid may escape unfavourable competition with water molecules [28]. Our experiments indicate also a strong change of physico-chemical properties of the components in the mixture towards an increased hydrophobicity. A part of the most hydrophilic fulvic acid (in neutral medium) which interacted with hydrophobic molecules of oleic acid became more hydrophobic and thus more adsorbable at the XAD-8 resin. The new hydrophobic neutral material, formed in the mixture of oleic acid and fulvic acid, has a tremendous influence on the adsorption behaviour at the mercury electrode as well. The result is that the hydrophobic neutral fraction represents 79.6% of the total surfactant activity of the mixture. The hydrophobic acid fraction with a higher organic carbon content but a lower adsorbability participates only with 18.1%

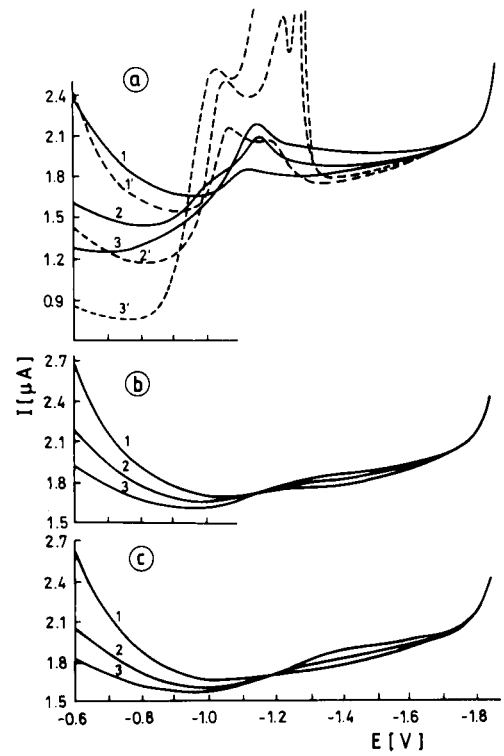

Fig. 3. Capacity current–potential curves of Mixture II and its components. (a) Mixture II before fractionation measured at dilution 1:2 (curves 1, 2 and 3), compared to electrochemical signal of 0.076 mg/l of oleic acid (curves 1′, 2′ and 3′). (b) Effluent solution after sorption of Mixture II on the resin in neutral medium (dilution 1:2). (c) 1 mg/l fulvic acid. Accumulation time: (1, 1′) 15 s, (2, 2′) 60 s and (3, 3′) 120 s.

in total surfactant activity. The hydrophilic fraction of the mixture is negligible, as expected.

3.6. Mixture III

The composition, concentration ratio and organic carbon ratio of the components in Mixture III are presented in Table 3. Naturally occurring hydrophobic neutral and highly adsorbable surface active substance (oleic acid), and less adsorbable hydrophilic polysaccharide (xanthan) were used. The electrochemical response represented by the capacity current–potential curves of the initial Mixture III and after sorption on the resin are given in Fig. 4a and b, respectively. It can be clearly seen that the effluent solution remained after sorption on the resin in neutral medium (Fig. 4b) resembles the adsorption behaviour of pure xanthan, given in Fig. 4c (the same concentration as used in the mixture), indicating a good separation of oleic acid from the mixture.

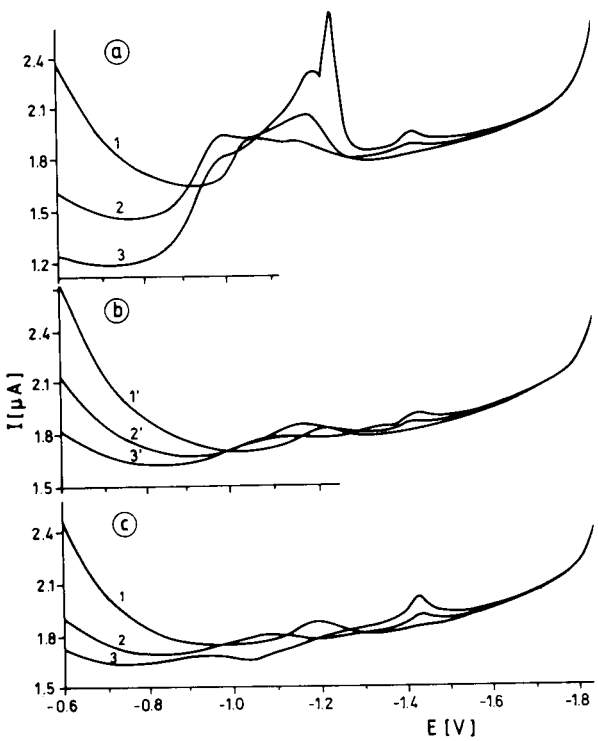

Fig. 4. Capacity current–potential curves of Mixture III and its components. (a) Influent solution of Mixture III before sorption on XAD-8 resin. (b) Effluent solution after sorption on the resin in neutral medium. (c) 9 mg/l xanthan. Accumulation time: (1) 15 s, (2) 60 s and (3) 120 s.

Table 6
Mixture III fractionated on XAD-8 resin

Fraction (%)		
Hydrophobic neutral	Hydrophobic acid	Hydrophilic
47.7	0	52.3
(15.3)	(6.4)	(78.3)

Values in brackets are obtained from DOC analysis.

The percentages of different fractions obtained from electrochemical measurements and from the DOC analysis are presented in Table 6. Both fractions, the hydrophobic neutral and the hydrophilic one, contribute to approximately the same extent to the adsorption effect at the mercury electrode. It is important to mention that the hydrophobic neutral fraction represents only 15.3% of organic carbon, while the hydrophilic fraction represents 78.3% of organic carbon of the mixture. The hydrophobic acid fraction, containing 6.4% of DOC, showed no measurable contribution to the adsorption effect at the mercury electrode. Similarly, as in the case of the above described Mixtures I and II, small amounts of hydrophobic organic substances, 0.14 mg/l of oleic acid in Mixture III, show dominant influence on adsorption at the hydrophobic mercury water interface in the presence of larger quantities of less adsorbable substance, 9 mg/l of xanthan in the Mixture III. The organic carbon content of the hydrophobic neutral fraction (15.3%) of the Mixture III is higher than would correspond to the participation of oleic acid and xanthan according to the data given in Tables 2 and 3. If possibility exists of modifying the xanthan molecules by interaction with oleic acid into a more adsorbable, hydrophobic material, this is however much less visible than in the case of the mixture of oleic acid and fulvic acid.

4. Conclusions

Fractionation of the SAS mixtures by sorption on the XAD-8 resin in neutral and acidic media

was followed by measuring DOC values and surfactant activity values at the mercury electrode in influent and effluent solutions. Comparing the percentage values of different fractions with respect to either the DOC content or the adsorbability at the mercury electrode, it is shown that small amounts of hydrophobic neutral material, like non-ionic surfactant Triton X-100 (log k_{ow} = 3.46, [29]), and long chain unsaturated fatty acid (oleic acid, log k_{ow} = 7.55, calculated from the hydrophobic fragmental constants) [30], have a dominant role in the adsorption at the hydrophobic mercury–water interface, even in the presence of larger quantities of less adsorbable hydrophilic (polysaccharides) or conditionally hydrophobic (fulvic acid) substances. The dominant adsorption of hydrophobic organic molecules in the mixture was confirmed by studying the oxidation–reduction processes of Cd(II) used as a molecular probe for the structure of the adsorbed layer.

The electrochemical analysis of well separated fractions of the mixture containing Triton X-100, fulvic acid and Dextran T-500, showed that the expected interaction between fulvic acid and Triton X-100 did not occur in spite of the generally known affinity of humic material to retain or fix hydrophobic compounds [31–34]. Oleic acid was found to be more reactive in this respect, either because of considerable higher log k_{ow} coefficient or the presence of a double bond. By attachment of oleic acid to the natural polymer fulvic acid, a new material is formed which is more adsorbable at the XAD-8 resin as well as at the mercury surface. Similarly, it was found for humic acid and oleic acid in our previous work [35] that the product of their interaction is also more stable during the treatment at increased temperature and pressure. In contrast to pure solutions of oleic acid and humic acid, the mixture is not accessible for further hydrophobic interactions. It was demonstrated in this work, using model SAS, that electrochemical measurements together with DOC analysis of fractions obtained on the XAD-8 resin, are a powerful tool in the study of the reactivity and physico-chemical characteristics of the complex mixtures of organic substances. This approach will be used in the analysis of natural marine, estuarine and freshwater samples.

Acknowledgments

The authors gratefully acknowledge Dr. Gustave Cauwet for his expert guidance in the isolation of humic material from the lagoon sediment at the Université de Perpignan, France. Financial support from the Croatian Ministry of Science is gratefully acknowledged.

References

[1] P.S. Liss, in Riley and Skirrow (Eds.), Chemical Oceanography, Vol. 2. Academic Press, New York, 1975.
[2] B. Ćosović, V. Žutić, V. Vojvodić and T. Pleše, Mar. Chem., 17 (1985) 127.
[3] J.C. Marty, V. Žutić, R. Precali, A. Saliot, B. Ćosović, N. Smodlaka and G. Cauwet, Mar. Chem., 26 (1989) 313.
[4] J. Buffle, Complexation Reactions in Aquatic Systems, Ellis Horwood, Chichester, 1988.
[5] W. Stumm and J.J. Morgan, Aquatic Chemistry, Wiley, New York, 2nd edn., 1981.
[6] J.A. Leenheer and E.W.D. Huffman Jr., J. Res. U.S. Geol. Surv., 4 (1976) 737.
[7] J.A. Leenheer, Environ. Sci. Technol., 15 (1981) 578.
[8] J.A. Leenheer, Mitt. Geol. Paleont. Inst. Univ. Hamburg. SCOPE/UNEP Sonderband, Heft, 58 (1985) 165.
[9] J.A. Leenheer and T.I. Noyes, J. Res. U.S. Geol. Surv. Water-Supply Pap., 2230 (1985a).
[10] B. Ćosović, V. Žutić and Z. Kozarac, Croat. Chem. Acta, 50 (1976) 260.
[11] T. Zvonarić and V. Žutić, Thalassia Jugosl., 15 (1979) 113.
[12] K.A. Hunter and P.S. Liss, Water Res., 15 (1981) 203.
[13] B. Ćosović and V. Vojvodić, Limnol. Oceanogr., 27 (1982) 361.
[14] B. Ćosović, V. Vojvodić and T. Pleše, Water Res., 19 (1985) 175.
[15] B. Ćosović and V. Vojvodić, Mar. Chem., 22 (1987) 363.
[16] B. Ćosović and V. Vojvodić, Mar. Chem., 28 (1989) 183.
[17] V. Vojvodić and B. Ćosović, Mar. Chem., 39 (1992) 251.
[18] B. Ćosović, in W. Stumm (Ed.), Chemical Processes in Lakes, Wiley, New York, 1985.
[19] B. Ćosović, in W. Stumm (Ed.), Aquatic Chemical Kinetics, Wiley, New York, 1990.
[20] Y. Sugimura and Y. Suzuki, Mar. Chem., 24 (1988) 105.
[21] Z. Kozarac, B. Ćosović and V. Vojvodič, Water Res., 20 (1986) 295.
[22] Z. Kozarac, PhD Thesis, University of Zagreb, Croatia, 1980.

[23] M. Plavšić and B. Ćosović, Mar. Chem., 36 (1991) 75.
[24] R.J. Cleven, PhD Thesis, University of Wageningen, Netherlands, 1984.
[25] C.H. Lochmuler and S.S. Saavedra, Anal. Chem., 58 (1986) 1978.
[26] R.J. Cleven and H. van Leeuwen, Int. J. Environ. Anal. Chem., 27 (1986) 11.
[27] M. Rinaudo and M. Milas, Carbohydr. Polym., 2 (1982) 264.
[28] P.M. Gschwend and R.P. Schwarzenbach, Mar. Chem., 39 (1992) 187.
[29] M. Ahel and W. Giger, Chemosphere, 26 (1993) 1478.
[30] R.R. Rekker, in The Hydrophobic Fragmental Constant, Elsevier, Amsterdam, 1977.
[31] S.U. Khan and M. Schnitzer, Geochim. Cosmochim. Acta, 36 (1972) 745.
[32] S.R. Larter and A.G. Douglas, Geochim. Cosmochim. Acta, 44 (1980) 2087.
[33] G.R. Harvey, D.A. Boran, L.A. Chesal and J.M. Tokar, Mar. Chem., 12 (1983) 119.
[34] M.A. Schlautman and J.J. Morgan, Environ. Sci. Technol., 27 (1993) 961.
[35] B. Ćosović and Z. Kozarac, Mar. Chem., 42 (1993) 1.

ELSEVIER

Analytica Chimica Acta 295 (1994) 85–91

ANALYTICA CHIMICA ACTA

Electrochemical determination of low levels of residual chlorine dioxide in tap water

François Quentel *, Catherine Elleouet, Christian Madec

URA CNRS 322, Université de Bretagne Occidentale, Laboratoire de Chimie Analytique, 6 Avenue Victor Le Gorgeu, B.P. 452, 29275 Brest Cedex, France

Received 17th December 1993; revised manuscript received 25th March 1994

Abstract

The reaction between 1,2-dihydroxyanthraquinone-3-sulphonic acid and chlorine dioxide, in phosphate buffer medium, was studied spectrophotometrically and electrochemically. An electroanalytical method is proposed for the determination of traces of ClO_2 with a detection limit of 2 $\mu g\ l^{-1}$. The stoichiometry of the reaction, the effects of various operational parameters and the influence of foreign ions are reported.

Key words: UV–Visible spectrophotometry; Voltammetry; Chlorine dioxide; Waters

1. Introduction

In the last decade, chlorine dioxide has been increasingly used for disinfecting drinking water in many countries. It is typically applied at doses of 0.3–0.5 mg l^{-1}. During water treatment and subsequent distribution, chlorine dioxide can undergo a variety of reduction and disproportionation reactions, forming primarily chloride but especially chlorite and chlorate, which have been shown to cause haemolytic anaemia. As these undesirable inorganic by-products increase in the water-pipes, the bactericidal reagent disappears. A sufficient residual concentration of chlorine dioxide in the drinking water is a guarantee for the protection of the consumer and therefore it is important to know the residual level of ClO_2 at the tap.

In many water-treatment plants, residual chlorine dioxide is conventionally monitored using Palin and Darral's DPD method [1]. However, it cannot be reliably determined at levels below 0.1 mg l^{-1} and, owing to its non-selectivity, the possibility of recording false-positive results cannot be eliminated, as we have often observed. This agrees with the comments of Fletcher and Hemmings [2]. Only two spectrophotometric methods have been identified as being suitable in the water-treatment context: the discoloration of Alizarin Violet 3R (AV3R) [3] and that of Chlorophenol Red (CPR) [4] by chlorine dioxide

* Corresponding author.

SSDI 0003-2670(94)00156-G

have been successfully utilized at levels of the latter down to 30 $\mu g\ l^{-1}$. The determination of lower levels in potable water therefore requires a more sensitive method.

This paper reports an electrochemical method that is simple, selective enough and has a range suitable for the determination of very low concentrations of ClO_2 (2–50 $\mu g\ l^{-1}$).

2. Experimental

2.1. Equipment

A Tacussel PRG5 polarographic analyser with a Metrohm EA 290 hanging mercury drop electrode was used for differential-pulse voltammetry. Cyclic voltammograms were recorded with an EGG 362 apparatus. An $Ag/AgCl/Cl^-$ half-cell was used as the reference electrode and a platinum wire as the auxiliary electrode.

UV–visible spectra of 1,2-dihydroxyanthraquinone-3-sulphonic acid (DASA; Alizarin Red S) and ClO_2 were recorded with an HP 8452 A diode-array spectrophotometer. pH was measured with an Orion 811 pH meter.

2.2. Reagents

Reagents were of analytical-reagent grade from Merck (Na_2HPO_4, NaH_2PO_4, EDTA). All solutions were prepared with ultrapure water produced by reverse osmosis, additional ion exchange and filtration through activated carbon (Millipore Milli-Q system).

Sodium chlorite was purchased from Aldrich. It was recrystallised twice from warm water (97% purity). Alizarin Red S (DASA) was purchased from Aldrich (dye content 70%) and was purified as follows. It was first dissolved in water and extracted twice with toluene, then Bu_4NCl was added to the aqueous solution and the DASA–Bu_4N ion pair was extracted with $CHCl_3$, which was then evaporated. A stock solution of DASA (10^{-3} mol l^{-1}) was prepared in methanol but all dilutions were made with water.

Chlorine dioxide was prepared by reaction of sodium chlorite with sulphuric acid (Atochem procedure) [5]:

$$5(Na^+, ClO_2^-) + 2H_2SO_4 \rightarrow 4ClO_2 + (Na^+, Cl^-) + 2(2Na^+, SO_4^{2-}) + 2H_2O$$

The concentration of the stock solution was determined by UV spectrophotometry at 360 nm with a molar absorptivity of 1200 l mol^{-1} cm^{-1}; the results obtained agreed well with those determined by the iodimetric method. Before and after its use, chlorine dioxide was measured. The level of the by-product ClO_2^- in the stock solution of chlorine dioxide was less than 1%.

3. Results and discussion

The electrochemical adsorptive properties of DASA are well known, especially in the determination of some trace metals [6,7]. Alizarin Violet is one of the two selective reagents used in spectrophotometry, having also an anthraquinoid nucleus. We investigated its electrochemical behaviour in order to improve the detection limit. Preliminary experiments showed, however, that this compound was not suitable for this purpose. Because an aqueous solution of DASA is discoloured in the same manner by the addition of chlorine dioxide, we chose to investigate in detail its behaviour towards the bactericidal reagent.

3.1. Mechanism

Spectrophotometric study

DASA is a diprotonic acid; the pK_a^0 values for the OH protons in aqueous solutions are 11.01 and 5.54 [8]. When the dye is dissolved in a phosphate-buffered solution (pH 6.8), it turns reddish ($\lambda_{max} = 516$ nm) (Fig. 1a). AV3R and DASA have similar absorptivities, 7750 and 7100 l mol^{-1} cm^{-1}, respectively. When chlorine dioxide is gradually added, the colour of the solution fades (Fig. 1b); DASA becomes colourless when 4 mol of ClO_2 are added whereas with Alizarin Violet only 2 mol of ClO_2 produce the

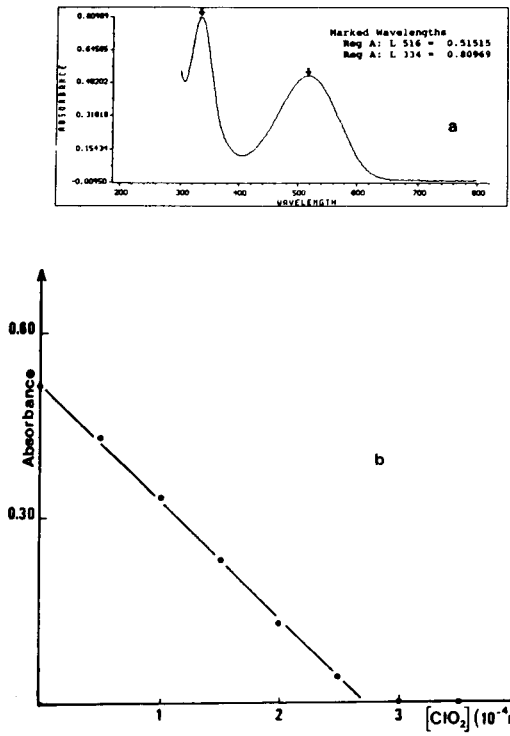

Fig. 1. (a) UV–visible spectrum of 7×10^{-5} mol l^{-1} DASA in phosphate buffer (pH 6.8). (b) Decrease in the absorbance at 516 nm on addition of ClO_2.

same effect. In addition, no hypsochromic shift was observed as with AV3R when the dye to oxidant ratio was decreased [3]. According to Masschelein [9], a selective attack of the anthraquinoid nucleus would take place with AV3R. The addition of two hydroxyl groups on the nucleus of DASA which can be oxidized in a first step in a keto form as in the quinone–hydroquinone system would explain the 4 mol of ClO_2 consumed per mole of dye in so far as the bactericidal reagent exchanges only one electron, ClO_2^- having no effect on the stability of DASA.

Electrochemical study

A few electrochemical experiments were carried out to confirm the previous results. In an aqueous phosphate buffer (pH 6.8), DASA exhibits two waves on vitreous carbon, an oxidation wave ($E_{1/2} = 0.420$ V) and a reduction wave ($E_{1/2} = -0.650$ V). The total disappearance of the oxidation wave was obtained for a ClO_2/DASA molar ratio of 4, which agrees with the spectrophotometric data. On the other hand, a new oxidation wave appeared at a more positive potential. As the addition of chlorite has no influence on the two waves of DASA, ClO_2 probably reacts in a monoelectronic step.

To confirm the assumption, that is the formation of ClO_2^- after the reaction of ClO_2 with DASA, we determined the chlorite concentration resulting from the addition of 4×10^{-4} mol l^{-1} chlorine dioxide to a solution of 1×10^{-4} mol l^{-1} DASA buffered at pH 6.8. The ClO_2^- concentration was measured by differential-pulse polarography [10], taking into account the ClO_2^- concentration determined in the ClO_2 stock solution. A level of 3.8×10^{-4} mol l^{-1} was found, which means that the reaction process can be summarized as follows:

$$4ClO_2 + DASA \rightarrow 4ClO_2^- + DASA^*$$

where DASA* corresponds to the oxidized form of DASA.

3.2. Electrochemical behaviour on the Hg electrode

The objective of this work was to determine very low levels of chlorine dioxide. Owing to the indirect character of the procedure, the concentration of the dye added to the sample also has to be low, which needs a preconcentration step to measure quantitatively its consumption. Most adsorptive procedures utilize the hanging mercury drop electrode, which offers the advantages of self-cleaning properties, reproducible surface area and automatic control. A few experiments were performed to investigate the electrochemical behaviour of DASA on the mercury electrode.

In phosphate buffer (pH 6.8), a $1\times10^-$ mol l^{-1} of DASA solution produces a reduction wave governed by diffusion. Two electrons and two protons are exchanged during the electrochemical process, corresponding to

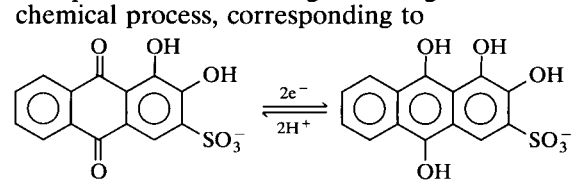

The reversibility was confirmed by cyclic voltammetry (Fig. 2a), where $\Delta E_p = E_{p_a} - E_{p_c} =$ 35 mV. When four equivalents ClO_2 were added to the solution the cathodic and anodic signals disappeared.

In dilute solution a signal was observed only if the cathodic sweep was preceded by an accumulation step. Cyclic voltammetry of 2×10^{-7} mol l^{-1} DASA showed reversible reduction of free adsorbed DASA after stirred accumulation (Fig. 2b).

3.3. Development of an electroanalytical method

Acidity

In the differential-pulse mode an adsorptive stripping peak of DASA was observed in phosphate buffer (pH 6.8) at a potential of −0.600 V vs. Ag/AgCl. The influence of pH on the reduction peak was examined. The peak current gradually increases with decreasing pH from 8 to 5 and decreases at pH lower than 5. The position of the peak also depends on pH and is shifted by 67 mV pH^{-1} between pH 3.9 and 7.8. Although the peak height of DASA is maximum around pH 5, a pH 7 buffer was chosen in the experiments for the following reasons: generally the reactivity of the oxidants decreases from acidic to neutral buffered solutions, which reduces the risks of losses of the reagent by side-reactions, and ClO_2^-, a by-product of the bactericidal reagent, gives at pH 5 a polarographic wave in the reduction range of DASA whereas the two systems exhibit a difference in potential of 0.300 V in a phosphate buffer (pH 7).

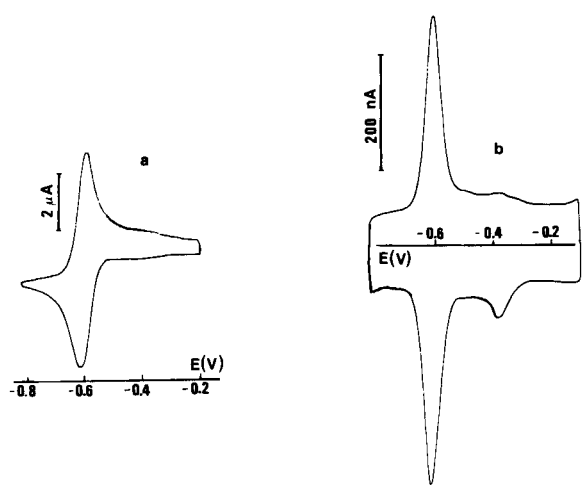

Fig. 2. Cyclic voltammetry at a scan rate of 100 mV s^{-1} in phosphate buffer (pH 6.8). (a) 1×10^{-4} mol l^{-1} DASA; (b) 2×10^{-7} mol l^{-1} DASA; 2 min at −0.100 V.

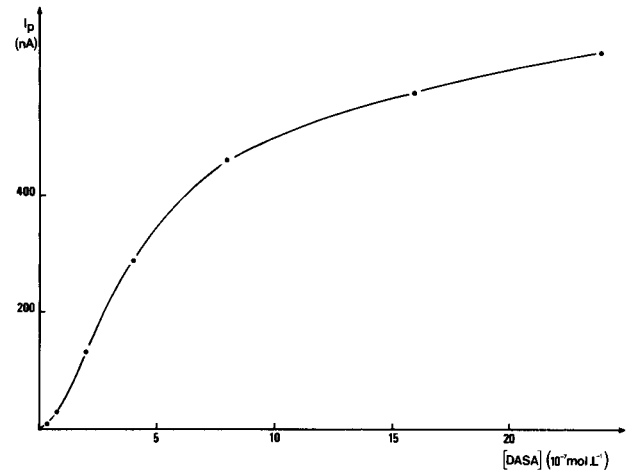

Fig. 3. Variation of peak height as a function of the concentration of DASA. $t_d = 1.5$ min; $E_d = -0.300$ V.

Concentration of DASA

The peak height of the dye was measured by adsorptive stripping voltammetry as a function of the DASA concentration; it was found (Fig. 3) that it increases strongly until about 8×10^{-7} mol l^{-1}. As in the spectrophotometric method, the electroanalytical procedure is based on the measurement of the decrease in the signal after the addition of ClO_2. The indirect character of the analysis requires the level of the residual oxidant to be known. According to the levels encountered in our samples, a concentration around 2×10^{-7} mol l^{-1} of DASA was used.

Accumulation time

The reduction current of a 2×10^{-7} mol l^{-1} DASA solution was measured as a function of the collection time (t_d) in phosphate buffer (pH 6.9). The relationship $i_p = f(t_d)$ is linear up to

3 min and then becomes curved owing to saturation of the mercury drop by free DASA (Fig. 4). For subsequent experiments a collection time of 1.5 min was selected.

Accumulation potential

Generally, the adsorption process at the electrode/solution interface depends on the electrode potential. The cathodic stripping peak height was therefore measured versus the adsorption potential. Stirred collection was carried out for 1.5 min at each selected potential. After a 10-s rest period, the potential was set to 0.000 V, where each scan was started (Fig. 5). As the accumulation potential (E_d) is higher than the reduction peak potential (E_p) of DASA, the peak height remains constant, whereas it decreases strongly when E_d is lower than E_p. A similar shape of the dependence of the peak current on

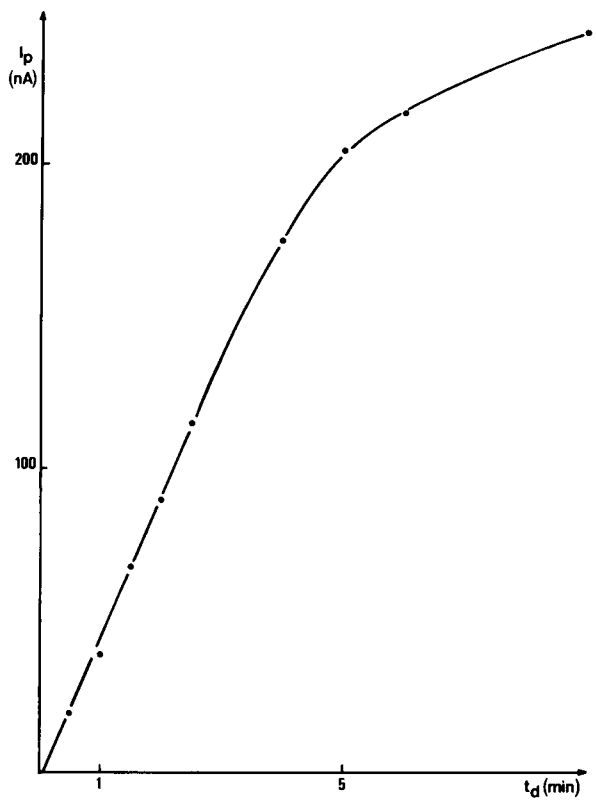

Fig. 4. Dependence of peak height on accumulation time in phosphate buffer. $E_d = -0.300$ V; 2×10^{-7} mol l^{-1} DASA.

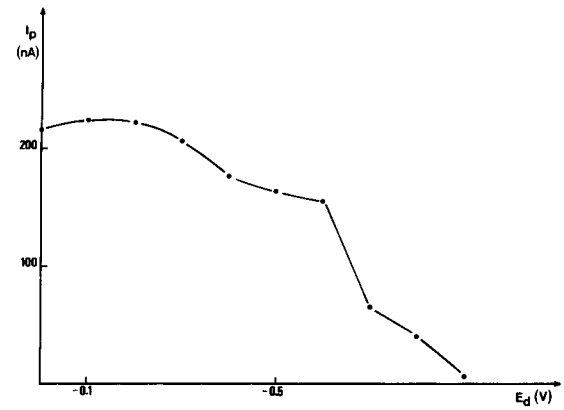

Fig. 5. Effect of collection potential on the differential-pulse stripping peak of 2×10^{-7} mol l^{-1} DASA in phosphate buffer, $t_d = 1.5$ min; $E_i = 0$ V.

potential has been observed for other adsorptive procedures [11]. At potentials more positive than -0.500 V (near the potential of zero charge (pzc)) the electrode surface is positively charged while the DASA ions have a negative charge which makes the adsorption easier. A value of -0.300 V was chosen in subsequent experiments.

ClO_2 concentration

Fig. 6 shows the relationship between the concentration of DASA and ClO_2 in distilled water (phosphate buffer). Under the prevailing experimental conditions (1.4×10^{-7} mol l^{-1} DASA), concentrations between 5×10^{-8} and 3×10^{-7} mol l^{-1} can be easily determined. However, the decrease in the signal versus ClO_2 concentration is linear only when the oxidant to dye ratio is < 2. In addition, the kinetics of the oxidation of DASA by ClO_2 are fast even in very dilute media.

Interferences

Interferences can arise from other residual oxidants which may also be used in water treatment or from trace metals which can form reducible and adsorbable chelates with the ligand.

Concentrations of up to 10^{-5} mol l^{-1} of chlorite (ClO_2^-) or hypochlorite (ClO^-) have no influence on the adsorptive stripping peak of DASA. Ozone, a reagent often used in a preliminary

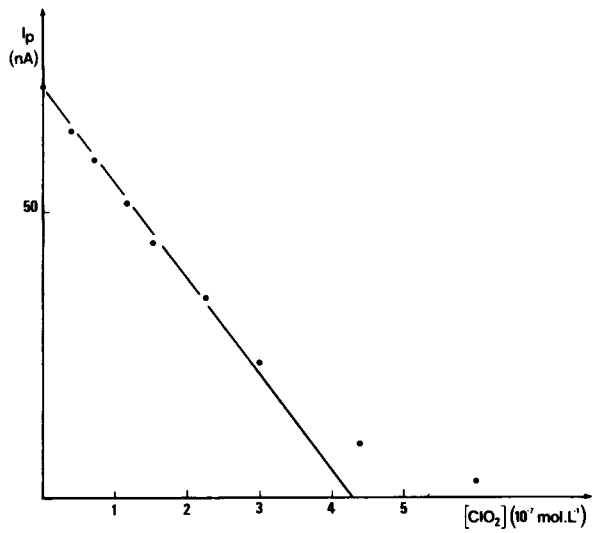

Fig. 6. Decrease in the differential-pulse adsorptive stripping peak of 1.4×10^{-7} mol l^{-1} DASA in phosphate buffer with increasing concentration of ClO_2. t_d = 1.5 min; E_d = −0.300 V.

step, on the other hand, reacts with DASA (4 mol of oxidant per mole of reagent); its presence must therefore be avoided in order to determine ClO_2 accurately. Although similar, the reaction of O_3 with DASA must be different in nature from that of ClO_2, which agrees with the comments of Masschelein [3] regarding AV3R.

In a previous work, we showed that copper forms a complex with DASA [7]. The addition of a masking agent such as EDTA eliminates this interference. Under the same conditions, other trace metals such as Al or Mn have no influence on the DASA signal.

Reproducibility and sensitivity

As the procedure is based on the decrease in the signal, it is necessary that the peak current of DASA in a ClO_2-free solution must be reproducible. For a 1.4×10^{-7} mol l^{-1} solution of DASA, the mean peak current ± standard deviation (n = 29) was 141 ± 7 nA, with a relative standard deviation of 5%.

The detection limit, defined as three times the signal-to-noise ratio, was 2 μg l^{-1}, which is much better than that of most sensitive spectrophotometric methods (20 μg l^{-1}).

Procedure for tap water

A 9.9-ml volume of tap water was pipetted into a quartz voltammetric cell and 0.1 ml of 0.5 mol l^{-1} phosphate buffer was added, giving a pH 6.8. A 20-μl volume of a 1×10^{-4} mol l^{-1} stock solution of DASA was added, corresponding to a final concentration of 2×10^{-7} mol l^{-1}. Finally, 50 μl of 0.1 mol l^{-1} EDTA solution were added. Before the electrochemical measurement the solution was degassed for 10 min. The measurement was made after a preconcentration step in which the solution was stirred (600 rpm) for 1.5 min at a potential of −0.300 V. At the end of the deposition time the stirring was stopped and after a rest period of 20 s the potential was scanned in the negative direction at a scan rate of 5 mV s^{-1}. The following values were used: drop area, 1.39 mm^2; pulse rate, 2 s^{-1}; and pulse amplitude, 20 mV.

The proposed method was applied to the determination of ClO_2 in tap water and compared with the direct *N,N*-diethyl-*p*-phenylenediamine (DPD) spectrophotometric method and the selective indirect Chlorophenol Red (CPR) spectrophotometric method (Table 1). There was a factor of 10 difference between the DPD and the DASA methods, probably owing to the non-selectivity of the spectrophotometric method. The DPD reagent is sensitive to light and can also be readily oxidized by some organic or inorganic substances dissolved in the sample.

Note

Ozonization is a prestep used in the treatment of the drinking water of the city of Brest. However, O_3 disappears more or less rapidly in the pipes owing to its reactivity with the dissolved organic substances and the by-product ClO_2^-. The oxidation of ClO_2^- by ozone would partly explain

Table 1
Determination of chlorine dioxide (mol l^{-1}) in tap water

Sample No.	DPD method	CPR method	This work
1	1.6×10^{-6}	$<3\times10^{-7}$	1.7×10^{-7}
2	1.7×10^{-6}	$<3\times10^{-7}$	1.9×10^{-7}

the formation of ClO_3^- ions (0.1–0.2 mg l^{-1}). After flowing for 48–72 h in the pipes, O_3 is not found and so does not introduce errors in the titration of chlorine dioxide.

References

[1] A.T. Palin and K.G. Darral, J. Inst. Water Eng. Sci., 33 (1979) 467.
[2] I.J. Fletcher and P. Hemmings, Analyst, 110 (1985) 695.
[3] W.J. Masschelein, G. Fransolet, P. Laforge and R. Savoir, Ozone Sci. Eng., 11 (1989) 209.
[4] D.L. Harp, R.L. Klein and D.J. Schoonover, J. Am. Water Works Assoc., (1981) 387.
[5] Information Atochem CAL, Centre d'Application de Levallois, 1978, ref. LCK 1319.
[6] C.M.G. Van Den Berg, K. Murphy and J.P. Riley, Anal. Chim. Acta, 188 (1986) 177.
[7] F. Quentel, C. Elleouet and C. Madec, Electroanalysis, in press.
[8] D.G. Perrin, Stability Constants of Metal-Ion Complexes, Part B (IUPAC Chemical Data series, No. 22), Pergamon Press, Oxford, 1979.
[9] W. Masschelein, Anal. Chem., 38 (1968) 1839.
[10] C. Madec, F. Quentel, J. Courtot-Coupez and M. Doré, Analusis, 15 (1987) 69.
[11] H. Li and C.M.G. Van Den Berg, Anal. Chim. Acta, 221 (1989) 269.

ELSEVIER

Analytica Chimica Acta 295 (1994) 93–100

ANALYTICA CHIMICA ACTA

Design criteria and implementation of hypermedia tools for structure elucidation of organic compounds with spectroscopic methods

Andreas Gloor [a], Marc Cadisch [a], Tamás Kocsis [a], Renate Bürgin Schaller [a], Hans-Jörg Hediger [a], Jean Thomas Clerc [b], Ernö Pretsch [a,*]

[a] *Department of Organic Chemistry, Swiss Federal Institute of Technology (ETH), Universitätsstr. 16, 8092 Zürich, Switzerland*
[b] *Department of Pharmacy, University of Bern, Baltzerstr. 5, 3012 Bern, Switzerland*

Received 15th November 1993; revised manuscript received 30th March 1994

Abstract

Hypermedia open up new possibilities for organizing and storing information. They are ideally suited to interrelate data according to various principles. Different logical structures encompassing the pieces of information can be implemented simultaneously.

Key words: Hypermedia; Molecular spectroscopy; Hypertext; Spectra interpretation

1. Introduction

Despite the progress made in understanding spectroscopic phenomena, applied spectroscopy is still more of an empirical art than pure science. The practical spectroscopist needs quick and easy access to a large body of data and rules compiled over the years. This knowledge is traditionally organized in books and other printed media. Recent developments in electronic data processing have resulted in other ways to make spectroscopic experience accessible. The most straightforward approach consists in converting the contents of books into computer-readable form, without significant modification apart from enlarging the conventional index systems by additional levels. In contrast, expert systems use spectroscopic rules and reference data as their knowledge base to derive conclusions about the chemical structure of unknown compounds.

The "electronic book" approach, as opposed to the printed book, makes access to spectroscopic facts and rules definitely more convenient and faster and allows for relatively easy insertion of additional, and revision of existing, data. However, it does not open new access roads and the levels of cross indexing remain limited. The same holds for computer-readable compilations of reference spectra.

Expert systems attempt to map the present state of knowledge by collecting basic facts and casting relations between facts into rules. The

* Corresponding author.

SSDI 0003-2670(94)00163-G

inference machine inherent in every expert system then tries to draw conclusions about the problem at hand by combining rules and facts. Thus, the inference process is not under direct control of the user. This is why only those pieces of information considered as relevant by the system designer delimit the decision chain and guide the user. Furthermore, modification of existing and installation of new rules are difficult and, due to unexpected interactions, risky. Hence, in the real world, expert systems are static, limited to standard cases and have a definite tendency to early obsolescence.

Here, we present SpecTool, a new hypermedia-based approach to make spectroscopic facts and rules easily accessible to the user by combining the strong points of the classical systems but avoiding their drawbacks.

2. The hypermedia concept

The classical medium for data storage is the book. Here, the information is physically organized in blocks, i.e., pages. This results in a natural linear order: each page has exactly one previous and one following page, except for the first and last, and the logical structure of the information is forced to follow the clear and simple organization along this path. The index of a book offers another linear structure providing access points to the main information stream.

In the classical data bank, on the other hand, the sequence of the information blocks becomes irrelevant and two succeeding blocks need not be logically related to each other. Thus, in contrast to books, browsing through a data bank is hardly ever useful. The number and types of indexes is, however, almost unlimited.

Hypermedia try to combine the strong points of both approaches. A data bank-like structure allows quick and easy access to any information block via classical indexing functions. This is of advantage when the user knows exactly what he is looking for. In addition, each information unit is linked to all other logically related blocks so that browsing through the data compilation as through a book is possible. The logical connections between the blocks depend on the context. They belong to different classes of links interweaving the data base in form of a network and enable the user to consider a topic under different aspects.

However, in contrast to books and data banks, the information in hypermedia also includes programs, graphics, animated graphics and sounds. A hypermedia application thus consists of facts, tools to manipulate them and connections between logically related clusters of facts and tools. The logical connections are called links, whereas the clusters of facts and/or data are referred to as nodes.

In SpecTool, the node contents cover the spectroscopic techniques most frequently used in the structure elucidation of organic compounds, i.e., mass spectrometry, ^{13}C and ^{1}H NMR spectroscopy as well as IR and UV–visible spectroscopy. The links implemented map the thought patterns of the analyst interpreting the spectra. The data structure is selected so as to render this mapping logical and easy.

The system has been realized using HyperCard® [1]. It handles textual, pictorial and acoustic information. The included HyperTalk, an interpreter language with run-time compilation, is suitable for developing versatile navigation tools to manage well-structured data representations. Furthermore, it is appropriate for performing simple calculations. For more involved computations, routines written in common programming languages, such as Fortran, Basic, Pascal or C, can be added as external commands. Interfaces to external files and stand-alone compiled programs are also available. Thus, more demanding applications can be attached. Even interfaces to external programs running on another computer, e.g., to spectroscopic data bases, can be established within the HyperCard® application.

The organization units of HyperCard® are cards (nodes) collected in stacks (files). A card may contain written and/or graphic information and have one or more special areas which upon mouse click show the information in a different form, jump to another card or invoke a program. These features allow for versatile data presentation, for designing flexible navigation structures

and performing fairly simple calculations. Due to the architecture of HyperCard®, processes implemented in HyperTalk run rather slowly so that more involved computations are better performed by calling external commands or programs.

In the following, the different components of the SpecTool hypermedia application are described.

3. Logical structure

3.1. Nodes

Nodes are the basic units of the data structure and are classified according to the spectroscopic method, type of information and compound class. Sometimes, not all information contained in a node can be displayed simultaneously. Therefore, by clicking specially underlined keywords, related information is brought to the front.

In case a table or text is too long to be displayed entirely on one card, scrollable fields are used. Various strategies allow quick access to the desired information. For example, in the table of Fig. 1, apart from usual scrolling, the compounds belonging to a particular substitution type appear at the top after clicking the corresponding index entry on the left. In addition, the table may be sorted according to increasing values of any of the columns by mouse click at the respective heading. In other cases, scrollable fields may be controlled via pop-up menus.

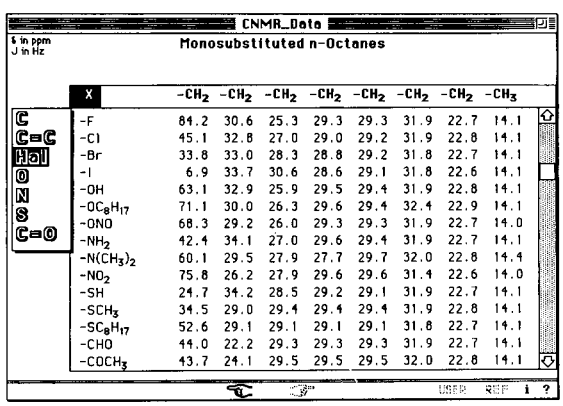
CNMR_Data

δ in ppm
J in Hz

Monosubstituted n-Octanes

C
C=C
Hal
O
N
S
C=O

X	-CH2	-CH2	-CH2	-CH2	-CH2	-CH2	-CH2	-CH3
-F	84.2	30.6	25.3	29.3	29.3	31.9	22.7	14.1
-Cl	45.1	32.8	27.0	29.0	29.2	31.9	22.8	14.1
-Br	33.8	33.0	28.3	28.8	29.2	31.8	22.7	14.1
-I	6.9	33.7	30.6	28.6	29.1	31.8	22.6	14.1
-OH	63.1	32.9	25.9	29.5	29.4	31.9	22.8	14.1
-OC8H17	71.1	30.0	26.3	29.6	29.4	32.4	22.9	14.1
-ONO	68.3	29.2	26.0	29.3	29.3	31.9	22.7	14.0
-NH2	42.4	34.1	27.0	29.6	29.4	31.9	22.7	14.1
-N(CH3)2	60.1	29.5	27.9	27.7	29.7	32.0	22.8	14.4
-NO2	75.8	26.2	27.9	29.6	29.6	31.4	22.6	14.0
-SH	24.7	34.2	28.5	29.2	29.1	31.9	22.7	14.1
-SCH3	34.5	29.0	29.4	29.4	29.4	31.9	22.8	14.1
-SC8H17	52.6	29.1	29.1	29.1	29.1	31.8	22.7	14.1
-CHO	44.0	22.2	29.3	29.3	29.3	31.9	22.7	14.1
-COCH3	43.7	24.1	29.5	29.5	29.5	32.0	22.8	14.1

Fig. 1. Table containing ^{13}C NMR shift values of monosubstituted *n*-octanes.

Whenever numerical data lend themselves to graphic representation, the user is given the choice of how he wants the information to be displayed. For example, clicking an entry in the abundance table of the MS tool "Isotope Table" results in a graphic display of the isotope pattern for the selected element. In some cases, even simple dynamic displays have been realized. For example, when applying the Karplus relationship [2,3] in the ^1H NMR section, a graph of coupling constant vs. torsion angle for the partial structure currently displayed is presented. By following the curve with the mouse pointer, the respective data pairs are shown numerically.

More sophisticated calculations are triggered by computational nodes which are similar to information nodes but are used for calling different kinds of programs. In case of simple calculations, they may be implemented in HyperTalk. On the other hand, certain programs for more demanding tasks do not have their own user interface but are invoked with a list of input parameters, execute their code instructions invisibly to the user and transfer the output values back to the invoking node, where the results are processed and displayed. This group consists of code resources that are physically integrated into a HyperCard® stack, enlarging the set of built-in HyperTalk commands, and of stand-alone applications that run without any user interaction. A further possibility is to call an external program that is completely independent of SpecTool and takes the full responsibility for all input and output so that the user is no longer within the SpecTool environment. After ending the job, the program flow returns to the invoking SpecTool node.

At present, programs are available for calculating molecular formulas (MolForm) [4], isotope patterns (using the algorithms from [5]), mass spectral fragmentations (patterned after MS-BREAK [6]) [7], ^{13}C [8] and ^1H NMR shift values [9] and spin systems as well as for assembling molecules [10]. Numerous other utilities mainly based on rules and relations taken from [11] allow to estimate chemical shifts and coupling constants for different skeletons. These computa-

tional nodes not only make use of available computing power but also guarantee a user-friendly presentation of certain hidden data tables. As an example, in linear additivity models for predicting ^{13}C and ^{1}H NMR chemical shifts of members of the most common compound classes, substituent increments are handled by means of computational nodes. The user is first presented with a drawing of the skeleton of the selected compound class. Using pop-up menus, he can then place substituents at the desired positions and the system immediately displays the chemical shift values predicted for the assembled compound.

Apart from browsing through the hyperspace of system nodes, the user can attach his own comments (text and pictures) to any card he desires. This individual information is stored on so-called user cards that are automatically connected to their parent node. So, once they have been created, they can be easily reached by clicking the USER button on the parent node. All user cards related to the same SpecTool stack are gathered in a user stack. In this way, the present data base can be considerably enlarged without any loss of clarity.

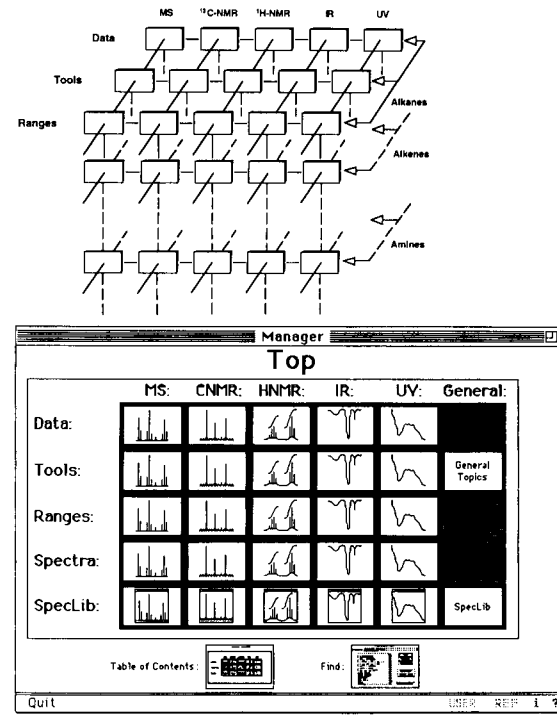

Fig. 2. Schematic representation of SpecTool hyperspace (top) and Top card (bottom).

3.2. Links

Logically related nodes are connected by links in a basically tree-like hierarchical structure whose root is represented by the Top card (Fig. 2, bottom). In addition, horizontal links as well as cross-links between nodes on different levels create a network allowing further possibilities of navigation.

The applied hierarchical classification scheme of organic compounds takes into account the peculiarities of each spectroscopic method. Every information is located according to three mutually orthogonal aspects, i.e., it relates to a particular spectroscopic method, a given type of information (namely numerical and spectral data as well as computational tools) and a specific compound class. The knowledge pool thus spans a 3-dimensional hyperspace, its three axes corresponding to the spectroscopic method, the type of information and the compound type, as shown schematically in Fig. 2 (top). Each box in this scheme contains itself a hierarchical tree connecting the individual compounds (or compound subclasses) collected in the respective node. Hence, the information space has more than three dimensions and is therefore referred to as hyperspace. The first level of the compound classification scheme is identical for all five spectroscopic methods considered. It is represented by the selection screen shown in Fig. 4 and corresponds to a column in Fig. 2 (top). The third dimension in the latter Figure, representing the type of information (Data, Tools, Ranges, Spectra, SpecLib), can be chosen from the Top card and, except for Ranges, via palette or menu bar.

Data cards contain textual and numerical information assigned to specific molecules or in the form of tables. Under Tools, different types of computational instruments are collected (for details, see "Nodes"). Ranges, on the other hand, provides an alternative entry to the system. For example, in the NMR and IR sections (cf. Fig. 3),

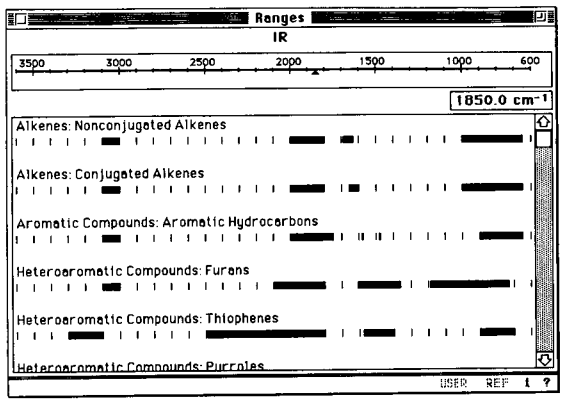

Fig. 3. Correlation table for IR ranges. The user selects the desired value by mouse click on the scale, upon which the appropriate table is displayed below. The items listed can be accessed by clicking at the corresponding line.

a correlation chart can be accessed via the Top card. By clicking at the desired value on the scale, a list of compound classes that typically satisfy this requirement is shown, from where an item may be selected for jumping to the corresponding data card. In Spectra, sets of reference spectra of prototype compounds are accessible, whereas in the more extensive SpecLib section, additional facilities, such as stretching and enlarging, are offered when examining spectra.

The definition of the main compound classes is similar to that found in many books containing spectroscopic information (e.g., [11]). Inevitably, it is a mixed concept because it consists partly of skeletons and partly of typical substituent groups (cf. Fig. 4). Redundancies are built in so that when in doubt, the user may find the same information in several places or be directed to the desired place via different routes. This is the case, for example, with phenol which has both a substituted aromatic skeleton and a OH group. Most of the 25 compound classes displayed in Fig. 4 are self-explanatory. The last icon in the fourth row symbolizes the periodic table. Under this entry, organic compounds containing elements that do not show up in the other classes can be found. Via the icon "Special", certain spectroscopic information is available that does not fit into the scheme of chemical compound classes (spectroscopic data of solvents, various overview and correlation tables).

On the next lower hierarchical level, nodes still have similar appearances but different contents. Only on the third level, the node entries become fully method-specific. Thus, for example, after having chosen ^{1}H NMR and clicked the icon for sp^3 hybridized amines and related compounds in Fig. 4, the user gets the screen shown in Fig. 5 allowing more specific selections. A click at one of these icons will present the pertinent data.

This structured way of data access guarantees that none of the navigation cards is overloaded with information so that quick orientation is possible. Several hundreds of nodes (data, tools and spectra cards) can be addressed in this two-step

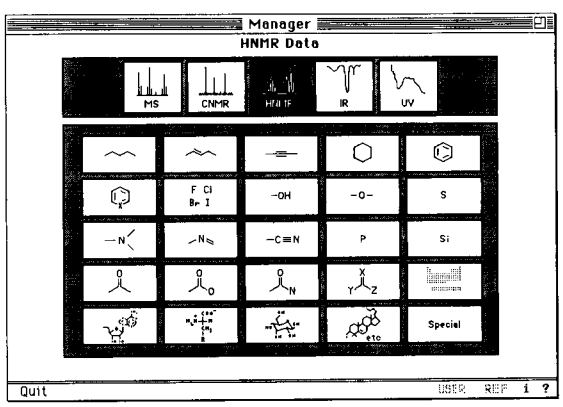

Fig. 4. Table of contents showing the compound groups of H NMR data. The same organization pattern is also followed in the other spectroscopic methods.

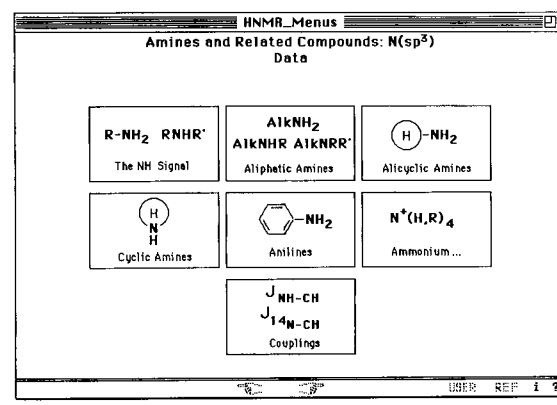

Fig. 5. Table of contents showing the data nodes of amines and related compounds in the ^{1}H NMR spectroscopy section.

process and none of the steps involves a selection from more than 25 items.

In contrast, horizontal navigation allows to remain on the same hierarchical level while switching between spectroscopic methods and types of information. This is achieved in one step via palette or menu bar. If the target node were inexistent, the next higher level is accessed. Starting from the menu card for Data shown in Fig. 5 and choosing, for example, "Spectra" via palette or menu bar, the corresponding ^{1}H NMR Spectra card is reached.

At every point of SpecTool, based on the currently presented information, the user decides which step to take next. Thus, he can browse through the system and backtrack whenever he is not satisfied. This implies the danger of going around in circles, becoming confused or getting outright lost. To minimize this problem, various precautions have been taken. At any place, the user may inspect the horizontal neighbours of the current card. By means of a pop-up menu appearing in the title field, he can also see (or move to) higher levels up to the Top card. On the other hand, a table of contents of the actual stack allows him to invoke a jump to any of the items listed. In addition, a global table of contents from where any node of the system can be accessed in one step, is available via palette, menu bar or Top card. Furthermore, backtracking is always possible till reaching familiar surroundings again.

3.3. Navigation tools

The navigation tools implemented have the form of menus, palettes or simple buttons and may be local or global but always involve a jump to another logically related place within the system. The target position may be defined independently of, or relative to, the current position. Local navigation tools are limited to absolute jumps and have a standardised appearance but vary in their contents. Global navigation tools are standardised with regard to appearance and contents, i.e., they look the same throughout the whole system. Their performance, however, may be context-dependent.

Following the direction of the coordinate axes of the hyperspace (cf. Fig. 2, top), switching between the columns means that the user can freely move between the different spectroscopic methods and between the types of information. Having selected these two coordinates, he may navigate among the compound classes, i.e., move vertically within a column of Fig. 2 (top).

There are several ways to enter the SpecTool system. Of course, a hierarchically structured table of contents is provided, similar to that of books but enriched with all the comfort hypermedia offer. Moreover, the user can dive into the data base by stepwise refining his choice: after selecting a combination of spectroscopic method and type of information on the Top card (cf. Fig. 2, bottom), he chooses a compound class (cf. Fig. 4) and finally, a particular item (cf. Fig. 5). As an alternative, he can specify a parameter value (cf. Fig. 3) upon which the system presents a set of fitting substructures; a further click at one of the entries gives access to the respective Data section. Furthermore, there is the possibility of searching for given keywords via a Find tool. In addition, the user may attach bookmarks to any node in order to enable direct access via menu bar.

3.4. File structure

The file structure of the system [12] has been designed with two goals in mind: it had to be transparent for development and updating as well as allow straightforward implementation of various logical structures. At present, the system consists of 35 stacks, i.e., 3 stacks devoted to general control and overall organization, 8 navigation stacks, 17 data, tools and spectra stacks, 6 help stacks and 1 stack for storing the settings of user-selectable parameters. Currently, SpecTool interfaces with 6 external applications. As mentioned above (see *Nodes*), any accessible stack may be provided with a supplementary, so-called user stack for individual data and comments.

The system is physically divided into two sections. One contains all read-only objects and could be transferred to CD-ROM in a future version. The other consists of dynamic data, including start-up modules, user settings, bookmark files

and user stacks, and must be located on a writeable storage medium.

4. Implementation

SpecTool was originally developed with HyperCard® 2.1 for Apple Macintosh computers. An MS DOS version based on ToolBook is in preparation. The Macintosh version requires at least 1 MByte RAM. In case of calling one of the interfaced external applications, another 500 to 1500 kBytes are needed. SpecTool consists of about 2000 nodes and nearly 80000 links and occupies a disk space of 8 MBytes. The attached spectrum library with approximately 3000 spectra of prototype compounds (500 to 1000 for each of the methods covered) needs another 23 MBytes disk storage.

Thanks to the internal architecture of HyperCard® and the current structure of SpecTool, updates are easy to implement. The modular organization allows for quick replacement as well as enhancement of the system. In addition, all routines designed for global tasks, such as navigation and menu handling, are centrally gathered in three special stacks. Thus, the general performance of the system can be modified just by changes within the program stacks without touching the data stacks.

5. How to use SpecTool

A major characteristic and advantage of hypermedia systems lies in the possibility to adapt their use to the problem at hand. Because of this almost unlimited flexibility of a well designed hypermedia application, a comprehensive description is almost impossible. Thus, only a few examples of its main features are given here by way of illustration, concentrating on problems typical in analytical chemistry.

SpecTool is not an expert system that aims at replacing the human analyst but rather a tool for relieving him from memorizing huge amounts of detail knowledge, retrieving data from books or data bases and doing extensive or trivial calculations. Thus, when the chemical structure of an unknown compound is to be determined from its spectra, the analyst must perform the initial interpretation steps. In a first superficial examination, he will collect a crude set of features of the sample compound, e.g., results from microanalysis, probable molecular mass values from the MS, conspicuous functional groups from the IR spectrum and the approximate numbers of C and H atoms from the NMR spectra, possibly also taking into account the UV–visible spectrum. SpecTool now supplies the tools for refining the educated guesses made on this basis and checking their consistency.

Let us assume, for example, that the molecular mass inferred is 248 and that further evidence from other spectra provides the limits for the number of atoms (e.g., from number of discernible ^{13}C NMR signals, integrals in ^{1}H NMR spectra, isotope patterns in MS) and of double bond equivalents (DBE; e.g., from UV spectrum and number of ^{13}C NMR signals of sp^2 carbons). Provided with the necessary parameters, the MolForm module now computes all molecular formulas compatible with the assumptions made. In the above example, with the limits set as C_{11-14}, H_{14-16}, N_{0-10} and O_{1-5}, four molecular formulas are found. If available, the results of a microelemental analysis may also be used. With this information, the initial list of possible structures can be pruned considerably. The analyst now has a set of loosely related pieces of information to be put into a reasonable and self-consistent context.

For example, if he suspects an oxime group to be present in the molecule, he looks up its spectral characteristics to see whether the corresponding data is compatible with the experimental facts. After jumping to the screen shown in Fig. 4, he selects the button for sp^2-hybridized nitrogen. This brings up the selection node for the respective compound classes (analogous to Fig. 5), among them for oximes if available. Then, the corresponding Data or Spectra card can be accessed where model compounds as well as outliers are presented with compound-specific and general rules. In the above example, ^{1}H NMR data for four prototype compounds are given

together with a rule for relating $\Delta\delta$ (between *syn* and *anti* protons) to the dihedral angle.

The unique advantage of hypermedia comes into action when the user wants to cross-check his tentative decisions. A simple selection operation invokes a jump to the oxime data of another spectroscopic method or information type. If there is no corresponding node on the target layer, the next higher hierarchical level is accessed instead. For example, as there is no MS Data card for oximes, a jump from the ^{1}H NMR Data card to the MS layer brings the user to the index screen of available sp^2-hybridized nitrogen compounds (analogous to Fig. 5).

In case the user doubts the oxime hypothesis or wants to double-check his assumptions, he goes up one step in the hierarchy and is brought again to the index node for sp^2-hybridized nitrogens. From there, he can select other icons in order to compare related types of compounds. If, on the other hand, he decides to inspect another class of compounds, e.g., other hydroxy derivatives, he simply switches by selecting this item from the palette or menu bar.

The series of operations described generally results in a list of monofunctional chemical substructures which have to be put together to form a meaningful molecule. For this step, SpecTool again offers a wide choice of useful tools, including a molecular assembler, tools assisting in the interpretation of mass spectra as well as NMR shift prediction and spin system simulation programs.

In order to transfer data from SpecTool to his own documents, the user may freely employ screen copying facilities or the built-in menu command "Take Picture" which puts an image of the current card into the clipboard or a file.

6. Conclusions

It is shown that hypermedia can be used to collect large amounts of data in a complex but transparent structure. Applied to molecular spectroscopy, the system calls for an organization scheme according to three mutually orthogonal aspects, i.e., spectroscopic method, type of information and chemical compound class. Whenever such mutually independent organization principles are relevant, hypermedia are especially attractive. However, building up a hypermedia system implies elaborate planning and a lot of work. An essential feature of SpecTool is the user interface which has been designed to be both self-explanatory and user-friendly. The selection and presentation of the reference data had to be made manually by chemists knowledgeable in spectroscopy and hypermedia.

To apply SpecTool, at least some basic knowledge of the spectroscopic methods covered is indispensable. Although hypermedia would be suitable for developing a tutorial for novices in spectroscopy, no efforts have been made in this respect. Based on the experiences described here, it is planned to publish the system (available from Chemical Concepts, Weinheim).

Acknowledgments

This work was partly supported by the Swiss National Science Foundation.

References

[1] HyperCard®, Claris Co., Santa Clara, CA, USA.
[2] M. Karplus, J. Am. Chem. Soc., 85 (1963) 2870.
[3] K. Imai and E. Osawa, Magn. Res. Chem., 28 (1990) 668.
[4] A. Fürst, J.T. Clerc and E. Pretsch, Chemom. Intell. Lab. Syst., 5 (1989) 329.
[5] H. Kubinyi, Anal. Chim. Acta, 247 (1991) 107.
[6] H. Kubinyi, in J. Gasteiger (Ed.), Software-Entwicklung in der Chemie 2, Springer Verlag, Berlin, 1988, p. 167.
[7] T. Brodmeier, A. Gloor, M. Cadisch, R. Bürgin and E. Pretsch, Anal. Chim. Acta, 277 (1993) 297.
[8] A. Fürst and E. Pretsch, Anal. Chim. Acta, 229 (1990) 17.
[9] R. Bürgin Schaller and E. Pretsch, Anal. Chim. Acta, (1994) in press.
[10] C.A. Shelley and M.E. Munk, Anal. Chim. Acta, 133 (1981) 507.
[11] E. Pretsch, J.T. Clerc, J. Seibl and W. Simon, Tables of Spectral Data for Structure Elucidation of Organic Compounds, Springer Verlag, Berlin, 2nd edn., 1989.
[12] M. Cadisch, M. Farkas, J.T. Clerc and E. Pretsch, J. Chem. Inf. Comput. Sci., 32 (1992) 286.

ELSEVIER

Analytica Chimica Acta 295 (1994) 101–107

ANALYTICA CHIMICA ACTA

Reliability of conversion–time dependencies as predicted from thermal analysis data

Sergey Vyazovkin *,[1], Wolfgang Linert

Institute for Inorganic Chemistry, the Technical University of Vienna, Getreidemarkt 9, Vienna A-1060, Austria

Received 21st January 1994; revised manuscript received 5th April 1994

Abstract

The isothermal dependencies of the conversion on time can be predicted from data resulting from thermal analysis experiments performed under non-isothermal conditions. The reliability of the predictions depends on an approach used to define the kinetic triplet (the activation energy, the pre-exponential factor and the reaction model). Five different approaches were examined and typical errors were pointed out. It was concluded that an approach (1) which uses only one thermal analysis experiment to define the kinetic triplet should not be used for predictions. In the case of a single-step process the approaches suggested by, correspondingly, the ASTM E648 (2), Malek (3) and Vyazovkin (4) are applicable, but (2) leads to crucial errors when the process does not obey a first-order reaction. For a complex process approaches by Kaisersberger and Opfermann (5) as well as (4) should be used. The predictions of (4) are expected to be more reliable because they are free from ambiguity which is peculiar to (5).

Key words: Conversion–time dependencies; Thermal analysis

1. Introduction

While exposing a substance to a programmed heating procedure, methods of thermal analysis can give comprehensive information on the thermal stability of a substance in a wide temperature interval. However, very often it is necessary to observe the behaviour of a substance at a constant temperature. A serious experimental problem occurs if the process being studied proceeds either very slowly or very fast at a temperature of interest. Such a problem is solved by means of predictions based on the kinetic characteristics of a process found at other temperatures.

To describe the kinetics of the conversion of a substance at a constant temperature T_0 the following equation is commonly used [1]

$$g(w) = k(T_0)t$$

It gives a theoretical description of the experimentally observed change in the degree of conversion (w) with time (t). The description includes the model of a process, $g(w)$, and the rate constant, $k(T_0)$. The $g(w)$ model may take different mathematical forms [1] depending on a specific reaction pathway. Influence of temperature

* Corresponding author.

[1] On leave from Institute for Physico-Chemical Problems, Byelorussian University.

SSDI 0003-2670(94)00167-K

on the process kinetics is given by the Arrhenius equation

$$k(T_o) = A \exp(-E/RT_o)$$

where A is the pre-exponential factor, E the activation energy and R the gas constant. Therefore, a description of the process kinetics over some temperature interval requires the knowledge of the complete kinetic triplet [E, A, $g(w)$].

From two above equations one can easily obtain the equation

$$t = g(w)/(A \exp(-E/RT_o)) \quad (1)$$

which allows for calculating time at which a given conversion will be reached at any constant temperature. According to the above equation we can predict the behaviour of a substance at any T_o if (1) the kinetic triplet was defined properly and (2) it remains the same when changing from the interval of experimental temperatures to a temperature of interest. Although the latter condition is not self-evident, we accept it without further discussion because this is an inevitable supposition of any extrapolation. The intention of this paper is to appraise different approaches to defining the kinetic triplet as applied to predicting the behaviour of a substance at a necessary temperature.

2. Analysis of the approaches used for predictions

It is obvious that the reliability of predictions depends on exactness with which the kinetic triplet is defined. The relative error of estimating t in Eq. 1 can be found by the well-known formula [2]

$$|\Delta f(x_1,\ldots,x_n)/f(x_1,\ldots,x_n)| = \sum|\Delta x_i \partial \ln f(x_1,\ldots,x_n)/\partial x_i|$$

A substitution of $n = 3$, $x_1 = g(w)$, $x_2 = A$, $x_3 = E$ leads to

$$|\Delta t/t| = |\Delta g(w)/g(w)| + |\Delta A/A| + |\Delta E/RT_o| \quad (2)$$

This relation can be used to analyse several kinetic approaches to define the kinetic triplet. The emphasis will be on the disclosure of the methodic errors specific to these approaches.

(i) The most popular approach to define the kinetic triplet is based on a thermal analysis experiment performed at only one heating rate. The E and A values computed in a such a way depend strongly on the choice of $g(w)$ model, which is always ambiguous [3]. As it was already shown [4], even a small error in the choice of $g(w)$ leads to significant errors in E and A. Upon prediction these errors become critical because each of the corresponding terms in the right hand side (RHS) of Eq. 2 exceeds completely [5].

Relatively reliable predictions can be expected only when T_o is equal to the isokinetic temperature (T_{iso}) [6]. The latter refers to an abscissa of a common intersection point of Arrhenius lines. It was shown previously [7] that the rate constant k_{iso}, found as an ordinate of the intersection point, is independent of $g(w)$ chosen and equal to the actual rate constant of the process occurring at T_{iso}. In such a case we can substitute the denominator in Eq. 1 by the value of k_{iso} which is supposed to be an exact value

$$t = g(w)/k_{iso}$$

Because of this the relative error in t computed this way only originates from the first term in RHS of Eq. 2. Fig. 1 shows the order of magnitude of this error when the model of a first-order reaction was wrongly chosen for the process which in fact follows one of six different models. It is seen that even this error may be excessive for predicting a substance behaviour. Therefore the reliability of the predictions made by approach (i) is on the whole rather doubtful.

(ii) An approach allowing to avoid the critical errors in E and A was suggested in the ASTM E698 standard [8]. Accordingly, several DSC or DTA experiments at different heating rates should be performed. The activation energy is calculated by either Ozawa's [9] or Kissinger's [10] method using the dependence of temperature of DSC/DTA peak maxima (minima) on the heating rate. Since these methods allow calculation of E without any suppositions about $g(w)$, the reliability of the values so obtained raises no doubts.

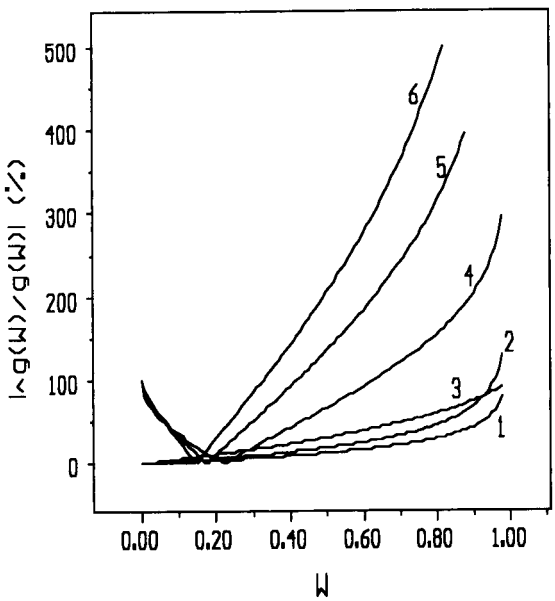

Fig. 1. Relative error appearing when the process obeys a non-first-order model: 1 = contracting sphere; 2 = contracting cylinder; 3 = second order; 4–6 = Avrami-Erofeev model with corresponding m values of 2–4.

The predictive errors of this approach relate to defining both $g(w)$ and A values. It is supposed [8] that the process being studied is a first order reaction, i.e., $g(w) = -\ln(1-w)$. This assumption is also used in ASTM E698 to calculate the pre-exponential factor as

$$A = q \cdot \exp(E/RT_m) \cdot E/RT_m^2 \qquad (3)$$

where q is the heating rate, the subscript m means that the value corresponds to the DSC/DTA peak maxima (minima).

In a common case, when the process obeys any model other than a first order one the predictive error is equal to the sum of two first terms in the RHS of Eq. 2. An application of the first term has been demonstrated in Fig. 1. It is evident that even if the error in computing the pre-exponential factor is neglected the predictive errors of the ASTM E698 approach can be very substantial, especially at high conversions.

Let us now estimate the contribution of the error in the pre-exponential factor appearing when the process does not obey first-order rules. For this purpose we should use a general equation suitable to compute the pre-exponential factor for a single-step process obeying an arbitrary reaction model. One can easily derive such an equation from the generally accepted rate equation

$$dw/dT = (A/q)\exp(-E/RT)f(w)$$

$f(w) = [dg(w)/dw]^{-1}$ is the differential form of the $g(w)$ model applying a condition of maxima ($d^2w/dT^2 = 0$) to it. The resulting equation

$$A = \left(-df(w_m)/dw\right)^{-1} q \cdot \exp(E/RT_m) \cdot E/RT_m^2 \qquad (4)$$

holds for any single reaction. Eq. 3 can easily be derived from this equation assuming a first-order reaction takes place, i.e., $f(w) = 1 - w$. Now we can estimate the relative deviation of A computed by Eq. 3 from the value computed by Eq. 4

$$|\Delta A/A| = |df(w_m)/dw + 1|$$

The estimates of the above error for different processes are presented in Table 1 from which it can be seen that the contribution of this error

Table 1
Relative errors in the pre-exponential factor value computed by the ASTM E698 approach provided the process obeys one of the following models

Model	$f(w)$	w_m [a]	$\lvert\Delta A/A\rvert$ (%)
Contracting sphere	$(1-w)^{2/3}$	0.680–0.700	2.5– 0.5
Contracting cylinder	$(1-w)^{1/2}$	0.725–0.735	4.7– 2.9
Second order	$(1-w)^2$	0.450–0.490	10 – 2.0
Avrami-Erofeev, $m = 2$	$(1-w)[-\ln(1-w)]^{1/2}$	0.610–0.625	55 –51
Avrami-Erofeev, $m = 3$	$(1-w)[-\ln(1-w)]^{2/3}$	0.623–0.630	69 –67
Avrami-Erofeev, $m = 4$	$(1-w)[-\ln(1-w)]^{3/4}$	0.630–0.638	76 –74

[a] The values of w_m were taken from [11].

may also be crucial. Therefore, the reliability of the predictions made by the ASTM E698 approach is very doubtful in the often occurring case when the process does not obey a first-order reaction.

(iii) The problems peculiar to the ASTM E698 approach have been overcome in an approach suggested by Malek [12]. This approach uses the Kissinger method to compute the activation energy. However, it differs significantly in its possibility to carefully determine both the model and the pre-exponential factor. Basically, this approach minimizes the errors related to the first two terms in the RHS of Eq. 2. Obviously the predictions made on the basis of the kinetic triplet defined by this approach will be much more exact than (ii). One must bear in mind, however, that this approach can be employed for a simple (single-step) process solely.

The problem appears when the process under consideration is a complex (multi-step) one which means that it cannot be described by the single kinetic triplet. This complexity can easily be detected [13] from the conversion dependence of the activation energy computed by the isoconversional method. In the case of a complex process the activation energies computed by (ii) and (iii) are relatively correct only for limited degrees of the conversion, namely that which correspond to the maxima (minima) of the differential (DSC, DTA, DTG) curve. Outside this conversion interval all three terms in the RHS of Eq. 2 contribute to the overall predictive error. Thus for a complex process reliable predictions can be made by approaches (ii) and (iii) only for a narrow interval of conversions. Failures of the approach (ii) to predict the dependence of the conversion on time for the model complex process have been demonstrated in [14]. Below we consider two approaches surmounting this limitation for complex processes.

(iv) An approach to kinetic processing of thermal analysis data on complex processes was suggested by Kaisersberger and Opfermann (Netzsch kinetics software) [15]. It allows to define the above kinetic triplets for consecutive, competitive and parallel independent reactions composing complex processes. However, it is the user's responsibility to choose a particular type of complex process. When a process has been chosen it becomes virtually a pure numerical problem to define the kinetic triplets for the single reactions and then to predict the conversion on time dependencies at any temperature. It is obvious, however, that the results of the predictions obtained in accordance with such approach depend on the choice of the complex process type which is never known a priori. This means that here we are again confronted with the problem of ambiguity as in (i). Therefore, when using this approach one must try all above types of complex processes and then compare the corresponding predictions each with other. Only if they coincide within a reasonable error, they can be considered as reliable ones.

(v) An alternative to (iv) are algorithms [16] based on the conversion dependence of the activation energy computed by the isoconversional method. This method allows the activation energy to be calculated at any degree of conversion from the parameters of the linear dependence $\ln(q/T_w^2)$ on $1/T_w$, where T_w is the temperature corresponding to the same degree of conversion at different heating rates. To predict the behaviour of a substance these algorithms need no additional information except the above-mentioned dependence and original thermal analysis data. In particular, the predictive dependence of the conversion on time can be calculated at any T_o by the following equation [16]

$$t = \int_0^{T_w} \exp(-E_w/RT)\, dT \Big/ \left(q \cdot \exp(-E_w/RT_o)\right) \quad (5)$$

where the subscript w implies that the value relates to a given degree of the conversion. This formula gives the time for which a given degree of conversion is reached if a process proceeds at the temperature T_o. T_w is an experimental value of the temperature corresponding to a given conversion at the heating rate equal to q. E_w is the activation energy computed by the isoconversional method for a given conversion. Varying T_w and E_w with respect to the degree of conversion

one can obtain the complete predictive curve by Eq. 5.

An advantage of this approach is that it is applicable to both simple and complex processes. It is seen from Eq. 5 that it does not contain $g(w)$ and A values, i.e., it does not contribute corresponding errors into the predictions. Using the Coats-Redfern approximation [17] of the temperature integral

$$t = \int_0^{T_w} \exp(-E_w/RT)\, dT$$

$$\approx RT_w^2 \exp(-E_w/RT)/E_w$$

we can find the relative error of estimating t in Eq. 5

$$|\Delta t/t| = |\Delta E(1/RT_0 - 1/RT - 1/E)| \quad (6)$$

Let us compare the error in time value estimated by Eq. 5 with the same error caused only by the error in the activation energy (third term in RHS of Eq. 2) when employing approach (iii). For such a purpose we accept that both the activation energy and the error in it estimated by approach (v) are equal to these values found by approach (iii). Assuming additionally that the activation energy is no less than 100 kJ mol^{-1}, it is easy to find that the following inequality

$$|\Delta E(1/RT_0 - 1/RT - 1/E)| < |\Delta E/RT_0| \quad (7)$$

is true when $T_0 < 2T$. In other words the approach (v) gives more exact predictions than (iii) when the temperature to which the experimental data are extrapolated exceeds the experimental temperature no more than twice. Fig. 2 shows the ratio of RHS to the left hand side (LHS) of Eq. 7 for the process proceeding in the temperature interval (T in Eq. 7) about 400 K with $E = 100$ kJ mol^{-1}. Such a case relates to the most commonly encountered processes. It is seen that the approach (v) makes the most notable gain in exactness when the predictions are performed at the temperature close to that of the experimental interval. More far-ranging predictions are expected to be comparable in exactness. Therefore, the reliability of the predictions made by approach (v), being applied to a simple process, is not less than that made by (iii).

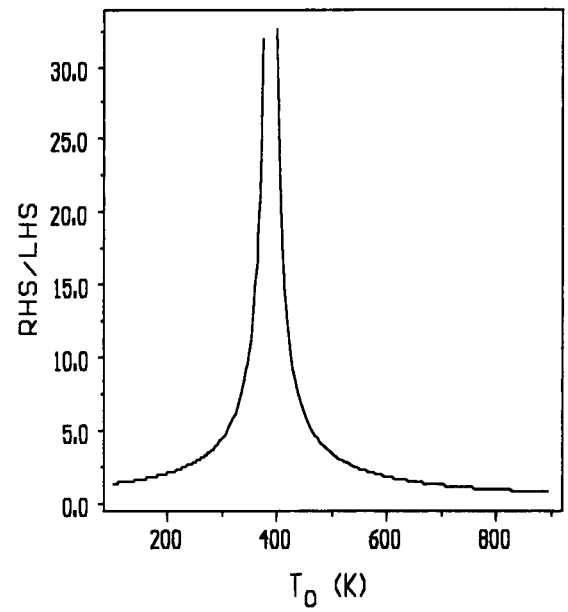

Fig. 2. Ratio of RHS to LHS (Eq. 7) for the process proceeding in the temperature interval of ca. 400 K with $E = 100$ kJ mol^{-1}.

For complex processes, high reliability of the predictions made by approach (v) was demonstrated for the model data in [14]. We also successfully used [18] it to predict the kinetic behaviour from thermal analysis data of HMX (1,3,5,7-tetranitro-1,3,5,7-tetrazocyclooctane) based compositions at burning temperatures. It should be emphasized here that this approach does not require specifying the complex process type. Consequently, its results, contrary to those of (iv), are not ambiguous. Therefore, approach (v) is considered to be the more preferable approach for predicting kinetic behaviour in the case of complex processes.

3. Further verification of approach (v)

Before approach (v) can be recommended for an extensive use, it is necessary to analyse another potential source of errors when actually applying it to a complex process. The conversion

dependence of the activation energy computed for the complex process is governed by the activation energies of the single reactions as well as by their contributions to the overall process rate. An increase in the heating rate, which normally shifts a process to higher temperatures, enhances the contribution of high temperature reactions. Therefore the E values, computed by the isoconversional method, should depend on the interval of the heating rates at which the experiments were performed. It is therefore necessary to elucidate how substantial this dependence is and how it influences the results of the predictions.

To investigate this we simulated data on a process comprising two parallel independent first-order reactions with the following Arrhenius parameters: $E_1 = 125.4$ kJ mol^{-1}, $A_1 = 10^{14}$ min^{-1}; $E_2 = 167.2$ kJ mol^{-1}, $A_2 = 10^{18}$ min^{-1}. Heating rates of 2, 5, 10, 20 and 40 K min^{-1} were selected for simulations because this interval accords to commonly used values of heating rates of the majority of the thermal analysis instruments available commercially. KinTool software [19] was used to compute the conversion dependencies of

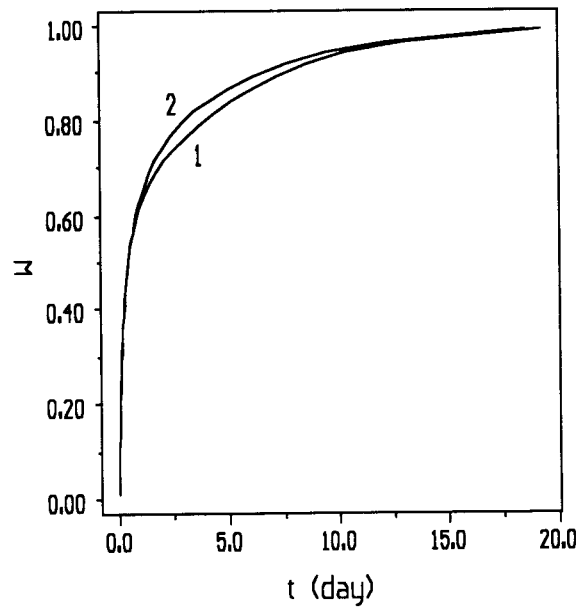

Fig. 4. Dependence of conversion on time at 400 K predicted when using the E on w dependence calculated for a heating rate of 2, 5 and 10 K min^{-1} (1) and 10, 20 and 40 K min^{-1} (2).

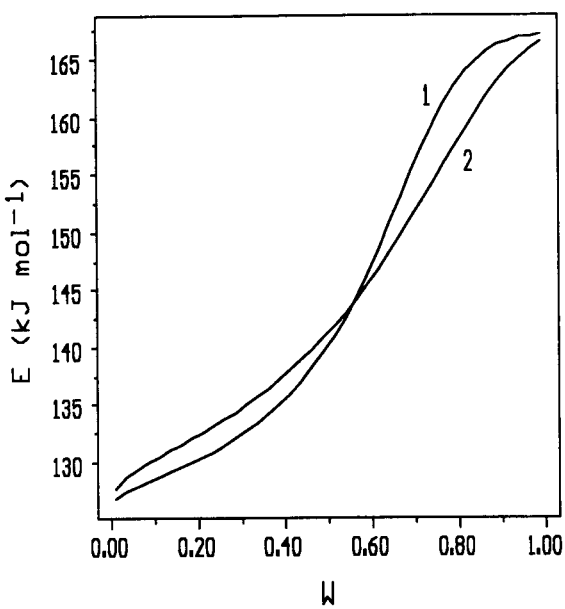

Fig. 3. Conversion dependence of the activation energy calculated for different values of heating rate: 2, 5 and 10 K min^{-1} (1) and 10, 20 and 40 K min^{-1} (2).

the activation energy by the isoconversional method as well as to predict dependencies of the conversion on time in accordance with Eq. 5.

Fig. 3 displays the conversion dependencies of the activation energy calculated for two different intervals of the heating rates. It is seen that the activation energies calculated from low heating rates are correspondingly lower at low conversions (and higher at high conversions) than those calculated from low heating rates. This result is characteristic for the process comprising two independent reactions with different activation energies. When increasing the heating rate, the temperature interval of the reaction shifts in inverse proportion to the activation energy of the reaction. Hence the relative contribution of the reaction with lower activation energy decreases at low conversions and increases at high conversions when increasing the heating rate. Furthermore, it is important to point out that the difference in the activation energies is not so substantial (< 5 kJ mol^{-1}).

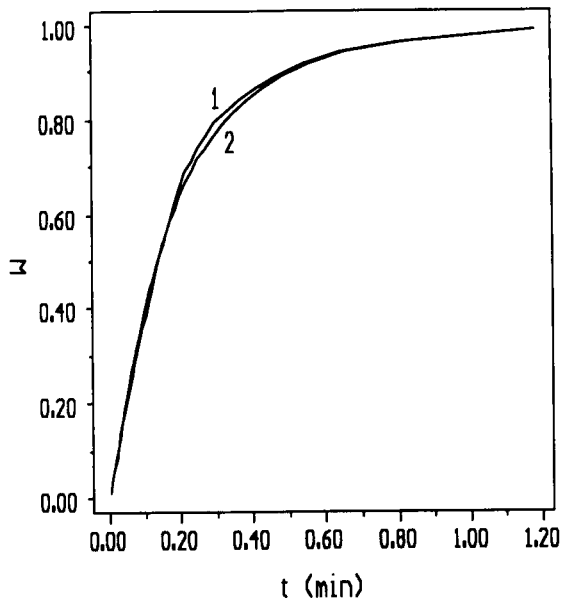

Fig. 5. Dependence of conversion on time at 500 K predicted when using the E on w dependence calculated for a heating rate of 2, 5 and 10 K min^{-1} (1) and 10, 20 and 40 K min^{-1} (2).

Fig. 4 and Fig. 5 show the predictive dependencies of the conversion on time plotted for two constant temperatures T_o. We can see that the above difference in the activation energies does not affect critically the results of the predictions.

4. Conclusions

Following the results of this paper we can recommend the following consequence of actions for reliably predicting kinetic behaviour of a substance from thermal analysis data. First, one should establish whether the process being studied is simple or complex. For this it is necessary to perform several thermal analysis experiments at different heating rates and to calculate the conversion dependence of the activation energy by the isoconversional method. If the process under study is simple (the activation energy does not depend on the conversion), approaches (iii) and/or (v) can be used to predict the kinetic behaviour of a substance. The reliability of both approaches seems to be close. When the process under study is found to be complex (the activation energy depends on the conversion), the approaches (iv) and/or (v) can be used. However, the predictions made in accordance with (v) are expected to be more reliable because they do not bear the ambiguity peculiar to (iv).

Acknowledgments

Thanks are due to the Fonds zur Förderung der wissenschaftlichen Forschung in Österreich for financial support under the projects 8795 and M0055.

References

[1] M.E. Brown, Introduction to Thermal Analysis, Chapman and Hall, London, 1988.
[2] G.A. Korn and T.M. Korn, Mathematical Handbook, McGraw-Hill, New York, 1968.
[3] S.V. Vyazovkin and A.I. Lesnikovich, J. Therm. Anal., 35 (1989) 2169.
[4] S.V. Vyazovkin and A.I. Lesnikovich, Thermochim. Acta, 165 (1990) 11.
[5] S.V. Vyazovkin and A.I. Lesnikovich, Thermochim. Acta, 182 (1991) 133.
[6] W. Linert and R.F. Jameson, Chem. Soc. Rev., 18 (1989) 477.
[7] S.V. Vyazovkin and A.I. Lesnikovich, J. Therm. Anal., 34 (1988) 609.
[8] Standard Test Method for Arrhenius Kinetic Constants for Thermally Unstable Materials (ANSI/ASTM E698-79), ASTM, Philadelphia, PA, 1979.
[9] T. Ozawa, J. Therm. Anal., 2 (1970) 301.
[10] H.E. Kissinger, Anal. Chem., 29 (1957) 1702.
[11] D. Dollimore, T.A. Evans, Y.F. Lee and F.W. Wilburn, Thermochim. Acta, 198 (1992) 249.
[12] J. Malek, Thermochim. Acta, 138 (1989) 337.
[13] S.V. Vyazovkin and A.I. Lesnikovich, Thermochim. Acta, 165 (1990) 273.
[14] S. Vyazovkin and V. Goryachko, Thermochim. Acta, 194 (1992) 221.
[15] E. Kaisersberger and J. Opfermann, Thermochim. Acta, 187 (1991) 151; ICTA 10th Congress Workbook, Hatfield, 1992, p. 105.
[16] S.V. Vyazovkin and A.I. Lesnikovich, Thermochim. Acta, 203 (1992) 177.
[17] A.W. Coats and J.P. Redfern, Nature, 201 (1964) 68.
[18] S.V. Vyazovkin, G.F. Levchik, V.I. Goryachko, A.I. Vyazovkina and A.I. Lesnikovich, Thermochim. Acta, 215 (1993) 315.
[19] S. Vyazovkin and V. Goryachko, Int. Labmate, 17 (1992) 21.

ELSEVIER

Analytica Chimica Acta 295 (1994) 109–118

ANALYTICA CHIMICA ACTA

Validation procedures in near-infrared spectrometry

M. Forina *[,a], G. Drava [a], R. Boggia [a], S. Lanteri [a], P. Conti [b]

[a] *Istituto di Analisi e Tecnologie Farmaceutiche ed Alimentari, Via Brigata Salerno (Ponte), I-16147 Genoa, Italy*
[b] *Dipartimento di Scienze Chimiche, Via S. Agostino 1, I-62032 Camerino, Italy*

Received 27th January 1994

Abstract

Three validation procedures, single evaluation set, cross-validation and repeated evaluation set, were tested on near-infrared spectrometric data to evaluate the predictive residual standard deviation and the complexity of the regression model based on partial least-squares (PLS) regression. Thirty-six combinations of response variables and predictor variables (originating from three response variables and spectra recorded on the same 60 samples in four laboratories with different instruments) were tested. Each validation method was used with several different percentages of objects in the evaluation sets, from very low percentages (leave-one-out) to 33%. The results show that the frequently used technique of the single evaluation set gives a bad estimate both of the residual standard deviation and of the complexity of PLS model. Cross-validation gives acceptable estimates when at least ten cancellation groups are used. The validation technique based on the repeated evaluation set, with a large number of repetitions of prediction, gives excellent estimates of residual standard deviation and of model complexity, but it requires a very long computing time.

Key words: Infrared spectrometry; Moisture; Multivariate calibration; Oil; Partial least-squares regression; Proteins; Soya flour; Validation procedures

1. Introduction

Near-infrared spectrometry (NIRS) is being increasingly used in process analysis and in analyses of perishable raw materials because of its speed and because it requires no or little sample preparation. As the number of measured reflectances or absorbances increased, from the first NIRS instruments to the instruments of today, the use of suitable regression techniques such as principal component regression (PCR) and partial least-squares regression (PLS) [1,2] became essential in the calibration phase, i.e., to extract from the spectra measured on a training set (the "standards" used for calibration) the multivariate regression equation, which computes the chemical quantity as a function of the measured physical quantities.

The regression equation computed by PCR or PLS [and also by the ordinary least-squares regression (OLS)] has to be validated. Validation means that the regression equation is used to compute the chemical quantity of samples not used to compute the regression equation.

* Corresponding author.

SSDI 0003-2670(94)00168-L

Table 1
Composition of soya samples

No	Moisture (%, w/w)	Proteins (%, w/w)	Oil (%, w/w)
1	9.9	34.6	22.4
2	14.0	32.5	19.8
3	13.7	32.6	19.7
4	15.0	36.7	15.8
5	11.4	31.7	22.2
6	10.9	35.3	17.1
7	9.0	29.0	20.7
8	8.3	29.6	20.5
9	12.9	32.3	19.7
10	13.5	32.6	18.1
11	15.4	36.6	15.9
12	10.2	39.8	14.7
13	17.2	35.8	15.6
14	9.5	33.5	22.3
15	13.3	32.2	21.0
16	6.0	42.4	16.6
17	15.5	32.0	19.7
18	9.0	41.3	16.4
19	12.9	34.3	21.4
20	9.0	43.4	15.6
21	6.3	40.9	17.8
22	13.3	37.7	19.1
23	15.5	37.0	15.4
24	17.1	35.8	15.4
25	11.2	36.5	16.9
26	5.9	43.1	17.0
27	7.3	38.6	17.9
28	8.4	29.5	21.8
29	9.5	29.5	22.2
30	14.9	32.0	19.8
31	10.1	34.3	20.5
32	12.6	29.1	20.9
33	9.1	34.1	22.9
34	11.1	34.6	20.3
35	13.1	30.3	20.3
36	12.4	32.1	17.7
37	12.0	34.0	21.0
38	14.2	32.4	17.1
39	16.2	34.7	16.2
40	18.4	33.8	16.3
41	10.9	34.2	19.7
42	13.1	35.4	16.7
43	8.5	31.9	20.1
44	8.9	37.7	18.3
45	17.9	31.7	17.6
46	9.3	37.3	17.1
47	16.7	36.6	15.3
48	9.4	34.4	21.8
49	16.4	36.9	15.4
50	15.8	36.1	16.2
51	13.2	35.8	18.7
52	7.5	42.4	16.1
53	12.7	33.9	21.0
54	13.4	34.8	19.8
55	10.6	33.2	21.0
56	8.9	34.7	22.2
57	13.6	34.9	20.7
58	9.0	34.3	20.8
59	10.0	34.8	21.0
60	9.9	35.6	22.5

The prediction error is the first result of validation. It measures the performance of the regression model. In PCR and PLS, a second result is the identification of the optimum complexity of the model, i.e., the number of principal components (PCR) or latent variables (PLS) used to obtain the regression equation, which ensures the minimum prediction error.

Finally, the third result is the "stability" of the model, i.e., the range of the number of principal components or of PLS latent variables for which the prediction error is not much greater than the minimum error corresponding to the optimum complexity.

Validation is usually performed with the method of the "single evaluation set" (SES). Samples are divided into two sets. The training set, usually with more than half of the samples, is used to compute the regression equation. The evaluation set is used to obtain the prediction error.

In this paper, the use of SES validation is compared with the method of cross-validation (CV) and the method of repeated evaluation set (RES).

CV divides data into some (D) "cancellation groups", so that the number of objects (samples) I divided by the number of cancellation groups is an integer. Each object is assigned to a cancellation group, with a systematic approach: the cancellation group of object i is

$$d = \mathrm{mod}(i - 1, D) + 1$$

where mod is the modulo arithmetic operation. The assignment of an object to a cancellation group can be changed by permutation. Hence the

result of validation depends on the order of objects.

The validation procedure is repeated as many times as there are cancellation groups. Each time the objects assigned to one of the cancellation groups form the evaluation set, the others are in the training set. At the end of the validation procedure each object has been once in the evaluation set and D-1 times in the training set.

When the number of cancellation groups is the same as the number of objects, the evaluation sets are constituted by only one object, and the result of validation is independent of the order of objects. Cross-validation in this case is referred as "leave-one-out validation".

RES repeats many times (generally more than I times) the procedure of SES. Given the number of objects N_e in the evaluation set, each time N_e objects are randomly selected to build the evaluation set. At the end of the validation procedure, an object should have been several times in the evaluation set and, if $N_e > 1$, generally with different companions.

This work was carried out as a collaborative study of the Italian Group for NIRS. Spectra were measured in four different laboratories, and the response variables were moisture, proteins and oil in 60 samples of soya flour.

2. Experimental

Sixty samples of soya seeds were collected from extensive soya fields in many Italian regions, to be representative of Italian soya production. Seeds were milled and subsamples from the 60 samples of soya flour were sent to four laboratories.

Chemical analyses were carried out with the following methods: moisture, gravimetric, by drying at 105°C for 4 h (inaccuracy as maximum error ±1%); proteins, determination of nitrogen by the Kjeldahl method with a selenic mixture as catalyst, the nitrogen percent are being multiplied by 6.25 to obtain the total protein content (inaccuracy as maximum error ±2.5%); and oil, determination by Soxhlet extraction (inaccuracy as maximum error ±1.5%)

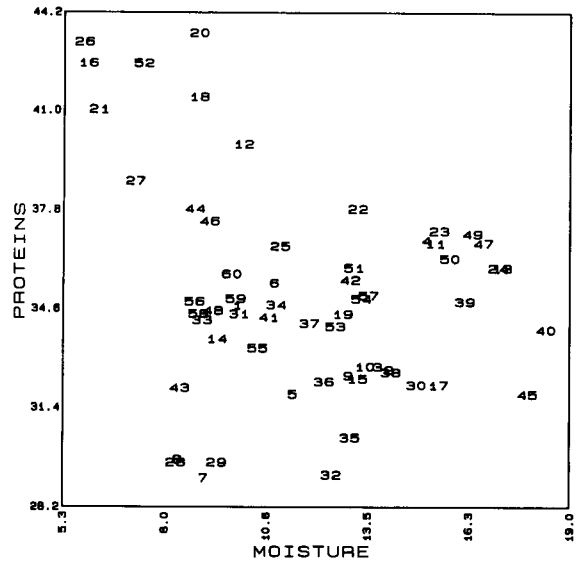

Fig. 1. Plot of the contents of moisture and proteins in the 60 samples (for compositions, see Table 1).

Table 1 and Figs. 1–3 show the main characteristics of the samples.

Spectra were recorded in four different laboratories on different instruments: (A) Technicon InfraAlyzer 400R (Bologna), 19 filters; (B) Tech-

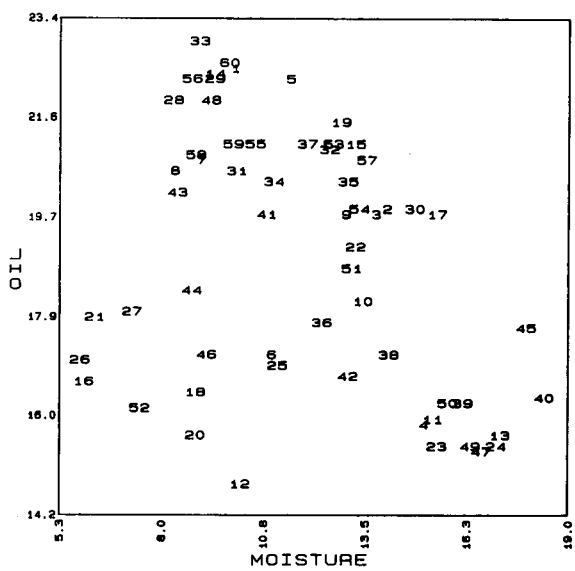

Fig. 2. Plot of the contents of moisture and oil in the 60 samples.

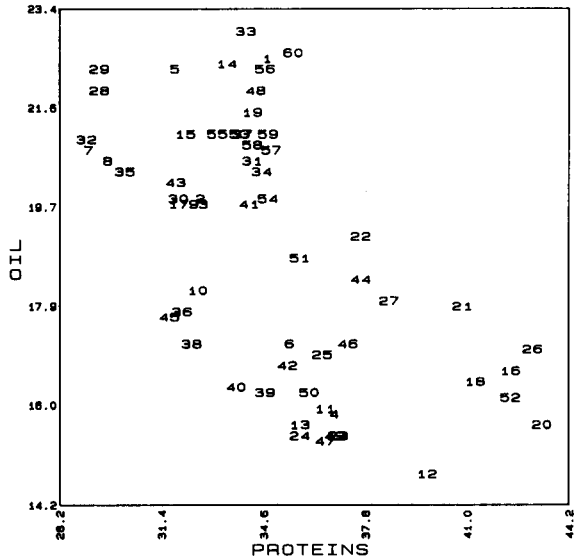

Fig. 3. Plot of the contents of proteins and oil in the 60 samples.

nicon InfraAlyzer 450 (Bari), 19 filters; (C) Technicon InfraAlyzer 500 (Lodi), 350 wavelengths; and (D) NIRSystem 6500 (Ferrara) 700 wavelengths. With instruments C and D only 175 wavelengths were used in data analysis (one every two and one every four, respectively).

3. Theory

The following notation will be used for a matrix:

$$ {}_I\mathbf{X}_V \tag{1} $$

where the left subscript indicates the number of rows and the right subscript the number of columns. The transpose of ${}_I\mathbf{X}_V$ is denoted by ${}_V\mathbf{X}_I$. Lower-case letters corresponding to the number of rows or columns are used to indicate a scalar, such as x_{iv}. Thus ${}_I\mathbf{x}$ is a column vector of I rows, and $\mathbf{x}_V$ is a row vector of V columns. ${}_I\mathbf{X}_V$ indicates the matrix of predictor variables (original physical quantities, or modified quantities such as derivatives, autoscaled data and centred data). ${}_I\mathbf{X}_M$, with $M = V + 1$, indicates the augmented matrix, where a column M of all 1 ($x_{iM} = 1$) is added to the original matrix ${}_I\mathbf{X}_V$. ${}_I\mathbf{Y}_3$ is the response matrix of three response variables (moisture, proteins, oil); ${}_I\mathbf{y}_k$ is the column vector of the kth response variable.

PLS regression computes, using the objects in the training set, the vector of the regression coefficients, so that

$$ {}_I\mathbf{y}_k = {}_I\mathbf{X}_M \, {}_M\mathbf{c}_k + {}_I\mathbf{e}_k \tag{2} $$

where ${}_M\mathbf{c}_k$ is the vector of the regression coefficients for the kth response variable and ${}_I\mathbf{e}_k$ is the vector of residuals. The value in row M of the vector of regression coefficient is the intercept.

Regression coefficients were computed by means of the algorithm of Marengo and Todeschini [3]; they depend on the number of latent variables (PLS components) P used in the PLS regression. P describes the complexity of the PLS regression model. As P increases, PLS tends to OLS regression, so that more noise is used by the regression equation to maximize the fitting to the experimental data. As P decreases, the bias increases. Hence the usual procedure in PLS regression is to detect the optimum complexity of the model, with the best compromise between bias and noise.

The values estimated by the regression are given by

$$ {}_I\hat{\mathbf{y}}_k = {}_I\mathbf{X}_M \, {}_M\mathbf{c}_k \tag{3} $$

and for a generic object

$$ \hat{y}_{ik} = {}_i\mathbf{x}_M \, {}_M\mathbf{c}_k \tag{3a} $$

The before-regression variance of the kth response variable, independent of the laboratory, is given by

$$ s^2_{bk} = \frac{\sum_i (y_{ik} - \bar{y}_k)^2}{I - 1} \tag{4} $$

where $\bar{y}_k$ is the mean of the response variable.

The (fitting) after-regression variance is

$$ s^2_{ak} = \frac{\sum_j (y_{ik} - \hat{y}_{ik})^2}{I - L} \tag{5} $$

when the regression model has been computed using all the available objects. L is 1 plus the number of latent variables; it is M in the ordinary least-squares regression.

The square root of this variance (residual standard deviation of fitting) is generally called the standard error of calibration (SEC).

The validated after-regression variance is

$$s_{ak}^2 = \frac{\sum_j (y_{jk} - \hat{y}_{jk})^2}{J} \quad (6)$$

where J is the number of objects for which prediction has been made, I in the case of cross-validation.

The square root of this variance (residual standard deviation of prediction) is generally called the standard error of prediction (SEP). Because prediction is the main objective of the calibration equation, SEP is the indicator of the goodness of the regression equation. The study of SEP against P, the number of PLS components, gives the optimum complexity of the PLS model. Generally SEP decreases with increasing P owing to the smaller bias. Then a minimum is reached, corresponding to the optimum model. With a further increase in P, SEP increases, as a consequence of the greater amount of noise used by the model. The stability of the model is described by the range of P, where SEP does not change significantly around its minimum, independently of the validation parameter [percentage of objects in the evaluation set(s)].

4. Results and discussion

The three techniques of validation, SES (single evaluation set) with 2, 3, 4, 6, 12 and 20 objects in the evaluation set, CV (cross validation) with 3, 5, 10, 15, 20, 30 and 60 cancellation groups (corresponding to 20, 12, 6, 4, 3, 2 and 1 objects respectively, in each cancellation group) and RES (repeated evaluation set) with 100 repetitions and 2, 3, 4, 6, 12 and 20 objects in each evaluation set, were applied to the validation of the regression equation for moisture, proteins and oil for the four laboratories A–D.

Three evaluation techniques were used for three response variables in four laboratories, for a total of 36 series where SEP was studied as a function of P and of the number of objects in the evaluation sets. Moreover, SES and CV were repeated ten times, with a different random choice of the objects in the evaluation set (SES), or after random permutations of the objects (CV), for some selected combinations of number of objects in the evaluation set, response variable and laboratory. In some instances RES was also repeated, with 10–10 000 repetitions.

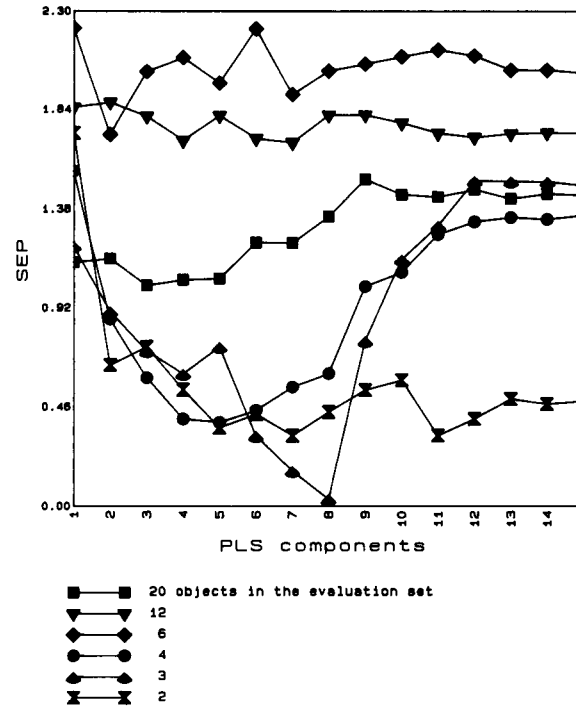

Fig. 4. Laboratory B, moisture: results of validation with SES (single evaluation set).

Results are reported in the form of SEP versus P (number of PLS components) plots in Figs. 4–13. The reported detailed results are only a fraction of the results obtained [7 series out of 36, and a limited part of the studies on the effect of different choice of the objects in the training sets (SES and CV) or of different number of repetitions (RES)]. However, the results reported in the figures are representative, at least with regard to the most important conclusions. Some results for all 36 series are reported in Table 2.

Fig. 4 shows that the technique of SES gives very irregular results: the minimum SEP changes

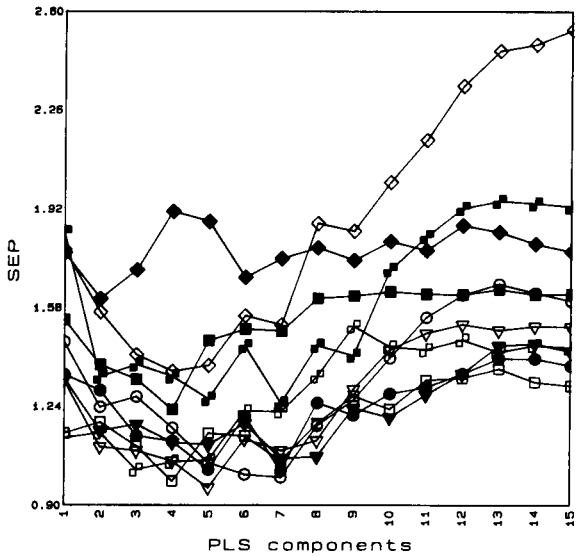

Fig. 5. Laboratory B, moisture: validation with SES and twenty objects in the evaluation set. Results for ten repeated runs with different objects (random selection) in the evaluation set.

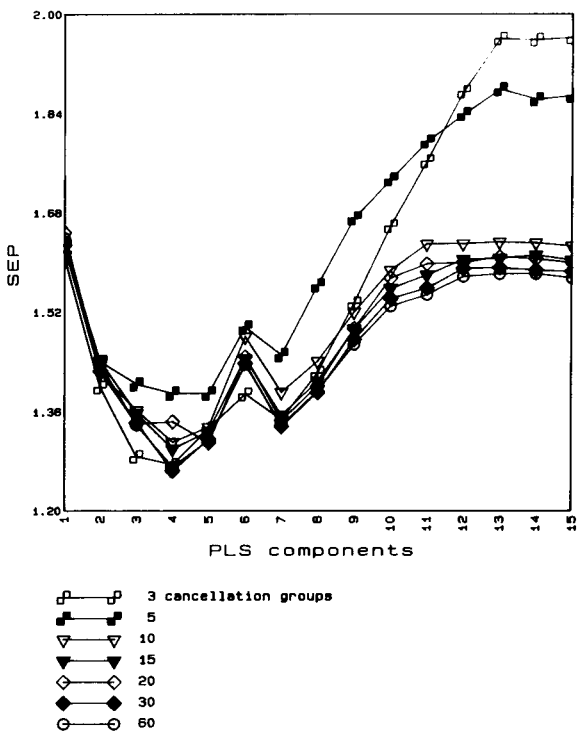

Fig. 6. Laboratory B, moisture: results of CV.

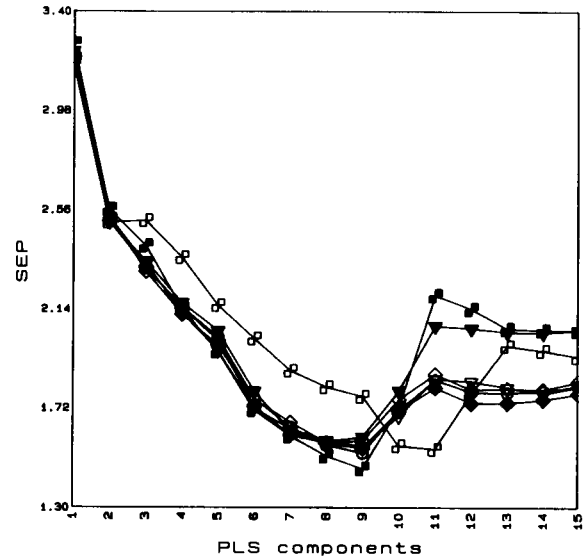

Fig. 7. Laboratory A, proteins: results of CV.

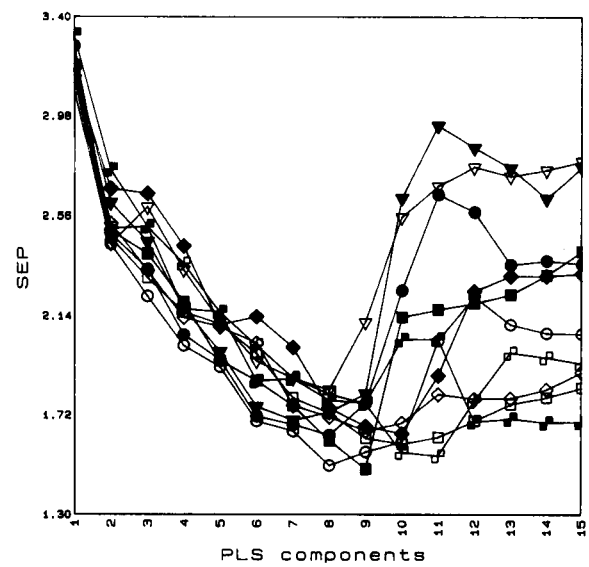

Fig. 8. Laboratory A, proteins: CV with three cancellation groups (twenty objects in each evaluation set). Results for 10 runs after random permutation of objects.

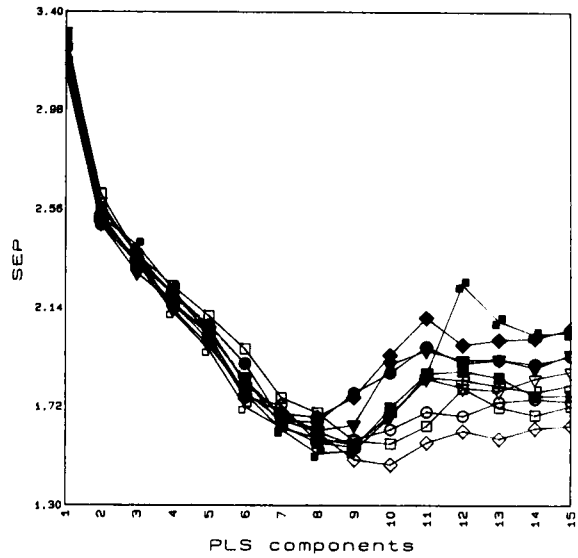

Fig. 9. Laboratory A, proteins: CV with ten cancellation groups (six objects in each evaluation set). Results for ten runs after random permutation of objects.

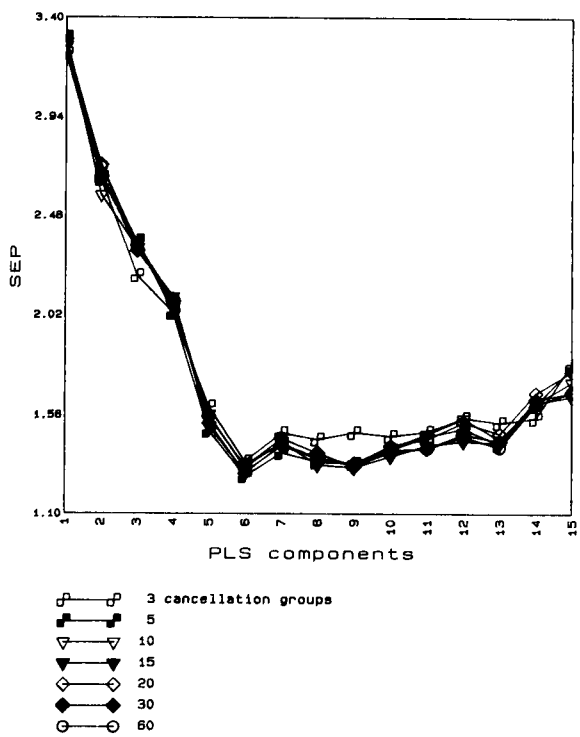

Fig. 10. Laboratory C, proteins: results of CV.

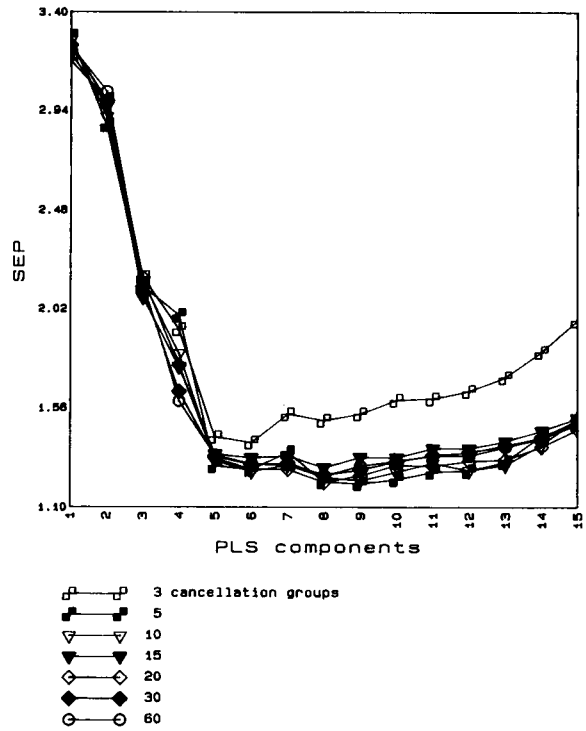

Fig. 11. Laboratory D, proteins: results of CV.

in the interval from about 0.03 to 1.7 (see Table 2) with the number of objects in the evaluation set. The corresponding optimum complexity of the PLS model changes from 2 to 8, with large variations of SEP in this range, so that the stability of the model seems very poor.

The results of validation with SES are strongly dependent on the choice of the objects in the evaluation set, especially when the number of objects in the evaluation set is small. Fig. 5 shows that, also in the case of one third (20) of the objects in the evaluation set, optimum SEP changes in the interval ca. 0.95–1.65, with an optimum complexity from 2 to 7. The very small value of the optimum SEP obtained with three objects in the evaluation set (Fig. 4) has to be interpreted as essentially due to the casual selection of the three objects. Although the validation by means of the SES is usually performed with 25–35% of the objects in the evaluation set, the reported results indicate that this method is completely unsuitable for validation, because the esti-

mates of both the prediction error and the complexity of the model have too high an uncertainty. The results in Figs. 4 and 5 refer to moisture; the results for proteins and oil are slightly better, probably because samples can be easily contaminated by the moisture of the environment during transport and storage.

SES was the first validation method suggested in chemometrics, so that it is still widely used today, in spite of the development and spreading of cross-validation.

With the same response variable, moisture, in the same laboratory, B, CV gives (Fig. 6) the optimum SEP in the range ca. 1.26–1.39 about, with 4 or 5 components. With 3–5 components the variations of SEP are small; this means a fairly good stability of the model, because the range of three latent variables is sufficiently large compared with the 19 predictor variables.

With proteins and laboratory A, CV gives the optimum SEP in the range ca. 1.46–1.58 with 8–11 components (Fig. 7). Figs. 8 and 9 show that

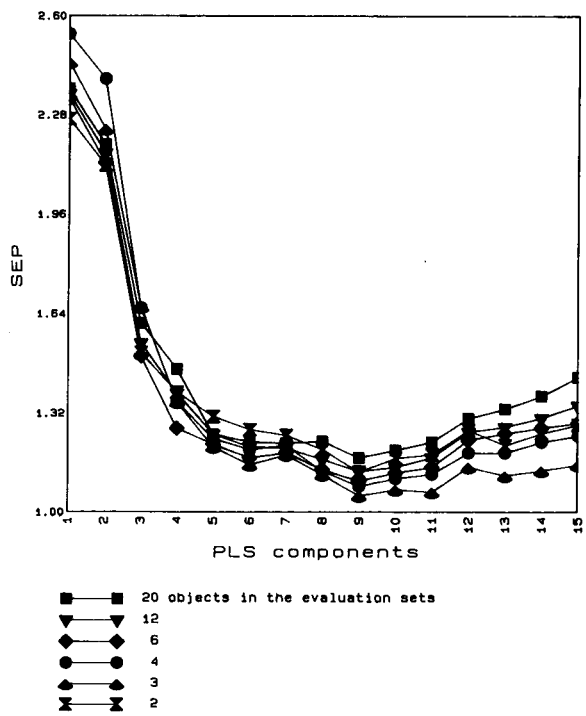

Fig. 12. Laboratory D, oil; results of RES (100 repetitions).

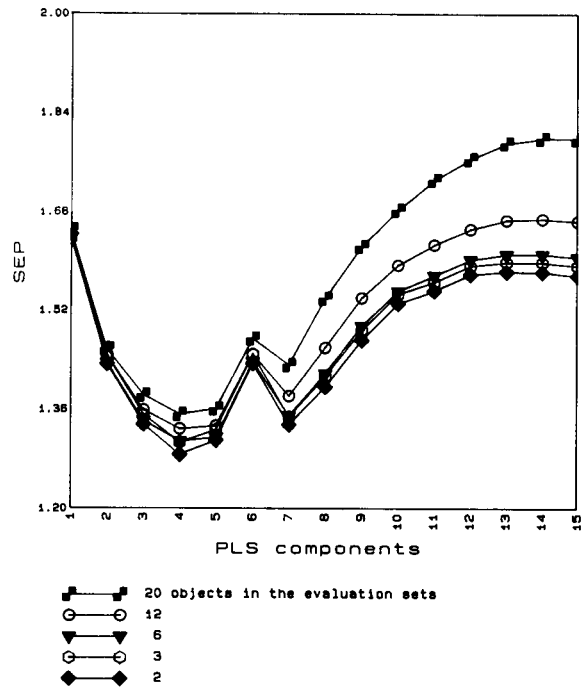

Fig. 13. Laboratory B, moisture: results of RES (10000 repetitions).

also with CV, a different choice of objects in the evaluation set can modify the result of validation. With three cancellation groups the minimum SEP is in the interval 1.5–1.8, and the optimum number of components is 8–11. As the number of cancellation groups increases, the variation of optimum SEP and of corresponding P, with the choice of objects in the evaluation sets, decreases, as Fig. 9, compared with Fig. 8, shows. Obviously, in the leave-one-out procedure, with as many cancellation groups as there are objects, the permutation of the objects (used here to obtain evaluation groups with different objects) does not produce different results.

Figs. 10 and 11 refer to CV for proteins and laboratories C and D, where the different instrumentation seems to be the main cause of the relative independence of the SEP–P relationship from the number of cancellation groups. Only in the case of three cancellation groups is the SEP–P curve different (and dependent on the objects in the cancellation groups).

Hence, generally, CV has to be considered as a good validation method, provided that the number of cancellation groups is relatively high.

The results with RES in Table 2 were obtained with 100 repetitions. The example in Fig. 12 shows that this method gives a compact and regular series of SEP–*P* curves. The regularity increases with increasing number of repetitions (see Fig. 13). The good results of RES are obtained at the expense of a long or very long computing time, and at present the use of RES with 10000 repetitions and with some selected percentages of objects in the evaluation set cannot be applied in the usual laboratory practice.

The improvements of results with RES are especially evident when the number of objects in the evaluation set is high. With 20 objects in the evaluation sets (corresponding in this instance to three cancellation groups with CV), SES studies only one evaluation set, CV gives the result as the mean of three evaluation sets and RES as the mean of 100 or more evaluation sets, so that the

Table 2
Range of minimum SEP and of corresponding *P* with different percentages of objects in the evaluation set(s)

Laboratory	Response variable	Validation technique	SEP		*P*	
			Min.	Max.	Min.	Max.
A	Moisture	SES	0.2795	1.2439	1	12
A	Moisture	CV	1.0533	1.1922	5	9
A	Moisture	RES	1.0229	1.2207	6	8
B	Moisture	SES	0.0307	1.7211	2	8
B	Moisture	CV	1.2643	1.3891	4	5
B	Moisture	RES	1.1649	1.3991	4	4
C	Moisture	SES	0.2320	1.1542	3	11
C	Moisture	CV	1.0231	1.1388	8	14
C	Moisture	RES	0.9416	1.1409	7	8
D	Moisture	SES	0.0985	0.4732	7	14
D	Moisture	CV	0.4370	0.4974	8	9
D	Moisture	RES	0.3953	0.4870	9	10
A	Proteins	SES	0.2662	1.7766	1	15
A	Proteins	CV	1.4646	1.5794	8	11
A	Proteins	RES	1.4757	1.7894	8	9
B	Proteins	SES	0.2484	1.8697	1	5
B	Proteins	CV	1.7849	1.8616	4	5
B	Proteins	RES	1.7660	1.9305	3	5
C	Proteins	SES	0.3373	1.3263	5	9
C	Proteins	CV	1.2745	1.3443	6	6
C	Proteins	RES	1.3093	1.4192	6	6
D	Proteins	SES	0.2136	1.5213	3	15
D	Proteins	CV	1.0842	1.4313	10	12
D	Proteins	RES	1.0532	1.2953	11	11
A	Oil	SES	0.6020	1.6946	5	13
A	Oil	CV	1.2844	1.4480	7	9
A	Oil	RES	1.2678	1.4160	6	9
B	Oil	SES	0.7752	1.2417	2	14
B	Oil	CV	1.2015	1.3423	6	7
B	Oil	RES	1.1799	1.3065	7	7
C	Oil	SES	0.1865	1.2461	6	12
C	Oil	CV	1.1367	1.2778	9	14
C	Oil	RES	1.1272	1.2344	9	10
D	Oil	SES	0.2469	1.1237	4	12
D	Oil	CV	1.0261	1.1161	7	9
D	Oil	RES	0.9742	1.1360	8	9

irregularities due to special combinations of objects in the evaluation sets vanish.

To have a good picture of the prediction error, measured by SEP, we have to use both low and high percentages of objects in the evaluation sets (few or many cancellation groups), because a large number of cancellation groups corresponds to validation with a small perturbation of the statistical sample, and generally to a too optimistic evaluation of SEP. A small number of cancellation groups corresponds to a heavy perturbation of the statistical sample, and so to a more pessimistic (perhaps more realistic) evaluation of the prediction error. A very large difference between the two extremes of SEP can also suggest that the whole set of chemical samples used for calibration has some heavy imperfections, such as a bad experimental design or the presence of contaminated samples.

Acknowledgements

This research was supported by the Italian Ministry for University and Research (MURST) (40% grant "Chemiometria", 60% grant "Azione Integrata Italia–Spagna") and by the National Council of Research (CNR, National Committee "Scienza e Tecnologia dell'Informazione"). Thanks are due also to P. Corti (Dipartimento Farmaco Chimico Tecnologico, University of Siena), R. Giangiacomo and C. Galliena (Istituto Sperimentale Lattiero Caseario, Lodi), R. Bigoni, I. Quartari and C. Serra (Eridania Laboratorio Chimico Centrale, Ferrara), D. Ferri (Istituto Sperimentale Agronomico, Bari) and O. Leoni and L. Lazzeri (Istituto Sperimentale per le Colture Industriali, Bologna) for the collection of samples, chemical analysis and measurements of NIR spectra.

References

[1] H. Martens, in B.R. Kowalski (Ed.), Chemometrics: Mathematics and Statistics in Chemistry, Reidel, Dordrecht, 1984, p. 147.
[2] S. Wold, Technometrics, 20 (1978) 397.
[3] E. Marengo and R. Todeschini, Chemometr. Intell. Lab. Syst., 12 (1992) 117.

ELSEVIER

Analytica Chimica Acta 295 (1994) 119–125

ANALYTICA CHIMICA ACTA

HOLMES: a program for target factor analysis

D. González-Arjona [a,*], J. Antonio Mejías [a], A. Gustavo González [b,*]

[a] Department of Physical Chemistry, and [b] Department of Analytical Chemistry, University of Seville, 41012 Seville, Spain

Received 7th March 1994

Abstract

A computer program called HOLMES, written in QuickBasic for performing target factor analysis, is outlined. Chemical data taken from the literature were processed with HOLMES and the results were compared with the data obtained when using well-known programs like TARGET90.

Key words: HOLMES program; Target factor analysis

1. Introduction

Target factor analysis (TFA) or target testing (TT) is a technique especially valuable for achieving meaningful transformations of the abstract factors emerged after eigenanalysis of cases. The mathematical bases of TFA are covered in the excellent text of Manilowski [1] and will not be described here. Apart from the successful application of TFA in all branches of chemistry, it has become especially useful for the analyst in areas like absorption and emission spectrometry, kinetic analysis, optical rotatory dispersion, mass spectrometry, nuclear magnetic resonance spectroscopy, chromatography and linear free energy relationships [1].

TFA enables us to individually test suspected parameters (such as physical properties or structural features of molecules) as possible real factors. This individual testing ability is one of the most valuable features of TFA.

Although some programs are available for performing TFA, TARGET90 [2,3] (developed by Malinowski and written in FORTRAN 77) is the most widely used.

In this paper a program called HOLMES is presented, which performs: (i) factor analysis (FA) of the data matrix; (ii) determination of the true number of underlying factors; (iii) target testing; and (iv) establishment of the definitive correlation model based on the factor loadings corresponding to the key combination of the accepted factors which perfectly reproduce the original data matrix.

HOLMES has been written in QuickBasic, a flexible structured computer language according to feasibility, user facilities and relative portability, for which no substantial knowledge of programming is needed. QuickBasic has already been used to create a wide range of applications from scientific packages and accounting systems to util-

* Corresponding authors.

SSDI 0003-2670(94)00169-M

ities. QuickBasic includes the majority of FORTRAN statements, aside from graphical sentences that FORTRAN lacks. Moreover, QuickBasic exhibits the possibility of managing FORTRAN and C libraries enabling us to make good use of routines developed in these languages and take advantage of the power of C in further applications.

2. Implementation

HOLMES provides capabilities for tackling real research problems. It has been implemented in a straightforward user-interactive way that practically overcomes the use of a user manual. HOLMES is a program whose source code is written in Microsoft QuickBasic 4.5 for use with an IBM compatible PC, XT or AT. In order to avoid slow computations it is advisable to use at least an 80286 processor.

Dealing with the memory usage and economy, QuickBasic allows the use of dynamic arrays [4] for optimizing the memory management. With these dynamic arrays HOLMES would use the amount of memory needed in each moment if available in the computer and accordingly, it could handle data matrices of any dimension and an arbitrary number of factors. However, QuickBasic presents some limitations when using dynamic arrays larger than 64 kilobytes. To use these large arrays called huge arrays, one must start the QuickBasic environment with the option /AH. The size of the elements in a huge array should be a power of 2; otherwise the dynamic array will be limited to 128 kbytes. In this case, for real double precision arrays, the number of bytes allowed by the element is 8. A maximum of 16384 elements may therefore be managed.

Listings of HOLMES (source code of about 620 total program lines) are available from the authors upon request. The HOLMES program (QuickBasic source file, QuickBasic executable stand-alone file and a sample ASCII data file) as well as a short user manual is also available after payment of material and mailing costs. The sample data file contains a worked example taken from literature enabling the user to get started quickly.

3. Computational details

The HOLMES program consists of the following principal procedures.

DATAIN: This procedure enables us to build step-by-step the data file (ASCII format) containing the data matrix and the target vectors. The data matrix has $nr \times nc$ dimension and the target vectors $nr \times 1$.

Three procedures dealing with matrix computations are used in this program: TRANSMATRIX for obtaining transposed matrices, INVMATRIX, which calculates the inverse of a given matrix, and DMULMATRIX to multiply suitable matrices [5]. Any of these routines may be invoked by other procedures of HOLMES that need matrix computations.

PREPROCESS is a procedure that (i) computes from the data matrix the sample covariance matrix and (ii) performs eigenanalysis of the covariance matrix calculating the eigenvalues and the corresponding eigenvectors.

A common procedure for performing eigenanalysis is the Jacobi transformation. However, for symmetric matrices of an order greater than about 10, the algorithm is slow. Therefore, in order to reach fast computations we select the Householder method [6] which reduces an $n \times n$ symmetric matrix to tridiagonal form by $n-2$ orthogonal transformations (routine TRED2D) and then finding the eigenvalues and eigenvectors of a symmetric tridiagonal matrix (routine TQLID). TRED2D and TQLID procedures are slightly modified versions of the routines tred2 and tqli which appeared in Numerical Recipes [7]. The combination of these two routines is the most efficient technique known for finding all the eigenvalues and eigenvectors of a real symmetric matrix [6]. Finally, PREPROCESS calls the routine EIGSRT that arranges the eigenvalues in decreasing order and selects accordingly the eigenvectors as the columns of an eigenvector matrix. The scores matrix is obtained by multiplying the data matrix by the eigenvector matrix. PREPROCESS produces as output the covariance matrix, the values of eigenvalues and the matrix is eigenvectors (printer or monitor).

MALINOV: This procedure selects the number f

of true underlying factors based on the empirical indicator function IND proposed by Malinowski [1,8,9] which is computed from the eigenvalues, *nr* and *nc*. IND reaches a minimum when the correct number of factors is employed.

Although the IND function has proved to be very sensitive for selecting the true number of factors, some other procedures would be of interest for the sake of comparison: MALIN_F (which utilizes a statistical *F*-test on eigenvalues) [10,11], RSD_F (which performs a similar statistical test on the relative standard deviation in the reproduction of the data matrix) [12] and WOLD (which carries out the Wold implemented cross-validation technique) [13]. Any of these later procedures may substitute the procedure MALINOV in the main program.

REPX: Once the true number of factors f is known, this procedure obtains the new eigenvector and scores matrix by deleting the columns $f+1$ to *nc* of each. Then the data matrix is reproduced from these new matrices and compared with the original data matrix. As output the following matrices are presented: new eigenvector matrix, original and new scores matrix and original and reproduced data matrix.

TFA: This procedure performs the target testing by means of a rotation matrix transformation [1]: the aim of target testing is to decide whether a proposed target can or cannot be accepted as a real factor. The criteria used for accepting/rejecting target vectors is based on the similarity between the target vector and the predicted target vector once information about the magnitudes of the real error predicted vector (REP), real error target vector (RET) and apparent error target test vector (AET) [1]. The target vectors to be assayed are read from the data file and stored as the columns of a target matrix. The proposed factors are evaluated on the basis of the SPOIL function (SPOIL = RET/REP) [1] as either acceptable ($0.0 < \text{SPOIL} < 3.0$), fair ($3.0 < \text{SPOIL} < 6.0$) or unacceptable (SPOIL > 6.0). TFA produces the matrix of target vectors as output as well as the result of the target testing for each (successful targeting/unsuccessful targeting), indicating also the value of the SPOIL.

LOADINGS: The definitive model for the original data matrix comes from the combinations of f accepted targets vectors which best reproduce the original data matrix, yielding the lowest root mean square (RMS). Thus, LOADINGS enables the user to select successively sets of accepted target vectors in order to compare the RMS of the reproduced data matrix. The set of f selected target vectors is arranged in a key combination matrix (the target vectors are the columns) which multiplied by the factor loadings matrix gives the reproduced data matrix. The factor loadings are the coefficients related to the weight of each value of the target vector on the elements of each column of the original data matrix. In a number of cases the evaluation of the factor loading matrix for the best combination is the goal and accordingly, one is faced with the task of estimating the reliability of the loadings. Among the diverse possibilities we have chosen the calculational method based on the covariance matrix of loading errors [14]. Thus, for each proposed set of f factors, the procedure LOADINGS produces as output: the RMS value, the matrix of factor loadings and the matrix of standard deviations of factor loadings.

In such a way, the user directed by theoretical considerations or chemical intuition may select all or some target combinations in order to attain the true one.

After debugging, HOLMES was tested with some scrutinized sample data and well-known examples in order to assess the reliability (accuracy and precision) of the procedures. The outputs were in all cases in excellent agreement with the true results.

4. Scope and features

As it was indicated above, HOLMES has been implemented in order to perform an FA of the data matrix by eigenanalysis, to select the proper number of factors and to attain the key factor combination which best reproduce the data matrix through the factor loadings. Nevertheless, HOLMES does not deal with special methods beyond FA and TFA [1] such as iterative key factor analysis (IKFA), evolving factor analysis (EFA),

Table 1
Data matrix. Acid dissociation constants of several solutes in dioxane–water mixtures

Dioxane (%, v/v)	HNCA	gly1	gly2	PropK	Sal1	Sal2
20	2.964	2.60	9.64	5.091	3.067	13.23
30	3.171	2.71	9.67	5.395	3.318	13.43
40	3.448	2.94	9.70	5.676	3.524	13.51
50	3.762	3.17	9.76	6.063	3.789	13.94
60	4.288	3.45	9.84	6.494	4.305	14.12
70	4.653	3.81	9.98	6.879	4.654	14.84

rank annihilation factor analysis (RAFA) or multimode factor analysis (MMFA).

Allowing for that the user would be interested in a comparison of the power of HOLMES with some other well-known programs, we have selected TARGET90, perhaps the most important program on FA most widely used today. TARGET90 is a set of 15 programs written by Malinowski [2,3] in a Microsoft version of FORTRAN 77. TARGET90 apart from other special methods, practically performs (although with different algorithms) the same TFA computations like HOLMES.

Within the TFA scope previously established by HOLMES, TARGET90 should therefore lead to the same results. Effectively, for several worked examples taken from the literature we have compared the results obtained by HOLMES with the results produced by TARGET90: In all cases the results were identical, apart from the non-significant statistical deviations.

Concerning user facilities, HOLMES is a complete program (implemented in a flexible-interactive way towards the user) whereas TARGET90 is a set of 15 programs that the user should apply in accord with theoretical or conceptual dictates. For applications within the TFA frame only, HOLMES could therefore be much more suitable for beginners on these topics. Effectively, Malinowski stated that: "TARGET90 is not designed to be an independent, self-contained teaching tool. It presupposes an exposure to the basic philosophical principles and terminology associated with target factor analysis" [1].

Table 2
Solvent parameters for water–dioxane mixtures

Dioxane (%, v/v)	α	β	π^*	n_2 [a]
20	0.81	0.296	1.124	0.05
30	0.74	0.379	1.088	0.083
40	0.67	0.433	1.049	0.123
50	0.61	0.474	0.989	0.174
60	0.57	0.486	0.92	0.241
70	0.54	0.469	0.849	0.33

[a] Molar fraction of dioxane.

5. A worked example

To show how the program works and for the sake of illustration we have selected a worked example taken from the literature.

The data for this example were taken from [15]. The paper deals with the study of the correlations between the acidity constants of a set of solutes [3-hydroxynaphthalene-2-carboxylic acid (HNCA), glycine (COOH group) (gly1), glycine (NH_2 group) (gly2), propionic acid (PropK), salicylic acid (COOH group) (Sal1) and salicylic acid (OH group) (Sal2)] and a series of solvent parameters (α, β and π^* Kamlet–Taft solvatochromic parameters and the molar fraction) in dioxane–water mixtures. The pK_a data matrix is shown in Table 1 (corresponding to the dashed box of Table 3 in [15]). The solvent parameters to be targeted, apart from unity, are depicted in Table 2 (taken from Table 2 [15]). Let test.dat be the input data file (which may be created using HOLMES) containing the data matrix and the target vectors. The program HOLMES produces the following outputs:

Target Factor Analysis

Filename test.dat

Covariance Matrix

0.8492D + 02	0.7088D + 02	0.2180D + 03	0.1342D + 03	0.8613D + 02	0.3104D + 03
0.7088D + 02	0.5922D + 02	0.1827D + 03	0.1122D + 03	0.7192D + 02	0.2600D + 03
0.2180D + 03	0.1827D + 03	0.5722D + 03	0.3473D + 03	0.2216D + 03	0.8116D + 03
0.1342D + 03	0.1122D + 03	0.3473D + 03	0.2127D + 03	0.1362D + 03	0.4937D + 03
0.8613D + 02	0.7192D + 02	0.2216D + 03	0.1362D + 03	0.8738D + 02	0.3154D + 03
0.3104D + 03	0.2600D + 03	0.8116D + 03	0.4937D + 03	0.3154D + 03	0.1152*D* + 04

Eigenvectors

0.1969D + 00	− .5123D + 00	− .9980D − 02	0.4102D + 00	0.1826D + 00	− .7050D + 00
0.1648D + 00	− .3270D + 00	− .2920D + 00	0.2599D − 01	0.7330D + 00	0.4927D + 00
0.5138D + 00	0.4531D + 00	0.5517D + 00	0.4074D + 00	0.2237D + 00	0.1014D + 00
0.3129D + 00	− .4261D + 00	0.5464D + 00	− .6492D + 00	− .2346D − 01	0.5469D − 02
0.2000D + 00	− .4516D + 00	0.1406D − 01	0.4298D + 00	− .5810D + 00	0.4834D + 00
0.7295D + 00	0.1996D + 00	− .5582D + 00	− .2429D + 00	− .2031D + 00	− .1273D + 00

Eigenvalues

0.2164D + 04	0.3917D + 01	0.3420D − 01	0.1710D − 01	0.4484D − 02	0.4959D − 03

Optimum # of factors	IND Function	Final RDS
2	0.3027D − 02	0.4843D − 01

Selected Eigenvector Matrix

0.1969D + 00	− .5123D + 00
0.1648D + 00	− .3270D + 00
0.5138D + 00	0.4531D + 00
0.3129D + 00	− .4261D + 00
0.2000D + 00	− .4516D + 00
0.7295D + 00	0.1996D + 00

Scores Matrices Y and New Y

0.1780D + 02	0.1120D + 01
0.1819D + 02	0.7543D + 00
0.1848D + 02	0.3540D + 00
0.1910D + 02	− .5361D − 01
0.1966D + 02	− .7591D + 00
0.2058D + 02	− .1178D + 01

0.1780D + 02	0.1120D + 01
0.1819D + 02	0.7543D + 00
0.1848D + 02	0.3540D + 00
0.1910D + 02	− .5361D − 01
0.1966D + 02	− .7591D + 00
0.2058D + 02	− .1178D + 01

Matrices X and New X

0.2964D + 01	0.2600D + 01	0.9640D + 01	0.5010D + 01	0.3067D + 01	0.1323D + 02
0.3171D + 01	0.2710D + 01	0.9670D + 01	0.5395D + 01	0.3318D + 01	0.1343D + 02
0.3448D + 01	0.2940D + 01	0.9700D + 01	0.5676D + 01	0.3524D + 01	0.1351D + 02
0.3762D + 01	0.3170D + 01	0.9760D + 01	0.6063D + 01	0.3789D + 01	0.1394D + 02
0.4288D + 01	0.3450D + 01	0.9840D + 01	0.6496D + 01	0.4305D + 01	0.1412D + 02
0.4653D + 01	0.3810D + 01	0.9980D + 01	0.6879D + 01	0.4654D + 01	0.1484D + 02

0.2930D + 01	0.2567D + 01	0.9652D + 01	0.5092D + 01	0.3054D + 01	0.1321D + 02
0.3194D + 01	0.2751D + 01	0.9687D + 01	0.5370D + 01	0.3297D + 01	0.1342D + 02
0.3458D + 01	0.2931D + 01	0.9658D + 01	0.5633D + 01	0.3537D + 01	0.1355D + 02
0.3788D + 01	0.3166D + 01	0.9791D + 01	0.6001D + 01	0.3845D + 01	0.1392D + 02
0.4260D + 01	0.3489D + 01	0.9759D + 01	0.6477D + 01	0.4275D + 01	0.1419D + 02
0.4656D + 01	0.3777D + 01	0.1004D + 02	0.6943D + 01	0.4649D + 01	0.1478D + 02

Estimated Target Matrix

0.7824D + 00	0.3478D + 00	0.1135D + 01	0.4075D − 01	0.1004D + 01
0.7396D + 00	0.3730D + 00	0.1090D + 01	0.8342D − 01	0.1002D + 01
0.6883D + 00	0.3977D + 00	0.1034D + 01	0.1289D + 00	0.9935D + 00
0.6470D + 00	0.4298D + 00	0.9934D + 00	0.1781D + 00	0.1001D + 01
0.5579D + 00	0.4741D + 00	0.8968D + 00	0.2586D + 00	0.9880D + 00
0.5251D + 00	0.5135D + 00	0.8702D + 00	0.3117D + 00	0.1011D + 01

Factor	Spoil	Comment
Alpha	3.349543451123226	successful targeting
Beta	18.40479276584182	unsuccessful targeting
PiStar	1.778313482154847	successful targeting
MolFract	2.49464085580481	successful targeting
Unity	2.098442860589044	successful targeting

Available Factors 4

Significant Factors 2

Select a sequence of 2 factors from 4 available factors

#	Factor Name
1	Alpha
2	Beta
3	PiStar
4	MolFract
5	Unity

Factor :? 3
Factor :? 5

RMS :0.556759D − 01

Matrices of Factors Loadings and their deviations

− .6264D + 01	− .4381D + 01	− .1181D + 01	− .6668D + 01	− .5781D + 01	− .5437D + 01
0.9998D + 01	0.7508D + 01	0.1095D + 02	0.1261D + 02	0.9575D + 01	0.1930D + 02
0.1629D + 00	0.1220D + 00	0.1080D + 00	0.3297D + 00	0.1978D + 00	0.5553D + 00
0.1641D + 00	0.1230D + 00	0.1088D + 00	0.3322D + 00	0.1993D + 00	0.5596D + 00

Another data series? (Y/N)

We have presented the output corresponding to the best factor combination of π^* and unity (RMS = 0.056) in order to avoid an extra amount of superfluous data.

The results obtained using HOLMES are in excellent agreement with the literature data [15] using TARGET90. For the sake of comparison, the most important outputs produced by HOLMES and TARGET90 are presented in Table 3.

6. Conclusion

HOLMES is a straightforward program written in QuickBasic for performing TFA. It is very easy

Table 3
Factor loadings for the best reproduction of data matrix using HOLMES and TARGET90

Solute	HOLMES (RMS = 0.056)		TARGET90 (RMS = 0.060)	
	π^* [a]	Unity	π^*	Unity
HNCA	−6.3(2)	10.0(2)	−6.3(1)	9.9(1)
gly1	−4.4(1)	7.5(1)	−4.38(9)	7.5(1)
gly2	−1.2(1)	11.0(1)	−1.18(9)	10.95(9)
PropK	−6.7(3)	12.6(3)	−6.4(2)	12.4(2)
Sal1	−5.8(2)	9.6(2)	−5.8(2)	9.5(2)
Sal2	−5.4(6)	19.3(6)	−5.4(4)	19.3(4)

[a] Values in parentheses are the errors associated with the last figures.

to handle for any user (even if not familiar with TFA). Compared with other large programs devoted to FA applications, such as TARGET90, HOLMES competes favourably (within its scope), leading to the same results in a more straightforward/interactive way.

Acknowledgement

Financial support from Direción General de Investigación Científica y Técnica de Espańa through Project PB92-0678 is gratefully acknowledged.

References

[1] E.R. Malinowski, Factor Analysis in Chemistry, Wiley, New York, 2nd edn., 1991.
[2] E.R. Malinowski, TARGET90, Stevens Institute of Technology, Hoboken, NJ, 1989.
[3] E.R. Malinowski, J. Chemometr., 3 (1988) 49.
[4] Microsoft QuickBasic 4.5 User Manual, Microsoft Co., 1990.
[5] A.G. González and D. González-Arjona, Anal. Chim. Acta, (1994) submitted for publication.
[6] W.H. Press, B.P. Flannery, S.A. Teukolski and W.T. Vetterling, Numerical Recipes in C, Cambridge Univ. Press, Cambridge, 1990.
[7] J.C. Sprott in association with Numerical Recipes Software, Numerical Recipes, Routines and Examples in BASIC, Cambridge University Press, Cambridge, 1991.
[8] E.R. Malinowski, Anal. Chem., 49 (1977) 612.
[9] E.R. Malinowski, in B.R. Kowalski (Ed.), Chemometrics: Theory and applications (ACS Symp. Series (52), American Chemical Society, Washington DC, 1977, Chap. 3.
[10] E.R. Malinowski, J. Chemometr., 1 (1987) 33.
[11] E.R. Malinowski, J. Chemometr., 3 (1988) 49; 4 (1990) 102.
[12] R.J. Sindreu, M.L. Moyá, F. Sánchez Burgos and A.G. González, J. Sol. Chem., (1994) submitted for publication.
[13] S. Wold, Technometrics, 20 (1978) 397.
[14] B.A. Roscoe and P.K. Hopke, Anal. Chim. Acta, 132 (1981) 89; 135 (1982) 379.
[15] E. Casassas, N. Domínguez, G. Forondona and A. de Juan, Anal. Chim. Acta, 283 (1993) 548.

ELSEVIER

Analytica Chimica Acta 295 (1994) 127–134

ANALYTICA CHIMICA ACTA

Algorithm for computer perception of topological symmetry

Chang-Yu Hu, Lu Xu *

Applied Spectroscopy Laboratory, Changchun Institute of Applied Chemistry, Academia Sinica, Changchun 130022, Jilin, China

Received 30th November 1993; revised manuscript received 5th April 1994

Abstract

For the exhaustive and irredundant generation of candidate structures in ESESOC (Expert System for the Elucidation of the Structures of Organic Compounds), a new algorithm for computer perception of topological equivalence classes of the nodes (non-hydrogen atoms) in molecular graphs or partial structures was developed. Two new matrices, node matrix (**N**) and bond matrix (**B**), are devised. A new graph invariant, the weight of the node, is suggested for characterizing the symmetry.

Key words: Expert systems; Computer perception; Structure elucidation; Topological symmetry

1. Introduction

An interactive computer system, ESESOC (Expert System for the Elucidation of the Structures of Organic Compounds) has been developed as a computer model of the intricate process by which the chemist reduces the spectroscopic data derived from an unknown compound to a molecular structure. It is a computer program system for automatically deducing all logical candidate structures on the basis of comprehensive information (chemical and spectroscopic information, etc.) [1–3]. It is composed of three parts: spectroscopic data analysis, structure generator and evaluation of the candidate structures. The heart of the ESESOC is the structure generator, as an integral part, which accepts the specific type information (molecular formula, substructure constraints, etc.) and produces an exhaustive and irredundant list of candidate structures [4].

Major requirements for any structure-generation algorithm include exhaustiveness, irredundancy, efficiency, duplicate elimination and prospective use of constraints. A good structure generator must be exhaustive (all possible structures should be generated from a given set of fragments), irredundant (the generation of identical structures should be avoided) and effective. All these mean that the generation should be fast and perceive the connections that lead to chemically or topologically impossible, identical structures correctly as soon as possible during the generation process. For example, a typical set of segments derived from the molecular formula $C_8H_{12}O$ is {1–O–, 2 $-CH_2-$, 3 $-CH_2-$, 4 $-CH_2-$, 5 $-CH_2-$, 6 $-CH<$, 7 $-CH<$, 8 $-CH<$, 9 $-CH<$}.

* Corresponding author.

SSDI 0003-2670(94)00170-Q

The partially assembled structure obtained after few steps of the generation is

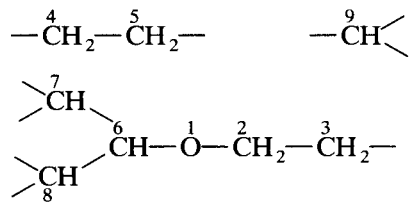

How is the next bond to be developed exhaustively and irredundantly? For exhaustiveness, all the segments with free valences should connected to each other alternatively. The segments 3, 4, 5, 7, 8 and 9 all have free valence, so the alternative connections of segment 3 are (3, 4), (3, 5), (3, 7), (3, 8) and (3, 9); the alternative connections of segment 4 are (4, 3), (4, 5), (4, 7), (4, 8) and (4, 9) and so on. The connections (3, 4) and (4, 3) are duplicate. Thus there are 15 (C_6^2) total alternative connections for the next bond, which are (3, 4), (3, 5) (3, 7), (3, 8), (3, 9), (4, 5), (4, 7), (4, 8) (4, 9), (5, 7), (5, 8), (5, 9), (7, 8), (7, 9) and (8, 9). The partially assembled structure obtained after the connection (3, 4) is

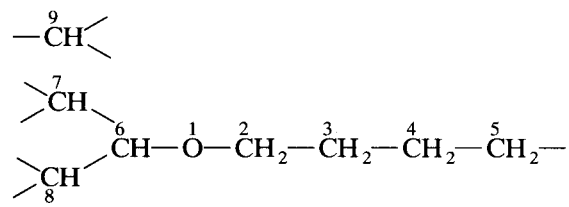

The partially assembled structure obtained after the connection (3, 5) is

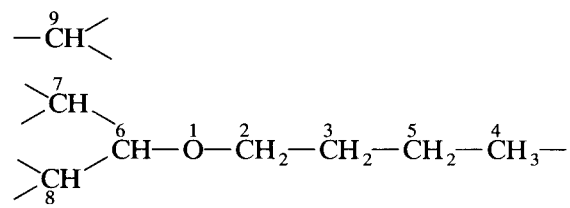

The connections (3, 4) and (3, 5) give the same partial structure, so they are redundant. In the same way as (3, 4) and (3, 5), the connections (4, 7), (4, 8), (5, 7) and (5, 8) are redundant. Thus, after removing the redundant connections, there are six valid connections to be developed alternatively, namely (3, 4), (3, 7), (3, 9), (4, 7), (4, 9) and (7, 9).

The redundancy of the connections (3, 4) and (3, 5) results from the topological equivalence of the segments 4 and 5. Hence the perception of the topological equivalence of the segments in molecular structures and partial structures is much more important for exhaustive and irredundant structure generation. It is also important for the assignment of a unique connection table for the molecular structure [5–9].

2. The published algorithm

Several algorithms have been developed for the computer perception of topological symmetry [6–12]. The algorithms designed by Morgan [7], Schubert and Ugi [9], Shelley and Munk [10–12] and the authors [6] all possess some characteristics of the graph theory, which all extend the node environments through the graph but include the different node properties and graph invariants to partition the nodes in the molecular graph.

The algorithm designed by Shelley and Munk [11] may be described as (1) set the class identifier (*CI*) of each node equal to $d \times 10 +$ elemental type (C = 2, N = 3, O = 4), where d is the connectivity; (2) count the number of different *CI* values (*NCI*) and assign new *CI* values between 1 and *NCI* to the *CI* of each atom; (3) if *NCI* is equal to the total number of nodes, then go to step 7, else assign a Trial Class Identifier (*TCI*) to each node, which specifies the neighbours' *CI* values; (4) count the number of different *TCI* values (*NTCI*) and assign new *TCI* values between 1 and *NTCI* to the *TCI* of each node; (5) if *NTCI* is not greater than *NCI* then go to to step 7; (6) set the *CI* of each node to its *TCI* and set *NCI* to *NTCI*, go to step 3; (7) end. The topological symmetry is represented by the class identifiers.

This algorithm completely partitions the nodes into equivalence classes for most molecular structures, but fails to partition the nodes in structures I and II and some structures in Figs. 5 and 6, etc. Therefore, another algorithm by using the permutation method was developed. This algorithm is rigorous, but it is more time consuming to construct the $\Pi(C_i)!$ permutations, where C_i is

the number of nodes in class i (partitioned by above algorithms) [10].

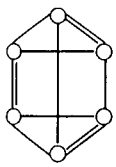

I

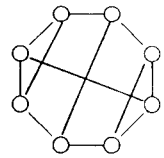

II

The authors modified Shelley and Munk's algorithm by using some new graph invariants, such as node properties, topological path and the smallest node ring index to set *CI* values [6]. In this paper, in order to partition the nodes in molecular graph, we use two new types of shell/layer matrices, node matrix (**N**) and bond matrix (**B**), patterned similarly to the matrices introduced by Diudea et al. [13].

3. Determination of topological symmetry

3.1. Node properties and bond codes

The connectivity of a molecule may be represented by a graph. A graph consists of a set of nodes and set of edges connecting the constituent nodes. A node of a chemical graph represents an atom in the molecule. In our system, the node properties include element type defining a specific non-hydrogen atom, the number of attached hydrogen atoms and the partial bonds by which it can join to other node. The partial bonds may be single, double, triple, aromatic, etc.

All the nodes containing elements, such as C, N, O, P, S, F, Cl, Br and I, were generated exhaustively and stored in the node library. An index number is assigned to each node in the node library. Table 1 shows various nodes in the node library.

The edges in the molecule graph are the bonds in the molecule; the bonds may be single, double, triple, aromatic, etc. In our system, a single bond is coded as 1, a double bond as 2, a triple bond as 3 and an aromatic bond as 1.5.

3.2. Matrices N and B

From the viewpoint of node i, the immediate neighbours of the node i form the first layer, the outer neighbours connecting immediately to the nodes of the first layer form the second layer, and so on. Then, a new type of layer matrix, node

Table 1
Various nodes of the node library

No.	Symbol	No.	Symbol	No.	Symbol
1	CH_3-	17	ArO	33	S=
2	$-CH_2-$	18	NH_2-	34	$\diagup$S=
3	$CH_2=$	19	–NH–	35	=S=
4	$\diagup$CH–	20	NH=	36	$\diagup$S(=)=
5	–CH=	21	$\diagup$N–	37	ArS
6	CH≡	22	–N=	38	H_2P-
7	$\diagup\diagdown$C$\diagup\diagdown$	23	N≡	39	–PH–
8	$\diagup\diagdown$C=	24	$\diagup$N(=)–	40	$\diagup$P–
9	–C≡	25	–N(=)=	41	=P$\diagup\diagdown$–
10	=C=	26	=N≡	42	F–
11	ArCH [a]	27	$N^{\ominus}$=	43	Cl–
12	ArC– [b]	28	$=N^{\oplus}=$	44	Br–
13	ArC [c]	29	$-N^{\oplus}\equiv$	45	I–
14	HO–	30	ArN		
15	–O–	31	HS–		
16	O=	32	–S–		

[a] Ar = aromatic. [b] Represents  . [c] Represents  .

matrix (**N**), is proposed, whose element n_{ij} is defined as the sum of index numbers in the node library for all nodes situated in the jth layer. Evidently, the entries n_{i1} in the first column represent the index number of the ith node in the node library. As an example, in structure IV, from the viewpoint of node 1, node 2 is in the first layer, the nodes of the second layer are 3 and 6 and nodes 4 and 5 are in the third layer. The index numbers of nodes 1, 2, 3, 4, 5 and 6 are 3, 8, 21, 4, 4 and 4, respectively (see Table 1). Hence $n_{11} = 3$, $n_{12} = 8$, $n_{13} = 21 + 4 = 25$ and $n_{14} = 4 + 4 = 8$. The **N** matrices of structures II, III, IV and V are shown in Fig. 1.

Similarly to the **N** matrix, the bond matrix (**B**) is proposed, whose element b_{ij} is defined as the

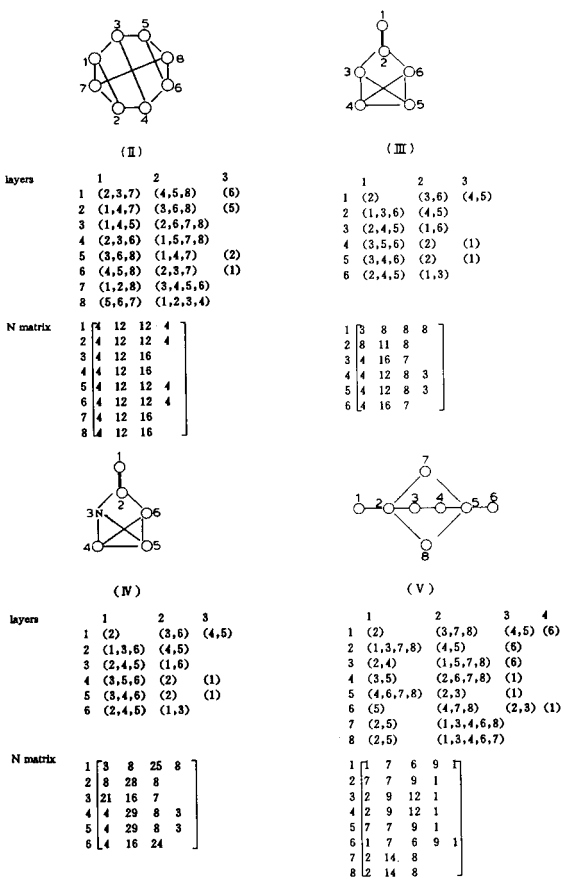

Fig. 1. The **N** matrices of structures II, III, IV and V.

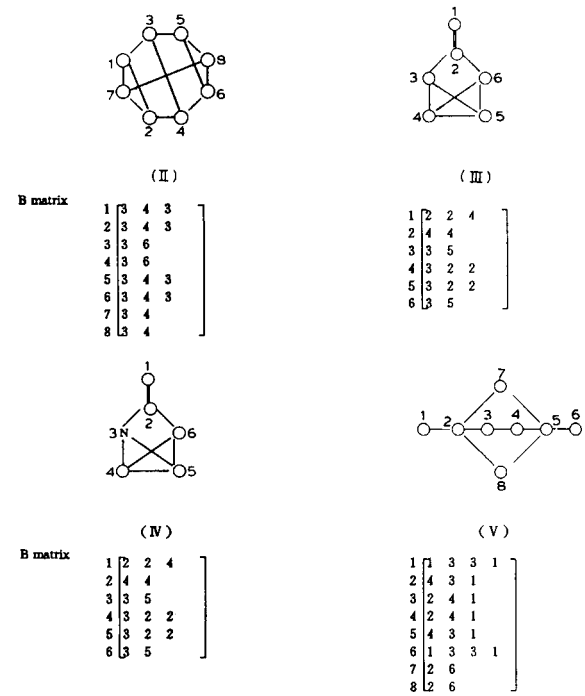

Fig. 2. The **B** matrices of structures II, III, IV and V.

sum of the codes of the bonds which are connected between the nodes of the jth layer and the nodes of the $(j-1)$th layer. As an example, there is one double bond between node 1 and the node in first layer in structure IV, so $b_{11} = 2$; there are two single bonds between the nodes of the first layer and the nodes of the second layer, so $b_{12} = 1 + 1 = 2$; there are four single bonds between the nodes of the second layer and the third layer, so $b_{13} = 1 + 1 + 1 + 1 = 4$. The **B** matrices of structure II, III, IV and V are given in Fig. 2.

3.3. Node weight calculation and topological symmetry perception

The **N** matrix characterizes the global environment of the nodes in a molecular graph from the viewpoint of every node and the **B** matrix expresses the global state of the edges in the molecular graph. Hence, the weight of a node is calcu-

lated by the following function, which specifies the global environments of the nodes and edges:

$$W[i] = n_{i1} + \sum_{j=1}^{K} n_{i(j+1)} \times b_{ij} \times 10^{-j}$$

where $W[i]$ is the weight of the ith node; n_{ij} and b_{ij} are the elements of the **N** and **B** matrices, respectively, and K is the number of layers from the viewpoint of node i. Fig. 3 shows the weight values of the nodes of structures II, III, IV and V.

The algorithm for the perception of topological symmetry is described as follows:

(1) Calculate the weight of each node (W) and count the number of different weight values (NW).
(2) If NW is equal to the total number of nodes then go to end, else calculate a Trial Node matrix (**TN**), whose element $(tn)_{ij}$ is defined as the sum of the weight values for all the nodes situated in the jth layer, and calculate a trial weight (TW) of each node by using the following function:

$$TW[i] = (tn)_{i1} + \sum_{j=1}^{K} (tn)_{i(j+1)} \times b_{ij} \times 10^{-j}$$

where $TW[i]$ is the weight of the ith node, $(tn)_{ij}$ and b_{ij} are the elements of the **TN** and **B** matrices, respectively, and K is the number of layers from the viewpoint of node i.
(3) Count the number of different TW values (NTW). If NTW is not greater than NW then go to 4, else set the W of each node to its TW, set NW to NTW, go to step 2.
(4) End. The topological symmetry is represented by W, i.e. if two nodes possess the equivalence weight value, then they are symmetrical.

Fig. 4 traces the algorithm for structure graph VI.

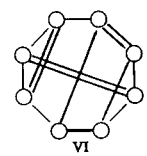

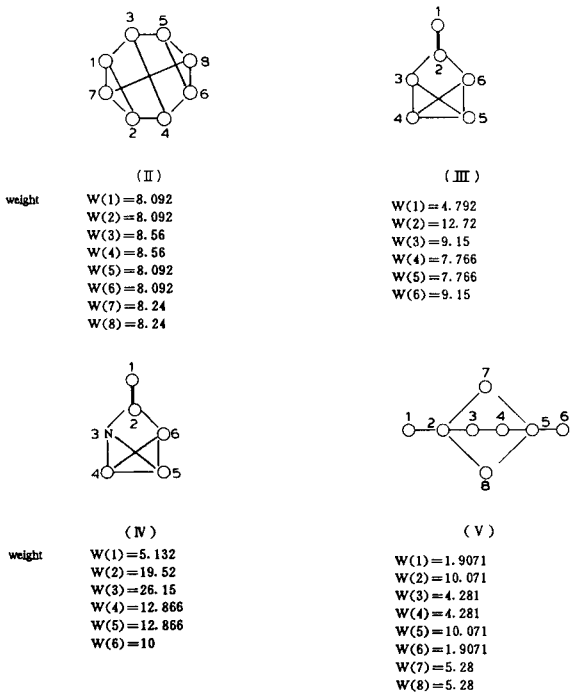

Fig. 3. The weight list of structures II, III, IV and V.

3.4. Tests of the method

For rigorous tests of the method, some complex polycyclic graphs were selected and examined. These graphs, employed by Randic et al. [14] and Carhart [15], are very complicated and interesting, and many published algorithms failed to detect the topological non-equivalent nodes in these graphs. The selected graphs are given in Fig. 5 and the results of the determination of topological equivalence are summarized in Table 2. From Fig. 5 and Table 2, it can be seen that the proper topological equivalence is indicated.

For more rigorous tests of the method, a set of highly regular graphs were examined. Regular graphs are graphs in which all nodes are the same. The regular graphs shown in Fig. 6 are exhaustively generated from the node sets containing 6–8 nodes of >CH–, >C<, >C=, etc. The

Table 2
Results of the determination of topological equivalence from Fig. 5

No.	Sets of equivalent nodes	Weight	CPU time (s)
A	(1, 2, 3, 4, 5, 6, 7, 8, 9)	20.44	< 0.01
B	(1, 2, 3, 4, 5, 6)	17.137216	< 0.01
	(7, 8, 9)	17.336896	
	(10)	19.46272	
C	(1, 3)	6.7464	< 0.01
	(2, 4)	4.02564	
	(6, 7)	6.952	
	(6)	4.1524	
	(8, 12)	4.1212	
	(9, 11)	6.5524	
	(10)	3.70016	
D	(1, 2, 11, 12)	8.36	< 0.01
	(3, 4, 9, 10)	8.1076	
	(5, 6, 7, 8)	7.77792	
E	(1, 4)	3.60408	< 0.01
	(2, 5)	3.52784	
	(3, 7)	6.9984	
	(6, 11)	8.73	
	(8, 12)	4.22184	
	(9, 13)	7.8724	
	(10, 14)	7.8408	
F	(1, 4)	4.10084	< 0.01
	(2, 3, 5, 7)	4.224	
	(6, 8, 11, 12)	7.7612	
	(9, 10, 13, 14)	6.994	
G	(1, 2, 5, 6)	3.475384	< 0.01
	(3, 4, 7, 8)	6.005992	
	(9, 10, 11, 12, 13, 14, 15, 16)	3.465456	
H	(1)	24.75622048	~ 0.02
	(2, 7)	15.233981448	
	(3, 6)	14.916111848	
	(4, 5)	22.93673288	
	(8)	40.4837768	
	(9)	39.8430224	
	(10, 13)	22.10664384	
	(11, 12)	14.275207384	
	(14)	20.77864384	
	(15, 16)	13.378296384	
I	(1, 7)	13.547844698970248	~ 0.02
	(2, 3, 9, 10)	7.6863674354378248	
	(4)	7.64196070383288	
	(5, 6)	10.5508064059717825	
	(8)	7.14569861427717824	
	(11)	17.52444054383288	
	(12, 18)	12.960960827946248	
	(13, 17, 19, 20)	7.3123984500778248	
	(14, 16)	10.0786489509317825	
	(15)	7.07151717405317824	
J	(1, 2, 3, 4, 5)	9.2928	~ 0.01
	(6, 7, 8, 9, 10)	9.4288	
	(11, 12, 13, 14, 15, 16, 17, 18, 19, 20)	9.4272	

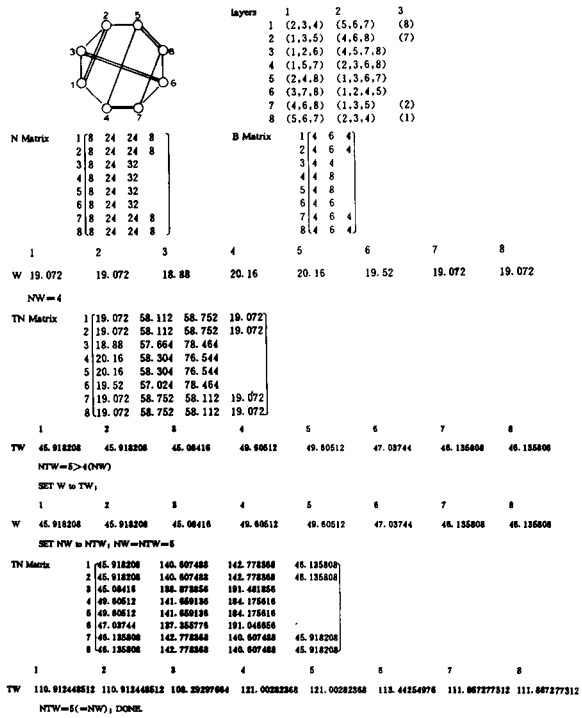

Fig. 4. The algorithm applied to structure VI.

determined results are given in Table 3. Again, the topological equivalence is determined correctly.

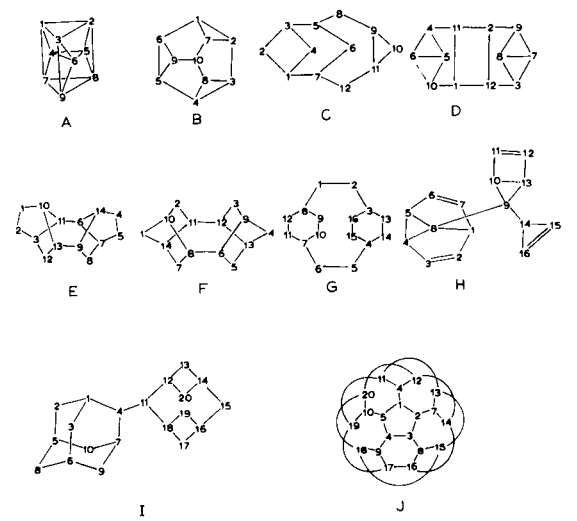

Fig. 5. Some selected graphs for the determination of topological equivalence.

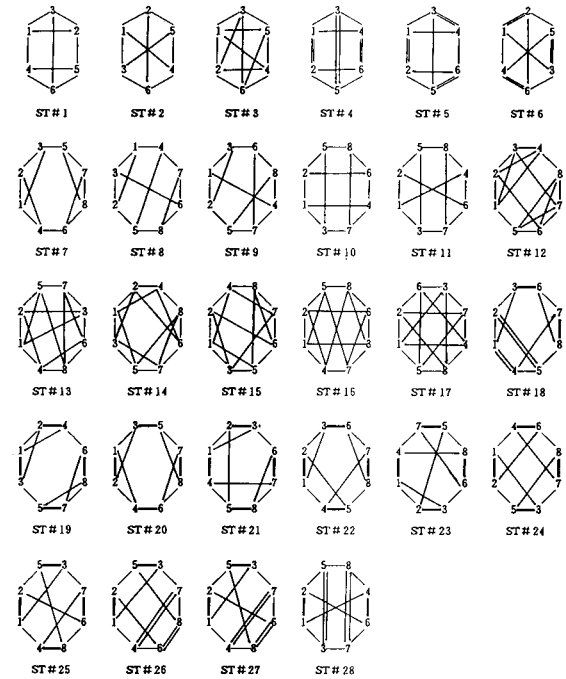

Fig. 6. Regular graphs for determination of topological equivalence.

4. Results and discussion

A simple scheme for computer perception of topological symmetry has been devised. It is considered to be rigorous in the identification of the topological equivalence class and relatively efficient in computer implementation. To substantiate the effectiveness, the CPU time needed for the evaluation of the graphs in Figs. 5 and 6 are also shown in Tables 2 and 3 (on an IBM PC 486/33 MHz), and the total CPU time needed for the evaluation of these 38 graphs (in Figs. 5 and 6) is 0.22 s.

This algorithm can also be applied to the partial structures. The results of its application to the partially assembled structure described in the Introduction are $W(1) = 16.5$, $W(2) = 5.456$, $W(3) = 2.3556$, $W(4) = 2.2$, $W(5) = 2.2$, $W(6) = 10.922$, $W(7) = 4.7822$, $W(8) = 4.7822$ and $W(9) = 4$, so segments 4 and 5 are in one topological equivalent class and segments 7 and 8 belong to another equivalent class.

Table 3
Results of the determination of topological equivalence from Fig. 6

No.	Sets of equivalent nodes	Weight	CPU time (s)
ST 1	(1, 2, 3, 4, 5, 6)	7.92	< 0.01
ST 2	(1, 2, 3, 4, 5, 6)	8.08	< 0.01
ST 3	(1, 2, 3, 4, 5, 6)	18.48	< 0.01
ST 4	(1, 2, 3, 4, 5, 6)	18.56	< 0.01
ST 5	(1, 2)	18.24	< 0.01
	(3, 4, 5, 6)	18.56	
ST 6	(1, 2, 3, 4, 5, 6)	18.88	< 0.01
ST 7	(1, 2, 7, 8)	7.792	< 0.01
	(3, 4, 5, 6)	8.092	
ST 8	(1, 2, 7, 8)	8.092	< 0.01
	(3, 6)	8.24	
	(4, 5)	8.56	
ST 9	(1, 2, 3)	17.1216	< 0.01
	(4, 5, 6)	18.184	
	(7, 8)	18.2608	
ST 10	(1, 2, 3, 4, 5, 6, 7, 8)	8.332	< 0.01
ST 11	(1, 2, 3, 4, 5, 6, 7, 8)	8.56	< 0.01
ST 12	(1, 2, 3, 4, 5, 6, 7, 8)	19.46	< 0.01
ST 13	(1, 2)	54.6028	< 0.01
	(3, 4, 5)	55.7536	
	(6, 7, 8)	54.46	
ST 14	(1, 2, 3, 4, 5, 6, 7, 8)	19.46	< 0.01
ST 15	(1, 8)	54.8212	< 0.01
	(2, 3, 6, 7)	56.2576	
	(4, 5)	56.1232	
ST 16	(1, 2, 3, 6)	19.88	< 0.01
	(4, 5, 7, 8)	20.3	
ST 17	(1, 2, 3, 4, 5, 6, 7, 8)	20.72	< 0.01
ST 18	(1, 2)	46.135808	< 0.01
	(3)	47.03744	
	(4, 5)	49.60512	
	(6)	45.08416	
	(7, 8)	45.918208	
ST 19	(1, 2, 7, 8)	18.016	< 0.01
	(3, 4, 5, 6)	19.072	
ST 20	(1, 2, 7, 8)	18.304	< 0.01
	(3, 4, 5, 6)	18.592	
ST 21	(1, 8)	18.592	< 0.01
	(2, 7)	19.072	
	(3, 6)	19.52	
	(4, 5)	20.16	
ST 22	(1, 2, 7, 8)	19.072	< 0.01
	(3, 6)	18.88	
	(4, 5)	20.16	
ST 23	(1)	45.7856	< 0.01
	(2, 3)	47.7824	
	(4)	50.1888	
	(5, 6)	50.3936	
	(7, 8)	50.5984	
ST 24	(1, 2, 3, 4, 5, 6, 7, 8)	19.552	< 0.01
ST 25	(1, 2, 3, 4, 5, 6, 7, 8)	20.16	< 0.01
ST 26	(1, 2, 3, 4, 5, 6, 7, 8)	19.552	< 0.01
ST 27	(1, 2, 3, 4, 5, 6, 7, 8)	20.16	< 0.01
ST 28	(1, 2, 3, 4, 5, 6, 7, 8)	20.16	< 0.01

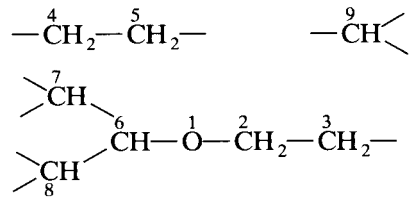

This algorithm has been incorporated in the ESESOC to determine the topological equivalence of the partial structures before the structure-generation step. This topic will be discussed further in a future publication [4].

Acknowledgement

The authors acknowledge the financial support of the National Natural Science Foundation of China.

References

[1] C.Y. Hu and L. Xu, Chin. J. Anal. Chem., 20 (1991) 643.
[2] C.Y. Hu and L. Xu, Chin. J. Org. Chem., 13 (1993) 129.
[3] C.Y. Hu and L. Xu, Sci. China (Ser. B), in press.
[4] C.Y. Hu and L. Xu, Anal Chim. Acta, in press.
[5] C.Y. Hu and L. Xu, Comput. Appl. Chem. (China), in press.
[6] C.Y. Hu and L. Xu, J. Chem. Inf. Comput. Sci., in press.
[7] L. Morgan, J. Chem. Doc., 5 (1965) 107.
[8] W.T. Wipke and M.T. Dyott, J. Am. Chem. Soc., 96 (1974) 4834.
[9] W. Schubert and I. Ugi, J. Am. Chem. Soc., 100 (1978) 37.
[10] C.A. Shelley and M.E. Munk, Anal. Chim. Acta, 103 (1978) 245.
[11] C.A. Shelley and M.E. Munk, J. Chem. Inf. Comput. Sci., 17 (1977) 110.
[12] C.A. Shelley and M.E. Munk, J. Chem. Inf. Comput. Sci., 19 (1979) 247.
[13] M.V. Diudea, O. Minailiuc and A.T. Balaban, J. Comput. Chem., 12 (1991) 527.
[14] M. Randic, G.M. Brissey and C.L. Wilkins, J. Chem. Inf. Comput. Sci., 21 (1981) 52.
[15] R.E. Carhart, J. Chem. Inf. Comput. Sci., 18 (1978) 108.

ELSEVIER

Analytica Chimica Acta 295 (1994) 135–141

ANALYTICA CHIMICA ACTA

Rapid photometric method for the determination of the mass concentration of nitrogen monoxide and nitrogen dioxide

K. Suzuki [a,*], T. Niimi [a], N. Yamamoto [a], M. Shibata [b], M. Saeki [c], A. Ono [c], T. Shirai [a,1], S. Yanagisawa [a]

[a] *Department of Applied Chemistry, Keio University, 3-14-1 Hiyshi, Kohoku-ku, Yokohama 223, Japan*
[b] *Aviation Environment Research Center, Airport Environment Improvement Foundation, 2-8-1 Haneda-Kuko, Ohta-ku, Tokyo 144, Japan*
[c] *Technical Development Bureau, Nippon Steel Coorporation, 1618 Ida, Nakahara-ku, Kawasaki 211, Japan*

Received 21st December 1993; revised manuscript received 30th March 1994

Abstract

A novel method has been developed for the photometric determination of nitrogen oxides (NO_x; NO and NO_2 gases). The sample gas is shaken with an NaOH–alkaline H_2O_2 solution in a container so that all the NO_x is converted to the NO_2^- form. After decomposition of the H_2O_2 by heating, the colour is developed using naphthylethylenediamine and the absorbance at 545 nm is determined. The reference calibration gases consisting of NO and NO_2 are determined within 20 min by adding catalase (enzyme) as a rapid decomposition reagent for H_2O_2 instead of the heating decomposition. This simple and rapid photometric method can be used to determine NO_x down to 0.5 ppm (v/v) (0.244 mg/m^3 as NO_2) in the case where a 1-l sampling flask is used.

Key words: Spectrophotometry; Manual determination; Nitrogen oxides

1. Introduction

Several methods have been employed for the determination of nitrogen oxides (NO_x; NO and NO_2) which are mostly emitted from exhaust gases by high temperature heating or combustion [1]. Some photometric measurements were adapted for the official domestic manual methods to determine NO_x in exhaust gases and standard calibration gases [1–3]. For instance, the Japanese Industrial Standard (JIS) has adapted three manual photometric measurements which include the zinc reduction naphthylethylenediamine (Zn–NEDA) method, the phenol disulfonic acid (PDS) method, and the Saltzman method [2]. Among them, we have been investigating for almost two decades the Zn–NEDA methods for the determination of NO_x in flue gases [4–8]. One of our developed Zn–NEDA photometric procedures was adapted by JIS in 1974 and is still used at present [2,4]. The major characteristic point of the Zn–NEDA method is to convert NO_x into NO_2^-, that is, (i) oxidation of NO to NO_2 with

* Corresponding author.
[1] Deceased.

SSDI 0003-2670(94)00160-N

ozone in the gas phase, (ii) absorption of NO_2 gas with a weak acidic solution in order to convert it into NO_2^- and NO_3^-, and (iii) catalytic reduction of NO_3^- to NO_2^- with zinc powder. The total NO_2^- is then determined based on the following colour development reactions with sulfanil amide (Eq. 1) and NEDA (Eq. 2) (see Scheme 1) in acidic medium and the measurement of absorbance of the azo dye at 545 nm [9,10].

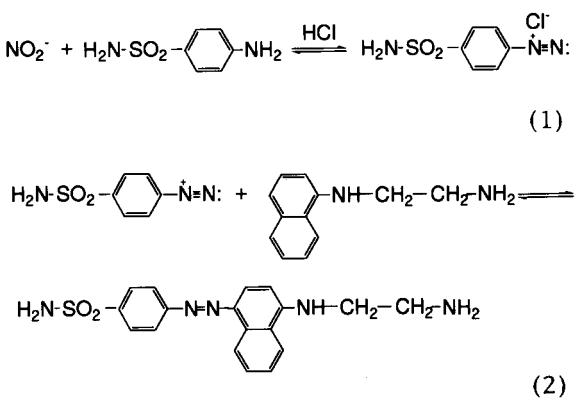

(1)

(2)

Scheme 1.

Regarding the Zn–NEDA method, two minor criticisms have been pointed out in the past. One is the use of ozone for the oxidation of NO to NO_2 in the gas phase and NO_2^- to NO_3^- in the aqueous phase. Ozone is a very active reagent and a harmful gas and requires a costly ozone generator for its preparation. The other is to use zinc which has a disposal problem. In addition, the reduction power is sometimes different with zinc powders from different suppliers. However, the last case has been solved in Japan by commercially supplying the same quality zinc materials for the nitrate reduction.

In the present report, we propose a rapid manual method for NO_x determination. The analytical procedure is briefly summarized in Fig. 1. It is also based on the colorimetric reactions indicated in Eqs. 1 and 2. The most characteristic point of the proposed method is that NO and NO_2 gases are converted into the NO_2^- (nitrite) form only in solution by shaking with an alkaline H_2O_2 solution in which H_2O_2 acts as a reducing agent in the solution. Using this procedure, ozone is not required since NO_3^- is not produced in the absorbed solution. In addition, zinc as a reducing agent is also not required. Hence, the previously mentioned critical points can be avoided.

After converting NO_x in the absorption solution as NO_2^-, the H_2O_2 residue in the sample solution disturbs the colour development with NEDA. Therefore, it must be decomposed. The H_2O_2 can be easily decomposed by placing the solution with Cu^{2+} as a catalyst in a water bath at 80°C for 30 min or by adding the enzyme catalase. In the latter case, the total analytical period is only 20 min starting from the NO_x gas sampling with the alkaline absorption solution through the final measurement of the absorbance of the coloured aliquot solution produced by the reaction with sulfanilamide and NEDA at a wavelength of 545 nm using a photometer.

As an application of this rapid manual photometric method, calibration NO and NO_2 gases in cylinders were measured and satisfactory results were obtained.

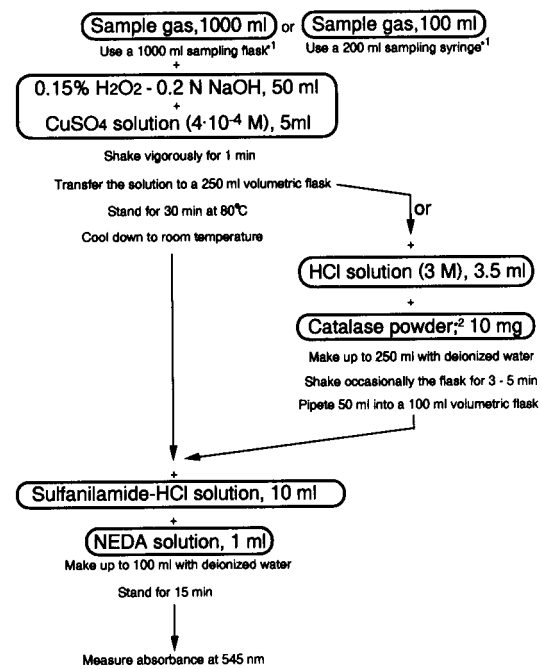

Fig. 1. Schematic diagrams of the manual methods for NO_x determination. *1See Ref. [2] (JIS K0104). *2Powdered enzyme extracted from bovine liver. Activity: 2000–5000 units/mg protein.

The present method for NO_x determination requires no special reagents, apparatus and techniques. Easy manual analytical procedures with inexpensive reagents provides many advantage in addition to the speed of the quantitative analysis.

2. Experimental

The analytical procedures, required reagents and their preparation for the proposed NEDA method for NO_x determination for reference and calibration gases are as follows.

2.1. Reagents

The following solutions are prepared for NO_x determination in which all chemicals are commercially available from most major chemical suppliers. Absorption solution: 0.2 M NaOH with 0.15% H_2O_2. $CuSO_4$ solution: 4×10^{-4} M. Sulfanilamide–HCl solution: 0.5% sulfanilamide with 20% HCl. NEDA (naphthylethylenediamine) solution: 0.1%. Standard $NaNO_2$ solution: 250 mg/l as NO_2^-. Diluted standard $NaNO_2$ solution: 20 mg/l as NO_2^-. HCl solution: 3 M. Catalase (EC 1.11.1.6): 10 mg (powdered protein, C_{10}, Sigma, St. Louis, MO; from bovine liver, activity 2000–5000 units/mg protein).

2.2. Apparatus

For calibration of capacities a 1000-ml sampling flask equipped with a three-way valve or a 200-ml sampling syringe was used. Spectrophotometric measurements were performed at 545 nm.

2.3. Gas sampling

The sampling apparatus basically consists of a sampling flask, manometer and a vacuum pump or sampling syringe [2]. (When the gas sampling syringe was used, the sampling volume is 100 ml and procedures 1–3 were not required. After connecting the syringe to a gas container or a sample gas bag with a silicone rubber tube, start from procedure 4.) The following gas sampling procedures were used.

(1) Connect the sampling flask to the sampling apparatus setup with silicone rubber tubing and connect a gas container or a sample gas bag to the three-way valve of the flask with silicone rubber tubing.
(2) Close the three-way valve of the sampling flask by opening the three-way valve of the manometer and draw a vacuum on the flask.
(3) Gently close the three-way valve of the manometer to the vacuum pump. Read the pressure (P_0) and ambient temperature (T_0).
(4) Open the three-way valve of the flask to introduce the sample gas and immediately close the three-way valve of the flask, and read the pressure (P_1) and the second ambient temperature (T_1).
(5) After closing the three-way valve of the manometer, detach the flask from the setup at the silicone rubber tubing.
(6) Inject 50 ml of the absorption solution and add 5 ml of the $CuSO_4$ solution to the sample flask or syringe using syringes.
(7) Immediately shake the flask vigorously for 1 min with intermediate rests.
(8) Transfer the sample solution from the flask into a 250-ml volumetric flask. Wash the sampling flask a few times with water and add it to the sample solution in the volumetric flask.

2.4. Decomposition of H_2O_2

The H_2O_2 residue in the absorption solution after gas sampling is decomposed by thermal heating or a catalytic promoter using catalase (In the case where the enzyme is used, add 3.5 ml of 3 M HCl to the sample solution in the flask and mix well. Add 10 mg of the catalase and mix by shaking until bubble generation stops. All these procedures are done at room temperature, in which steps 1 and 2 are not required.)
(1) Remove the lid of the flask and put the flask into a bath at 80°C for 30 min.
(2) Remove it and shake the flask. Cool the flask with running water.
(3) Add water to the 250-ml volumetric flask up to the mark and mix. This solution will be used as the sample solution for the following colour development step.

2.5. Colour development and photometric measurement

The azo dye for use in the photometric measurement is produced from NO_2^- by reactions 1 and 2. The following procedures are for photometry with NEDA as a colorimetric reagent.
(1) Pipet 20 ml of the sample solution (aliquot) into a 100-ml volumetric flask.
(2) Add 10 ml of the sulfanilamide–HCl solution.
(3) Add 5 ml of the NEDA solution, fill up to the mark with water and shake well.
(4) Allow this solution to stand for about 15 min at room temperature, and measure the absorbance with a spectrophotometer at a wavelength of 545 nm using the flask solution as the reference solution.

2.6. Preparations of calibration solutions and calibration graph

For the determination of the NO_2^- converted form NO_x, the following calibration solutions are prepared and the calibration graph is made with the solutions.
(1) A set of calibration solutions having NO_2^- concentrations of 0 (blank), 0.2, 0.4, 0.6, 0.8 and 1.0 μg/ml are prepared by pipetting, 0 (blank), 1, 2, 3, 4 and 5 ml of the diluted $NaNO_2$solution, respectively, into a series of 100-ml volumetric flasks.
(2) According to the former section of colour development and photometric measurement, the absorbance at 545 nm of the produced azo-dye solutions are measured.
(3) Plot a calibration graph with the absorbance of each calibration solution versus the concentration of NO_2^-. A linear calibration graph is obtained in the range 0.2–1.0 μg ml^{-1} NO_2^-. The slope of the straight line in the graph is given by Eq. 3.

$$\frac{\Delta A}{\Delta C} = \frac{1}{f} \tag{3}$$

where A is the absorbance, C is the mass concentration of NO_2^- in μg/ml, and f is the calibration factor in μg/ml related to a 1 cm optical cell ($\Delta A/\Delta C$).

Calculation of the mass concentration of NO_x in the sample gas

(1) Calculate the amount of sample gas taken at standard atmospheric conditions (0°C, 101.3 kPa) following Eq. 4.

$$V_s = V_a \cdot \frac{273}{101.3} \cdot \left(\frac{P_1}{273 + T_1} - \frac{P_0}{273 + T_0} \right) \tag{4}$$

where V_s is the amount of sample gas taken in ml, V_a is the capacity of the sampling flask or syringe in ml, P_0 is the pressure in the flask before gas sampling in kPa, P_1 is the pressure in the flask after gas sampling in kPa, T_0 is the temperature of the flask before gas sampling in °C, and T_1 is the temperature of the flask after gas sampling in °C (in the case when the temperature of the sample gas is the same as the ambient temperature, $T_1 = T_0$).
(2) Calculate the mass concentration of NO_x in the sample gas as nitrogen dioxide using Eq. 5.

$$C = f \cdot \frac{A}{b} \cdot \frac{nV_t}{V_s} \cdot 10^3 \tag{5}$$

where C is the mass concentration of NO_x in the sample gas in mg/m^3 which is multiplied by 10^3, f is the calibration factor of the solution in μg/ml, A is the absorbance, b is the optical cell length in cm, n is the dilution ratio of the sample solution (100/20 = 5), V_t is the volume of the total sample solution in ml (250 ml), and V_s is the volume of the sample gas in its normal state in ml as calculated using Eq. 4.

3. Results and discussion

3.1. Optimum composition of the absorption solution

The schematic analytical procedures are shown in Fig. 1 and their details are described in the Experimental section. The major role of the absorption solution is that all NO_x is converted to the NO_2^- form in the solution. In the case where

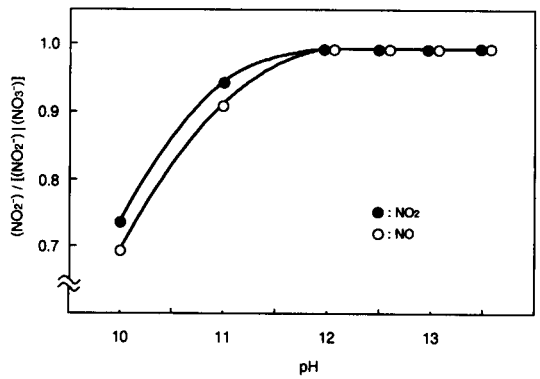

Fig. 2. Dependence of conversion of NO or NO_2 on the pH of the absorption solution (0.15% alkaline H_2O_2–NaOH solution). NO: 128 (v/v) ppm; NO_2; 180 (v/v) ppm (1 ppm = 0.487 mg/m^3 as NO_2).

H_2O_2 content in the solution kept constant (0.15%), the conversion ratio of NO and NO_2 to NO_2^-/NO_3^- is increased with increasing pH of the solution as shown in Fig. 2 and finally NO_x is converted into the NO_2^- form only in the pH region > 12.0. In the case when there is no H_2O_2 present in the alkaline solution of pH 12, the conversion ratio of NO_2^-/NO_3^- is approximately 2:1. However, when the solution involves > 0.05% of H_2O_2, NO_x is completely converted to the NO_2^- form. In the practical procedure, the absorption solution is adjusted to pH 13.3 with 0.2 M NaOH and 0.15% H_2O_2 is adequate for the determination of NO_x as a calibration/reference gas.

The most characteristic point of this new NO_x determination method is that the alkaline–H_2O_2 solution with a pH > 12.0 converts NO_x to NO_2^- only. This reaction equilibrium is discussed using the oxidation–reduction potential–pH diagram developed by Pourbaix [11]. In the alkali region, NO_2^- is produced from NO and NO_2 by reacting with HO_2^- as shown in Eqs. 6 and 7.

$$NO + HO_2^- + e^- \rightleftharpoons NO_2^- + OH^- \quad (6)$$

$$NO_2 + HO_2^- \rightleftharpoons NO_2^- + H^+ + e^- \quad (7)$$

On the other hand, H_2O_2 is considered to react with NO_3^- as shown in reaction 8.

$$NO_3^- + HO_2^- \rightleftharpoons NO_2^- + OH^- + O_2 \quad (8)$$

However, experimental facts indicated that the conversion reaction of NO_2^- to NO_3^- in an alkaline H_2O_2 solution did not proceed. Thus, reactions 6 and 7 are the actual major reactions to be considered. The conversion of NO and NO_2 of up to 2000 ppm (v/v) (974 mg/m^3 N as NO_2) into NO_2^- is almost quantitative (= 100%) in a 0.15% H_2O_2 alkaline solution of pH 13. The preservation of the aliquot after sampling of NO_x has no effect on the resulting absorbance for up to 24 h. Furthermore, after the decomposition of H_2O_2, the aliquot can be preserved for at least 48 h.

The addition of copper ion (Cu^{2+}) has the advantage of catalytically accelerating the conversion rate of NO_x into NO_2^-. However, this ion also accelerates the decomposition of H_2O_2, therefore, the solution containing Cu^{2+} and the alkaline H_2O_2 absorption solution should not be stored. The optimum concentration of Cu^{2+} addition is 4×10^{-4} M (5 ml/50 ml absorption solution) while further addition of this ion produces a positive error on the resulting absorbance.

3.2. Decomposition procedure of H_2O_2 in the absorption solution

The H_2O_2 residue in the absorption solution must be decomposed because it interferes with the colour development of NO_2^- when using NEDA. The H_2O_2 is easily decomposed by heating even if it is dissolved in alkaline solution. For instance, in the case where the alkaline solution of pH 13 contains 0.15% H_2O_2, the peroxide can be fully decomposed after 90 min at 80°C. According to the proposed analytical procedures (see Experimental section), the aliquot in the decomposition step contains Cu^{2+}, so that the decomposition rate of H_2O_2 is accessible. The time required for the decomposition of 0.15% H_2O_2 in the alkaline solution of pH 13 is 30 min at 80°C, 75 min at 70°C, and 90 min at 60°C. This reaction time for the decomposition of the H_2O_2 is a major part of the total required time for NO_x analysis. Thus, the rapid enzyme decomposition of H_2O_2 was examined using catalase. As we expected, adding catalase is very effective for the

decomposition of H_2O_2 even at room temperature. For utilizing the enzymatic reaction more effectively, the alkaline absorption solution is neutralized with hydrochloric acid before adding the enzyme. The optimum amounts of catalase and the neutralizing acid solutions are 10 mg (e.g., 2000–5000 units/mg protein extracted from bovine liver, see Experimental section) and 3 M HCl, 3.5 ml (per 50 ml absorption solution), respectively (see Fig. 1). The larger amounts of catalase are much more effective for the decomposition rate of H_2O_2. However, a too high amount of enzyme sometimes produced a yellowish precipitate in the solution. Therefore, this optimum amount was experimentally determined. The time required for the decomposition of 0.15% of H_2O_2 was completed in 5 min, so that the total time required for NO_x determination is approximately 20 min. This is one of the major advantages of this manual method for NO_x determination in addition to the economical merits caused by requiring no special reagents.

3.3. Application of the determination of NO_x as a calibration gas in the cylinder

Standard reference and calibration gases are mostly supplied in a metal cylinder which is commercially available from major gas and reagent suppliers. However, the true concentration varies with time, especially for NO_2 gas which is water soluble and has strong absorbing property. Hence, absolute determination is often required when it is used. As a test of the proposed method, five samples of newly prepared and almost one year-old NO_x gases in metal cylinders were measured with the present method involving the thermal (80°C, 30 min) or enzymatic H_2O_2 decomposition procedures. The analytical results are summarized in Table 1. The resulting analytical values compared with the present method is in good accordance with those determined by the official Zn–NEDA method that appears in JIS K0104 [2]. Using the present method with the enzyme H_2O_2 decomposition procedure, the analytical period for one determination is shortened by about 60 min compared to the official Zn–NEDA JIS method.

For additional information concerning the present method for NO_x determination, the influence of some interference gases on the resulting analytical NO_x values can be described as follows. (i) No interference was caused from coexisting hydrocarbons (HC), N_2O, CO and CO_2. In this case, CO_2 as an acidic gas, decreases the pH of the absorption solution when it is absorbed. However, no interference was observed using the absorption solution of over pH 12.0. (ii) A large concentration of coexisting SO_2 gas causes a negative error in the resulting NO_x value. However, this is a classical problem in gas sampling, because SO_x reacts with NO_x in the gas phase. (iii) NH_3 and other alkali gases have no influence on the resulting value of NO_x, because the present method uses alkaline absorption solution for gas sampling, whereas most of the other manual

Table 1
Analytical results for NO_x determination.

NO_x (total) [a] ($n = 2$) (v/v) ppm [b]	Composition $NO + NO_2$	NO_x (total) determined with the method		$\frac{NO_x(\text{present method})}{NO_x(\text{JIS method})^{*a}} \times 100$ (%)
		Mean (v/v) ppm [b] ($n = 8$)	C.V. (%)	
92.0	0.8 + 1	91.3	0.89	99.2
189	1.7 + 1	185	0.25	97.9
356	1.3 + 1	351	0.54	98.6
668	3.3 + 1	654	0.78	98.0
202 [c]	1 + 1	204	0.28	101

[a] Determined with the Zn–NEDA method (JIS k0104) [2].
[b] 1 (v/v) ppm NO_x indicates 0.487 mg/m^{3}N as NO_2.
[c] One year old NO_x gas in a metal sylinder (supplied as 110 ppm NO and 110 ppm NO_2).

methods use acidic solutions in which alkali gases produce positive errors in the resulting analytical values of NO_x.

In conclusion, the present manual method is very effective for the rapid determination of NO_x for standard calibration and reference gases. This method could be applied to the measurement of NO_x in flue and exhaust gases which are currently under investigation.

References

[1] Nitrogen Oxides, Committee on Medical and Biologic Effects of Environmental Pollutants, National Research Council, National Academy of Sciences, Washington, DC, 1977 (Japanese version: O. Wada and M. Okuda (translation), Tokyo Kagaku Dojin, Tokyo, 1979).
[2] JIS K 0104-1984, Japanese Standards Association, Tokyo, 1984.
[3] ASTM D 1608-60, American Society for Testing and Materials, Philadelphia, PA, 1967.
[4] JIS K 0104-1974, Japanese Standards Association, Tokyo, 1974.
[5] S. Yanagisawa, T. Shirai, T. Kutsusaka, M. Tanaka and N. Takada, Bunseki Kagaku, 25 (1976) 275.
[6] Y. Shichi, S. Fukushima, H. Kato, H. Inoue, T. Shirai and S. Yanagisawa, Bunseki Kagaku, 28 (1979) 187.
[7] S. Fukushima, H. Inoue, T. Shirai and S. Yanagisawa, Bunseki Kagaku, 29 (1980) 410.
[8] K. Isobe, H. Akada, S. Yanagisawa, H. Inoue and T. Shirai, Bunseki Kagaku, 32 (1983) 425.
[9] A.C. Bratton and E.K. Marshall, Jr., J. Biol. Chem., 128 (1939) 537.
[10] B.E. Saltzman, Anal. Chem., 26 (1954) 1949.
[11] M. Pourbaix, Atlas d'equilibres electrochimques: Azote 493, Eau 97, Eau Oxygenee 106, Cebelcor, Paris, 1963.

ELSEVIER

Analytica Chimica Acta 295 (1994) 143–149

ANALYTICA CHIMICA ACTA

Solid-state microprocessor-controlled detector for doublet peak measurements in flow-injection analysis

Mary K. Carroll [1], Michael Conboy, Asaph Murfin, Julian F. Tyson *

Department of Chemistry, University of Massachusetts at Amherst, Box 34510, Amherst, MA 01003-4510, USA

Received 7th December 1993; revised manuscript received 24th March 1994

Abstract

A solid-state detector for time-based transmission measurements in flow-injection analysis (FIA) based on a light-emitting diode (LED) source and photodiode (PD) transducer with microprocessor controller is described. The instrument components cost less than US$ 500. A simple peak-finding algorithm was capable of accurate measurements of the time interval between doublet peaks (Δt). Comparison of results, obtained using the detector, with theory for an acid–base reaction with bromothymol blue indicator is made. Linear relationships between the measured Δt and the logarithm of the injected concentration were obtained for two systems whose injection volumes were 987 and 1650 μl. The correlation coefficients, based on 14 and 13 data points, were 0.99_9 and 0.99_2, respectively. The detector could measure transmittance signals corresponding to 0.00098 absorbance above the baseline.

Key words: Flow injection; Solid state microprocessor-controlled detector

1. Introduction

Considerable effort has been made in the development of inexpensive flow-injection systems for research and pedagogical use. Hansen and Ruzicka [1] developed a modular system for use in teaching laboratories shortly after flow-injection analysis (FIA) was introduced. Davis [2] has presented an extremely inexpensive detector, constructed in-house, and of relatively crude design, for use in a variety of laboratory situations. Recently, Dasgupta et al. [3] reviewed the literature on LED-based detectors for absorption measurements. In that article, they described the advantages and disadvantages of various instrumental components (LEDs vs. laser diodes, photodiodes vs. phototransistors) and configurations, and stressed the need for a reference-based instrumental design, in order to avoid long-term instrumental drift [3].

The use of time-based measurements obviates both the need to eliminate or compensate for long-term drift of the source or detector, and the requirement that the signal have a linear response to concentration [4]. Ordinarily, FIA measurements are based on peak height. Doublet peaks, which form if the analyte is in excess at the profile center when the sample bolus reaches the detector, are seen as disadvantageous, limiting

* Corresponding author.

[1] Present address: Department of Chemistry, Union College, Schenectady, NY 12308, USA.

SSDI 0003-2670(94)00165-I

the upper range of the determination. However, by choosing appropriate manifold lengths and reagent concentrations such that doublets occur for even relatively low concentrations of analyte, the analytical chemist can expand the working range of the determination [4].

If the assumption is made that dispersion occurs only in the mixing chamber of the manifold, in accordance with that of a single well-stirred tank, the time between the two peaks, Δt, can be related to a number of system parameters by the following equation:

$$\Delta t = (V/Q)\ \ln\{[S][\exp(V_i/V) - 1]/[R]\} \quad (1)$$

where V is the volume of the mixing chamber, Q is the flow rate, [S] is the concentration of analyte in the sample injected into the manifold, [R] is the concentration of reagent in the carrier stream, and V_i is the volume of sample injected [4]. Hence, a plot of Δt versus ln[S] will be linear. Moreover, the relative error introduced in determination of unknown concentrations arising from the precision of the Δt measurements and the logarithmic relationship can be small in comparison with the uncertainty introduced from the calibration process [5].

Dasgupta and Loree [6] have developed instrumentation for peak width measurements in FIA and liquid chromatography (LC). Previous work by our group involved the development of a simple instrument for doublet-peak measurements suitable for use in teaching laboratories [7]. This instrument had as its optical sources LEDs and as detectors PDs; the output from the PD was plotted on an integrator, and Δt values were calculated based on the difference in recorded time of each peak [7]. In an effort to streamline the process, and to develop an instrument that is both more versatile and more easily portable than the first iteration, a microprocessor has been incorporated into the new instrument. The present instrument, referred to here as the doublet peak detector (DPD), has the FI manifold, detector electronics, microprocessor controller and readout contained within the same unit. It can be used as a self-contained instrument, or interfaced with a computer or an oscilloscope.

2. Experimental

2.1. Flow-injection manifold design

A schematic of the DPD is shown in Fig. 1. It is desirable to protect the electronic components from being flooded if a leak develops within the manifold system; hence, manifold components and the detector module are located below the electronic components in a project box ($13 \times 25 \times 30$ cm, McKinstry Metal Works). The majority of the manifold components are located within the DPD unit as illustrated in Fig. 1A.

A Rheodyne 6-port valve is mounted in the front side of the project box; small segments of flow tubing (0.9 mm i.d., Chemplast, Chemfluor® Teflon® spaghetti tubing) are used to connect the ports for injection loop, sample introduction, and waste output to unions mounted in the container wall. For purposes of testing the performance of the DPD, a simple, single-line manifold was chosen, of the type used in our previous studies [7,8]; however, the DPD has additional ports for use in more complicated manifold configurations. The mixing component used is a 60-cm length of flow tubing, and is more tightly coiled than that used in the previous LED-based instrument, in order to better approximate a well-stirred tank [7]. This component is connected to the detector module by a short segment of flow tubing.

Alteration of the manifold components housed within the DPD is facile, but it is not practical to do so within an experiment because components are anchored with cable ties. Because sample loop volume is used commonly as a variable in flow-injection experiments, the sample loop is connected externally to the box through two unions, which lead to valve ports. This has one disadvantage: it allows a certain amount of room light to enter the DPD through the tubing, resulting in a higher background signal. Significant problems with light leakage were not noted with this system; however, it would be possible to reduce stray light ingress by use of opaque tubing.

Likewise, because flow rate is commonly controlled by changing pump tubing or pump settings during the course of an experiment, the peri-

staltic pump is not contained within the DPD. Pump tubing is connected through a union to one of the valve ports. In the work presented here, we used a variable-speed peristaltic pump (Ismatec); however, a less expensive pump could be substituted.

Samples are injected into the sample loop using a disposable plastic syringe, which connects to a union on the side of the DPD unit. Waste from the injection valve and from the detector effluent is transported out of the DPD through additional unions.

2.2. Calibration of manifold components

The volume of each sampling loop was measured by filling the loop with 0.0464 M NaOH, injecting this sample into a carrier stream of deionized distilled water, collecting the effluent, and titrating with 0.0130 M HCl, employing a suitable acid–base indicator. Three replicate measurements were made for each sample loop. Flow rates for the solid-state instrument manifold were calculated from the time necessary to fill a 10.00-ml calibrated flask. Three replicate measurements were performed for each flow rate.

2.3. Transmission detector design

Three ultrabright light-emitting diodes (LEDs, Newark Electronics) are used as detector source elements, one of each of the following colors: red (630 nm), yellow (585 nm), green (565 nm), where each LED has a bandwidth of approximately 30 nm and the wavelength indicated is the wavelength of maximum emission. PIN photodiodes (PDs, Newark Electronics) were used as the detection components. The LEDs and PDs were mounted perpendicular to the direction of flow in appropriately sized holes in a small block of aluminum, as illustrated in Fig. 1A. The LEDs are not glued into place, but fit snugly into the drilled holes. The active area of each PD is centered across the flow cell from the corresponding LED,

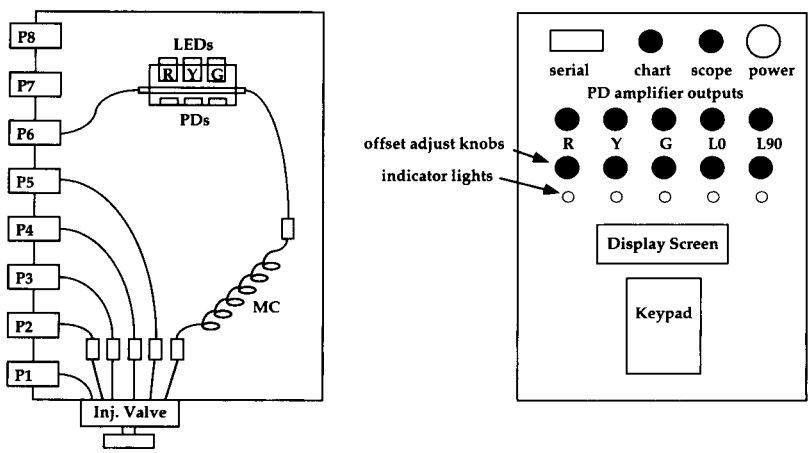

A B

Fig. 1. (A) Inside view of manifold components in doublet peak detector (DPD) unit. Inj. valve is a six-port rotary valve; MC is the mixing component, a coiled segment of flow tubing. PDs are the photodiode detector elements; each is paired with a light-emitting diode (LED) source. R, Y, G refer to the positions of the red, yellow and green LEDs. P1-P8 are union ports into the DPD. In the present study, a single-line manifold is used and the following connections have been made: the sample loop is connected between P1 and P2; injection syringe attaches to P3; the flow from the peristaltic pump enters through P4; P5 and P6 carry waste from the valve and detector, respectively, out of the DPD. P7 and P8 are not used, but could be employed in more complicated manifold designs. (B) Top view of DPD unit. The labelled circles are BNC connectors. R, Y and G refer to the outputs from photodiodes paired with red, yellow, and green LEDs, respectively. L0 and L90 are outputs from PDs to be paired with a laser diode for transmission and fluorescence measurements, respectively.

resulting in improved optical alignment over the previous detector version [7]. Because the case of each PD is connected to positive (not ground), and it is not desirable to have the cathodes of the three PDs in electrical contact with the aluminum block and each other, the PD cases are wrapped in Teflon tape prior to insertion into the detector module. The corners of the detector module are attached to the base of the DPD unit with silicone sealant.

The flow cell is a piece of square-cross-section capillary tubing ($1 \times 1 \times 50$ mm, Wale Apparatus); it is connected to the flow tubing by a short segment of pump tubing (red/red), and the connection is sealed with clear silicone as described previously [8]. Square-cross-section tubing was used in order to have a fixed path length in the cell, and to allow the detection of smaller signals. The initial design used flow tubing as the flow cell [7]; such tubing absorbed and scattered significant amounts of light in the visible region (as evidenced by its blue-gray color) and, because it was circular in cross section, the path length varied across the cell. In the current design, path length is 1 mm and is uniform across the cell; the sampled volume of the flow cell at each LED/PD detector pair is approximately 1 μl.

2.4. Controller design

The heart of the microprocessor unit is a single-chip microcomputer (DS5000, Dallas Semiconductor). It is programmed in code to collect and store the data, calculate the time between the two peaks in the doublet (in the range 10–240 s), and display the results to the nearest 0.01 s. The sampling frequency is 1 kHz.

The circuitry used to power the LEDs, perform current-to-voltage conversion of the signal from the PDs, and to offset the output voltage is modified slightly from that described previously [7]. It differs from the earlier circuit design in the voltage reference for the offset circuitry; complete circuit diagrams may be obtained from the authors. The object of the offset is to bring the background signal to zero volts, so that the gain settings may be used to the fullest extent. The instrument user sets the offset, while pumping

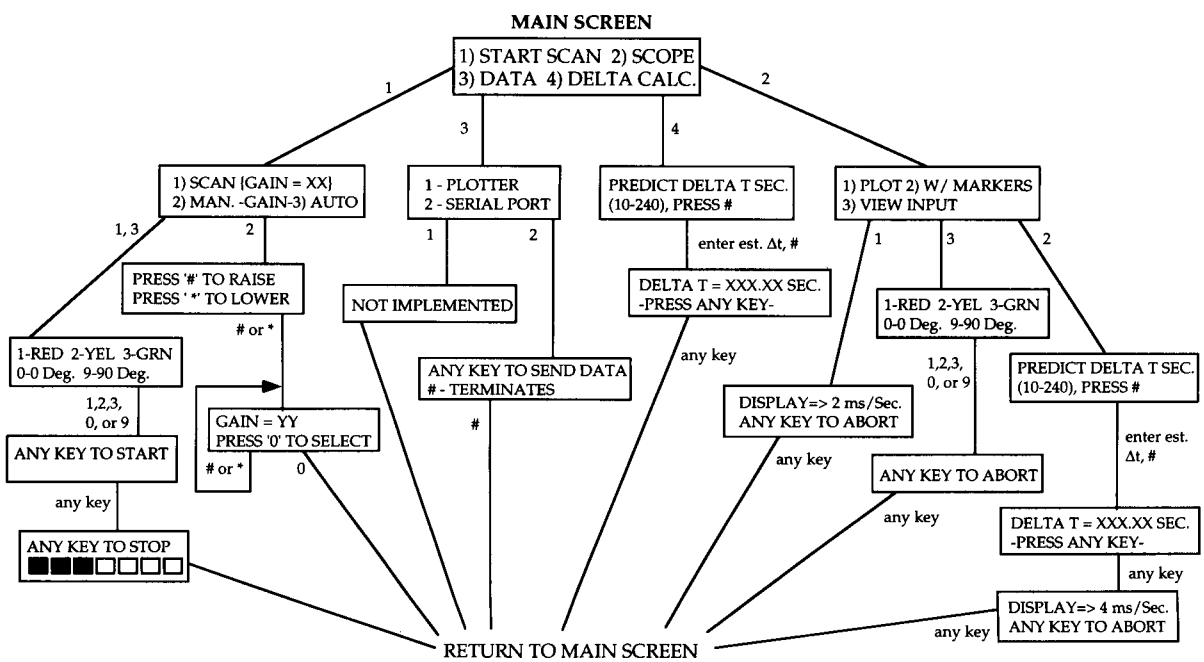

Fig. 2. Flow chart of operation of doublet peak detector (DPD). Note that when the data is displayed, a certain number of milliseconds of readout on the oscilloscope corresponds to 1 s of doublet peak data (designated ms/Sec. in the flow chart).

carrier stream through the DPD; a separate control for each detector PD is located on the instrument top panel (Fig. 1B).

Each PD has a fixed gain of 10^6 V/A in the current-to-voltage conversion step. Additional signal amplification (by a factor of 2^n, $n = 0$–7) is performed in the microprocessor.

After the signal has passed through the current-to-voltage converter, it is sent to an 8-bit analog-to-digital converter (AD7569, Analog Devices). The data is digitized and stored in memory for the duration of the experiment. The offset, amplified signal can be output to a stripchart recorder, integrator, or other readout device through a BNC connector if the user desires to view the amplified (but unprocessed) signal.

Detailed circuit diagrams may be obtained from the authors. The total cost of the electronic and manifold components used to construct the DPD is less than US$ 500.

2.5. Controller operation

Fig. 2 is a flow chart of the operation of the microprocessor controlled DPD unit. The keypad is used to enter numbers for the various selections. There are four selections on the main screen: (1) collect a new data set, (2) view most recently collected data on oscilloscope (this can include calculation of Δt), (3) send stored data to plotter or serial port of a computer, (4) calculate Δt. A data file is kept in memory until the next set of data is collected.

Data collection with the DPD unit consists of several steps. First, the user selects a gain setting or chooses autogain. Next, the source/detector combination to be monitored is chosen: RED, YEL and GRN refer to red, yellow, or green LED/PD combination, respectively; 0 Deg and 90 Deg refer to PDs placed 180° and 90° from a diode laser source (not described here) for transmittance-based or fluorescence-based measurements, respectively. The user then injects the sample into the flowing carrier stream and presses a key to start data collection. The signal is displayed as a bar graph (see Fig. 2); as the sample passes through the detector, a peak in the signal (dip in transmittance) is indicated by a rise in the number of illuminated blocks in the bar graph. After the second peak is observed, the user can stop the data collection; otherwise data collection continues until 240 s have elapsed since the start of the run. If the autogain setting was chosen, the microprocessor collects the data, then calculates the gain setting that should be employed to maximize the observed signal; however, it does not amplify the data. Consequently, if the signal is small, the data collection should be repeated using the gain setting selected by the microprocessor and given in the gain window as "1) SCAN {GAIN = XX}", where XX is the gain factor (2^n, $n = 0$–7).

Once it has collected the data, the microcomputer uses a simple algorithm for the double peak detection (more complicated algorithms could be programmed into the DPD). The user inputs an estimate of the time between peaks, Δt_{input}, within the range of 10–240 s. Each data point is compared to the previous one and the first peak is located; then, the microprocessor waits $\Delta t_{input}/2$ s before beginning to compare data points again. It locates the second maximum in the same way as the first, and then computes the time between the two peaks and displays the calculated Δt on the screen.

The output of the DPD can be sent to a plotter, to an oscilloscope, or in ASCII binary to a computer. If the data is sent to the oscilloscope, the user has the option of displaying tick marks that indicate the points chosen by the controller as the two peaks of the doublet.

2.6. Reagents used

The solvent used for all solutions was distilled, deionized water. For the purposes of characterizing the performance of the DPD, the same simple acid–base reaction with indicator that was used in previous work is employed [7]. The carrier stream contained 1.0×10^{-5} M HCl and 6.0×10^{-6} M bromothymol blue (BTB) indicator, and had the characteristic yellow color of the acid form of BTB. Sample solutions of NaOH were prepared by dilution of a 0.5 M stock solution with appropriate amounts of water. Alkaline solutions of BTB are a deep blue in color, and

absorb significantly at the wavelengths emitted by the LEDs used here; the acidic form of BTB does not absorb appreciably at these wavelengths.

2.7. Experimental procedure to test performance of DPD

The carrier stream was allowed to flow through the DPD. The red LED has the best overlap with the absorbance maximum of the blue form of BTB; thus, the signal from the red-LED/PD pair was monitored. The offset for the red LED/PD pair was adjusted manually to zero volts. A sample of NaOH solution was injected into the carrier stream, resulting in an on-line titration. Because the NaOH is in excess in the profile center when the sample bolus reaches the detector, the transmittance of the stream was observed to dip before and after the center of the sample bolus (doublet "peaks" if the signal is inverted, as was done in this circuitry, or if transformed to units of absorbance). The Δt calculated by and displayed on the DPD was recorded manually. To verify whether the identification of the two peaks, and therefore the calculation of Δt, was successful, the output of the DPD was displayed with markers on an oscilloscope (Hameg, Model HM205-3). Any discrepancy between the Δt recorded on the oscilloscope and that calculated by the DPD was noted. Three to five replicate measurements were made for each sample solution; the flow rate was fixed at 1.32 ml/min.

Five sample solutions, with concentrations of NaOH ranging from 1.10×10^{-5} M to 1.10×10^{-1} M, were used. Two different sample loops were tested, one 987 μl in volume, the other 1.65 ml in volume.

3. Results and discussion

With the exception of the data for the 1.10×10^{-5} M NaOH, the Δt values recorded by the DPD were all within 3 s of the Δt measured from the oscilloscope screen ("true" Δt); the first peak was identified correctly, but noise spikes near the second peak were often chosen by the microprocessor as the second peak, resulting in erroneous Δt values. Accurate location of the first peak is simplified by the fact that the first peak is relatively sharp for this particular chemical system; however, the second peak is broad. Doublet peak shapes vary for different chemical systems; a thorough study of doublet peak shapes for a variety of chemical systems has been performed [9].

Peaks observed for the least concentrated solution of NaOH studied were misidentified by the DPD because of the relatively large noise spikes observed, and because no smoothing of the data took place before peak identification. The signal-to-noise ratio was sufficiently large that precise measurements of Δt could be made when the DPD output was displayed on an oscilloscope screen. Modification of the microprocessor code so that the algorithm contains some level of smoothing would eliminate this shortcoming of the DPD.

The DPD is sensitive to small changes in absorbance; for the 1.10×10^{-5} M NaOH sample, the peak signal (least transmission) observed for the BTB indicator was equivalent to 0.00098 absorbance. The major source of electronic noise in the detection circuitry appears to be from the microprocessor circuitry. Improved shielding of the microprocessor from the detection electronics should result in improved signal-to-noise ratio, and allow the DPD to be used for samples that absorb even less strongly than those studied here.

Experimental results were in good agreement with Eq. 1. For the 987 μl sample loop, the plot of Δt (in s) versus [NaOH] (in M) gave a good fit to the line: $\Delta t = 107.4(\pm 0.6) + 7.8(\pm 0.2) \cdot \log[\text{NaOH}]$, $r^2 = 0.99_9$. (The values in parentheses are standard deviations of the intercept and slope, respectively; 14 points were used in the correlation.) Measured values of Δt ranged from 18.8 to 92.4 s. The working range covers four orders of magnitude of NaOH concentration. It should be noted that this fit includes the data for the 1.10×10^{-5} M solution of NaOH. The DPD calculations of Δt for solutions of this concentration were erroneous, so the Δt measured from the oscilloscope tracing was used; if these data points are omitted, there is no significant change in the curve-fit line. For solutions of the other

concentrations, Δt values calculated by the DPD were used, even though more accurate results could be obtained from the oscilloscope. Three replicate injections of a 6.60×10^{-4} M solution were made. The average calculated value of Δt was 51.4 s, with standard deviation 0.9 s; this corresponds to a sample concentration at the 95% confidence interval of 8.28×10^{-4} M > [NaOH] > 6.13×10^{-4} M (data treatment as in [5]).

Dispersion does occur in the sample loop, as well as in the mixing component, which is simply a more tightly coiled segment of the same tubing used in the rest of the manifold; hence, we would expect deviations from theory to be more pronounced as the size of the sample loop increases. Use of the larger sample loop, 1.65 ml, resulted in data that fit reasonably well to the line expected by theory, but the fit is not as good as that for the smaller sample. For this set of 13 data points, $\Delta t = 150(\pm 2) + 1.6(\pm 0.6) \cdot \log[\text{NaOH}]$, $r^2 = 0.99_2$. Values of Δt ranged from 42.5 to 127.9 s. As can be seen from these data, changing the volume of sample injected has a relatively small effect on the slope of the line, but a large effect on the Δt for a particular sample concentration.

The doublet peak detector (DPD) has several advantages: it is a relatively sensitive detector, inexpensive to construct, portable and rugged, and is suitable for many chemical systems whose products absorb light in the green to red region of the spectrum. The main limitations of the current version of the DPD are the short path length, the wavelength limitations imposed by the use of LEDs as light sources, and the current algorithm used to identify peaks and calculate the time between the two peaks in the doublet.

References

[1] E.H. Hansen and J. Ruzicka, J. Chem. Educ., 56 (1979) 677.
[2] L.C. Davis, J. Chem. Educ., 70 (1993) 511.
[3] P.K. Dasgupta, H.S. Bellamy, H. Liu, J.L. Lopez, E.L. Loree, K. Morris, K. Petersen and K.A. Mir, Talanta, 40 (1993) 53.
[4] J.F. Tyson, Analyst, 112 (1987) 523.
[5] R.T. Echols and J.F. Tyson, Anal. Chim. Acta, 286 (1994) 169.
[6] P.K. Dasgupta and E.L. Loree, Anal. Chem., 58 (1986) 507.
[7] M.K. Carroll and J.F. Tyson, J. Chem. Educ., 70 (1993) A210.
[8] M.K. Carroll and J.F. Tyson, Appl. Spectrosc., 48 (1994) 276.
[9] R.T. Echols and J.F. Tyson, Analyst, (1994) in press.

ELSEVIER

Analytica Chimica Acta 295 (1994) 151–157

ANALYTICA CHIMICA ACTA

Determination of traces of calcium and magnesium in rare earth oxides by flow-injection analysis

Duong Thanh Thuy [a], Dini Decnop-Weever [a], Wim Th. Kok [a,*], Pham Luan [b], Tu Vong Nghi [b]

[a] *Laboratory for Analytical Chemistry, University of Amsterdam, Nieuwe Achtergracht 166, 1018 WV Amsterdam, Netherlands*
[b] *Department of Analytical Chemistry, University of Hanoi, 19 Le Thanh Tong, Hanoi, Viet Nam*

Received 3rd January 1994; revised manuscript received 13th April 1994

Abstract

Flow-injection analysis has been applied for the determination of traces of calcium and magnesium in rare earth oxide samples. The method is based on the fluorescence of the calcein complexes of calcium and magnesium in a solution with high pH. The analyte ions are separated from the rare earth ion matrix on an in-line ion-exchange column. Matrix concentrations up to 500 mg l^{-1} of rare earth ions can be used. To discriminate between calcium and magnesium, 8-hydroxyquinoline is used as masking agent for magnesium and EGTA for calcium. Without masking agent the sum of calcium and magnesium is obtained. The relative standard deviation of the peak height for 25 μmol l^{-1} calcium was 0.4%. The lower limits of determination are 2 μmol l^{-1} or 0.1 mg g^{-1} in the rare earth oxide for calcium and 1 μmol l^{-1} or 0.04 mg g^{-1} for magnesium. Results obtained with the proposed method agree well with inductively coupled plasma atomic emission spectrometric results for a raw rare earth oxide sample

Key words: Flow injection; Fluorimetry ; Calcium; Magnesium; Rare earth oxide; Calcein

1. Introduction

The determination of traces ($\leq 0.1\%$) of calcium and magnesium in rare earth (RE) oxides such as Nd_2O_3 and Gd_2O_3 is important in the RE production industry in Vietnam and other countries. Numerous methods for the determination of calcium and magnesium are available, but only few are suitable for the low concentration levels expected after dissolution of the RE oxide matrices. Atomic absorption spectrometry (AAS) or inductively coupled plasma atomic emission spectrometry (ICP-AES) can be used for the determination. However, for these methods expensive instrumentation is required, which is not always available at the production sites in developing countries. Here, a method of analysis would be preferred which requires only simple instrumentation.

Flow-injection analysis (FIA) has been shown to be a relatively simple, reliable technique with a high sample throughput [1–3]. For matrices such

* Corresponding author.

SSDI 0003-2670(94)00177-N

as drinking water, brine, biological fluids, or minerals after dissolution, FIA has often been used for the determination of calcium and magnesium. Detection can be performed by potentiometry with ion-selective electrodes [4,5], by absorption spectroscopy with various colour reagents [6–9] or by fluorimetry with Quin-2 reagent [10].

Recently, the use of the fluorescence reagent calcein (bis[*N*,*N*′-bis(carboxymethyl)aminomethyl]fluorescein) in a flow-injection set-up has been described [11]. Calcein has been used before as an indicator in complexometric titrations [12,13] and for direct fluorimetric determinations in batch experiments [14,15]. In aqueous solutions with high pH calcein is not fluorescent itself while its calcium or magnesium complexes are [16,17]. The selectivity and high fluorescence yield of the reagent make it a promising choice for use in FIA. The FIA method was applied for the determination of calcium in mineral samples with a high calcium content. Good agreement was found with the nominal values of certified reference samples.

In our laboratory we have also studied the use of calcein as a reagent for calcium and magnesium in FIA with fluorescence detection. The system was optimized with respect to sensitivity for calcium and magnesium. The elimination of the interference of the RE matrix and the discrimination between calcium and magnesium by using different masking agents have been investigated.

2. Experimental

2.1. Apparatus

A Gilson (Villiers-le-Bel, France) Minipuls II pump was used, with polyethylene pump tubes, delivering flows of typically 1 ml/min pro line. Samples were introduced by means of a Rheodyne injection valve with a 100 μl sample loop. Connecting tubing and mixing coils were made from 1/16″ o.d., 1 mm i.d. PTFE tubing. Glass columns of 4 mm i.d. were used with PTFE wool as end frit. The fluorescence was measured with a Shimadzu RF-530 flow-through detector, operated with excitation and emission wavelengths of 300 and 515 nm, respectively. Signals were registered on a strip-chart recorder.

2.2. Chemicals and solutions

Calcein was obtained from Baker (Baker Grade) and from Janssen Chimica (Fluorexon, indicator grade). Standard solutions of RE metals (1000 mg/l lanthanum, praseodymium, neodymium, samarium and gadolinium in 2–3% HNO_3) were obtained from Hicol. Chelex 100 (50–100 mesh, sodium form) was obtained from Bio-Rad. The resin was rinsed with 0.01 mol l^{-1} HCl before use. Other chemicals used were of p.a. quality. Doubly deionized water was used.

Calcein stock solutions ($1.5 \cdot 10^{-4}$ mol l^{-1}) were prepared in concentrated potassium hydroxide solutions and stored in a refrigerator. Fresh reagent solutions were prepared by dilution in 0.2 mol l^{-1} KOH daily. Standard solutions of calcium and magnesium (1000 mg/l, Spectrosol-BDH), prepared from their nitrates, were appropriately diluted in 0.01 mol l^{-1} hydrochloric acid before use. RE oxide samples (10–50 mg) were dissolved in 5 ml 15% hydrochloric acid. After dissolution, the excess of acid was removed by evaporation, and the sample solution was reconstituted in the desired volume with 0.01 mol l^{-1} HCl.

All solutions were prepared and stored in polyethylene bottles. Before and during analysis, carrier and reagent solutions were degassed with helium.

ICP-AES determinations were carried out with a Thermo Jarrell Ash ICAP 61 instrument. For calcium the 393.366 nm line and for magnesium the 280.270 nm line was used.

3. Results and discussion

3.1. Calibration curves for calcium and magnesium

Calibration curves for calcium were constructed using 0.01 mol l^{-1} HCl as carrier solution and various concentrations of calcein in 0.2 mol l^{-1} KOH as reagent. After merging of the

two solutions a 20 cm mixing coil was used, since with this coil the highest signals were obtained. Fig. 1 shows the results obtained. Comparable with previous observations in batch experiments [14,15] and FIA [11], typical sigmoid curves are found when the peak height is plotted against the calcium concentration. Wallach and Steck [16] explained the relative low sensitivity at low calcium concentrations as a result of the fact that only the 2:1 calcium–calcein complex is fluorescent. The increase of the concentration-offset with increasing reagent concentration, as observed in our experiments, is consistent with this model. However, in our experiments it was found that the extent of the effect depended somewhat on the source and age of the calcein used. Also, according to the experiments of others [18], only the 1:1 complex is formed. Robinson and Weatherell [14] ascribed the low sensitivity at low calcium concentration to quenching of the fluorescence by free calcein. This, however, is contradicted by the appearance of the effect at the much lower concentrations as used in FIA. Demertzis [19] found that neither of the above mentioned processes can explain the dependency of the fluorescence intensity on the calcium and reagent concentrations. He assumed the involvement of the sodium or potassium ions of the alkali solution in the complexation reactions.

At high calcium concentrations a plateau value of the fluorescence intensity is found, proportional to the reagent concentration. This may be explained by the depletion of the free reagent at these high concentrations. The accessible calcium concentration range of the method is therefore determined at both sides by the reagent concentration, which should be adapted to the expected sample concentrations. In further experiments, a concentration of 7.5 μmol l^{-1} calcein was used. With this reagent concentration, the linear range was from 2 to 12 μmol l^{-1}, and calcium concentrations from 1 to 20 μmol l^{-1} could be determined.

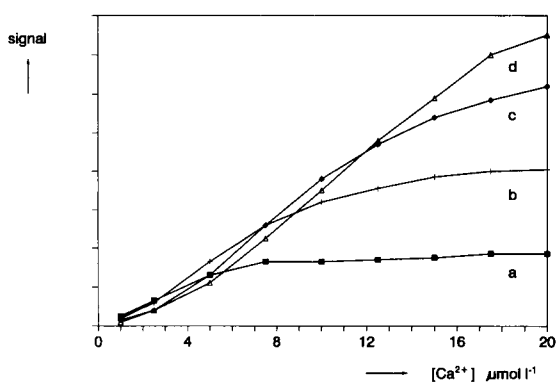

Fig. 1. Influence of the reagent concentration on the calibration lines for calcium. Calcein concentration: (a) 2.5, (b) 5.0, (c) 7.5 and (d) 10 μmol l^{-1}.

For magnesium ions approximately the same sensitivity was found as for calcium in the linear range of the method. The offset at low concentrations, however, was much smaller than with calcium, so that for low concentrations higher peaks were observed for magnesium. This is also in agreement with the results of Wallach and Steck [16]. From the solubility product of magnesium hydroxide (log $S = -11.15$ [20]) it would be expected that precipitation of magnesium would occur when the acidic carrier solution is merged with the alkaline reagent solution. This was not observed. Apparently, the complexation equilibrium with the calcein reagent prevents precipitation. An attempt was made to discriminate between calcium and magnesium by premixing of the carrier with a potassium hydroxide solution and the use of an in-line filter before merging with the reagent. This attempt failed: a reduction of the sensitivity for magnesium was not observed. Either the precipitation reaction is too slow, or the precipitate too finely divided to be filtered out.

3.2. Matrix interference

Although RE ions do not give fluorescent complexes with calcein, interference of the matrix on the calcium and magnesium signals is found due to the competition for the available reagent. In Fig. 2 peak heights obtained for a 15 μmol l^{-1} calcium solution with different concentrations of neodymium in the sample are shown, relative to the signal obtained without neodymium. The sensitivity for calcium at RE concentrations above 10 mg l^{-1} is strongly decreased.

To eliminate the matrix interference a 4 mm i.d. column, packed with macroparticulate (50–100 mesh) Chelex-100 ion-exchange resin, was inserted in the carrier line, before the point of merging with the reagent solution. Since the affinity of the packing material for RE ions is higher than for calcium or magnesium ions [21], a separation of the matrix was expected. In Fig. 2 the relative peak heights for a 15 μmol l^{-1} calcium solution with different neodymium concentrations, using a 5 cm Chelex column in the system, are included. In the absence of neodymium the calcium peak height is approximately three times lower than without column, due to an increased dispersion of the sample. However, as is shown in Fig. 3, with increasing RE matrix concentration, the calcium peaks become sharper and higher. A decrease of the peak heights is again observed at matrix concentrations of 100 mg l^{-1} and higher, but the sensitivity for calcium is still satisfactory up to a neodymium concentration of 500 mg l^{-1}. The sharpening of the calcium peaks may be attributed to a displacement effect by the neodymium ions on the ion-exchange column. The presence of high RE ion concentrations ($\geq$ 200 mg/l) in the sample is visible on the recorder traces as a depression of the background signal after the passage of the calcium peak (Fig. 3). This depression is also visible when the sample contains the RE ion only.

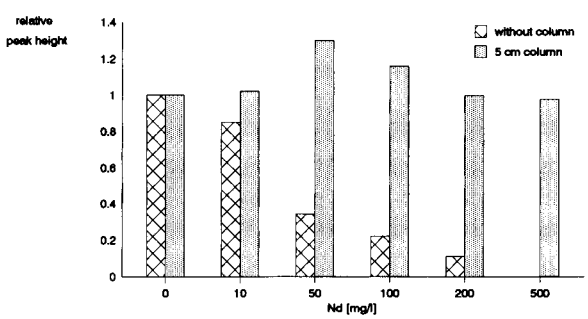

Fig. 2. Influence of the RE matrix concentration in the sample on the relative peak heights for 15 μmol l^{-1} calcium, with or without in-line ion-exchange column. Column bed length 5 cm. Reagent concentration 7.5 μmol l^{-1}.

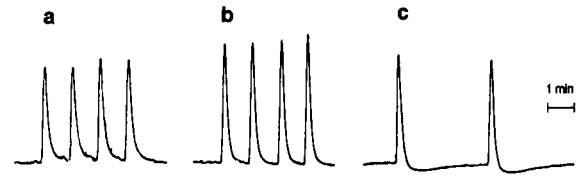

Fig. 3. Recorder traces obtained with the injection of 15 μmol l^{-1} calcium in a matrix of (a) 0, (b) 100 and (c) 500 mg l^{-1} Nd. Column bed length 5 cm.

Apparently, with the elution of the RE ions from the column, the background fluorescence of the calcein reagent is suppressed. Since a similar background suppression was also found when EDTA was added to the reagent solution, the source of the background signal may be a contamination of the solutions with calcium or magnesium.

Between the different RE ions tested as matrix component (La, Pr, Nd, Sm, Gd) no significant differences were found. Since with the 0.01 mol l^{-1} HCl carrier solution the retention of the RE ions on the resin is low, regeneration of the column during use is not necessary. However, the time interval between injection should be long enough ($\geq$ 2 min) to avoid interference by the matrix of the previous sample.

Different lengths of the ion-exchange resin bed have been tested. The tolerance of the system for the RE matrix increases with the length of the bed. While with a 2 cm bed the presence of 200 mg l^{-1} neodymium decreases the calcium peaks with approximately 50% (depending on the calcium concentration), with a 4 cm bed the peak heights are almost unaffected and with an 8 cm bed the sensitivity increases by 25% due to the sharpening of the peaks. With magnesium this effect was not found; in the presence of RE ions the magnesium signals were decreased. Fig. 4 shows calibration plots for calcium and magnesium in the absence and presence of 200 mg l^{-1} of neodymium, measured with a column length of 8 cm. Although the sensitivity for Ca and Mg depends on the presence of the RE ions, this is not a problem in practice, since the matrix concentration can easily be kept constant.

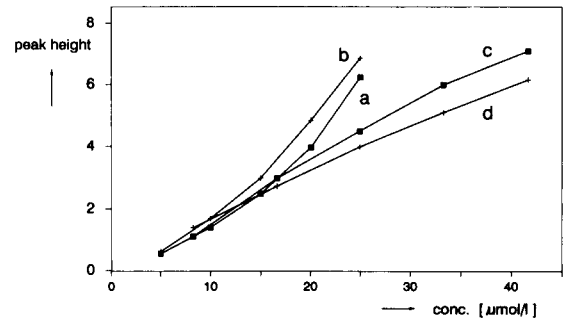

Fig. 4. Effect of the matrix on the calibration lines for Ca and Mg. Samples contain (a) Ca; (b) Ca with 200 mg l^{-1} Nd; (c) Mg and (d) Mg with 200 mg l^{-1} Nd.

3.3. Discrimination between calcium and magnesium

Several reagents have been tested as masking agent for calcium or magnesium. The masking reagents were added with a separate line, merging with the carrier stream after the ion-exchange column. The complete set-up, which was used in subsequent experiments, is shown in Fig. 5. Due to the different dilution of sample and reagent, sensitivities were changed compared with previous experiments. For the masking of magnesium, the best results were obtained with a 5 mmol l^{-1} solution of 8-hydroxyquinoline (8-HQ) in 0.01 mol l^{-1} KOH. The sensitivity for Mg decreased to approximately 3% of that obtained without masking agent, while the sensitivity for Ca decreased only to approximately 50%. For the masking of Ca, a solution of 0.5 mmol l^{-1} EGTA in 0.01 mol l^{-1} KOH could be used. The calcium signals completely disappeared, while the sensitivity for Mg was virtually unaffected by the presence of EGTA. Fig. 6 shows calibration lines for calcium and magnesium in a 200 mg l^{-1} RE matrix with both masking agents.

Mixtures of Ca and Mg in different ratios, in a

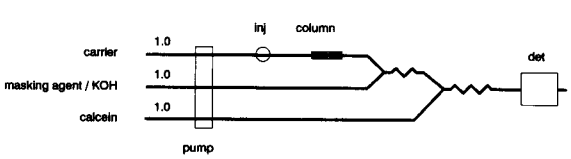

Fig. 5. Set-up of the FIA system with masking-agent line.

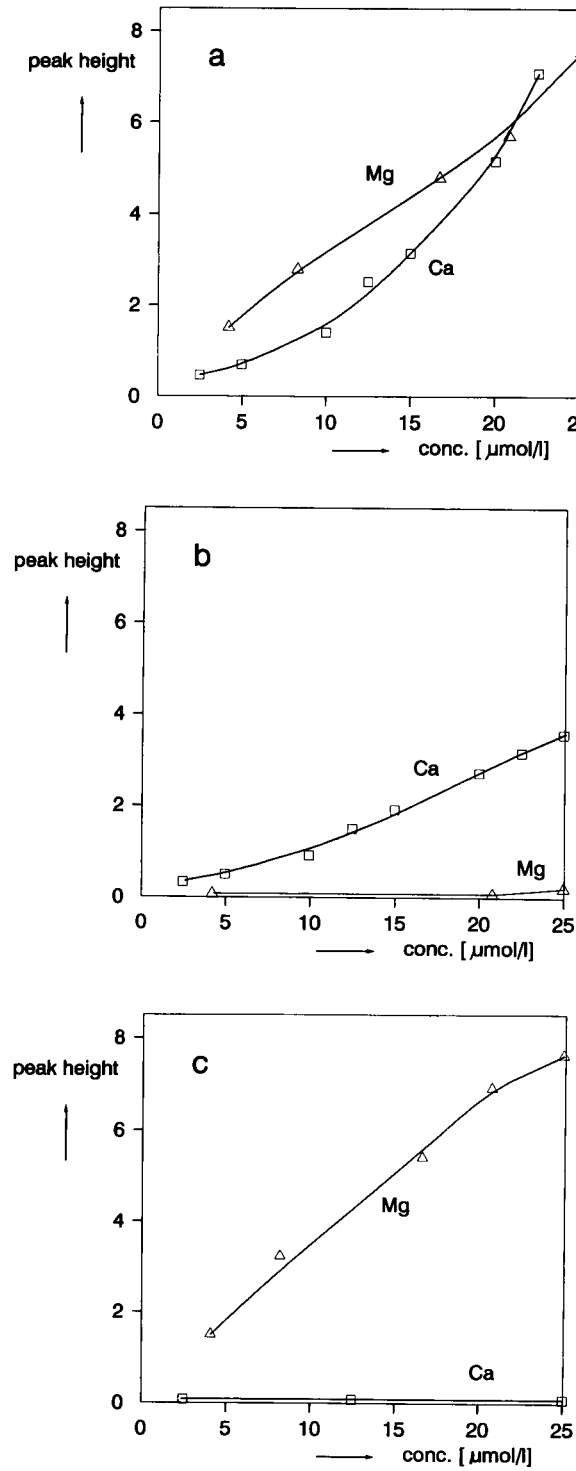

Fig. 6. Calibration lines for Ca and Mg in a 200 mg l^{-1} RE matrix with the use of masking agents. The masking-agent line contains 0.01 mol l^{-1} KOH, (a) without masking agent; (b) with 5 mmol l^{-1} 8-HQ and (c) with 0.5 mmol l^{-1} EGTA.

200 mg l^{-1} RE matrix, were injected with 8-HQ, EGTA or a blank KOH solution in the masking-agent line of the set-up. The results of these experiments are given in Table 1. The calcium concentrations in the mixtures were determined using the 8-HQ masking agent, by comparison with a calibration line measured with calcium standards. The magnesium concentrations in the mixtures were determined using EGTA as masking agent, with a magnesium calibration line. As can be seen in Table 1, the accuracy for the single ions is reasonable. By measurement of the peak heights obtained without masking agent, the sum of the calcium and magnesium concentrations could be determined. Peak heights were compared with a calibration line measured with calcium standards. Again, a reasonable accuracy is found. Only when the mixture contains a relatively high amount of magnesium, the sum of the calcium and magnesium concentrations is underestimated.

3.4. Analytical performance

The interference of other metal ions possibly present in RE oxide samples has been studied. The results are summarized in Table 2. Apart from the interference by barium, strontium and cadmium, which also give fluorescent complexes with calcein at high pH, the effect of other metal ions in high concentration on the calcium peak heights is probably due to a similar competition effect as with the RE ions. These experiments have been performed without the ion-exchange column.

Table 1
Analysis of mixtures of calcium and magnesium in a 200 mg l^{-1} RE matrix with and without masking agents

Sample	Added (μmol l^{-1})			Found (μmol l^{-1})		
	Ca	Mg	Ca+Mg	Ca [a]	Mg [b]	Ca+Mg [c]
1	5.0	8.3	13.3	4.0	6.9	14.7
2	12.5	20.8	33.3	11.8	21.8	31.0
3	22.5	4.2	26.7	18.5	4.1	25.7
4	2.5	37.5	40.0	2.5	40.0	32.2

[a] With 8-HQ.
[b] With EGTA as masking agent.
[c] Without masking.

Table 2
Effect of the presence of other metal ions in the sample on the signal for calcium

Metal ion	Effect
Li^+, Na^+, K^+, Al^{3+},	No effect
Bi^{2+}, Si^{4+}, V^{5+}, Cr^{6+}	No effect up to 50 mg/l
Ba^{2+}, Sr^{2+}, Cd^{2+}	Increase of signal
Ni^{2+}, Co^{2+}, Fe^{3+}, Cr^{3+}	Decrease of signal at concentrations $\geq$ 10 mg/l

The standard deviation of the peak heights obtained with repeated injections of a calcium standard in a 200 mg l^{-1} RE matrix varies from $\pm 0.4\%$ ($n = 6$) for a 25 μmol l^{-1} solution to $\pm 8\%$ ($n = 6$) for a 2.5 μmol l^{-1} calcium solution. The lower limit of determination is 2 μmol l^{-1} in solution. Since matrix concentrations up to 500 mg l^{-1} of the RE ions could be used, this lower limit corresponds to 0.1 mg of calcium per gram of RE oxide or 0.01% (w/w). For magnesium the lower limit is 1 μmol l^{-1} in solution or 0.004% (w/w) in the RE oxide. The upper concentration limit of the method is approximately 50 μmol l^{-1}. The sample throughput of the method was, depending on the dilution of the matrix, 20–30 h^{-1}.

Two samples of a raw lanthanum oxide material were processed and analyzed for calcium and magnesium by the proposed FIA method and by ICP-AES. The sum of the calcium and magnesium content as found by FIA was 0.52 ± 0.05 mg/g (mean $\pm 95\%$ confidence interval). With ICP-AES a calcium content of 0.56 ± 0.02 mg/g and a magnesium content of 0.01 ± 0.005 mg/g were found in the sample.

Acknowledgments

Thanks are due to S. Remijnse for her participation in the experimental work.

References

[1] J. Ruzicka and E.H. Hansen, Flow Injection Analysis, Wiley, New York, 1981.
[2] M. Valcarcel and M.D. Luque de Castro, Flow-Injection

Analysis, Principles and Applications, Ellis Horwood, Chichester, 1987.
[3] B. Karlberg and G.E. Pacey, Flow Injection analysis, A Practical Guide, Elsevier, Amsterdam, 1989.
[4] E.H. Hansen, J. Ruzicka and A.K. Ghose, Anal. Chim. Acta, 100 (1978) 151.
[5] H. Wada, T. Ozawa and G. Nakagawa, Anal. Chim. Acta, 211 (1988) 213.
[6] W.D. Basson and J.F. van Staden, Analyst, 103 (1978) 296.
[7] A.O. Janintho, E.A.G. Zagatto, B.F. Reis, L.C.R. Pessenda and F.J. Krug, Anal. Chim. Acta, 130 (1981) 361.
[8] G. Nakagawa, H. Wada and C. Wei, Anal. Chim. Acta, 145 (1983) 135.
[9] J.F. van Staden and A. van Rensburg, Analyst, 115 (1990) 605.
[10] H. Wada, H. Atsumi and G. Nakagawa, Anal. Chim. Acta, 261 (1992) 275.
[11] N. Chimpalee, D. Chimpalee, R. Jarungpattananon and S. Lawratchavee, Anal. Chim. Acta, 271 (1993) 247.
[12] K. Mori, Arch. Biochem. Biophys., 83 (1959) 552.
[13] J.A. Weatherell, Clin. Chim. Acta, 5 (1960) 61.
[14] C. Robinson and J.A. Weatherell, Analyst, 93 (1968) 722.
[15] S. Meites, Stand. Methods Clin. Chem., 6 (1970) 207.
[16] D.F.H. Wallach and T.L. Steck, Anal. Chem., 35 (1963) 1035.
[17] H. Diehl, Calcein, Calmagite, and *o,o'*-Dihydroxyazobenzene. Titrimetric, Colorimetric and Fluorometric Reagents for Calcium and Magnesium, The G. Frederick Smith Chemical Co., Columbus, OH, 1964.
[18] E.A. Bozhevolnov and S.U. Kreingold, J. Anal. Chem., USSR, 17 (1962) 558.
[19] M.A. Demertzis, Anal. Chim. Acta, 209 (1988) 303.
[20] R.M. Smith and A.E. Martell, Critical Stability Constants, Vol. 4, Plenum Press, New York, 1976.
[21] E.B. Sandell and H. Onishi, Photometric Determination of Metals, Part I, Wiley, New York, 1978.

ELSEVIER

Analytica Chimica Acta 295 (1994) 159–163

ANALYTICA CHIMICA ACTA

Flow spectrophotometric method for determination of hydrogen peroxide using a cation exchanger for preconcentration

A.M. Almuaibed *, A. Townshend

School of Chemistry, University of Hull, Hull HU6 7RX, UK

Received 26th January 1994; revised manuscript received 16th March 1994

Abstract

A flow spectrophotometric method for the preconcentration and determination of hydrogen peroxide is developed. It is based on the formation of the titanium(IV) peroxo complex and its retention on a minicolumn cation exchanger, elution with sulphuric acid and spectrophotometric detection at 410 nm. The calibration graph is linear over the range 4×10^{-6}–6×10^{-5} M. The 2σ detection limit is 1×10^{-6} M (34 ng ml^{-1} and the exchange capacity is 1.1 mmol H_2O_2 g^{-1} dry weight.

Key words: Flow system; Ion exchange; Spectrophotometry; Hydrogen peroxide; Preconcentration

1. Introduction

The determination of H_2O_2 is important in clinical applications for measuring the concentration of a variety of biological species such as glucose, uric acid and cholesterol based on enzyme (oxidase)-catalysed reactions [1]. The determination of very low concentrations of aqueous hydrogen peroxide has received great attention in atmospheric studies because it is believed that it rapidly oxidises hydrogensulphate ions in water at pH < 4.5 and this contributes to the generation of sulphuric acid [2,3]. On-line preconcentration offers some advantages such as the removal of matrix effects, and improvement of the selectivity and detection limit of some common analytical procedures. It enables comparatively large representative samples to be treated and therefore decreases the sampling error [4]. Many flow analysis procedures combined with on-line preconcentration techniques for trace metal ions have been developed [5–13]. The preconcentration of H_2O_2 in flow systems, however, has not been reported. This paper describes the determination of H_2O_2 based on preconcentration of the titanium(IV)–H_2O_2 complex on a cation exchange minicolumn. The complex is eluted with sulphuric acid and monitored spectrophotometrically at 410 nm [14].

2. Experimental

2.1. Chemicals and reagents

Distilled deionized water was used throughout. Hydrogen peroxide (30 volumes) was obtained

* Corresponding author.

SSDI 0003-2670(94)00153-D

from Fisons (Loughborough). The hydrogen peroxide stock solution (1×10^{-3} M) was prepared by dilution of 2.5 ml of the H_2O_2 to 100 ml with water; the solution was standardized iodimetrically [15]. Standard solutions containing $< 1 \times 10^{-5}$ M H_2O_2 were freshly prepared before use. $Ti(SO_4)_2$ solution (15% w/v) was obtained from BDH (Poole). Dowex 50W resin (4% cross-linked, 100–200 mesh) was obtained from Sigma (Poole).

2.2. Apparatus

Spectrophotometric measurements were made with an LKB Ultrospec II spectrophotometer equipped with a flow cell (30 μl, light path 10 mm). The components, including injection valve, pump, manifold and reaction coil tubing (0.5 mm i.d.) were as reported earlier [16].

2.3. Direct flow injection manifold and procedure

The manifold used for direct determination of H_2O_2 is shown in Fig. 1. The H_2O_2 solutions were injected into the carrier stream (2×10^{-3} M $Ti(SO_4)_2$ in 0.1 M H_2SO_4) and the absorbance was measured at 410 nm.

2.4. Preconcentration flow manifold and procedure

The manifold used for on-line preconcentration of H_2O_2 is shown in Fig. 2. The H_2O_2 solutions were continuously pumped for exactly 4 min at 1.5 ml min^{-1}, merging with 1×10^{-3} M $Ti(SO_4)_2$ containing 0.02 M H_2SO_4. The Ti–H_2O_2 complex formed was retained on a Dowex 50W

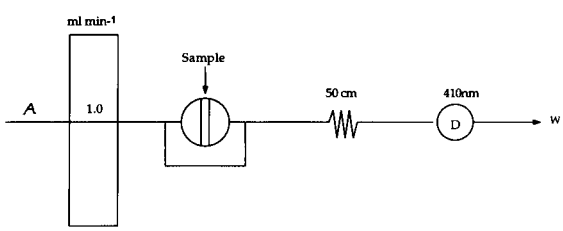

Fig. 1. Manifold used for direct determination of H_2O_2: A, 1×10^{-1} M Ti(IV) containing 0.1 M H_2SO_4; D, spectrophotometer; W, waste.

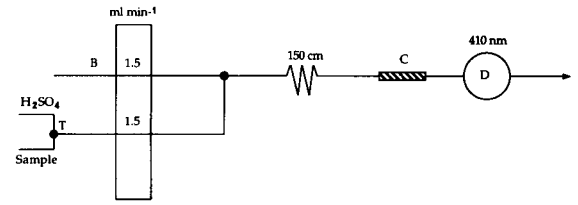

Fig. 2. Manifold used for preconcentration and determination of H_2O_2: B, 1×10^{-3} M Ti(IV) containing 0.02 M H_2SO_4; T, three-way valve; C, cation exchange minicolumn; D, spectrophotometer; W, waste.

cation exchanger minicolumn (2.5 mm × 0.25 mm i.d.), and eluted by pumping 1.2 M H_2SO_4 through the column by turning the three-way valve. The eluate was pumped to the spectrophotometer and monitored at 410 nm.

2.5. Preparation of the cation exchanger minicolum

Dowex-50W resin was used in the H^+ form. It was washed with 0.2 M sulphuric acid followed by water to remove fine particles, soaked for one day in water and packed into the minicolumn. A thin layer of glass wool was put at each end to prevent the movement of resin particles by the carrier stream. A small piece of silicone rubber tubing was pushed into each end of the column to achieve a very tight connection.

3. Results and discussion

3.1. Direct injection

The manifold shown in Fig. 1 was used for the determination of H_2O_2. H_2SO_4 concentration, titanium concentration, flow rate, sample volume and coil length were optimized using 2×10^{-4} M H_2O_2. The optimal conditions established are: sample volume, 70 μl; H_2SO_4 concentration, 0.1 M; flow rate, 1.0 ml min^{-1}; titanium concentration, 2×10^{-3} M; coil length, 50 cm.

Under the conditions established above, the calibration graph was linear over the range 4×10^{-5}–4×10^{-4} M H_2O_2. The least squares regression line and correlation coefficient were peak height absorbance = $157[H_2O_2](M) + 3 \times 10^{-3}$

and 0.998 ($n = 6$), respectively. The detection limit (2σ) and sample throughput were 2×10^{-5} M (1.5 nmol) and 65 h^{-1}, respectively. The relative standard deviation (R.S.D.) for 10 replicate injections of 1×10^{-4} M H_2O_2 was 1.0%.

3.2. Optimization of variables for the preconcentration system

H_2O_2 reacts with titanium(IV) in the presence of H_2SO_4 to form a peroxo complex, probably $Ti(O_2)^{2+}$ [17], which is retained on the resin. It was reported that H_2SO_4 can have an important effect on the retention of $Ti(O_2)^{2+}$ on the resin; too high a concentration of H_2SO_4 caused some complex to be washed through the column [18]. Therefore the effect of H_2SO_4 on the adsorption of the peroxo complex on the resin was investigated by preparing the titanium solution (1×10^{-3} M) in solutions of different H_2SO_4 concentration (0.02–0.1 M). The retained complex was eluted with 1.6 M H_2SO_4. Maximum absorption of the complex for 4×10^{-5} M H_2O_2, as indicated by the amount eluted, was found at 0.02 M acid, which was used for further investigations.

The influence of titanium concentration over the range 1×10^{-4}–2×10^{-3} M containing 0.02 M H_2SO_4 was examined. It was found that the peak height absorbance for 4×10^{-5} M H_2O_2 increased up to 1×10^{-3} M Ti(IV), then levelled off. So 1×10^{-3} M Ti^{4+} was used in further investigations.

H_2SO_4 was used to elute the retained $Ti(O_2)^{2+}$ from the column. Initially an injection valve with a 50 μl loop was inserted before the column in the manifold shown in Fig. 2. 1.6 M H_2SO_4 was injected to elute the complex; ca. 5 injections were required to elute all the complex. The injection of the acid also led to an apparent signal because of a refractive index change. For this reason, this approach was not used further in this investigation.

Another approach, in which the H_2SO_4 could be continuously aspirated through the column, was used throughout the remainder of this study, as shown in Fig. 2. The influence of different concentrations of H_2SO_4 over the range 0.2–2.2 M on the peak height absorbance for 4×10^{-5} M H_2O_2 was studied. The results are shown in Fig. 3. The peak height absorbance increased as the concentration of H_2SO_4 increased from 0.2 to 1.6 M, and the peak width decreased. This indicates that at lower H_2SO_4 concentrations the complex is released slowly. After the elution of the complex with 0.2 M H_2SO_4, 1.6 M H_2SO_4 M was pumped through and no peak was obtained, showing that all the retained complex has been eluted by 0.2 M H_2SO_4. In subsequent experiments, 1.2 M H_2SO_4 was used for elution to minimize the effect of refractive index unless otherwise stated. The 0.02 M H_2SO_4 then replaces the 1.6 M solution before sample loading is restarted.

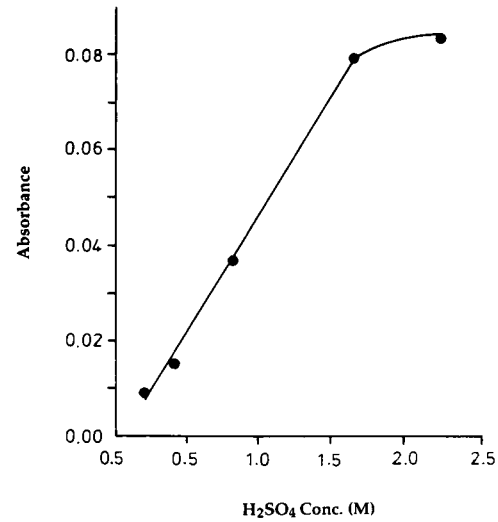

Fig. 3. Effect of eluting agent (H_2SO_4) concentration on the peak height absorbance for 4×10^{-5} M H_2O_2.

The process of sample loading onto a packed column is a key link in the entire preconcentration procedure [19]. Different procedures have been applied for sample loading on a minicolum such as the injection of a definite volume of sample from a simple loop [8,9], continuous aspiration of a fixed volume of sample [11], and continuously pumping the sample through the column at a constant rate for a constant time [12,13]. Each procedure has its advantages and disadvantages. The first approach (by injection) was not used because it is inconvenient to load

the injection valve with a large volume of sample (ca. 4 ml or so). It also needs a washing stage to remove the somewhat dispersed sample completely from the loop. The continuous aspiration of a fixed volume appears to be a useful approach. It is suitable for atomic absorption spectrometry or related detection techniques, but not for spectrophotometric measurements because pumping the last drops of sample sucks some air bubbles into the system, which affects the measurements, while it has no significant effect in atomic absorption spectrometric measurements. The last approach (loading of sample for a fixed time) was used in this investigation because it is simple to load the sample directly onto the column without prior introduction into a loop. The only limitation is its dependence on the stability of the flow rate. The sample flow rate should therefore be checked regularly. Aspiration of sample for exactly 4 min at 1.5 ml min^{-1} (6.0 ml) was used throughout unless otherwise stated.

The effect of coil length (10, 70 and 150 cm) to allow a reaction between Ti(IV) and H_2O_2 was studied. The results for 4×10^{-5} M H_2O_2 showed that peak height absorbance increased by ca. 20% as the length of coil increased from 10 to 150 cm; 150 cm was used for further experiments.

The influence of total flow rate over the range 2–3 ml min^{-1} was studied. The flows in both lines are equal to promote more reproducible mixing. The peak height absorbance for 4×10^{-5} M decreased by 15% as the flow rate increased from 2 to 3 ml min^{-1}. This is probably due to dispersion and less contact time between the exchanger and the complex. 3 ml min^{-1} was used to achieve a reasonably high sample throughput, although a lower flow would give greater sensitivity if that was desirable.

Washing the column with water after the elution of complex had no effect on the signal in the subsequent experiment. Thus no washing step was needed.

The effect of using ion exchange columns of 2 or 4 cm with the same diameter (0.25 mm) was studied. It was found that there was no significant different in the peak height absorbance for 4×10^{-5} M H_2O_2 using either column. So 2 cm was used for further investigations.

3.3. H_2O_2 recovery

The manifold shown in Fig. 2 was used for this study. A 1×10^{-3} M or 4×10^{-4} M H_2O_2 solution was merged with 1×10^{-3} M Ti(IV) containing 0.02 M H_2SO_4. The experiment was carried out with and without the column. The waste was collected in a 10-ml volumetric flask in each instance, and the absorbance was measured at 410 nm. The retention values on the column calculated from the two measurements were found to be 93 and 97%. The complex retained on the cation exchanger in the above experiment was eluted with 1.6 M acid and collected in a 10-ml volumetric flask. The absorbance was again measured at 410 nm and the H_2O_2 concentration was calculated from the calibration graph prepared by the batch method [14]. The recovery was found to be 92%.

3.4. Exchange capacity

The resin was dried at 60°C for 4 h and cooled in a desiccator. A solution (25 ml) of 0.02 M H_2O_2 and 1×10^{-3} M Ti(IV) prepared in 0.02 M H_2SO_4 was added to the cation exchanger (0.460 or 0.558 g). The mixture was allowed to equilibrate for 7 h with stirring at room temperature (20°C). The absorbance of the filtrate was measured manually at 410 nm. The capacity C was calculated from the following equation [20] : $C = C_i - C_f V/W$, where C_i is the initial concentration of H_2O_2 before equilibration, C_f is the concentration of H_2O_2 after equilibration, and V and W are the volumes of the test solution and the resin weight, respectively. The Ti–H_2O_2 complex uptake capacity of the cation exchanger, calculated as described above, was found to be 1.1 mmol H_2O_2 g^{-1} dry weight.

3.5. Analytical characteristics

Under the conditions established, the calibration graph for H_2O_2 was linear over the range 4×10^{-6}–6×10^{-5} mol l^{-1} for 4 min (6.0 ml) sample uptake. The least squares calibration equation over this range was peak height is repre-

sented by: absorbance = $1987[H_2O_2](M) - 2.7 \times 10^{-3}$. The correlation coefficient was 0.999 ($n = 5$). The R.S.D. for 5 replicate injections of 1×10^{-5} M H_2O_2, and the sample throughput were 2% and 10 h^{-1}, respectively. The detection limits (2σ) for 4 min and 8 min sample uptake were 2×10^{-6} M (68 ng ml^{-1}, 12 nmol) and 1×10^{-6} M (34 ng ml^{-1}, 12 nmol), respectively.

It is interesting that the sensitivity (calibration slope) is ca. 13 times greater than the direct injection procedure, although the volume of sample solution used has increased from 70 μl to 6 ml. Likewise the absolute detection limit has increased from 1.4 nmol to 12 nmol. This seems to indicate that an appreciable amount of peroxide is not retained on the column, notwithstanding the recovery experiments described above. However, sufficient is retained to give a significant increase in sensitivity.

4. Conclusions

A simple, inexpensive and sensitive preconcentration procedure for determination of H_2O_2 has been developed. Sensitivity is 10 times greater than the direct flow injection procedure. The detection limit could undoubtedly be improved by decreasing the flow rate or by increasing the volume of the sample loaded onto the minicolumn and by using a mixed ligand complex such as, Ti – 2(5-bromopyridyl)azo-5-propyl-*N*-sulfopropyl(amino)-phenol – H_2O_2, which has higher molar absorptivity than Ti – H_2O_2 [21].

References

[1] P.W. Carr and L.D. Bowers, Immobilized Enzymes in Analytical Chemistry and Clinical Chemistry, Wiley, New York, 1986.
[2] S.A. Penkett, B.M.R. Jones, K.A. Brice, and A.E. Eggleton, J. Atmos. Environ., 13 (1979) 123.
[3] D. Moller, Atmos. Environ., 14 (1980) 1067.
[4] Y.A. Zolotov and N.M. Kuz'min, Preconcentration of Trace Elements, Elsevier, Amsterdam, 1990.
[5] X. Wu and Q.I. Wy, Anal. Chim. Acta, 214 (1988) 279.
[6] Z. Fang, J. Ruzicka and E.H. Hansen, Anal. Chim. Acta, 164 (1984) 23.
[7] F. Malmas, M. Bengtsson and G. Johansson, Anal. Chim. Acta, 160 (1984) 1.
[8] Z. Fang, S. Xu and S. Zhang, Anal. Chim. Acta, 164 (1984) 41.
[9] M.A. Marshall and H.A. Mottola, Anal. Chem., 57 (1985) 729.
[10] M.R. Pereiro Garcia, M.E. Diaz Garcia and A. Sanz Medel, J. Anal. At. Spectrom., 2 (1987) 699.
[11] S. Devi, K.A.J. Habib and A. Townshend, Quim. Anal., 8 (1989) 159.
[12] I. Sekerka and J.F. Lechner, Anal. Chim. Acta, 234 (1990) 199.
[13] J. Havel, M. Vrchlabsky and Z. Kohn, Talanta, 39 (1992) 795.
[14] Z. Marczenko, Separation and Spectrophotometric Determination of Elements, Wiley, New York, 1986.
[15] G.D. Christain, Analytical Chemistry, Wiley, New York, 4th edn., 1986, p. 581.
[16] A.M. Almuaibed and A. Townshend, Anal. Chim. Acta, 198 (1987) 37.
[17] D.T. Burns, A.H. Carter and A. Townshend, Inorganic Reaction Chemistry, Vol. 2, Horwood, Chichester, 1981, p. 464 and references cited therein.
[18] J.S. Fritz and J.E. Abbink, Anal. Chem., 34 (1962) 1080.
[19] Z. Fang, S. Xu and S. Zhang, Anal. Chim. Acta, 200 (1987) 35.
[20] D.E. Berge and J.E. Going, Anal. Chim. Acta, 123 (1981) 19.
[21] C. Matsubara, K. Kudo, T. Kawashisa and K. Takamura, Anal. Chem., 57 (1985) 1107.

ELSEVIER

Analytica Chimica Acta 295 (1994) 165–172

ANALYTICA CHIMICA ACTA

Impulse-response functions of flow-through detectors based on the membrane-stabilised liquid–liquid interface Part II. Experimental verification

Stefan Wilke *

Martin-Luther-Universität Halle-Wittenberg, Fachbereich Chemie, 06217 Merseburg, Germany

Received 7th December 1993; revised manuscript received 22nd March 1994

Abstract

The impulse-response functions of an amperometric and potentiometric flow-through detector based on the membrane stabilised water–nitrobenzene interface have been determined by measuring the response to a short concentration pulse which was generated by a flow-injection system. The response time determining diffusion layer was represented by a cellulose membrane separating the flowing aqueous solution and the ion-sensing stationary organic phase. The shape of the experimentally obtained signal–time responses was found to be in excellent agreement with the theoretical curves calculated by the models derived recently. As expected from the theory, the response in amperometry was found to be faster than in potentiometry. Diffusion coefficients of the species in the membrane were determined by fitting the parameters of the model to the measured curve. The following values were calculated from the amperometric response (in 10^{-10} m^2/s): 7.3 (thiocyanate), 8.6 (iodide) and 1.7 (dodecylsulfate). From the dimensions of the flow system, the width of the exciting concentration pulse was estimated to be less than $0.02d^2/D_M$. It has been proved by numerical simulations, that the shape of the detector signal is almost identical with the impulse-response function itself under this condition.

Key words: Amperometry; Flow system; Potentiometry; Cellulose membrane; Dynamic response; Impulse-response function; Liquid–liquid interface

1. Introduction

Amperometric flow-through electrodes have found numerous applications in the analytical chemistry of liquid samples. Their advantages are the excellent sensitivity and the possibility to adapt the selectivity of the detector to the analytical problem through the applied working potential and permeable selective coatings on the surface of the electrode (see e.g. [1–4]). The classical amperometric or voltammetric detection is based on reduction or oxidation of the species of interest. A new detection principle is based on the electrically induced transfer of ions across the water–oil interface and can be applied to the determination of ions that are not electroactive in the classical (redox) sense [5–7]. However, the

* Corresponding author.

SSDI 0003-2670(94)00158-I

half-wave potential of the ion transfer must be within the window governed by the transfer of the supporting electrolyte ions employed in the two phases. Hydrophilic salts like LiF, Li_2SO_4 and $MgSO_4$ and hydrophobic salts like tetraalkylammonium tetraphenylborates are used in the aqueous and in the organic phase, respectively. The new principle of detection extends the applicability of electrochemical detection to such species which cannot be reduced or oxidised.

The problem of the mechanical stabilisation of the electrified liquid–liquid interface has been solved by the solidification of the organic phase through gel formation with PVC [8] or by the use of arrays of micro liquid–liquid interfaces [9]. The stabilisation of liquid–liquid interfaces by porous membranes has been successfully applied in the construction of liquid-state ion-selective electrodes [10], in the investigation of interfacial phenomena in liquid–liquid extraction processes [11] and in the study of ion transfer reactions at electrified liquid–liquid interfaces [12–17]. Moreover, the membrane-stabilised liquid–liquid interface has been utilised for the voltammetric or amperometric determination of Na^+ and K^+ [14], volatile amines [15] and common inorganic anions like nitrate and chloride [16,17]. Since a hydrophilic membrane, whose pores are filled with the aqueous electrolyte solution, must be crossed by the electroactive ions to come to the ion-sensing membrane/oil phase, both the static and the dynamic response of the detector are expected to be changed. Since the dynamic response can be crucial in flow applications such as flow-injection analysis (FIA) and liquid chromatography (LC), the problem has been treated mathematically [18] using the concept of the impulse-response function [19,20]. The response signal $s(t)$ of a detector to a concentration function $c(t)$ is determined by both $c(t)$ and the impulse-response function $g(t)$ via the convolution integral

$$s(t) = \int_0^t c(\tau) g(t-\tau)\, d\tau \qquad (1)$$

Eq. 1 can be written also in the form $s(t) = c(t) * g(t)$ where the $*$ denotes the convolution procedure. In flow-injection potentiometry with ion-selective electrodes, the carrier stream is often spiked with a constant concentration c^* of the ions to be measured. On account of this background concentration, $\Delta c(t) = c(t) - c^*$ rather than $c(t)$ will be used in the following. The absolute signal $s(t)$ will be also replaced by the signal difference to the baseline $\Delta s(t)$. Assuming the simple case that the electroactive species have to cross only the hydrophilic membrane, i.e., a single aqueous diffusion layer of uniform thickness (adjacent to a planar electrode surface), and the current $i_{lim}(t)$ is monitored, the dynamic response in amperometry is described by the convolution

$$\Delta s_{lim}^{amp}(t) = i_{lim}(t) = \Delta c(t) * g_{lim}^{amp}(t) \qquad (2)$$

$$g_{lim}^{amp}(t) = \frac{zFAD_M^{1/2}}{\pi^{1/2} t^{5/2}} \sum_{n=0}^{\infty} \left\{ \left[(2n+1)^2 \frac{d^2}{2D_M} - t \right] \times \exp\left[-(2n+1)^2 d^2 / 4D_M t \right] \right\} \qquad (3)$$

where $g_{lim}^{amp}(t)$ is the impulse-response function of the amperometric detector working in the range of the limiting diffusion current [18]. D_M, z, F, A, t and d are the diffusion coefficient in the membrane and the charge number of the electroactive species, the Faraday constant, the electrode area, time and the thickness of the hydrophilic membrane, respectively. When the oil phase contains a hydrophobic salt of the ion to be measured, and the potential difference between both liquid phases is measured by means of two reference electrodes and a voltmeter of high impedance, a liquid-state potentiometric detector can be realised [10]. Since one is finally interested to see the dynamic behaviour of the detector in the linear concentration scale rather than in the logarithmic voltage scale, the impulse-response function in potentiometry is related to the concentration in the aqueous membrane immediately at the membrane/oil interface $c_{x=0}(t)$ which is in fact "seen" by the electrode (respectively the difference $\Delta c_{x=0}(t) = c_{x=0}(t) - c^*$). The imaginary potentiometric signal $\Delta s^{pot}(t)$ is then described by the general formula

$$\Delta s^{pot}(t) = \Delta c_{x=0}(t) = \Delta c(t) * g^{pot}(t) \qquad (4)$$

Assuming negligibly small transfer of mass and charge across the electrode surface, the impulse-response function of the potentiometric detector is [18]

$$g^{pot}(t) = \frac{d}{\pi^{1/2} D_M^{1/2} t^{3/2}} \sum_{n=0}^{\infty} \left\{ (-1)^n (2n+1) \times \exp\left[-(2n+1)^2 \frac{d^2}{4 D_M t} \right] \right\} \quad (5)$$

When the peak width of $g(t)$ is much smaller than of $\Delta c(t)$, i.e., the excitation is slow compared with the impulse-response function of the detector, the detector has enough time to reach the steady state. The functions $\Delta s(t)$ and $\Delta c(t)$ are then identical except for a constant factor, the static sensitivity $h(\infty)$. Eq. 1 is then simplified to

$$\Delta s(t) = \Delta c(t) h(\infty) \quad (6)$$

$$h(\infty) = \int_0^{\infty} g(t)\,dt \quad (7)$$

In the other case, the excitation is too fast for the "slow" detector, so that the dynamic response of the signal is determined only by the impulse-response function and Eq. (1) is simplified to

$$\Delta s(t) = \Theta\, g(t) \quad (8)$$

where the "action" of the concentration pulse is characterised by the integral

$$\Theta = \int_0^{\infty} \Delta c(t)\, dt \quad (9)$$

As it can be seen from Eq. 8, the impulse-response function can be observed directly if the δ-function is experimentally approached by the concentration input function $c(t)$. In this work, a simple flow-injection system has been used to apply a short concentration pulse to the detector and to obtain the impulse-response function directly from the detector signal. The response time determining diffusion layer has been represented by a hydrophilic cellulose membrane separating the flowing aqueous solution from the ion-sensing stationary organic phase. The rather great thickness of the membrane (≈ 120 μm) has caused a relatively slow response, so that the requirements concerning the width of the concentration pulse have been easier to fulfil.

A more rigorous approach for the experimental determination of impulse-response functions has been presented by van der Linden and coworkers [21,22]. Impulse-response functions of various components of a flow-injection system such as tubes, mixing coils, T-pieces [21] and various detectors [22] have been measured employing a deconvolution method based on the Fourier transformation. Although the exciting concentration pulse does not need to be negligibly short in comparison with the impulse-response function to be measured, the function $c(t)$ must be known for the deconvolution procedure.

2. Experimental

Hydrophilic membrane filters of cellulose (RC 58, Schleicher and Schuell) were used to stabilise the water–nitrobenzene interface. As reported by the manufacturer, this membranes were fabricated by hydrolysis of foamed membranes of cellulose acetate. The thickness of the swollen membranes was determined to be 120 ± 5 μm (dry 85 μm), and the diameter of the pores was 0.2 μm nominally. The flow-through cell used was already described in a previous paper [17], the geometric area of the interface was 0.07 cm^2. The inner compartment of the flow cell was filled with a 10 mM solution of tetra(dodecyl)ammonium tetrakis(4-chlorophenyl)borate (Fluka) in nitrobenzene (purified as in Ref. [17]). A modular flow-injection system (EVA, Eppendorf-Netheler-Hinz) comprising a peristaltic pump (flow rate: 7.3 ml/min) and a loop injector (8-way valve, loop volume: 15 μl) was used to generate the concentration pulse in the detector (Fig. 1). All tubes were of poly(tetrafluoroethylene), PTFE, and had an inner diameter of 0.5 mm. The distance between the outlet of the injector and the nozzle of the wall-jet cell was 12 cm (around 24 μl). The distance between the nozzle and the membrane was 4 mm. In amperometry, the potential difference across the water–nitrobenzene interface was controlled by the four-electrode potentiostat described previously [23], but no

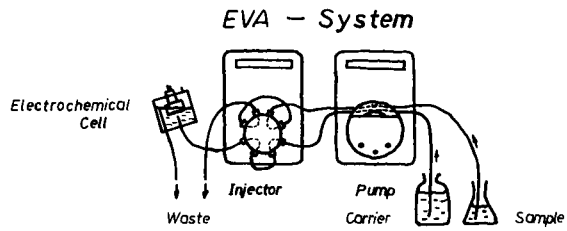

Fig. 1. Scheme of the flow-injection system used.

compensation of the ohmic potential drop was applied because of the low currents. The working potential was −90 mV, being equivalent to a Galvani potential difference of −290 mV, so that all ions of interest were transferred with the limiting diffusion current. For the potentiometric investigations, the same device was used as differential amplifier to measure the potential difference between the reference electrodes in the aqueous and organic phase, respectively. The inner compartment of the cell was then filled with a 1 mM solution of μ-nitrido-bis(triphenylphosporus) thiocyanate in nitrobenzene, prepared by shaking 0.5 ml of a 1 mM solution of μ-nitrido-bis(triphenylphosporus) chloride [24] with 2 ml of a 100 mM solution of KSCN. The detector signals were recorded with a strip chart recorder (endim 621.02, Messapparatewerk Schlotheim) with usually a paper speed of 1 cm/s. All solutions were prepared from redistilled water and analytical-reagent grade chemicals. The measurements were carried out at laboratory temperature (27 ± 2°C).

3. Results and discussion

The excellent agreement between the measured response of the amperometric detector to thiocyanate and iodide on the one hand and the impulse-response calculated by the Eqs. 3 and 8 on the other hand is illustrated in Figs. 2 and 3. The parameters d^2/D_M and Θ of Eqs. 3 and 8, respectively, have been chosen so that the best fit between calculated and measured data is obtained in each case. In the case of dodecylsulfate, a deviation between calculated and measured response at the root of the peak has been found. Since the pattern of this deviation has been observed also when the pure carrier solution was injected itself, it is proved that this phenomenon is only an "injection peak" caused by the breakdown of the flow when the injection valve (without by-pass) is turned. The fact that this effect is found only for dodecylsulfate rather than for thiocyanate and iodide is explained by the higher sensitivity of recording in the former case. Taking this injection peak into consideration, the agreement between the calculated and the measured curve is very good for all three ions investigated. Hence, it can be supposed that Eq. 3 is adequate for the modelling of the amperometric impulse-response function under the chosen conditions of the experiment. It should be mentioned, that the flow rate used in this work is about four times higher than in most FIA systems used in analytical practice. A main drawback of this high flow

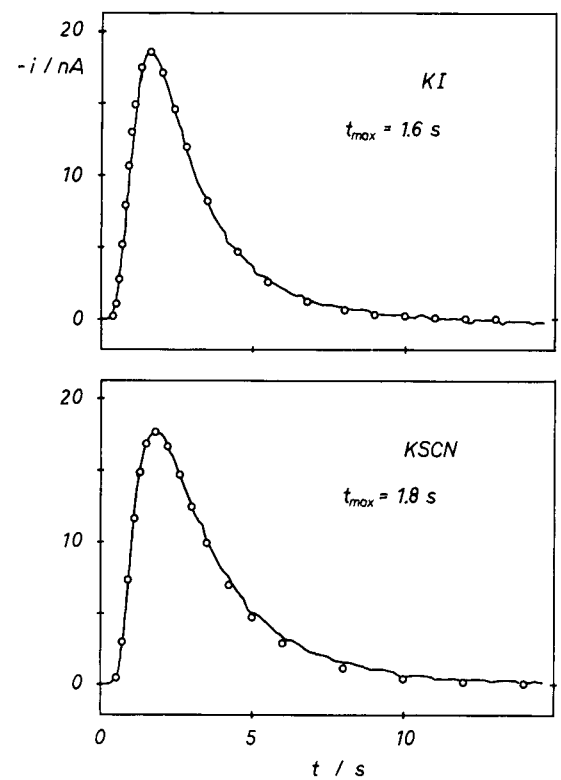

Fig. 2. Measured (solid line) and calculated (Eqs. 3 and 8; circles) amperometric response to a concentration pulse (Δc_{inj} = 0.1 mM) of iodide (upper curve) and thiocyanate (lower curve).

rate is that the dispersion is controlled mainly by the convective transport of the sample accompanied by a rather high random error of the signals. However, the unusual and in some aspects unfavourably high flow rate has been determined by the need to apply a sufficiently short concentration pulse to the detector so that this drawback has to be accepted. When the flow rate is much slower than in our case, or when thinner membranes are used, e.g., to get a faster response, deviations from the simple single-layer model described by Eq. 3 are expected since the hydrodynamic boundary layer cannot be neglected further. The single-layer model must be replaced by a more adequate two-layer model that accounts for the diffusion in both dialysis membrane and hydrodynamic boundary layer. A two-layer model has been treated in terms of the statistical moments using numerical simulations [25], but no impulse-response functions have been reported so far.

From the time constants d^2/D_M for the various ions, diffusion coefficients in the membrane have been calculated and compiled in Table 1. The rather similar response of the detector to iodide and thiocyanate is not surprising, since both ions have almost the same limiting diffusion coefficient in water ($D_M(SCN^-) = 2.05 \times 10^{-9}$ m^2/s, $D_M(I^-) = 1.75 \times 10^{-9}$ m^2/s). The ratio of the diffusion coefficient in the membrane and in water is 0.42 for both iodide and thiocyanate and 0.3 for dodecylsulfate. It can be concluded from these three values, that the diffusion coefficient of common single-charged anions in the membrane is around half or third of the corresponding value for water. For comparison, diffusion coefficients of these ions in dialysis membranes are in the range between 0.7 and 1.2×10^{-10} m^2/s for various membranes [12]. The relatively high diffusion coefficients in the filter membrane are probably due to the foamy, sponge-like structure and the larger diameter of the pores in comparison with the dialysis membranes. There is also a visible difference between the filter membranes and the dialysis membranes. The membrane filters used look opaque, while the dialysis membranes are transparent. Because of the rather heterogeneous structure of the filter membranes, the diffusion coefficients should be considered as apparent diffusion coefficients.

Table 1
Experimental parameters evaluated from the measured impulse response (mean of three measurements)

	t_{max} (s)	d^2/D_M (s)	Peak height	$10^{10} \times D_M$ ($m^2\ s^{-1}$)	Θc_{inj}^{-1} (s)
Amperometry					
Thiocyanate	1.82	19.8	17.4 nA	7.3	0.14
Iodide	1.54	16.7	18.8 nA	8.6	0.11
Dodecylsulfate	7.60	82.6	0.7 nA	1.7	0.10
Potentiometry					
Thiocyanate	2.75	16.2	4.0 mV	8.9	0.16

Values of Θ which, multiplied by the flow rate, is actually the amount of the injected electroactive species have been calculated using Eqs. 3 and 8. After reducing them to Δc_{inj}, the injected concentration minus the background concentration in the carrier stream, they have been compiled in Table 1. Theoretically, a value of $\Theta/\Delta c_{inj} = 0.123$ s is expected in each case. This value is determined by the ratio V_S/v, that is governed by the volume V_S of the injected standard and the volume flow rate v. This ratio can be considered to be the width of the exciting concentration pulse assuming a rectangular shape of the pulse, i.e., the original sample plug in the injector would not be changed by any dispersion while moving to the detector. The scatter of the experimental results around the theoretical value is rather high and probably attributed to the unfavourably high contribution of convection to the dispersion because of the high flow rate, but no significant systematic deviation from the theoretical value can be established. A more sophisticated FIA system or the use of much thicker membranes could probably circumvent the problem of the poor reproducibility.

Potentiometric investigations have been made for thiocyanate only. 15 μl of a standard solution ($c_{inj} = 1$ mM KSCN) have been injected in a carrier stream of $c^* = 0.1$ mM KSCN and 10 mM Na_2SO_4. The thiocyanate has been added to the carrier for three reasons. The first is, that it provides a stable baseline, and all concentration values applied to the electrode are within of the Nernstian range. A slope of $S = 58.6$ mV be-

tween 10^{-4} and 10^{-3} mol/l has been found in steady state measurements, which is rather close to the theoretical 59.6 mV at 27°C. Second, the relative change of the concentration of thiocyanate that the electrode "sees" is small, so that the potential response of the electrode to the concentration is approximately linear rather than logarithmic as usual in potentiometry. Starting from the Nernst equation

$$E - E^* = S \log(c/c^*) \quad (10)$$

the approximated linear relationship

$$c/c^* = \ln(10)(E - E^*)/S \quad (11)$$

can be derived employing the approximation $\ln(1 + x) \approx x$ for small values of x. Here, E^* is the baseline voltage for the carrier solution with the background concentration c^*. Since the peak height of the voltage signal recorded is 4 mV only, it is equivalent to a relative concentration change of $\Delta c/c^* = 0.17$, the relative error due to this linearisation is less than 2% so that the experimentally obtained and in Fig. 4 shown voltage vs. time curves can be taken directly as impulse-response function in terms of concentration as defined here. Finally, the mass transfer due to the charging of the double layer can be neglected for this small voltage change. As for the amperometric measurements, an excellent agreement between measured and calculated data is evident from Fig. 4, that supports the validity of the model under the chosen experimental conditions. The diffusion coefficient of thiocyanate in the membrane obtained from the potentiometric response is somewhat higher than those obtained from amperometry. This rather high deviation cannot be explained by the random error of the measurements that was usually 5%. The amperometric and potentiometric measurements have

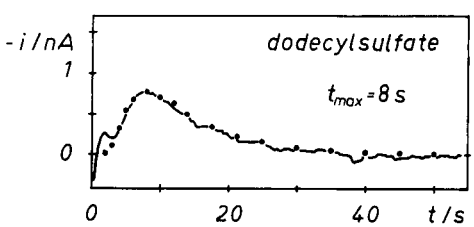

Fig. 3. As in Fig. 2, but for the dodecylsulfate ion.

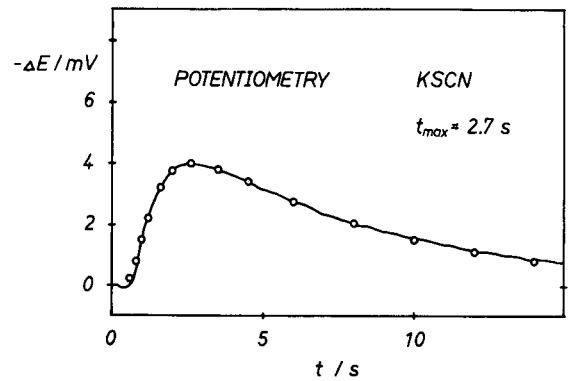

Fig. 4. Measured (solid line) and calculated (Eqs. 5, 8 and 11; circles) potentiometric response to a concentration pulse of thiocyanate ($\Delta c_{inj} = 0.09$ mM).

been made using the same membrane, but at different days, so that slight changes of the thickness of and the diffusion coefficients in the membrane by aging must be assumed.

Eq. 8 is employed for the direct determination of impulse-response functions and is based on the assumption that the width of the exciting concentration pulse is much smaller than those of the impulse-response function. It appears to be important to know how short or how long the exciting concentration pulse can or must be in comparison with the time constant d^2/D_M without noticeable changes in the response signal. Furthermore, it would be interesting to see how the response changes while increase the pulse width. Numerical simulations have been made to roughly estimate the influence of the pulse width on shape and parameters of the amperometric signal. The rectangular pulse shape has been chosen for this simulations because it is simple and the meaning of the term "pulse width" is clear. The detector response has been calculated by convoluting the impulse-response function with rectangular pulse functions of different width. The product of c_{inj} and the pulse width t_{pulse} has been kept constant, so that all pulses have the same "action" Θ. The magnitude of the signals is then approximately the same in each case. In other words, the time of contact between the sample and the membrane is varied while keeping the injected amount of the electroactive species cor

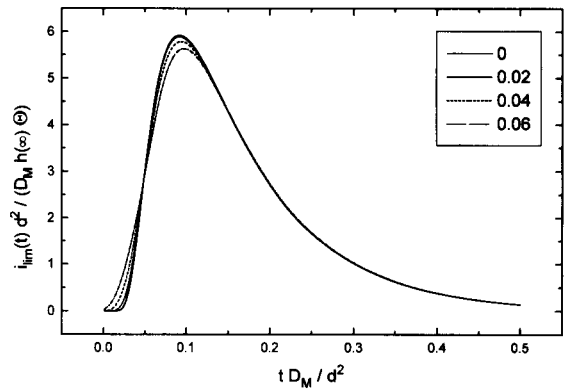

Fig. 5. Simulated response (by Eqs. 2 and 3) of an amperometric detector to rectangular concentration pulses of the same midpoint ($t = 0$) and concentration–time product Θ, but having different pulse widths (given in the legend).

stant. The results of the convolution are shown in Fig. 5 for $0 < t < 0.5d^2/D_M$. To virtually fix the center of the pulses at $t = 0$, the resulting functions have been shifted to the negative direction by $t_{pulse}/2$. It becomes evident from Fig. 5, that both shape and parameters of the response function remain nearly constant as long the peak width is around $0.02d^2/D_M$ or smaller. When the pulse width is increased further, the rising part of the signal becomes less and less steep and the peak hight is decreased more and more. The peak maximum is shifted slightly to higher values of the time scale. For a pulse width of $0.06d^2/D_M$, the peak height is decreased by 4%, and the rising part of the curve is changed significantly. Even higher pulse widths have not been considered since they are not relevant for the direct determination of impulse-response functions.

In the experiments described above, the time constant of the membrane was $d^2/D_M = 16.7$ s for the iodide ion as the most mobile ion investigated in this work. If the injected solution would move like a plug without any dispersion from the injector to the detector, the width of the pulse were $V_S/v = 0.123$ s. From the geometry of the flow system, the dispersion of the sample has roughly been estimated to be in the order of two. Assuming in a first approximation, that the pulse shape is similar to a rectangle still, but of half height and double width, the mean width of the peak in the detector would be around 0.25 s or $0.015\ d^2/D_M$. Comparing these numbers with the results of the simulations, the peak width should be $\leq 0.02d^2/D_M = 0.33$ s for the iodide ion. Although the dispersion in the flow system was only roughly estimated, it can be stated that the concentration pulses used fulfil the requirements concerning the peak width, and the measured signals represent the impulse-response functions of the detectors really without noticeable deviations. This is also proved by the excellent agreement between the measured response and the calculated impulse-response functions.

References

[1] G. Sittampalam and G.S. Wilson, Anal. Chem., 55 (1983) 1608.
[2] J. Wang and L.D. Hutchins, Anal. Chem., 57 (1985) 1536.
[3] J. Wang, P. Tuzhi and T. Golden, Anal. Chim. Acta, 194 (1987) 129.
[4] J. Wang, T. Golden and P. Tutzhi, Anal. Chem., 59 (1987) 740.
[5] E. Wang and Z. Sun, Trends Anal. Chem., 7 (1988) 99.
[6] J. Koryta, Ion-Selective Electrode Rev., 5 (1983) 131.
[7] M. Senda, T. Kakiuchi and T. Osakai, Electrochim. Acta, 36 (1991) 253.
[8] T. Osakai, T. Kakutani and M. Senda, Bunseki Kagaku, 33 (1984) E371.
[9] F. Silva and C.M. Pereira, Charge Transfer Processes at Liquid/Liquid Interfaces, Symposium of the 182nd Meeting of the Electrochem. Soc., Toronto, Oct. 11–16, 1992
[10] J. Ross, Science, 156 (1967) 1378.
[11] W.J. Albery, R.A. Choudhery and P.R. Fisk, Faraday Discuss. Chem. Soc., 77 (1984) 53.
[12] B. Hundhammer, S.K. Dhawan, A. Bekele and H.-J. Seidlitz, J. Electroanal. Chem., 217 (1987) 253.
[13] S. Sawada, T. Osakai and M. Senda, Bunseki Kagaku, 39 (1990) 539.
[14] Y. Yamamoto, T. Osakai and M. Senda, Bunseki Kagaku, 39 (1990) 655.
[15] Y. Yamamoto, T. Nuno, T. Osakai and M. Senda, Bunseki Kagaku, 38 (1989) 589.
[16] B. Hundhammer and S. Wilke, J. Electroanal. Chem., 266 (1989) 133.
[17] S. Wilke, H. Franzke and H. Müller, Anal. Chim. Acta, 268 (1992) 285.
[18] S. Wilke and R. Picht, Anal. Chim. Acta, 291 (1994) 41–52.
[19] J.C. Sternberg, in J.C. Giddings and R.A. Keller (Eds.), Advances in Chromatography, Vol. 2, Marcel Dekker, New York, 1966, p. 205.
[20] H. Poppe, Anal. Chim. Acta, 114 (1980) 59.

[21] I.C. van Nugteren-Osinga, M. Bos and W.E. van der Linden, Anal. Chim. Acta, 214 (1988) 77.
[22] I.C. van Nugteren-Osinga, E. Hoogendam, M. Bos and W.E. van der Linden, Anal. Chim. Acta, 239 (1990) 245.
[23] S. Wilke, J. Electroanal. Chem., 301 (1991) 67.
[24] J.K. Ruff and W.J. Schlientz, in G.W. Parshall (Ed.), Inorganic Synthesis, Vol. 15, McGraw-Hill, New York, 1974, p. 84.
[25] W.Th. Kok, A.J. Tüdös and H. Poppe, Anal. Chim. Acta, 228 (1990) 39.

ELSEVIER

Analytica Chimica Acta 295 (1994) 173–179

ANALYTICA CHIMICA ACTA

Separation of enantiomers by microcolumn liquid chromatography with methylated β-cyclodextrin as mobile phase additive

Rongzong Hu [a], Toyohide Takeuchi *[,b], Ji-Ye Jin [b], Tomoo Miwa [b]

[a] *Department of Chemistry, Xiamen University, Xiamen, Fujian, China*
[b] *Faculty of Engineering, Gifu University, 1-1 Yanagido, 501-11 Gifu, Japan*

Received 23rd November 1993; revised manuscript received 30th March 1994

Abstract

Enantiomers can be separated by microcolumn liquid chromatography with methylated β-cyclodextrin (β-CD) as a mobile phase additive. Effects of the mobile phase composition on the retention behaviour of the analytes were examined. The separation factor achieved with heptakis(2,3,6-tri-*O*-methyl)-β-CD as the chiral selector for 1,1′-binaphthyl-2,2′-diyl hydrogenphosphate enantiomers was up to 3. Heptakis(2,6-di-*O*-methyl)-β-CD achieved poor enantioselectivities for the enantiomers examined.

Key words: Liquid chromatography; Cyclodextrins; Enantiomer separation

1. Introduction

Several kinds of cyclodextrins (CDs) have been found which differ in the number of glucose units. Native and functionalized CD-bonded stationary phases have been extensively employed for chiral separations in liquid chromatography (LC) [1]. Among the CD-bonded stationary phases, β-CD and its derivatives have been the most widely used as the chiral stationary phase in LC.

The use of CD as a mobile phase additive in LC is another approach to establishing chiral resolution. However, there are a few disadvantages when CD is used as the mobile phase additive, including low solubility of CD in aqueous/organic solutions, prohibitive cost and poor efficiency. Miniaturization of separation columns facilitates the use of such expensive CDs as the mobile phase additive, e.g., columns of 0.35–1.0 mm i.d. allow the separation of analytes in a reasonable time at flow-rates of 3–30 μl min^{-1} [2,3].

Although the solubility of the CD can be improved by increasing the pH of the mobile phase or adding urea to the mobile phase [4], the conditions adopted in turn restrict the applicability.

The solubility of CDs can also be improved by derivatization, e.g., by methylation. There are a

* Corresponding author.

SSDI 0003-2670(94)00161-E

few derivatized β-CDs commercially available such as heptakis(2,6-di-*O*-methyl)-β-CD (DM-β-CD) and heptakis(2,3,6-tri-*O*-methyl)-β-CD (TM-β-CD), and these reagents have been employed as mobile phase additives for the enantiomeric separation of barbiturates in LC [3,5,6]. These methylated β-CDs adsorb on hydrophobic stationary phases, which makes the optimization of the separation conditions difficult.

Methylated CDs have been also employed as chiral selectors in capillary zone electrophoresis (CZE) [7], in which various racemic drugs were resolved. CZE provides various advantages over regular LC, including rapid and efficient separations and the feasibility of using expensive or commercially unavailable chiral selectors owing to the small volume of the CZE system. The latter advantage is also shared by microcolumn LC. One of disadvantages of CZE is that the chemical and physical properties of the migration tube wall greatly affect the separation and reproducibility.

This paper describes the feasibility of using methylated β-CDs as mobile phase additives for the separation of enantiomers in microcolumn LC and examines the mobile phase conditions for the optimization of the enantiomeric separation. Microcolumn LC facilitates the detailed examination of a wide range of mobile phase conditions.

2. Experimental

2.1. Apparatus

The microcolumn liquid chromatograph was assembled from a microfeeder (Azumadenki Kogyo, Tokyo) equipped with an MS GAN050 gastight syringe (0.5 ml) (Ito, Fuji) as a pump, an ML-522 microvalve injector with an injection volume of 20 nl (Jasco, Tokyo), a 150 × 0.35 mm i.d. micropacked separation column, a Uvidec-100V UV absorbance detector (Jasco) with a laboratory-made flow cell, and a Chromatopac C-R4A data processor (Shimadzu, Kyoto). The detector was operated at 220 nm. The separation column was made from fused-silica tubing (GL Science, Tokyo). The packing material employed was Develosil ODS-5 (5 μm) (Nomura Chemical, Seto). The separation column was prepared by the slurry-packing technique reported previously [8] and dipped in a water-bath in operation to mini-

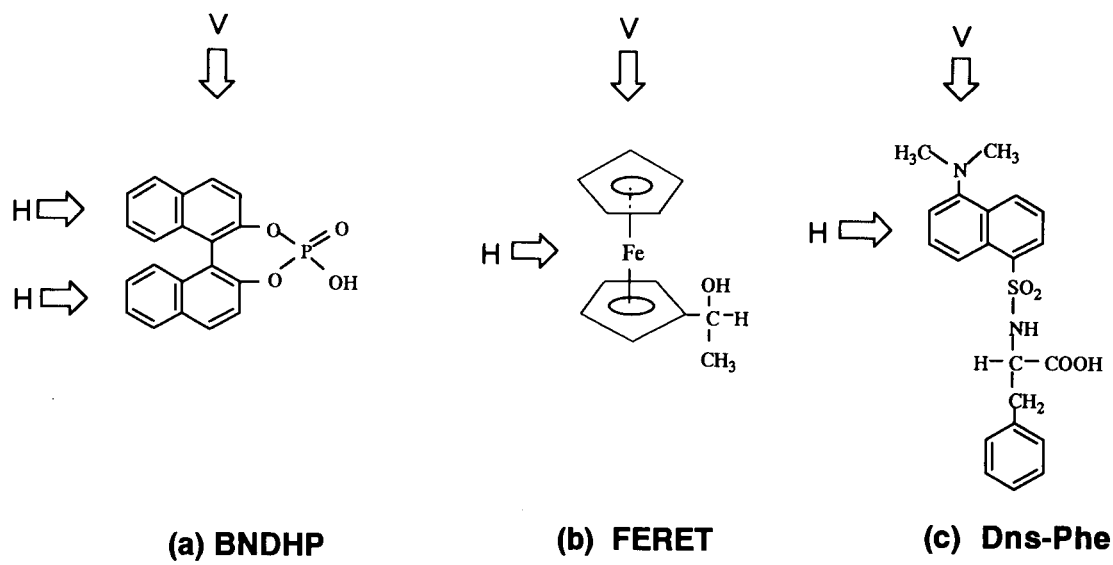

Fig. 1. Structures of the enantiomers examined. V, vertical direction; H, horizontal direction.

mize the variations of the column temperature. The separation was carried out at room temperature (ca. 25–30°C).

2.2. Reagents

The reagents employed were of guaranteed-reagent grade from Nacalai Tesque (Kyoto), unless indicated otherwise. The reagents were employed without any further treatment. Purified water was prepared from distilled water using a Milli-Q Plus system (Millipore, Molsheim, France). Racemic 1-ferrocenylethanol (FERET), (*R*)-(−)-1,1′-binaphthyl-2,2′-diyl hydrogenphosphate [(*R*)-(−)-BNDHP] and (*S*)-(+)-BNDHP were of extra-pure grade from Tokyo Chemical Industry (Tokyo). Non-derivatized (native) β- and γ-CD were obtained from Nacalai Tesque and DM-β-CD and TM-β-CD from Sigma (St. Louis, MO). Racemic dansylphenylalanine (Dns-Phe) and Dns-L-Phe were purchased from Sigma. The (+)- and (−)-FERET enantiomers were isolated by using a 250 × 4.6 mm i.d. Develosil ODS-5 column, and the isomers were assigned as reported previously [9]. The structures of the enantiomers considered in this paper are illustrated in Fig. 1.

3. Results and discussion

3.1. Effects of CD concentration

BNDHP enantiomers

It has been reported that the elution order of barbiturate enantiomers alters with variation in the DM-β-CD concentration [3], because DM-β-CD adsorb on the hydrophobic stationary phase. The resolution of the enantiomers in dilute DM-β-CD solution was governed by the process of inclusion complexation of the analytes with DM-β-CD adsorbed on the surface of the stationary phase, whereas at higher concentrations of DM-β-CD it was governed mainly by inclusion complexation of the analytes with DM-β-CD in the mobile phase [3].

The effects of TM-β-CD concentration on the retention behaviour of BNDHP enantiomers were examined by using aqueous acetonitrile solution (15%, v/v) as the mobile phase. When three phases are involved in the process of retention, a linear relationship between the concentration of CD and the reciprocal of the capacity factor (k') should be observed, as described by the following equation [10]:

$$1/k' = 1/k'_0 + [(CD)_m]/K_D k'_0 \quad (1)$$

where k'_0 is the capacity factor of a solute in the absence of CD in the mobile phase, $[(CD)_m]$ is the concentration of CD in the mobile phase and K_D is the CD–solute dissociation constant. As methylated CDs adsorb strongly on hydrophobic stationary phases [3,5,6], four phases exist, i.e., the original hydrophobic stationary phase (L_s), CD molecules adsorbed on the stationary phase $[(CD)_s]$, CD molecules in the mobile phase $[(CD)_m]$ and bulk solvent. In the same manner as in the above three-phase model, when four phases are involved in the process of retention, the capacity factor of the analyte solute is derived in the usual way:

$$k' = \frac{V_L[AL_s] + V_{(CD)s}[(A\text{–}CD)_s]}{V_m[A_m] + V_{(CD)m}[(A\text{–}CD)_m]} \quad (2)$$

where V_L is the volume of the hydrophobic stationary phase, $V_{(CD)_s}$ is the volume of CD adsorbed on the hydrophobic stationary phase, $V_{(CD)_m}$ is the volume of CD existing in the mobile phase, V_m is the volume of the bulk solvent, $(A\text{–}CD)_s$ and $(A\text{–}CD)_m$ represent the analyte associated with CD in the stationary and the mobile phases, AL_s represents the analyte partitioning in the hydrophobic stationary phase and A_m represents the analyte existing in the bulk solvent. The equilibrium equations relating to the partitioning of the analyte are as follows:

$$A_m + L_s \overset{K_1}{\rightleftharpoons} AL_s \quad (3)$$

$$A_m + (CD)_m \overset{K_2}{\rightleftharpoons} (A\text{–}CD)_m \quad (4)$$

$$A_m + (CD)_s \overset{K_3}{\rightleftharpoons} (A\text{–}CD)_s \quad (5)$$

The combination of Eqs. 2–5 yields the following expression for the capacity factor:

$$k' = \frac{K_1 V_L[L_s] + K_3 V_{(CD)_s}[(CD)_s]}{V_m + K_2 V_{(CD)m}[(CD)_m]} \quad (6)$$

Eq. 6 indicates that linear relationships between the reciprocal of the capacity factor and the concentration of CD in the mobile phase, $[(CD)_m]$, should be observed in the following cases: when $[(CD)_s]$ is independent of $[(CD)_m]$; when the amount of CD adsorbed on the hydrophobic stationary phase is much smaller than that of the hydrophobic stationary phase; and when K_1 is much larger than K_3.

Fig. 2 illustrates the reciprocal of the capacity factor and the separation factor of the BNDHP enantiomers as a function of TM-β-CD concentration, with ODS as the stationary phase. The capacity factor was calculated by assuming that nitrate is not retained on the stationary phase. It was found that the *S*-(+)-isomer eluted before the *R*-(−)-isomer and that the capacity factor decreased with increasing TM-β-CD concentration in the mobile phase. The relationships between the reciprocal of the capacity factor and the TM-β-CD concentration were not linear. The result indicates that the condition in Fig. 2 is not valid for any of the above three cases.

On the other hand, the separation factor varied in a complex way with the TM-β-CD concentration, and the maximum separation factor was obtained at a concentration of ca. 25 mM.

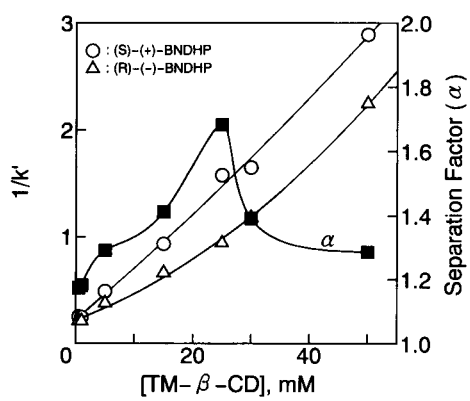

Fig. 2. Retention behaviour of BNDHP enantiomers as a function of TM-β-CD concentration in the mobile phase. Column, Develosil ODS-5 (150×0.35 mm i.d.); mobile phase, aqueous acetonitrile solution (15%, v/v) containing TM-β-CD; flow-rate, 2.8 μl min^{-1}; sample volume, 20 nl; wavelength of UV detection, 220 nm, ○ = $1/k'$ of (*S*)-(+)-BNDHP; △ = $1/k'$ of (*R*)-(−)-BNDHP; ■ = α of both analytes.

When aqueous acetonitrile solution (15%, v/v) containing 12 mM native β-CD was employed as the mobile phase, (*S*)-(+)-BNDHP eluted before the *R*-(−)-isomer. Under this condition, it is expected that native β-CD molecules do not adsorb on the stationary phase, i.e., native β-CD molecules in the mobile phase recognize the chirality of the analytes. The separation factor achieved with native β-CD was ca. 1.1, which was much smaller than that observed for TM-β-CD. Further, it should be noted that the peak shapes were poor for TM-β-CD and native β-CD, especially for native β-CD. The cavity size of β-CD is small so that only one naphthyl group of BNDHP can be included in the horizontal direction (see Fig. 1). It is presumed, therefore, that there could exist BNDHP molecules associated with one or two β-CD molecules, leading to poor peak shapes owing to the existence of different species.

On the other hand, when aqueous acetonitrile solution (15%, v/v) containing 12 mM native γ-CD was employed as the mobile phase, (*R*)-(−)-BNDHP eluted before the (*S*)-(+)-isomer. The elution order observed for native γ-CD was opposite to that observed for native β-CD and TM-β-CD. The peak shapes observed for γ-CD were good and the separation factor was 1.12. It is expected that the cavity size of native γ-CD allows the inclusion of BNDHP molecules in the vertical direction (see Fig. 1).

As native β- and γ-CD are hydrophilic and are not retained on the stationary phase under the usual conditions, it can be concluded that the chirality is recognized by CD molecules present in the mobile phase. The opposite elution order observed between native β- and γ-CD may be caused by different orientations of BNDHP in the CD cavities. The poor peak shapes observed for native β-CD may be caused by the existence of BNDHP molecules associated with one and two CD molecules.

Considering these experimental results, it can be presumed that the abnormally large separation factors observed for TM-β-CD are attributable to the situation that BNDHP forms an inclusion complex with two TM-β-CD molecules and methylation of β-CD may stabilize such an inclusion complex in comparison with native β-CD.

FERET enantiomers

For FERET enantiomers, the effects of the TM-β-CD concentration on the retention behaviour were examined by using aqueous acetonitrile solution (20%, v/v) as the mobile phase. At concentrations of TM-β-CD in the mobile phase from 25 to 50 mM, the capacity factor decreased with increasing TM-β-CD concentration, whereas the separation factor remained constant in the regions examined, viz., 1.2, as shown in Fig. 3. The elution order of the FERET enantiomers was the same as that observed when native β-CD was employed as the mobile phase additive, and the separation factor achieved with native β-CD was ca. 1.1 [9].

On the other hand, when native γ-CD was used as a chiral selector, no resolution of FERET enantiomers was achieved. This can also be explained by the different configuration of inclusion complexes. Native β-CD and TM-β-CD include FERET in the vertical direction as shown in Fig. 1, whereas native γ-CD includes it in horizontal direction. Such a different configuration has been confirmed for a crystalline state in the literature [11]. These results lead to the conclusion that CD molecules present in the mobile phase dominantly contribute to the resolution of the FERET enantiomers for both native β-CD and TM-β-CD as the chiral selector.

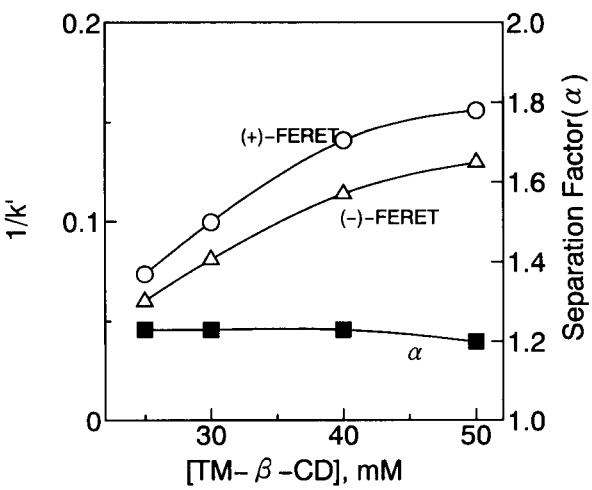

Fig. 3. Retention behaviour of FERET enantiomers as a function of TM-β-CD concentration in the mobile phase. Mobile phase, aqueous acetonitrile solution (20%, v/v) containing TM-β-CD; other operating conditions as in Fig. 2. ○ = $1/k'$ of (+)-FERET; △ = $1/k'$ of (−)-FERET; ■ = α of both analytes.

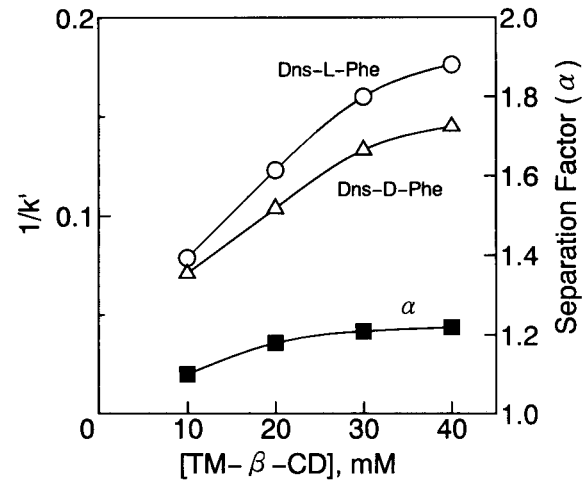

Fig. 4. Retention behaviour of Dns-Phe enantiomers as a function of TM-β-CD concentration in the mobile phase. Mobile phase, aqueous acetonitrile solution (10%, v/v) containing TM-β-CD and 40 mM ammonium acetate; other operating conditions as in Fig. 2. ○ = $1/k'$ of Dns-L-Phe; △ = $1/k'$ of Dns-D-Phe; ■ = α of both analytes.

Dns-Phe enantiomers

For Dns-Phe, a different retention behaviour was observed, as shown in Fig. 4. When 10–40 mM TM-β-CD dissolved in aqueous acetonitrile solution (10%, v/v) was used as the mobile phase, the L-isomer eluted first. It should be noted that the elution order of the Dns-Phe enantiomers was opposite to that obtained with native β- and γ-CD as the mobile phase chiral selector. This result indicates that TM-β-CD adsorbed on the stationary phase dominantly contributes to the chiral recognition of the analytes. It is seen in Fig. 4 that the reciprocal of the capacity factor increases with increasing TM-β-CD concentration, and the separation factor also increases with increasing TM-β-CD concentration. Again, the former relationship was not linear.

Table 1 compares the elution orders of the enantiomers examined in this work for three different chiral selectors.

Table 1
Comparison of the elution order of the enantiomers examined

CD	Isomer eluted first		
	BNDHP	FERET	Dns-Phe
TM-β-CD	(*S*)-(+)-	(+)-	L-
Native β-CD	(*S*)-(+)- [a]	(+)-	D-
Native γ-CD	(*R*)-(−)-	NR [b]	D-

For eluent, see text. [a] Poor peak shape. [b] Not resolved.

3.2. Effects of acetonitrile concentration

The effects of the acetonitrile concentration on the retention behaviour were examined for the BNDHP, FERET and Dns-Phe enantiomers. For the BNDHP and Dns-Phe enantiomers the TM-β-CD concentration was kept at 30 mM, whereas for the FERET enantiomers it was kept at 25 mM. Fig. 5 illustrates the separation factor as a function of acetonitrile concentration. The elution order did not change for the enantiomers in the regions examined in Fig. 5. The separation factor increased with decreasing acetonitrile concentration for BNDHP and FERET, whereas a different relationship was observed for Dns-Phe. It should be noted that at 3% (v/v) acetonitrile the separation factor achieved for BNDHP was ca. 3, which was much larger than that achieved for

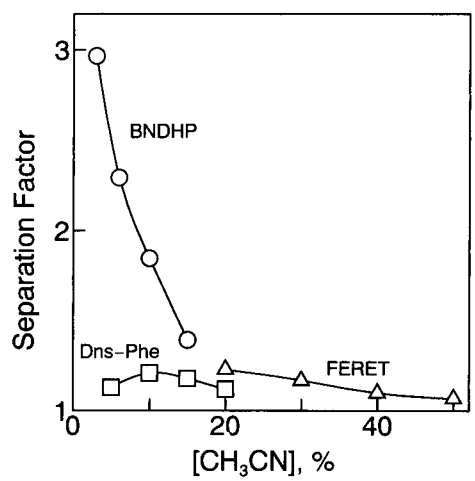

Fig. 5. Effect of acetonitrile concentration on the separation factor. Mobile phases, acetonitrile–water mixtures containing 30 mM TM-β-CD for BNDHP and Dns-Phe or 25 mM TM-β-CD for FERET; analytes, (○) BNDHP, (△) FERET and (□) Dns-Phe; column and flow-rate as in Fig. 2.

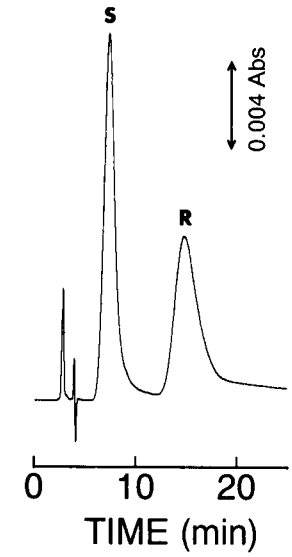

Fig. 6. Separation of BNDHP enantiomers with TM-β-CD as the mobile phase additive. Mobile phase, aqueous acetonitrile solution (3%, v/v) containing 30 mM TM-β-CD; analytes, 0.025% (w/v) of each isomer; other operating conditions as in Fig. 2.

FERET and Dns-Phe. Such a high separation factor for the BNDHP enantiomers cannot be achieved with native CDs as the chiral selector.

In addition, almost linear relationships between the logarithm of the capacity factor of the analytes and the acetonitrile concentration were observed for BNDHP and FERET, whereas the relationship was not linear for Dns-Phe, possibly because ODS dominantly contributes to the retention of the analytes in the former instance, whereas TM-β-CD adsorbed on the ODS dominantly contributes to the retention in the latter. The amount of TM-β-CD can be varied by changing the acetonitrile concentration, which affects the retention of the analytes.

3.3. Separation of enantiomers

Fig. 6 demonstrates the enantiomeric separation of BNDHP using 30 mM TM-β-CD dissolved in aqueous acetonitrile solution (3%, v/v) as the mobile phase. It should be noted again that the elution order was the same as that observed when native β-CD was used as the mobile phase additive.

The enantiomeric separation of FERET is demonstrated in Fig. 7. Baseline separation of the enantiomers was achieved in 50 min. The elution order was the same as that observed when native β-CD was used as the mobile phase additive [9].

Another example of the enantiomeric separation is demonstrated in Fig. 8, in which enantiomers of Dns-Phe were resolved and the separation factor of the analytes achieved was 1.18. Under the conditions in Fig. 8 the elution order was opposite to that observed when native β-CD was employed as the mobile phase additive [2].

Finally, it should be noted that the use of DM-β-CD as the mobile phase additive failed to separate BNDHP and FERET enantiomers, whereas Dns-Phe enantiomers could be partially separated by using DM-β-CD as the mobile phase additive. In the latter instance, the elution order of the enantiomers was the same as that obtained by using TM-β-CD, and the separation factor was 1.10 when aqueous acetonitrile solution (10%, v/v) containing 40 mM DM-β-CD was used as the mobile phase.

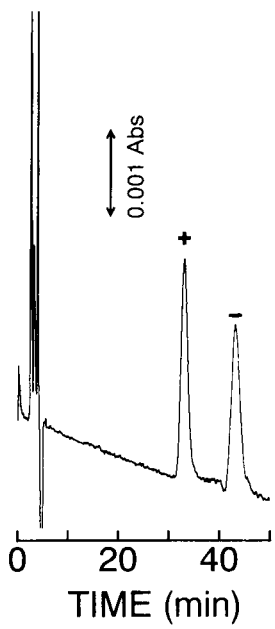

Fig. 7. Separation of FERET enantiomers with TM-β-CD as the mobile phase additive. Mobile phase, aqueous acetonitrile solution (20%, v/v) containing 25 mM TM-β-CD; analytes, 0.05% (w/v) of each isomer; other operating conditions as in Fig. 2.

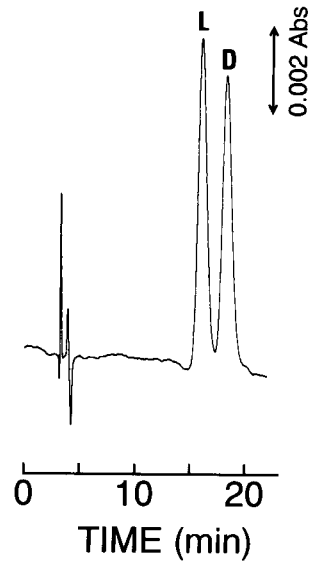

Fig. 8. Separation of Dns-Phe enantiomers with TM-β-CD as the mobile phase additive. Mobile phase, aqueous acetonitrile solution (15%, v/v) containing 30 mM TM-β-CD and 40 mM ammonium acetate; analytes, 0.1% (w/v) of each isomer; other operating conditions as in Fig. 2.

References

[1] R.A. Menges and D.W. Armstrong, in S. Ahuja (Ed.), Chiral Separations by Liquid Chromatography (ACS Symposium Series, No. 471), American Chemical Society, Washington, DC, 1991, Ch. 4, p. 67.
[2] T. Takeuchi, H. Asai and D. Ishii, J. Chromatogr., 357 (1986) 409.
[3] J. Zukowski, D. Sybilska and J. Bojarski, J. Chromatogr., 364 (1986) 225.
[4] D.Y. Pharr, A.S. Fu, T.K. Smith and W.L. Hinze, Anal. Chem., 61 (1989) 275.
[5] J. Zukowski, D. Sybilska, J. Bojarski and J. Szejtli, J. Chromatogr., 436 (1988) 381.
[6] J. Zukowski and R. Nowakowski, J. Liq. Chromatogr., 12 (1989) 1545.
[7] M.W.F. Nielen, Anal. Chem., 65 (1993) 885.
[8] T. Takeuchi and D. Ishii, J. Chromatogr., 213 (1981) 25.
[9] T. Takeuchi and T. Miwa, J. Chromatogr., 666 (1994) 439.
[10] K. Fujimura, T. Ueda, M. Kitagawa, H. Takayanagi and T. Ando, Anal. Chem., 58 (1986) 2668.
[11] A. Harada, Y. Hu, S. Yamamoto and S. Takahashi, J.

ELSEVIER

Analytica Chimica Acta 295 (1994) 181–186

ANALYTICA CHIMICA ACTA

Anion detection in capillary electrophoresis with ion-selective microelectrodes

P.C. Hauser *, N.D. Renner, A.P.C. Hong

The University of Auckland, Department of Chemistry, Private Bag 92019, Auckland, New Zealand

Received 24th November 1993; revised manuscript received 29th March 1994

Abstract

The use of potentiometric microelectrodes as detectors for anions in capillary electrophoresis is demonstrated. The detector electrode with a tip diameter of 3 μm is inserted into the end of a fused silica separation capillary with an internal diameter of 25 μm. The separation and detection of Cl^-, NO_3^-, NO_2^-, Br^-, I^- and ClO_4^- down to concentrations of 10 $\mu g\ kg^{-1}$ is reported.

Key words: Electrophoresis; Ion selective electrodes; Microelectrodes

1. Introduction

The use of capillary electrophoresis for the separation of large biologically relevant molecules has received much attention in recent years. The method also provides an attractive alternative to the prevalent ion chromatographic determination of small inorganic anions [1–6]. Capillary electrophoresis instrumentation is simpler, the method shows fewer matrix effects, a higher number of theoretical plates and a separation sequence different to the one commonly obtained in ion chromatography [1–6]. However, as is true for capillary electrophoresis for any analytes, detection of the separated species is difficult because the technique requires capillaries of small diameters to allow high resolution and efficient cooling of the column. For the presently commercially available capillary electrophoresis systems 50–100 μm i.d. capillaries are used and detection is generally carried out by the method of indirect UV absorption. This procedure allows measurements only over a limited dynamic range. Optical means of detection are also not well suited for capillaries narrower than 50 μm because of the reduced pathlengths. Conductivity detection has also been reported [7,8], but here again a property of the bulk of the solution is sampled and detection is therefore affected by the available volume. Electrochemical detectors in contrast require only minute volumes since they rely on surface reactions. The use of amperometric microelectrodes inserted as on-column detectors into capillaries with diameters as small as 2 μm has been reported [9]. These electrochemical detectors however require that the detected species are electroactive. This is not necessary for ion-selective microelectrodes, which in principle respond to all species with the correct charge. The

* Corresponding author.

SSDI 0003-2670(94)00162-F

logarithmic response obtained with potentiometric sensors should also allow detection over a wide dynamic range. The use of ion-selective microelectrodes for the detection of inorganic cations in electrophoresis with capillaries of 25 and 10 μm internal diameter has been reported by Simon and co-workers [10–12]. The detection of anions is described here.

2. Experimental

2.1. Microelectrodes

Glass micropipettes of approx. 3 μm tip diameter were drawn from borosilicate glass tubes (GC150T-10, o.d. 1.5 mm, i.d. 1.17 mm, Clark Electromedical Instruments, Pangbourne, UK) using a two-stage vertical puller (Narishige PP-83). The micropipettes were silanized and filled according to established procedures [12]. The filling solutions were identical to the electrolyte used in the electrophoresis with the exception that 1 mM potassium chloride was also included. This salt was included in order to satisfy the internal reference electrodes which consisted of a chlorinated silver wire (0.5 mm diameter, immersed in 3% sodium hypochlorite solution overnight). The TDMAC-membrane consisted of a solution of 3% of the ionophore (tridodecylmethylammonium chloride, Fluka) in *o*-nitrophenyl octyl ether (Fluka). The manganese porphin cocktail was prepared according to Kondo et al. [13] and consisted of 5% MnTPP (5,10,15,20-tetraphenyl-21*H*,23*H*-porphin manganese(III) chloride, Aldrich), 1% tetradodecylammonium tetrakis(*p*-chlorophenyl)-borate (Fluka), 4% 1-decanol (BDH) and 90% *o*-nitrophenyl octyl ether. New microelectrodes were usually prepared every day, but it was found that the lifetime can be longer if they are stored in the electrolyte overnight. A microelectrode with the tip broken to approx. 50 μm diameter served as reference electrode.

2.2. Electrolyte solutions

These were made up from analytical grade reagents obtained from a variety of suppliers.

2.3. Determination of selectivity coefficients

The selectivity coefficients (K^{pot}) were determined by using the single solution method (SSM) with 0.1 M solutions of the respective anion as the sodium or potassium salt. The values were calculated according to the Nicolsky formalism from the respective anion activities.

2.4. Apparatus

The high voltage power supply was a Model 230-30R from Bertran (Hicksville, NY). The high voltage end of the separation capillary was placed together with a platinum electrode (−30 kV) in a container with the electrolyte. This end of the capillary was contained in a perspex box fitted with a micro-switch to interrupt the mains to the high voltage power supply as a safeguard. The separation capillaries were uncoated fused silica capillaries with 25 μm i.d. obtained from Scientific Glass Engineering (SGE), Melbourne. The detection end of the capillary was placed in a low angle into a shallow vessel of the electrolyte solution. A platinum wire of 0.3 mm diameter positioned 270–280 μm from the end of the capillary served as the counter electrode for the applied high voltage. This alignment was carried out under a microscope (Olympus, Model E, magnification 150 ×). A view of the arrangement at the detector end of the capillary is given in Fig. 1. In order to avoid extra-column band broadening, which can be very severe in the light of the narrow diameters used, it is beneficial to carry out on-column detection by inserting the detector directly into the end of the capillary. This however implies that the detector is located ahead of the grounding wire and is exposed to the electrophoretic field (e.g., 30 mV μm^{-1} within a capillary of 1 m length and an applied potential of 30000 V). The electrophoretic field therefore superimposes a voltage on the membrane potential of the microelectrode and the measured value becomes sensitive to slight changes in the alignment and any turbulence in the electrolyte. It has been demonstrated by Nann and Simon [11] for potentiometric detection and by Sloss and Ewing [9] for amperometric detection, that the electrical

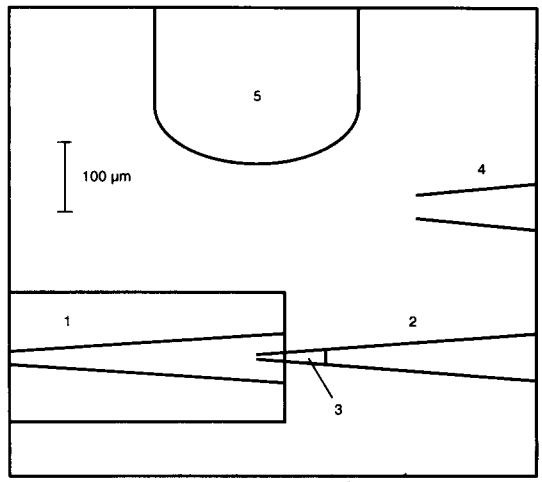

Fig. 1. View of the arrangement at the detector end of the capillary as seen under the microscope: (1) capillary end showing the conical etch, (2) ion-selective microelectrode, (3) membrane, (4) reference electrode, (5) counter electrode for the application of the electrophoretic voltage.

field at the end of a capillary can be significantly reduced by conical etching and a good compromise in terms of bandbroadening and electrical noise can be obtained. This procedure was adopted and the end of the capillary etched in 40% HF solution for 40 min to give a conical opening of 75 μm width at the end and approx. 500 μm depth. The tip of the ion-selective microelectrode was inserted about 40 μm. The microscope stage was employed as a micromanipulator to facilitate this alignment. The end of the separation capillary was mechanically fixed and the microelectrode mounted on the microscope stage which allowed movement in the three dimensions. The microelectrode was connected to an electrometer operational amplifier (AD 549 from Analog Devices, Norwood, MA) in the voltage follower configuration mounted in close proximity in order to lower the impedance of the measured voltage. The reference electrode was also placed as near as feasible to the end of the separation capillary, but the exact position was found not to be critical. A conventional two-electrode electronic amplifier system was used with the reference electrode connected to the common amplifier. The microscope, electrode assembly and amplifier were contained in a Faraday cage and the amplifier was further shielded in a grounded metal box. The electropherograms were acquired on a Macintosh IIci personal computer (Apple) equipped with a 16 bit analog-to-digital converter card (NB-MIO-16XL-42 from National Instruments). The data acquisition software was written in LabVIEW 2 (National Instruments).

3. Results and discussion

3.1. Selectivity considerations

The potential response of an ion-selective electrode may be described by the following form of the Nicolsky-Eisenman equation:

$$E = E' + s \log \left\{ K_1^{\text{pot}} (a_1)^{1/z_1} + K_2^{\text{pot}} (a_2)^{1/z_2} + K_3^{\text{pot}} (a_3)^{1/z_3} + \ldots K_n^{\text{pot}} (a_n)^{1/z_n} \right\}$$

1 to n stand for the ions that the electrode is responsive to, z for the charge on the respective ion, s for the slope measured for a monovalent ion and E' for a constant potential. The K^{pot} values are the respective selectivity coefficients. It is usually desirable that an ion-selective electrode responds to one species only, i.e., the selectivity coefficient for the ion of interest should be very high and all the other values negligible. In the case where such an electrode is to be used as a detector in capillary electrophoresis the response should ideally be the same for all ions, i.e., all the K^{pot} values should be identical. The electrode also should show no response or a very limited response only to a background electrolyte present, i.e. possess a very small K^{pot} value for the background ion. This desired behaviour is illustrated in the first column of Fig. 2.

Ion-selective electrodes for anions are often based on quaternary amines such as tridodecylmethylammonium chloride (TDMAC). These charged ionophores invoke a selectivity behaviour that follows the so-called Hofmeister pattern [14] and is dependent on the hydration energy of the ions [15]. The selectivity obtained for a microelectrode based on TDMAC is given in the second column of Fig. 2. The pattern suggests the use of sulphate or acetate in the background electrolyte and should allow the determination of the other

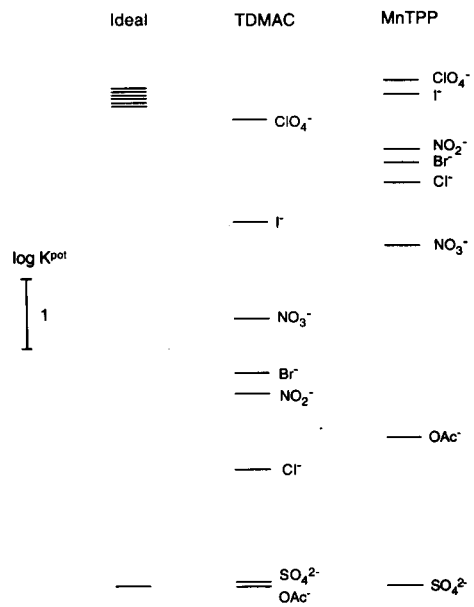

Fig. 2. Logarithmic selectivity coefficients (log K^{pot}) for anion selective microelectrodes. First column: desired for a potentiometric detector in capillary electrophoresis. Second column: obtained for tridodecylmethylammonium chloride (TDMAC). Third column: obtained for 5,10,15,20-tetraphenyl-21*H*,23*H*-porphin manganese(III) chloride (MnTPP).

anions with the detection limit decreasing in the order of Cl^-, NO_2^-, Br^-, NO_3^-, I^-, ClO_4^-. Clearly the pattern is far from the ideal. It should for example not be possible to determine chloride at concentrations much lower than about one order of magnitude below the level of the background electrolyte. A microelectrode based on 5,10,15,20-tetraphenyl-21*H*,23*H*-porphin manganese(III) chloride (MnTPP) shows a pattern much closer to the desired one. This electrode was developed for intra-cellular chloride determinations [13]. The selectivities obtained for MnTPP are illustrated in the third column of Fig. 2. This pattern promises to allow the determination of the six anions Cl^-, NO_2^-, Br^-, NO_3^-, I^-, ClO_4^- with good detection limits by using sulphate as the background electrolyte.

3.2. Electrophoresis

The separation of an anion mixture 10^{-4} M in Br^-, Cl^-, NO_3^- and NO_2^- and 10^{-5} M in I^- and ClO_4^- in a 25 μm fused silica capillary is illustrated in Fig. 3. A microelectrode based on TDMAC as detector was employed. The separation was performed by applying a potential of 30 kV with the detector end as the anodic side. Injection was carried out in the electrokinetic mode by dipping the sampling end into a container with the anion mixture and applying a potential of 5 kV for 7 s. A buffer solution of 10 mM acetic acid–sodium acetate at pH 5 was employed as electrolyte and the anion mixture was prepared in this electrolyte solution. All six anions were found to elute between about 8 and 10 min and baseline separation is achieved with the exception of iodide and chloride. Clearly, the peak heights follow the expected selectivity sequence taking the different concentrations into account. Chloride is just detected at a level of 10^{-4} M (3.5 mg kg^{-1}) and the peak for nitrite is fairly small as well. The lowest concentration of perchlorate that can be detected, the ion the electrode is most responsive to, was estimated to be around 10^{-7} M (10 μg kg^{-1}). The lowest detectable concentrations for the other ions are between these two extremes. As was expected, the peak heights were found to show a dependence on the position of the microelectrode tip.

The electropherogram obtained for the same anion mixture using a microelectrode based on

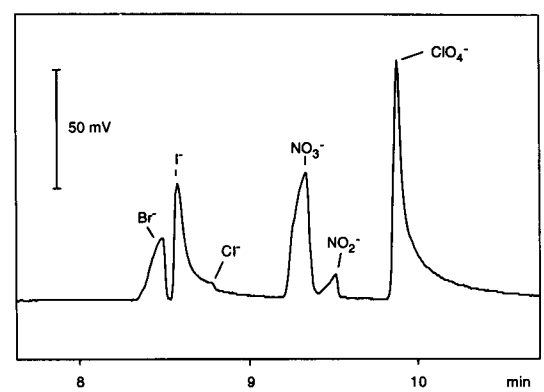

Fig. 3. Electropherogram obtained for a mixture of six anions using a microelectrode based on TDMAC. Concentrations: 10^{-4} M in Br^-, Cl^-, NO_3^- and NO_2^- and 10^{-5} M in I^- and ClO_4^-. Electrokinetic injection, 5 kV, 7 s. Separation potential: 30 kV. Capillary: length 1 m, diameter 25 μm. Electrolyte: 10 mM HOAc–NaOAc, pH 5.0.

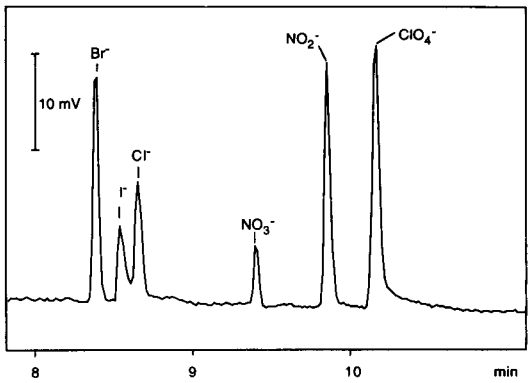

Fig. 4. Electropherogram obtained for a mixture of six anions using a microelectrode based on MnTPP. Concentrations: 10^{-4} M in Br^-, Cl^-, NO_3^- and NO_2^- and 10^{-5} M in I^- and ClO_4^-. Electrokinetic injection, 5 kV, 7 s. Separation potential: 30 kV. Capillary: length 1 m, diameter 25 μm. Electrolyte: 10 mM K_2SO_4.

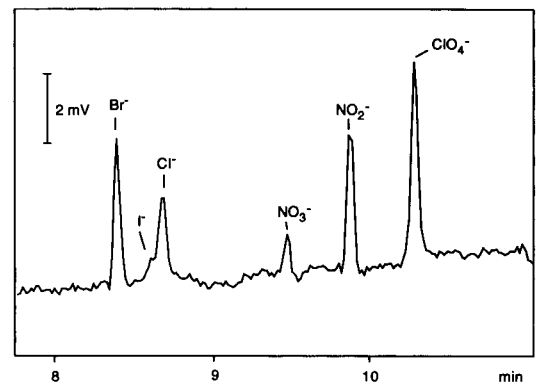

Fig. 5. Electropherogram obtained for a mixture of six anions using a microelectrode based on MnTPP. Concentrations: 10^{-5} M in Br^-, Cl^-, NO_3^- and NO_2^- and 10^{-6} M in I^- and ClO_4^-. Electrokinetic injection, 5 kV, 7 s. Separation potential: 30 kV. Capillary: length 1 m, diameter 25 μm. Electrolyte: 10 mM K_2SO_4.

MnTPP as detector is given in Fig. 4. Here a 10 mM K_2SO_4 solution was used as electrolyte. The elution times are almost the same in this electrolyte. Here the peak heights are more uniform and follow the selectivity sequence expected for the electrode. It is possible to determine chloride and nitrite easily at the 10^{-4} M level with this detector. The only species suffering a relative loss of sensitivity is nitrate.

An electropherogram was acquired for a tenfold dilution solution of the anion mixture (10^{-5} and 10^{-6} M). The result is given in Fig. 5. As the level of noise on the baseline illustrates, the concentrations are near the detection limits. The lowest detectable concentration for nitrate, the least responsive anion, is in the order of 10^{-5} M and that for perchlorate below 10^{-7} M. An improvement of one order of magnitude compared to the detector based on the quaternary amine was therefore achieved for the respective least responsive ions.

A typical calibration curve obtained for chloride using the latter electrode as detector is given in Fig. 6. It clearly illustrates the wide dynamic range obtainable with this type of detection. The multiple injection of a solution of 10^{-3} M Cl^- concentration gave a relative standard deviation of 1.8% ($n = 5$) in peak height. Due to the logarithmic response this corresponds to a relative error of 7% in concentration. For the repeated injection of a solution of 3×10^{-5} M Cl^- a relative standard deviation of 7.9% ($n = 5$) in peak height was obtained. The shape of the calibration curve at the low end makes the determi-

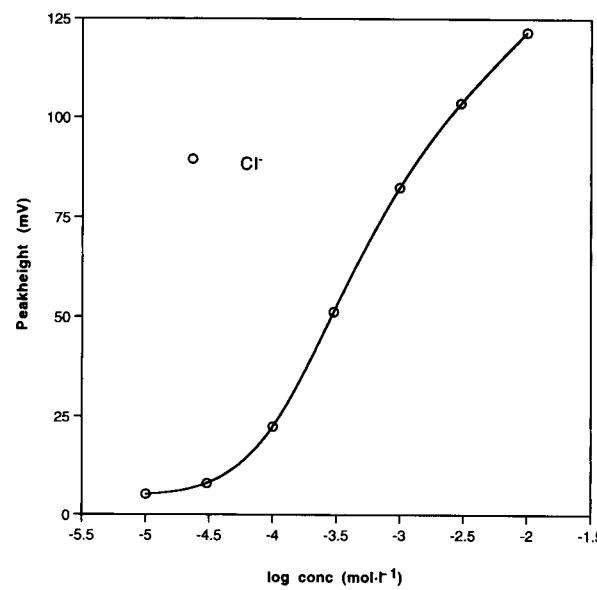

Fig. 6. Calibration curve for chloride obtained using a microelectrode based on MnTPP. Electrokinetic injection, 5 kV, 7 s. Separation potential: 30 kV. Capillary: length 1 m, diameter 25 μm. Electrolyte: 10 mM K_2SO_4.

nation of the detection limit somewhat arbitrary. However, based on the latter quoted value of precision and an average gradient of the calibration curve of 17 mV per decade between 10^{-5} M and 10^{-4} M a detection limit for chloride of 1.5×10^{-5} M or 0.5 mg kg^{-1} is obtained (concentration corresponding to a signal 3 times its standard deviation at the low end of the calibration curve).

Hydrodynamic injection of the 10^{-4}–10^{-5} M mixture (10 cm elevation at the sample end, 30 s) yielded a peak height of 16 mV for perchlorate (28 mV for the electrokinetic injection of the same concentration, 5 kV, 7 s). The peak heights relative to each other remained unchanged. It was further found to be possible to also determine thiocyanate either with hydrodynamic or electrokinetic injection. The elution time was in the order of 12 min. Based on the selectivity consideration it should also be possible to determine acetate, albeit with relatively poor detection limit, with the MnTPP-based detector. This was not attempted however.

Acknowledgments

The authors thank Assoc. Prof. J. Kistler and Dr. P. Donaldson from the Cell Biology department of the University of Auckland for the use of the micropipette puller and Prof. C.J. O'Connor for the loan of the microscope. We are also grateful to Assoc. Prof. G.A. Wright and the staff of the departmental electronics workshop for helpful advice. Grants from New Zealand Lottery Science (SR 022159) and the University of Auckland Research Council are gratefully acknowledged.

References

[1] P.E. Jackson and P.R. Haddad, Trends Anal. Chem., 12 (1993) 231.
[2] J. Romano, P. Jandik, W.R. Jones and P.E. Jackson, J. Chromatogr., 546 (1991) 411.
[3] W.R. Jones and P. Jandik, J. Chromatogr., 608 (1992) 385.
[4] W. Buchberger and P.R. Haddad, J. Chromatogr., 608 (1992) 59.
[5] G. Bondoux, P. Jandik and W.R. Jones, J. Chromatogr., 602 (1992) 79.
[6] W.R. Jones and P. Jandik, J. Chromatogr., 546 (1991) 445.
[7] N. Avdalovic, C.A. Pohl, R.D. Rocklin and J.R. Stillian, Anal. Chem., 65 (1993) 1470.
[8] X. Huang, J.A. Luckey, M.J. Gordon and R.N. Zare, Anal. Chem., 61 (1989) 766.
[9] S. Sloss and A.G. Ewing, Anal. Chem., 65 (1993) 577.
[10] C. Haber, I. Silvestri, S. Rööslі and W. Simon, Chimia, 45 (1991) 117.
[11] A. Nann and W. Simon, J. Chromatogr., 633 (1993) 207.
[12] A. Nann, I. Silvestri and W. Simon, Anal. Chem., 65 (1993) 1662.
[13] Y. Kondo, T. Bührer, K. Seiler, E. Frömter and W. Simon, Pflügers Arch., 414 (1989) 663.
[14] F. Hofmeister, Arch. Exp. Pathol. Pharmakol., 24 (1888) 247.
[15] J. Rais, Collect. Czech. Chem. Commun., 36 (1971) 3080.

ELSEVIER

Analytica Chimica Acta 295 (1994) 187–197

ANALYTICA CHIMICA ACTA

Electrothermal atomic absorption spectrometric determination of Al, Cu, Fe, Pb, V and Zn in clinical samples and in certified environmental reference materials

Jorge E. Tahán, Víctor A. Granadillo, Romer A. Romero *

Laboratorio de Instrumentación Analítica, Facultad Experimental de Ciencias, La Universidad del Zulia, Maracaibo, Zulia, Venezuela

Received 21st December 1993; revised manuscript received 12th April 1994

Abstract

This work presents the electrothermal atomic absorption spectrometric (ETAAS) determination of aluminum (Al), copper (Cu), iron (Fe), lead (Pb), vanadium (V) and zinc (Zn) in whole blood, blood components, bone and urine specimens from hemodialyzed azotemic patients and healthy subjects, and in certified environmental reference materials. Prior to the ETAAS analysis, test portions of the samples were diluted at different ratios in appropriate solvents: (i) whole blood, blood plasma, blood serum and red blood cells, in 0.1% v/v Triton X-100; (ii) urine, in 0.1% v/v Triton X-100 + 0.01 mol l^{-1} nitric acid; and (iii) mineralized samples (e.g., bone, pond sediment, vehicle exhaust particulates and sargasso), in 0.01 mol l^{-1} nitric acid. For Al, Cu, Fe and Zn, the diluent solutions also acted as the analyte isoformation solutions. For Pb and V, the analyte isoformation solutions were 0.5 mg l^{-1} of palladium +2% m/v of citric acid and 0.1 mg l^{-1} of palladium +2% m/v of citric acid in 0.01 mol l^{-1} nitric acid–0.1% v/v Triton X-100, for the former and for the latter, respectively. These analytical isoformers were not combined directly with the specimens in order to eliminate any precipitate formation, particularly with whole blood and its components. The detection limits (3σ, $\mu g\ l^{-1}$), were 0.5 (Al), 0.3 (Cu), 0.5 (Fe), 0.1 (Pb), 0.4 (V) and 0.1 (Zn). Accuracy was evaluated by using whole blood, human serum, freeze-dried urine, pond sediment, vehicle exhaust particulates and sargasso reference materials. For all metals present in real samples, precision was better than 3.0% R.S.D. The proposed methods were used to establish the metal concentrations found in the clinical samples under consideration. The methods were free from interferences, reliable and reproducible.

Key words: Electrothermal atomic absorption spectrometry; Aluminum; Copper; Iron; Lead; Vanadium; Zinc; Renal patients; Clinical samples; Environmental samples

1. Introduction

The study of trace metals in humans is of foremost importance because they play a definitive role in the intrinsic mechanisms regulating vital biological processes. Patients with chronic renal failure (CRF), treated with periodic hemodialysis, may present complex metabolic disturbances, such as dialysis encephalopathy, aluminum-induced osteomalacia, microcytic anaemia, copper fever, arterial hypertension, hypogo-

* Corresponding author.

SSDI 0003-2670(94)00175-L

nadism and sexual dysfunction, delayed growth and wound healing, acrodermatitis enteropathica, etc. Some of these disorders are related to the particular manner that aluminum (Al), copper (Cu), iron (Fe), lead (Pb), vanadium (V) and zinc (Zn) are corporally distributed in the renal insufficiency [1].

Electrothermal atomic absorption spectrometry (ETAAS; the graphite furnace technique) has been used successfully in our laboratory for the past eight years to investigate the mobilization of metals during the hemodialysis of renal individuals, in the diagnosis of metal-related diseases and in the follow-up of their clinical treatments. This technique is highly sensitive for determining $\mu g\ l^{-1}$ levels at which the above metals are found in the samples under consideration; additionally, ETAAS has an excellent selectivity and decreased sample handling requirements. However, ETAAS is prone to spectral and non-spectral interferences, many of which may induce severe analytical errors. For this reason, extreme care must be exercised to develop precise, accurate and interference-free ETAAS-based methodologies that can provide full analytical confidence to the metal data supporting clinical studies.

The purpose of the present work is to report on the ETAAS determination of Al, Cu, Fe, Pb, V, and Zn in whole blood, blood components (e.g., blood plasma, blood serum and red blood cells), urine and bone samples from hemodialyzed azotemic patients and healthy subjects. Certified environmental reference materials (e.g., Pond Sediment, Vehicle Exhaust Particulates and Sargasso) were also considered and analyzed.

2. Experimental

2.1. Reagents

All chemicals used were of analytical-reagent grade. The metal stock solutions (ca. 1000 mg l^{-1}) were prepared from Titrisol concentrates (Merck). Standard solutions were freshly prepared by serial dilution of the stocks with grade I (as established by the American Society for Testing and Materials, ASTM, ca. electrical resistivity $> 16.6\ M\Omega\ cm^{-1}$ at 25°C) [2] triply distilled, deionized water; nitric acid (Riedel-de Haën) was added to produce a 0.01 mol l^{-1} nitric acid concentration. The blanks of the $Pd(NO_3)_2$ (Aldrich), citric acid ($C_6H_8O_7 \cdot H_2O$, Riedel-de Haën), Triton X-100 (Riedel-de Haën) and sodium heparin (anticoagulant, Eli Lilly) used were below the ETAAS detection limits of the metals under study.

For accuracy evaluation, the following standard reference materials were used: Control Blood for Metals 1 (OSSD 20/21) from Behring Institute (Marburg, Germany); Trace-Metal Serum Control-A (Contox No. 0146 Level II) from Kaulson Labs. (West Caldwell, NJ); NIST SRM 909 Human Serum and NIST SRM 2670 Toxic Metals in Freeze-Dried Urine from the National Institute of Standards and Technology (Gaithersburg, MD); Pond Sediment (NIES No. 2), Vehicle Exhaust Particulates (NIES No. 8) and Sargasso (NIES No. 9) from the National Institute for Environmental Studies (Ibaraki, Japan).

Test portions of the samples were diluted at different ratios in appropriate solvents: (i) whole blood, blood plasma, blood serum and red blood cells, in 0.1% v/v Triton X-100; (ii) urine, in 0.1% v/v Triton X-100 + 0.01 mol l^{-1} nitric acid; and (iii) the mineralized samples (e.g., bone, Pond Sediment, Vehicle Exhaust Particulates and Sargasso), in 0.01 mol l^{-1} nitric acid.

All plasticware was cleaned with an alkaline phosphate-free detergent (Sodosil, Riedel-de Haën) by soaking for 24 h in a ca. 0.1% v/v detergent solution, and rinsed with grade I ASTM triply distilled, deionized water. Extreme care was exercised to avoid metal contamination of samples and solutions from dust, tap water, glassware, chemicals, etc., particularly for the ETAAS determination of Al and Zn, as suggested elsewhere [1]. In this sense, sample manipulation, solution preparation and instrumental measurements were conducted in a clean room with Class-100 work area.

2.2. Apparatus

A graphite furnace atomizer (Perkin-Elmer Model HGA-500) was mounted on an atomic

Table 1
Optimum furnace temperature parameters used for the ETAAS determination of the metals under consideration[a]

Metal	Pyrolysis [b]		Atomization [b,c]
	Temperature (°C)	Time (ramp/hold) (s)	Temperature (°C)
Al [d]	700	5/10	2300
	1500	5/5	
Cu [d]	900	10/5	2200
	1200	5/5	
Fe [d]	500	5/10	2500
	1300	10/15	
Pb [e]	600 [f]	30/15	2000
	600	0/10	
V [e]	800 [f]	20/15	2700
	800	0/10	
	1100	10/10	
	1700 [g]	5/5	
Zn [d]	500	10/15	2100
	1300	5/1	

[a] For 20-μl injections of the test portions mixed with the analytical isoformer (for Al, Cu, Fe and Zn) or for 10-μl injections of the test portions and of the isoformation solution via the alternate volume mode of the autosampler (for Pb and V); deuterium-arc background correction.
[b] Temperatures given represent the digital settings on the control panel of the HGA-500 temperature programmer.
[c] Internal Ar flow: 0 ml min^{-1}. Maximum power heating used. Holding time was 5 s for all metals but 6 s for V.
[d] Wall atomization in uncoated graphite tubes.
[e] In pyrolytic graphite coated graphite tubes with pyrolytic graphite platforms.
[f] Internal alternate gas: air at 300 ml min^{-1}.
[g] Internal alternate gas: CO at 300 ml min^{-1}.

absorption spectrometer (Perkin-Elmer Model 2380). Sample introduction was effected with an autosampler (Perkin-Elmer Model AS- 40). Data were recorded on a printer-sequencer (Perkin-Elmer PRS-10). Integrated absorbance signals computed by the atomic absorption spectrometer were employed throughout.

Table 1 shows the optimum analytical parameters used for the ETAAS determination of the metals studied. The drying temperature used for all these metals and matrices analyzed was 120°C. The light sources were single-element hollow-cathode lamps and a deuterium arc for background correction. The operating parameters of the hollow-cathode lamps used for the ETAAS determination of the metals under consideration were those given by the manufacturer, except for the spectral bandwidth of Pb, set at 0.2 nm to overcome a background interference probably due to an overcompensation of the background absorption by the deuterium-arc background corrector, as reported elsewhere [3]. Argon was employed in the graphite furnace as external and internal gas, and the flow of the latter was interrupted during atomization. For Pb and V, pyrolysis under an oxygen atmosphere was achieved using air as internal alternate gas during the first pyrolysis step, as shown in Table 1. In some experiments with vanadium, carbon monoxide was used as the internal alternate gas for 5 s prior to the atomization step (see Table 1).

2.3. Procedures

Blood samples were obtained from azotemic patients, undergoing hemodialysis at Maracaibo University Hospital, and from volunteers (controls) by venipuncture using 20-ml metal-free polystyrene syringes. The following protocol was used in order to establish the amount of metal attributable to contamination from the stainless steel needles: two portions of 3 ml each of blood were used to rinse the needle and were collected separately and preserved; posteriorly, 12 ml of blood were collected and preserved. Contamination from the needle was calculated by subtracting the amount of metal found in the first two blood fractions from that of the last fraction; no significant contamination was found. Routinely, 12 ml of blood were divided into three portions as follows: (i) a 4-ml blood aliquot was transferred into a metal-free polypropylene tube with cap, which contained 100 μl of sodium heparin (1000 IU ml^{-1}) (used for whole blood metals); (ii) another 4-ml heparinized aliquot was centrifuged at 1000 *g* for 10 min and plasma and red blood cells were separated and introduced into metal-free polypropylene tubes (used for plasma and red blood cells metals); (iii) the last 4 ml of blood were allowed to clot in order to obtain serum, which was kept separately in capped tubes. All blood specimens were preserved at 4°C until analyzed (within 48 h).

Bone biopsies were performed on the poste-

rior superior iliac spine with a No. 6 Yamshidi needle, constructed at the university machine shop [4]. Bone specimens came from three different sources: (i) hemodialyzed CRF patients; (ii) individuals undergoing surgical exposure of the iliac crest for the purpose of taking a bone fragment for grafting; and (iii) at postmortem examination. Informed consent was obtained from all patients and from the next of kin in the case of postmortem samples. All surgical procedures were approved by an ad hoc committee of the Maracaibo University Hospital and were performed by qualified surgeons; these were told about the risk of metal contamination from dust, surgical glove powder, surgical instruments, etc. Bone test portions were transferred into metal-free polypropylene tubes, containing 70% (v/v) analytical-grade ethanol, capped and kept at −20°C until analysis (within 4 days of collection). Bone metal losses were not detected in the ethanol solution. Before the ETAAS analysis, the bone aliquot was dehydrated at 40°C for 24 h, weighed (ca. 100 mg) and mineralized in a 23-ml high-pressure bomb (Parr Instrument Co. Model 4745) with 1 ml of concentrated nitric acid and 3 ml of grade I ASTM triply distilled, deionized water, being the system placed in a pre-heated oven at 150°C and kept at this temperature for 4 h for complete dissolution. The bone digestion solution was then transferred quantitatively into a 50-ml polypropylene calibrated flask (Nalgene Labware) and diluted to volume with grade I ASTM triply distilled, deionized water.

The certified environmental reference materials from the National Institute for Environmental Studies were mineralized as follows: approximately 1 g of sample was weighed accurately into the microwave digestion vessel of a laboratory microwave oven (CEM Model MDS-2000), 1 ml of grade I ASTM triply distilled, deionized water and 3 ml of concentrated nitric acid were added. The vessel was capped, inserted in the oven and irradiated for 10 min (at 100% power, equivalent to 600 W and 2450 MHz). The test solutions of the Vehicle Exaust Particulates and Pond Sediment materials required a second microwave mineralization with 3 ml of concentrated hydrochloric acid and 3 ml of hydrofluoric acid for 5 min at 100% power. After cooling to ambient temperature, the caps were removed and the contents were transferred quantitatively into 50-ml polypropylene calibrated flasks and diluted to volume with grade I ASTM triply distilled, deionized water.

Prior to ETAAS analysis, the samples and standard reference materials were diluted with an appropriate solvent, as described above, in the metal-free microvials of the autosampler, using Gilson air displacement pipettes (Gilson Medical Electronics). In general, dilutions of 1 + 3 (blood plasma and blood serum), 1 + 9 (whole blood, red blood cells and urine) and 1 + 19 (mineralized test portions of the bone specimens and of the certified environmental reference materials) were achieved. For Al, Cu, Fe and Zn, the diluent solutions also acted as the analyte isoformation solutions, term taken from Granadillo and Romero [5]. For the ETAAS determination of these four metals, 20-μl aliquots of diluted test portions under analysis (or aqueous standards) were injected into the graphite tube. The analyte isoformation solutions for Pb and V were 0.5 mg l^{-1} of Pd + 2% m/v of citric acid and 0.1 mg l^{-1} of Pd + 2% m/v of citric acid in 0.01 mol l^{-1} nitric acid–0.1% v/v Triton X-100, respectively; these analytical isoformers were not combined directly with the specimens in order to eliminate any precipitate formation, particularly with whole blood and its components. Hence, by using the alternate volume mode of the AS-40 autosampler, 10-μl aliquots of diluted test portions under analysis (or aqueous standards) and 10 μl of the respective isoformation solutions were injected in sequence onto the L'vov platform; the 10 μl of the analyte isoformation solutions contained either 5 ng of Pd and 200 μg of citric acid (for Pb) or 1 ng of Pd and 200 μg of citric acid (for V).

2.4. Statistical analysis

Statistical comparisons between groups were carried out by non-parametric (Mann-Whitney two-sample test) methodology because S.D. values were often significantly different in CRF patients and in the control group. Differences were

considered significant when $p < 0.05$. Associations were tested by linear regression analysis.

3. Results and discussion

The analytical isoformers employed in the present work for the ETAAS determination of Al, Cu, Fe and Zn were Triton X-100 and/or nitric acid. Magnesium nitrate has been used for the analytical isoformation of these four metals [6]; potassium dichromate-induced isoformation for Al has also been reported [7]. We prefer simpler analytical isoformers to decrease the risk of contamination and avoid multi-step analytical procedures [8]. Pre-atomization losses of these analyte elements were not observed even in the presence of complex matrices such as whole blood and red blood cells; the formation of thermally-stable atomic precursors should have been induced. No interference effects on the integrated absorbance signals were observed for the wall atomization of these four metals, as reported by other authors [9,10]. Graphite furnace analyses were also carried out using pyrolytic graphite coated graphite tubes with and without pyrolytic graphite platforms, and results obtained were compared with those obtained with uncoated graphite tubes. No significant differences ($p > 0.001$) were found for the precision and sensitivity for the three tube designs.

For lead, volatilization losses of the analyte element were controlled by using Pd-induced isoformation in conjunction with the carbon-reducing effect achieved by the addition of citric acid. It was found that maximum sensitivity was achieved at 5 ng of Pd for both the aqueous Pb standards and the samples; the use of 5 ng of Pd was assessed to be sufficient for the analysis of the different type of samples using ETAAS. When the determination of Pb was carried out with excess of Pd (> 20 ng of Pd) or without citric acid even at low masses of Pd (< 10 ng of Pd), it was found that the graphite platform and the graphite tube were worn faster (e.g., the tube broke down after 15–20 firings). Consequently, the reproducibility (R.S.D. $> 15\%$) and sensitivity ($> 30\%$ decrease) of the analyses were adversely affected. This could be the result of the fatigue of the graphite structure induced by Pd(II) using up the carbon atoms of the graphite surface for its reduction. This spectroscopic behavior was recently discussed by Granadillo and Romero [5]. They postulated a carbon-dependent mechanism for the reduction of the atomic precursor PbO to form atomic Pb with production of CO, assuming that a carbon source other than the graphite furnace (in our case, citric acid) was available and was participating actively in the redox reaction. Additionally, oxygen-ashing pyrolysis was successfully employed to prevent the build-up of carbonaceous material that could block the optical beam and to induce the formation of PbO [5].

The spectroscopic behavior of vanadium in aqueous and biological matrices was studied using three different analytical isoformers: Pd, citric acid and nitric acid. A composite Pd–citric acid–nitric acid isoformer was also tested. Pyrolytic graphite coated graphite tubes with inserted pyrolytic graphite coated graphite platforms proved to be an adequate instrumental design for the ETAAS determination of V, in spite of the fact that this is a refractory element. Platform atomization of V caused a slight drop in sensitivity ($< 5\%$) but guaranteed neat absorbance–time profiles without deflections below the baseline. On the other hand, wall atomization for V yielded to a much lower reproducibility (15–20% R.S.D.). A background attenuation-type spectral interference, lower integrated absorbance signals (15–20% lower) and poor reproducibility (20–25% R.S.D.) resulted when nitric acid alone was employed for real samples. The best analytical results were achieved with the following isoformer mixture: 0.1 mg l^{-1} of Pd + 2% m/v of citric acid in 0.01 mol l^{-1} nitric acid–0.1% v/v Triton X-100. An appearance time (e.g., time in seconds required to reach the maximum height of the absorption peak at the atomization temperature) [5] for atomic V of 2.38 s was equally obtained for aqueous standards and samples when argon was the internal gas and the above isoformation mixture was used. This clearly indicated an efficient isoformation effect achieved in both aqueous V and real V. To the best of our knowledge, no other ETAAS paper has reported similar appear-

ance time for V in unmatched standards and samples. To success in doing this, a sufficient amount of carbon from a source other than that of the graphite tube (ca. 200 μg of citric acid) was required; as a result, adequate absorbance–time profiles and accurate and precise analyses were obtained. However, the V peak was delayed from 2.38 s to 2.50 s when an excessive amount of citric acid was added (ca. > 300 μg). Additionally, CO also delayed the atomization of V to 2.48 s. Altogether, these results suggested that the rate-limiting step for the atomization of V in the graphite tube, under our experimental conditions, should have been the formation of vanadium carbide and this step is carbon-dependent [11].

Table 1 presents the pyrolysis and atomization temperatures established for the ETAAS determination of the six metals in the clinical and environmental materials considered. Optimization of these analytical parameters was done by steadily increasing the temperature at fixed concentrations of the metal under study and observing the highest integrated absorbance readings. Pyrolysis and atomization curves with pronounced maxima were obtained. Below the optimum pyrolysis temperatures, the effects of the matrix were seen, and above these temperatures volatilization losses of the analyte elements probably accounted for the decreased absorbance signals. In addition, decreased absorbance signals were observed below the optimum atomization temperatures, probably because of incomplete volatilizations of the analyte elements; at higher temperatures, the integrated absorbances decreased probably because diffusional losses of atoms increased [12]. Pyrolysis [5,13–15] and atomization [9,16,17] curves with pronounced maxima have also been reported by others. The atomization curve for V (Fig. 1) behaves differently because this refractory metal requires an atomization temperature higher than the maximum temperature supplied by the graphite furnace HGA-500 (ca. 2700°C). However, the atomization of V at 2700°C should have been accomplished

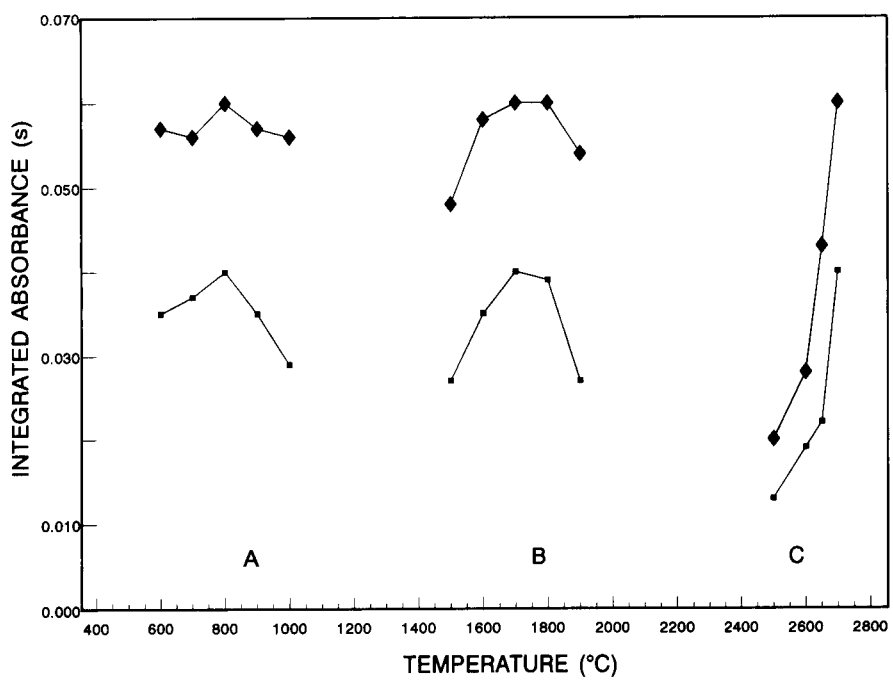

Fig. 1. Pyrolysis (A,B) and atomization (C) curves for V with the use of Pd-induced isoformation (1 ng of Pd + 200 μg of citric acid in 0.01 mol l^{-1} nitric acid–0.1% v/v Triton X-100; 10-μl injection volume) in the presence of O_2: ♦ aqueous standard (300 pg V); ■ mineralized bone sample (200 pg V). See text for details.

Table 2
Analytical figures of merit for the electrothermal atomic absorption spectrometric determination of metals in whole blood, blood plasma, blood serum, red blood cells, urine, bone specimens, pond sediment, vehicle exhaust particulates and sargasso

Metal	Calibration curve [a]	Correlation coefficient	Linear range ($\mu g\,l^{-1}$)	Standard error of the estimate ($S_{y.x}$) (s)	Standard deviation of intercept (s)	Standard deviation of slope ($s \cdot l\,\mu g^{-1}$)	Detection limit [b]		Characteristic mass [d] (pg)	Precision R.S.D., [e]%
							Solution ($\mu g\,l^{-1}$)	Solid [c] ($\mu g\,g^{-1}$)		
Al	$Y = 0.0050X - 0.0004$	0.9999	100	0.002	0.0012	0.00003	0.5	0.025	19 (10)	1.0
Cu	$Y = 0.0244X + 0.0005$	1.0000	50	0.002	0.0011	0.00004	0.3	0.015	3 (8)	1.9
Fe	$Y = 0.0123X + 0.0024$	0.9994	50	0.005	0.0035	0.00025	0.5	0.025	3 (5)	0.8
Pb	$Y = 0.0034X - 0.0002$	0.9999	50	0.003	0.0001	0.00002	0.1	0.005	13 (12)	2.2
V	$Y = 0.0026X - 0.0001$	0.9994	50	0.0004	0.0003	0.00005	0.4	0.020	35 (40)	3.0
Zn	$Y = 0.0325X + 0.0006$	0.9999	5	0.0008	0.0006	0.0002	0.1	0.005	2 (9)	2.0

[a] X and Y are the analyte concentration ($\mu g\,l^{-1}$) and the integrated absorbance (s), respectively.
[b] Defined as three times the standard deviation of the blank.
[c] For Pond Sediment, Vehicle Exhaust Particulates and Sargasso. For bone, detection limits were 10-fold lower.
[d] Amount of analyte, in picograms (pg), contained in 20-μl injection volume of test solution mixed with the analytical isoformer (for Al, Cu, Fe, Zn; see text for dilution ratios used) or 10-μl injection volume of test solution (for Pb, V), that produces an integrated absorbance of 0.0044 s; internal argon flow stopped. Characteristic mass values in parenthesis were taken from reference 6 (reference 13 for Zn; injection volume of 5 μl) and were obtained using 20-μl injection volume and the stabilized temperature platform furnace (wall atomization for V) with Zeeman correction.
[e] Average R.S.D., for real samples only. Triplicate samples for each matrix under consideration; seven runs each analysis.

efficiently as proven by the excellent analytical figure of merits obtained and presented below. Two pyrolysis steps were used for V (Curves A and B; Fig. 1). Firstly, the temperature was risen to 800°C and pyrolysis occurred under an oxygen atmosphere to remove carbonaceous concomitants; posteriorly, air was evacuated from the graphite tube (at 800°C for 10 s), palladium reduced at 1100°C and another pyrolysis at 1700°C was pursued for analyte isoformation.

Table 2 shows the analytical figures of merits for the ETAAS determination of Al, Cu, Fe, Pb,

Table 3
Accuracy of the ETAAS determination of metals in clinical and environmental materials

		Mean concentration ± 1 S.D. ($\mu g\ l^{-1}$)	
Reference material	Metal	Certified value	Measured value
OSSD 20/21 [a]	Pb	413 ± 51	424 ± 18 ($n = 12$)
Trace Metal Serum Control-A [b]	Cu	1500 ± 300	1438 ± 120 ($n = 7$)
	Fe	2100 ± 420	2050 ± 200 ($n = 7$)
	Zn	2000 ± 400	2040 ± 100 ($n = 8$)
SRM 909 [c]	Cu	1290 ± 80	1250 ± 30 ($n = 6$)
	Fe	2340 ± 240	2410 ± 80 ($n = 9$)
	Pb	23.7 ± 2.1	20.6 ± 3.2 ($n = 10$)
	V	3.19 ± 0.55	3.36 ± 0.10 ($n = 6$)
SRM 2670 [d]	Al	180 [e]	179 ± 10 ($n = 7$)
	Cu	370 ± 30	380 ± 15 ($n = 9$)
	Pb	109 ± 4	106 ± 5 ($n = 5$)
	V	120 [e]	125 ± 21 ($n = 6$)
NIES No. 2 [f]	Al	10.6 ± 0.5 [i]	11.0 ± 0.6 [i] ($n = 9$)
	Cu	210 ± 12 [j]	201 ± 13 [j] ($n = 7$)
	Fe	6.53 ± 0.35 [i]	6.50 ± 0.12 [i] ($n = 8$)
	Pb	105 ± 6 [j]	102 ± 4 [j] ($n = 8$)
	V	250 [e,j]	250 ± 28 [j] ($n = 5$)
	Zn	343 ± 17 [j]	350 ± 8 [j] ($n = 6$)
NIES No. 8 [g]	Al	0.33 ± 0.02 [i]	0.32 ± 0.01 [i] ($n = 7$)
	Cu	67 ± 3 [j]	65 ± 4 [j] ($n = 7$)
	Pb	219 ± 9 [j]	214 ± 4 [j] ($n = 8$)
	V	17 ± 2 [j]	17.5 ± 1.3 [j] ($n = 9$)
	Zn	0.104 ± 0.005 [i]	0.103 ± 0.002 [i] ($n = 5$)
NIES No. 9 [h]	Al	215 [e,j]	213 ± 8 [j] ($n = 6$)
	Cu	4.9 ± 0.2 [j]	5.0 ± 0.2 [j] ($n = 7$)
	Fe	187 ± 6 [j]	189 ± 4 [j] ($n = 7$)
	Pb	1.35 ± 0.05 [j]	1.31 ± 0.02 [j] ($n = 8$)
	V	1.0 ± 0.1 [j]	1.0 ± 0.1 [j] ($n = 7$)
	Zn	15.6 ± 1.2 [j]	16.2 ± 0.4 [j] ($n = 7$)

n = Number of test portions analyzed; 7 analyses of each portion were made.
[a] Control Blood.
[b] Control Blood Serum.
[c] Human Serum.
[d] Toxic Metals in Freeze-Dried Urine.
[e] Provisional value.
[f] Pond Sediment.
[g] Vehicle Exhaust Particulates.
[h] Sargasso.
[i] In %, m/m.
[j] In $\mu g\ g^{-1}$.

Table 4
Metal concentrations (mean ± 1 S.D., $\mu g\ l^{-1}$) found in whole blood, blood components, bone and urine samples of azotemic patients (CRF) and controls (C) established by electrothermal atomic absorption spectrometry. Ranges are shown in parentheses (in $\mu g\ l^{-1}$, except for bone: $\mu g\ g^{-1}$)

Metal		Whole Blood	Plasma	Serum	Red blood cells	Bone [a]	Urine
	CRF	98 ± 18 (n = 50) *	63 ± 9 (n = 42) *	73 ± 10 (n = 46) *	107 ± 11 (n = 50) *	29 ± 17 (n = 18) *	NO
Al		(50–120)	(45–78)	(58–91)	(90–125)	(9–55)	
	C	4 ± 1 (n = 38)	4 ± 0.3 (n = 43)	3 ± 0.2 (n = 25)	3 ± 0.5 (n = 16)	13 ± 11 (n = 14)	20 ± 1 (n = 20)
		(2–7)	(3.5–4.8)	(2.1–4.3)	(2.0–3.9)	(2–34)	(18–21)
	CRF	905 ± 43 (n = 50) *	930 ± 40 (n = 50) *	904 ± 36 (n = 50)	540 ± 17 (n = 50)	0.19 ± 0.16 (n = 18)	NO
Cu		(850–963)	(870–992)	(852–973)	(493–591)	(0.01–0.43)	
	C	724 ± 19 (n = 52)	760 ± 33 (n = 52)	999 ± 31 (n = 51)	533 ± 17 (n = 52)	470 ± 14 (n = 52)	6 ± 4 (n = 20)
		(700–758)	(720–830)	(942–1055)	(484–562)	(450–495)	(2–12)
	CRF	235 ± 8 (n = 50) **	0.6 ± 0.1 (n = 14)	1.3 ± 0.2 (n = 14)	884 ± 16 (n = 50)	940 ± 133 (n = 18) **	NO
Fe		(215–249)	(0.2–0.7)	(1.0–1.5)	(862–899)	(798–1150)	
	C	470 ± 14 (n = 52)	0.9 ± 0.1 (n = 15)	1.2 ± 0.2 (n = 15)	913 ± 13 (n = 52)	263 ± 49 (n = 14)	6.2 ± 3.0 (n = 20)
		(405–496)	(0.7–1.1)	(0.9–1.5)	(880–930)	(210–350)	(2.1–10.5)
	CRF	155 ± 7 [b] (n = 50)	UD	UD	349 ± 15 (n = 50)	10 ± 2 (n = 18)	NO
Pb		(48–169) [b]			(189–383)	(7–16)	
	C	148 ± 27 (n = 40)	UD	UD	326 ± 60 (n = 40)	7.8 ± 2.8 (n = 14)	10.2 ± 3.8 (n = 40)
		(51–271)			(123–452)	(3.9–11.5)	(2.7–18.2)
	CRF	13 ± 2 (n = 19) **	15 ± 2 (n = 19) **	7 ± 1 (n = 19) *	18 ± 1 (n = 19) **	3 ± 0.4 (n = 18) *	NO
V		(8–17)	(11–19)	(5–8)	(16–19)	(2.5–3.6)	
	C	< 1.2 (n = 10) [c]	5 ± 3 (n = 10)	3 ± 1 (n = 10)	< 1.2 (n = 10) [c]	1 ± 0.4 (n = 14)	UD
			(1–8)	(1–4)		(0.2–4.3)	
	CRF	3800 ± 110 (n = 50) *	720 ± 40 (n = 50) *	500 ± 40 (n = 50) *	17200 ± 400 (n = 50) *	0.11 ± 0.02 (n = 18)	NO
Zn		(3620–4050)	(672–778)	(452–559)	(16500–18000)	(0.07–0.16)	
	C	8400 ± 200 (n = 52)	400 ± 31 (n = 46)	810 ± 33 (n = 50)	12700 ± 310 (n = 52)	0.11 ± 0.02 (n = 14)	1341 ± 734 (n = 20)
		(8005–8820)	(354–438)	(768–869)	(12000–13420)	(0.08–0.15)	(505–2200)

n = Number of specimens analyzed.
[a] Bone metal concentration in $\mu g\ g^{-1}$. Differences between CRF and C as follows: * $p < 0.01$, ** $p < 0.005$. NO = CRF patients did not have urine output.
[b] Values corrected for hematocrit. UD = Undetectable by ETAAS.
[c] In diluted sample.

V and Zn in whole blood, plasma, serum, red blood cells, urine, bone specimens, pond sediment, vehicle exhaust particulates and sargasso. Precision was evaluated in real samples of these clinical materials. Three aliquots of each material were analyzed (seven runs each analysis) using the proposed methods. For all metals, precision (R.S.D.) was better than 3.0%, for both the within- and between-run precision, which can be considered adequate for these types of analyses of real samples. The characteristic masses presented in Table 2 are in good agreement with values reported in the current literature [6,13].

Accuracy was verified by analyzing seven standard reference materials supplied by four different international agencies; the certified environmental reference materials were mineralized as stated above to provide aqueous solutions whose final concentrations were within the range of the metal contents expected in the clinical materials evaluated. The results are given in Table 3. The reliability of the analytical methods was further assessed through recovery studies. Recoveries were done by six replicate spectrometric determinations of the metals under consideration in three real samples of each clinical material studied. The average recoveries were 101% (range 98–103%). The standard addition method was also used for quantification and comparison purposes. Samples of whole blood (three specimens), plasma (three specimens), serum (four specimens), red blood cells (six specimens), bone (six specimens) and urine (five specimens), and the reference materials Whole Blood OSSD 20/21, Urine SRM 2670 and Sargasso NIES No. 9, were analyzed by the method of standard additions and produced graphs with slopes statistically indistinguishable from those of the aqueous standard calibration graphs. This implied the absence of non-spectral interferences in the ETAAS analyses by the proposed methods and permitted the use of either the calibration graphs or the standard addition method for quantification.

A continuum source background corrector (e.g., a deuterium arc) was used to compensate for background attenuation-type spectral interferences. A study of the background was carried out in order to evaluate the performance of this correction system and to ensure its efficacy. Integrated absorbance signals were registered under different modes: (1) hollow cathode–deuterium arc (AA-BG, absorption measurement taken with background correction), (2) hollow cathode only (AA, uncorrected absorption signal), and (3) deuterium arc only (BG, measurement of the background). Relative errors were calculated assuming that a true analyte absorption was obtained with mode (1). This procedure has been described by Navarro et al. [3]. Relative errors (%) below 3 (Al), 1 (Cu), 1 (Fe), 3 (Pb), 2 (V) and 3 (Zn) were found, which corresponded to metal concentrations of less than 0.6 μg Al l^{-1}, 0.2 μg Cu l^{-1}, 0.2 μg Fe l^{-1}, 0.8 μg Pb l^{-1}, 0.5 μg V l^{-1} and 0.3 μg Zn l^{-1}. Therefore, compensation of the background attenuation-type spectral interferences should have been achieved by the corrector used.

Altogether, the above analytical figures indicated that the ETAAS-based methodologies were precise, accurate and interference-free, providing full analytical confidence to the metal data presented below.

The proposed methods were used in our laboratory to establish the concentrations as well as the ranges of Al, Cu, Fe, Pb, V and Zn found in whole blood, blood plasma, blood serum, red blood cells, bone and urine samples of CRF patients, undergoing hemodialysis at the Maracaibo University Hospital, and healthy subjects (Table 4). These data demonstrated that plasma or red blood cells were appropriate analytical targets for Al and Zn; Pb should be determined in red blood cells, and V and Cu should be tested in plasma. Romero et al. [1] proved that the determinations of trace metals in serum are less likely to be useful in clinical studies; this is the corollary of the present work. CRF patients' blood Al concentrations reported in the present study are considered to be pathetically representative of the values found in azotemic patients undergoing hemodialysis programs in Venezuela because Al content in the hemodialysis water exceeds by far (ca. > 350 μg l^{-1}) the acceptable concentration of < 10 μg l^{-1} [18]. Aluminum intoxication in these individuals has been well documented in previous communications [1]. It should be pointed

out that our controls' plasma vanadium (mean ± S.D. = 5 ± 3 $\mu g\ l^{-1}$) was higher than that reported by Hosokawa and Yoshida (0.4 ± 0.2 $\mu g\ l^{-1}$) [19], but it was not significantly different ($p > 0.005$) from the plasma vanadium data of Steffen et al. (3.1 ± 1.2 $\mu g\ l^{-1}$) [20]. This apparently high plasma vanadium is perhaps a characteristic of the population examined. In this sense, the thermoelectric plant that provides electricity to Maracaibo City is fed with coke (a fuel with a high carbon content obtained by the cracking of petroleum); this coke contains huge amounts of vanadium and nickel, a well-known feature of the Venezuelan petroleum. For this reason, Maracaibo's dwellers are exposed to a vanadium-contaminated environment as reported elsewhere [21]. The ETAAS determination of Cu and Zn in plasma and serum was straightforward and preferred to flame AAS; sample dilution (ca. 1 + 24 for Cu; 1 + 99 for Zn) ensured the elimination of non-spectral interferences, adequately. To achieve this, contamination had to be carefully controlled, as mentioned above.

In conclusion, the ETAAS-based methods described above are sufficiently sensitive, accurate and precise, and, therefore, should be of interest to the scientists and analytical chemists concerned with biometal research. Additionally, these methods provide an important alternative for the evaluation of trace metals in different clinical and biological materials, and in a wide range of concentrations. Finally, the uncoated graphite tubes used in the present study for Al, Cu, Fe and Zn are cheaper and, under our furnace conditions, can tolerate more than 250 firings; thus, they can be recommended for clinical and hospital laboratories engaged in routine analyses, and whenever operating costs should be carefully considered.

Acknowledgments

This research was partially supported by Consejo Nacional de Investigaciones Científicas y Tecnológicas (CONICIT; grants F-142 and S1-2499) and Consejo de Desarrollo Científico y Humanístico (CONDES, La Universidad del Zulia). The authors gratefully acknowledge research support from FUNDAYACUCHO (Venezuela).

References

[1] R.A. Romero, J.A. Navarro, B. Rodríguez-Iturbe, R. García, O.E. Parra and V.A. Granadillo, Trace Elem. Med., 7 (1990) 176.
[2] American Society for Testing and Materials: Standard Speciation for Water, Philadelphia, PA, ASTM D, 1977, p. 1193.
[3] J.A. Navarro, V.A. Granadillo, O.E. Parra and R.A. Romero, J. Anal. At. Spectrom., 4 (1989) 401.
[4] D.J. Sherrard, Semin. Nephrol., 6 (1986) 5.
[5] V.A. Granadillo and R.A. Romero, J. Anal. At. Spectrom., 8 (1993) 615.
[6] W. Slavin and G.R. Carnrick, At. Spectrosc., 6 (1985) 157.
[7] K.S. Subramanian, Prog. Anal. Spectrosc., 11 (1988) 511.
[8] R.A. Romero, J.A. Navarro, V.A. Granadillo and O.E. Parra, paper presented at the 1st Rio Symposium on Furnace Atomic Absorption Spectrometry, Rio de Janeiro (Brazil), 1988, paper 38.
[9] J.M. Marchante, J. Pérez, A. Sanz-Medel and C.S. Fellows, J. Anal. At. Spectrom., 7 (1992) 743.
[10] D.E. Bass and J.A. Holcombe, Anal. Chem., 60 (1988) 578.
[11] V.A. Granadillo and R.A. Romero, in M. Anke (Ed.), Trace Elements in Man and Animals (TEMA-8), Jena, 1993, p. 86.
[12] R.E. Sturgeon, C.L. Chakrabarti and C.H. Langford, Anal. Chem., 48 (1976) 1792.
[13] P.C. D'Haese, L.V. Lamberts, A.O. Vanheule and M.E. De Broe, Clin. Chem., 38 (1992) 2439.
[14] A.A. Almeida, M.L. Bastos, M.I. Cardoso, M.A. Ferreira, J.L. Lima and M.E. Soares, J. Anal. At. Spectrom., 7 (1992) 1281.
[15] D.C. Paschal and G.G. Bailey, At. Spectrosc., 11 (1990) 65.
[16] J. Arnaud, A. Favier and J. Alary, J. Anal. At. Spectrom., 6 (1991) 647.
[17] W. Penninckx, D.C. Massart and J. Verbeke-Smeyers, Fresenius' J. Anal. Chem. 343 (1992) 526.
[18] Association for the Advancement of Medical Instrumentation: American National Standard for Hemodialysis Systems (RD5), Arlington, VA, 1981.
[19] S. Hosokawa and O. Yoshida, Nephrol. Dial. Transplant., 4 (1989) 282.
[20] R.P. Steffen, M.B. Pamnai, D.L. Clough, S.J. Hout, S.M. Muldoon and F.J. Haddy, Hypertension, 3 (1981) 1173.
[21] R.A. Romero, J.A. Navarro, V.A. Granadillo, O. Salgado and B. Rodríguez-Iturbe, Acta Cient. Ven., 42 (Suppl. 1) (1991) 176.

ELSEVIER

Analytica Chimica Acta 295 (1994) 199–204

ANALYTICA CHIMICA ACTA

Synthesis of a chelating polymer matrix by immobilizing Alizarin Red-S on Amberlite XAD-2 and its application to the preconcentration of lead(II), cadmium(II), zinc(II) and nickel(II)

Reena Saxena [a], Ajai K. Singh *,[a], S.S. Sambi [b]

[a] *Department of Chemistry, Indian Institute of Technology, New Delhi 110 016, India*
[b] *Department of Chemical Engineering, Indian Institute of Technology, New Delhi 110 016, India*

Received 14th September 1993; revised manuscript received 1st March 1994

Abstract

A very stable chelating resin matrix was synthesized by covalently linking Alizarin Red-S with the benzene ring of the polymer Amberlite XAD-2 through an –N=N– group. The resin was characterized by elemental analyses, thermogravimetric analysis and IR and reflectance spectra. One dye molecule was found to be present per repeat unit of the polymer. The resin was used for the preconcentration of Zn(II), Cd(II), Ni(II) and Pb(II) prior to their determination by flame atomic absorption spectrometry (AAS). For the quantitative sorption and recovery of Zn, Cd, Ni and Pb the optimum pH and eluents were pH 5–6 and 4 M HCl or 1 M HNO_3 for Zn, pH 5–6 and 4 M HNO_3 for Cd, pH 3–4 and 4 M HCl or 2 M HNO_3 for Ni and pH 6 and 3–4 M HNO_3 for Pb. The sorption capacity of the resin was 511, 124, 139 and 306 μg per gram of the resin for Zn, Cd, Ni and Pb, respectively. Tolerance limits of NaF, NaCl, Na_2SO_4, Na_3PO_4 and $NaNO_3$ on the sorption of these metal ions are reported. Sodium nitrate interfered in the sorption of all the metal ions except Pb(II). The preconcentration factor was 40 for all four metals and the lower limit of preconcentration was 0.01 mg dm^{-3}. The simultaneous determination of all the four cations is possible. The relative standard deviation (R.S.D.) is in the range 3.7–8.2%. Zn, Cd, Ni and Pb in well-water samples were determined by AAS after preconcentrating them with the resin. Ni and Cd were found to be absent. The R.S.D. was 2.7–6.5% and 4.7–10.1% for zinc and lead, respectively.

Key words: Atomic absorption spectrometry; Cadmium; Chelating resin; Lead; Nickel; Preconcentration; Waters; Zinc

1. Introduction

The determination of metal ions at very low concentration levels is often carried out by atomic absorption spectrometry (AAS), particularly in the analyses of water, high-purity materials and biological fluids. Prior to such determinations the concentration of the analytes is raised by adopting a preconcentration procedure. The most popular methods for this purpose are liquid–liquid extraction and ion exchange. The use of function-

* Corresponding author.

Elsevier Science B.V.
SSDI 0003-2670(94)00136-A

alized or chelating agent-loaded polymers for preconcentration has the additional advantage of selectivity. Consequently, there is continuing interest [1–8] in developing chelating resins of good stability, which have a high capacity for metal ions and a low analyte–matrix effect and do not need very strict working conditions.

Recently chelating resins were developed [7,8] by loading Pyrocatechol Violet and Xylenol Orange on a polymer matrix through ion exchange and π–π dispersion forces. These resins have good capacities but not the desired high stability. It was therefore thought worthwhile to synthesize a new chelating resin by linking Alizarin Red-S (ARS) with a commercially available styrene–divinylbenzene copolymer, Amberlite XAD-2, through an –N=N– group because such a link is considered to enhance the stability of the resin. A high loading of this moderate-size dye is expected and hence its immobilization in this manner may also give a matrix of reasonably good capacity.

In this paper, the synthesis of Alizarin Red-S-loaded Amberlite XAD-2, its sorption characteristics and its application to the preconcentration of Zn(II), Cd(II), Ni(II) and Pb(II) prior to their determination by flame atomic absorption spectrometry are reported. This matrix was also used to preconcentrate the four metal ions in well-water samples before determining them by flame AAS.

2. Experimental

2.1. Apparatus

AAS measurements were made with a Hitachi Model Z-8100 atomic absorption spectrometer using an air–acetylene flame with air and acetylene flow-rates of 15 and 1.5 $dm^3\ min^{-1}$, respectively. pH measurements were made on an Elico Model LI 120 digital pH meter. Reflectance spectra in the UV–visible region were recorded on a Hitachi Model 330 UV spectrophotometer. IR spectra (4000–200 cm^{-1}) were recorded on a Nicolet DX-5 Fourier transform infrared spectrometer. Thermal analyses were carried out on a Stanton Redcroft Model STA-780 thermal analyser.

2.2. Reagents

Stock standard solutions of Zn(II), Cd(II), Ni(II) and Pb(II) were prepared by dissolving appropriate amounts of analytical-reagent grade cadmium(II) nitrate, zinc(II) nitrate, nickel(II) nitrate and lead(II) acetate, respectively, in doubly distilled water acidified with a small amount of the corresponding acid and standardized titrimetrically [9] with EDTA before use. pH adjustments were made with 0.01–1.0 M HCl and NaOH.

Amberlite XAD-2 resin (surface area 330 $m^2\ g^{-1}$, pore diameter 90 Å and bead size 20–60 mesh) was obtained from Aldrich. Alizarin Red-S (Aldrich) was used as received. All other reagents used were of analytical-reagent grade. The glassware used was soaked in 5% HNO_3 for 1 week before use and cleaned with doubly distilled water. Well-water samples were collected from Janak Puri, New Delhi and Patel Nagar, Gurgaon (India), situated 31 km from New Delhi.

2.3. Synthesis of Alizarin Red-S-loaded Amberlite XAD-2

Amberlite XAD-2 (5 g) was stirred with a nitrating mixture (10 cm^3 of concentrated HNO_3 + 25 cm^3 of concentrated H_2SO_4) on an oil-bath at 60°C for 30 min. The reaction mixture was poured into ice–water. The nitrated resin was filtered, repeatedly washed with water until free from acid, mixed with $SnCl_2$ (40 g), concentrated HCl (45 cm^3) and ethanol (50 cm^3) and refluxed for 10 h at 90°C. The amino-polymer was filtered off and washed with water and 2 M NaOH, which released the free amino-polymer according to the following equation:

$$(RNH_3)_2SnCl_6 + 8NaOH \rightarrow 2RNH_2 + Na_2SnO_3 + 6NaCl + 5H_2O \quad (1)$$

The amino-polymer was treated with 2 M HCl, washed with water to remove excess of HCl, suspended in 350 cm^3 of ice–water and mixed

with 1 M HCl–1 M $NaNO_2$ solution (added in aliquots of 1 cm^3) until the reaction mixture began to give a permanent blue colour with starch–iodide paper. The diazotized polymer was filtered, washed with cold water and reacted with Alizarin Red-S (2 g in 400 cm^3 of water and 200 cm^3 of glacial acetic acid) at 0–3°C for 24 h. The brown beads were filtered and washed. Elemental analysis: found, C 54.72, H 3.43, N 6.02, S 6.72; calculated for $C_{22}H_{19}SN_2O_9$, C 54.21, H 3.90, N 5.80, S 6.60%.

2.4. Recommended procedure for preconcentration and determination of zinc, cadmium, lead and nickel

A glass column (1 cm i.d.) was packed with 1 g of Amberlite XAD-2 loaded with ARS. It was treated with 20 cm^3 of 4 M HCl and washed with water until free from acid. A suitable volume of solution containing zinc(II), cadmium(II), lead(II) or nickel(II) at levels from 10 $\mu g\ dm^{-3}$ to 25 μg per 50 cm^3 was passed through this column after adjusting its pH to an appropriate level as given in Table 1 at an optimum flow-rate (Table 1) so that the total load of metal on the column was 10–25 μg. The column was washed with 15 cm^3 of HCl or HNO_3 (concentrations are given in Table 1). The volume of the eluate was made up to 25 cm^3 and its zinc, cadmium, lead or nickel content was determined directly at 213.9, 228.8, 212 and 232 nm, respectively, by aspirating it into the flame of the AAS instrument standardized prior to the determination.

3. Results and discussion

The ARS-loaded Amberlite XAD-2 (resin–ARS) is formed as a result of the sequence of chemical reactions shown.

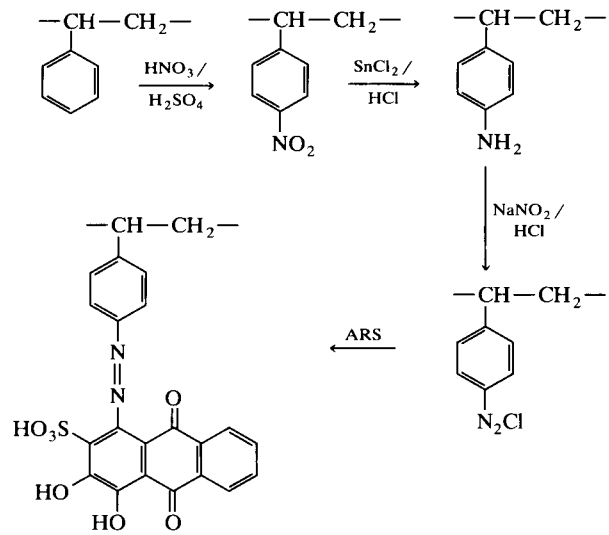

(2)

The reflectance spectrum of resin–ARS exhibits a broad shoulder from 400 to 490 nm. Pure Amberlite XAD-2 exhibits very little absorbance in this region, whereas Alizarin Red-S shows a

Table 1
Optimum conditions for sorption and desorption of metal ions

Parameter	Metal ions			
	Zn(II)	Cd(II)	Ni(II)	Pb(II)
pH range	5–6	5–6	3–4	6
Flow-rate ($cm^3\ min^{-1}$)	2–5	2	3	3–4
Acid concentration for desorption	1 M HNO_3 or 4 M HCl	4 M HNO_3	4 M HCl or 2 M HNO_3	3–4 M HNO_3
Capacity of sorption ($\mu g\ g^{-1}$ resin)	511	124	139	306
Average recovery (%)	97	98	98	97
Standard deviation [a] ($mg\ dm^{-3}$)	0.123	0.55	0.103	0.073
R.S.D. (%)	8.2	4.1	3.7	6.6

[a] In six determinations of 1.5 $mg\ dm^{-3}$ Zn, 1.4 $mg\ dm^{-3}$ Cd, 2.8 $mg\ dm^{-3}$ Ni and 1.1 $mg\ dm^{-3}$ Pb.

broad peak at 470 nm. This observation is in agreement with formation of ARS-loaded resin in reaction 2. The thermogravimetric analysis (TGA) curve for resin–ARS shows a very slow but steady weight loss up to 600°C. It was 8% up to 130°C, supporting the presence of two molecules of H_2O per unit of polymer. The elemental analysis of resin–ARS suggests that on average one dye molecule per unit of polymer is present. As dinitration of the benzene ring of the polymer is not expected under the present experimental conditions, it is reasonable to assume that with each ring one dye molecule is covalently bonded through an azo group. Most probably it occupies a position *para* to the $-CH-CH_2-$ group, owing to electronic effects and steric reasons. The infrared spectrum (Fig. 1) of resin–ARS exhibits additional bands at 1640, 1535 and 1440 cm^{-1} which do not appear in the IR spectrum of Amberlite XAD-2. These originate from ARS and are characteristic of 1,4-quinone, the $-N\equiv N-$ group and the C–O bond, respectively. All these observations point to the formation of an ARS-loaded polymer matrix.

Table 2
Tolerance limits of electrolytes in sorption

Metal ion	Electrolyte (mol l^{-1})				
	NaF	NaCl	$NaNO_3$	Na_2SO_4	Na_3PO_4
Cd(II)	0.50	0.05	Int [a]	0.05	Int
Pb(II)	0.50	0.50	0.20	0.10	0.01
Ni(II)	0.50	0.01	Int	0.01	Int
Zn(II)	0.50	0.20	Int	0.20	0.01

[a] Int = interferes.

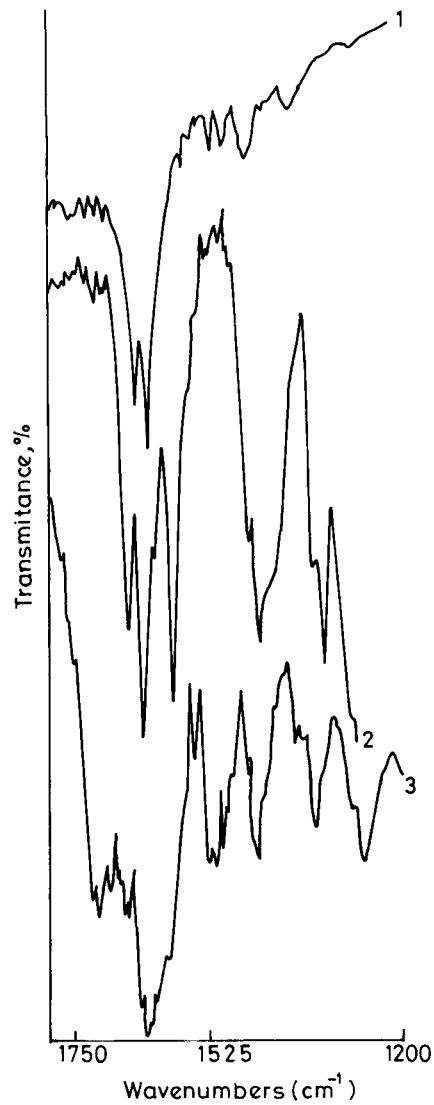

Fig. 1. Infrared spectra: 1 = Amberlite XAD-2; 2 = Alizarin Red-S; 3 = Alzarin Red-S-loaded Amberlite XAD-2.

3.1. Optimum conditions for sorption

A column of 1 cm i.d. was filled with nearly 1 g of ARS-loaded Amberlite XAD-2, treated with 20 cm^3 of 4 M HCl and washed with water. It was standardized for sorption and desorption of Zn(II), Cd(II), Ni(II) and Pb(II). The optimum conditions for ca. 100% sorption and desorption are given in Table 1. Flow-rates less than 2 cm^3 min^{-1} were not studied in order to avoid a long analysis time. Similarly for desorption an acid concentration > 4 M was not used because it would have to be partially neutralized in the eluate, which would lower the preconcentration factor.

3.2. Effect of electrolyte and cations

The effect of fluoride, chloride, nitrate, sulphate and phosphate ions (added as sodium salts) on sorption was studied. The results are reported

Table 3
Parameters at preconcentration limit

Metal ion	Volume of solution passed [a]	Concentration (mg dm^{-3})	Recovery (%)	Preconcentration factor [b]
Cd(II)	1000	0.01	95	40
Pb(II)	1000	0.01	100	40
Ni(II)	1000	0.01	95	40
Zn(II)	1000	0.01	100	40

[a] The total amount of each metal ion was 10 μg.
[b] The final volume after elution from column was 25 cm^3.

in Table 2. NO_3^- does not interfere much with Pb(II) as reported earlier [4] for a resin derived by reaction of semicarbazone of 2-hydroxyacetophenone, substituted benzoic acid and formaldehyde. Hg(II) does not interfere up to 2 mg dm^{-3} in the determination of 1 mg dm^{-3} Zn and 2 mg dm^{-3} of Cd or Pb; 0.5 mg dm^{-3} of Cu(II), Co(II), Fe(II), and Cr(III) can co-exist with 1 mg dm^{-3} of either of the four metal ions.

3.3. Limit of preconcentration and preconcentration factor

The recovery of Zn, Cd, Pb and Ni was $\geqslant 95\%$ at the 0.01 mg dm^{-3} concentration level (Table 3). At lower concentrations than these limiting values the results were not quantitative and showed poor reproducibility. The preconcentration factor was 40 for all four metals. They can be preconcentrated simultaneously if their total amount does not exceed the capacity of the resin column.

3.4. IR spectra of metal ion-sorbed Amberlite XAD-2 loaded with Alizarin Red-S

Under optimum conditions the four metal ions were sorbed on the chelating resin and the IR spectra of the resins were compared with that of the metal ion-free chelating resin. The bands due to the 1,4-quinone and –N≡N– groups undergo a red shift of 10–12 cm^{-1} whereas the C–O frequency undergoes a blue shift of 20 cm^{-1}. The νOH band appears between 3400 and 3500 cm^{-1} as a sharp band in these spectra. This suggests that metal ions are coordinated by oxygen of the 1,4-quinone and nitrogen of the azo group during sorption on the chelating matrix. The pH of maximum sorption also agrees with the non-involvement of phenolic OH in the coordination of the dye with the metal ions during their retention on the chelating resin matrix.

The main advantage of the present matrix in comparison with other commonly used resins is its high precision. The most promising chelating resin having a lower analyte–matrix effect suitable for determining these metal ions in water samples is Chelex 100 [10–12]. The present resin has a lower preconcentration factor than Chelex 100 but gives a much better precision at ng cm^{-3} concentrations as the relative standard deviation obtained with Chelex 100 is $\geqslant 15\%$. In comparison with other chelating matrices such as quinolin-8-ol-loaded silica [13] used for these metal ions, the preconcentration factor with the present resin is comparable, but the additional advantage is the greater tolerance limits for anions. The preconcentration factor of the present resin is better than that of mercapto-modified silica gel [14] and dithizone-loaded Amberlite XAD-2 [15]. The sorption capacity was maximum for Zn because of its smaller size. The recoveries are comparable to those obtained [1] with ion exchangers, other chelating resins, polyurethane foam and polystyrene beads. The desorption is instantaneous, which is also an advantage of the present chelating resin. The sorption of all four metal ions is faster than or comparable to that with other commonly used chelating resins and ion exchangers. The resin is very stable because the dye is not released on repeated use for several months. This is evident from the sorption capacity, which is found to be almost unchanged even after using the same column several hundred times after regenerating it with 4 M HCl every time.

3.5. Determination of zinc and lead in well water

Well-water samples collected from New Delhi and Gurgaon (India) were subjected to the recommended procedures directly and after stan-

Table 4
Determination of Pb and Zn in the underground water samples

Origin of sample	Method	Amount of zinc ($\mu g\ dm^{-3}$)	R.S.D. (%)	Amount of lead ($\mu g\ dm^{-3}$)	R.S.D. (%)
New Delhi	Direct	1.5	6.5	0.07	10.1
	SA	1.7	5.2	0.05	4.7
	Extraction [a]	1.4	5.0	0.05	5.2
Gurgaon	Direct	3.6	2.7	0.12	9.2
	SA	3.8	3.2	0.11	5.3
	Extraction [a]	3.4	2.6	0.10	6.0

[a] APDC–MIBK extraction method [16].

dard additions for determining their Ni, Pb, Zn and Cd contents. Ni and Cd were found to be absent. The results for Pb and Zn are given in Table 4. The relative standard deviation in the direct determination of lead is higher owing to its lower concentration levels.

Acknowledgement

Financial support of this work from the Council of Scientific and Industrial Research (India) is gratefully acknowledged.

References

[1] C. Kantipuly, S. Katragadda, A. Chow and H.D. Gesser, Talanta, 37 (1990) 491.
[2] G. Persaud and F.F. Cantwell, Anal. Chem., 64 (1992) 89.
[3] X. Cheng, X. Luo, G. Zhan and Z. Su, Talanta, 39 (1992) 937.
[4] T.K. Bastia, S. Lenka and P.L. Nayak, J. Appl. Polym. Sci., 46 (1992) 739.
[5] M.C. Yebra-Biurrum, A. Bermejo-Barrera and M.P. Bermejo-Barrera, Analyst, 116 (1991) 1033.
[6] M.C. Yebra-Biurrum, M.C. Garcia-Dopazo, A. Bermejo-Barrera and M.P. Bermejo-Barrera, Talanta, 39 (1992) 671.
[7] A.K. Singh, and S.K. Dhingra, Analyst, 117 (1992) 891, and references cited therein.
[8] A.K. Singh and P. Rita, Microchem. J., 43, (1991) 112.
[9] A.I. Vogel, A Text Book of Quantitative Inorganic Analysis, Longman, London, 3rd edn., 1973.
[10] A.J. Paulson, Anal. Chem., 58 (1986) 183.
[11] R.R. Greenberg and H.M. Kingston, Anal. Chem., 55 (1983) 1160.
[12] H.M. Kingston, I.L. Barnes, T.J. Brady, T.C. Rains and M.A. Champ, Anal. Chem., 50 (1978) 2064.
[13] R.E. Sturgeon, S.S. Berman, S.N. Willie and J.A.H. Desanlriens, Anal. Chem., 53, (1981) 2337.
[14] J.W. McLaren, A.P. Mykytiuk, S.N. Willie and S.S. Berman, Anal. Chem., 57 (1985) 2907.
[15] J. Chwastowska and E. Kosiarska, Talanta, 35 (1988) 439.
[16] R.R. Brooks, B.J. Presley and I.R. Kaplan, Talanta, 14 (1967) 809.

ELSEVIER

Analytica Chimica Acta 295 (1994) 205–210

ANALYTICA CHIMICA ACTA

Determination of sulphur by tin, aluminium and indium monosulphide molecular absorption spectrometry using sharp line irradiation sources

Pekka Parvinen *, Lauri H.J. Lajunen

Department of Chemistry, University of Oulu, SF-90570 Oulu, Finland

Received 8 January 1994

Abstract

Methods for the determination of sulphur by high-temperature molecular absorption spectrometry were investigated. Sulphur was determined via the molecular absorption of aluminium, indium and tin sulphides using hollow-cathode lamps of different elements as irradiation sources for the measurements. The best result was obtained when sulphur was measured as tin sulphide and was almost as good when measured as indium sulphide. The methods were tested for the determination of sulphur in some organic compounds and in rain-water samples.

Key words: Atomic absorption spectrometry; Molecular absorption spectrometry; Sulphur

1. Introduction

Current methods for the determination of sulphur are often cumbersome, insensitive and time consuming and require substantial sample pretreatment, e.g., by ion exchange. Direct atomic absorption spectrometric (AAS) methods for the determination of sulphur are impossible because the resonance lines of sulphur lie in the vacuum ultraviolet region. For the determination of sulphur a simple, sensitive and precise molecular absorptiometric method would provide a much needed analytical tool. Molecular absorption of aluminium and indium sulphides has been proposed earlier for the determination of sulphur [1]. Aluminium sulphide formed in the graphite furnace has a strong molecular absorption band at 219.2 nm and indium sulphide at 234.5 nm. In previous studies a deuterium lamp was used as a light source. However, the use of a continuum light source causes some problems related to slit width and background correction. In the case of the slit width, the sensitive measurement of molecular absorption requires a narrow spectral bandpass and if the background correction is performed at the same wavelength a wide spectral bandpass is needed. That is why the absorption intensity measured at a point where molecular absorption is minimal was subtracted from that measured at the molecular absorption band using a two-channel spectrometer [2]. These two

* Corresponding author.

SSDI 0003-2670(94)00173-J

problems can be avoided by using a line-like irradiation source for the molecular absorption measurements.

In this work, the use of atomic lines of different elements was examined for the determination of sulphur as aluminium and indium sulphides. In addition to aluminium and indium sulphides, the absorption of tin and barium sulphide [3] was tested for determination of sulphur by molecular absorption spectrometry.

2. Experimental

2.1. Apparatus

The molecular absorption of aluminium and indium sulphides was measured with PU 9200 and Pye Unicam SP-9 and tin and barium sulphides with Pye Unicam SP-9 atomic absorption spectrometers equipped with deuterium lamp background correction systems for simultaneous background correction. Measurements were made using ordinary uncoated graphite furnaces. Argon was used to purge the air from the furnace. Cathodeon iron, copper and tungsten hollow-cathode lamps were used as irradiation sources for the determination of aluminium sulphide molecular absorption and Cathodeon arsenic, cobalt and nickel hollow-cathode lamps for the molecular absorption of indium sulphide. In the measurement of the molecular absorption of tin sulphide Cathodeon iron, molybdenum, tungsten and chromium hollow-cathode lamps were used. The spectral bandwidth of the monochromator was usually set at 0.2 nm.

2.2. Procedure

The experimental conditions for the measurement of aluminium and indium sulphide molecular absorption are given in Table 1 and for the measurement of tin sulphide in Table 2. Cobalt and strontium (0.01 M) were added to the aluminium solution (0.01 M) and iron (0.01 M) to the indium solution (0.01 M) in order to enhance the sensitivity and to improve the precision of the measurements. The measurement of tin sulphide molecular absorption was done using tin(II) chloride solution (0.01 M).

Table 1
Experimental conditions for determination of sulphur via aluminium and indium sulphide molecular absorption spectrometry

Conditions	AlS	InS
Injection of sulphur solution	10 μl	10 μl
Injection of aluminium solution	15 μl	15 μl
Drying conditions	110°C, 10 s	110°C, 10 s
Ashing conditions	700°C, 10 s	200–600°C, 10 s
Evaporation and measurement conditions	2200°C, 3 s	2200°C, 3 s

2.3. Chemicals

All the reagents were of analytical-reagent grade from Merck. Standard solutions were prepared by dissolving the corresponding metal nitrates or chlorides and sodium sulphate in deionized, distilled water.

3. Results and discussion

3.1. Aluminium sulphide molecular absorption

The aluminium sulphide molecular absorption maximum lies at 219.2 nm. Iron, copper and tungsten have suitable emission lines for the determination of aluminium sulphide molecular absorption at this maximum [4]. The wavelengths of the emission lines and the absorption intensities measured are given in Table 3. On the basis of these data, the iron hollow-cathode lamp seems

Table 2
Experimental conditions for the determination of the sulphur via tin sulphide molecular absorption spectrometry

Injection of the tin solution	10 μl
Drying	110°C, 10 s
Ashing	800°C, 10 s
Injection of sulphur solution	10 μl
Drying	110°C, 10 s
Ashing	400°C, 10 s
Evaporation and measurement	2200°C, 4 s

Table 3
Molecular absorption of aluminium sulphide measured by emission lines of different elements

Element	Wavelength (nm)	Relative absorption (%)
Fe	219.18	100
Cu	219.23	8
W	219.21, 219.45	31

to be the most suitable light source for the measurement of the aluminium sulphide molecular absorption. For copper and tungsten the observed absorbances were weak. Different types of aluminium solution were investigated in order to find the most suitable aluminium reagent solution to bind the sulphur during the drying and ashing steps. The most difficult problem is the escape of sulphur as sulphur dioxide during these steps. The solutions tested were aluminium with silver, cobalt, barium and strontium and their mixtures as 0.01 M solutions. Comparisons of these aluminium solutions were done by measuring the absorptions caused by 100 mg l^{-1} sulphur using each of these solutions (Table 4). The best results were obtained by using pure aluminium solution, but almost as good results were given by aluminium–cobalt–strontium solutions. The detection limit when measuring sulphur as aluminium sulphide was 6 mg l^{-1}.

Table 4
Molecular absorption of aluminium sulphide measured using different aluminium solutions

Al solution used	Concentration (M)	Relative absorption measured (%)
Al	0.01	100
Al–Co	0.01	16
Al–Ag	0.01	44
Al–Sr	0.01	31
Al–Ba	0.01	40
Al–Ag–Sr	0.5	123
Al–Ag–Sr	0.01	67
Al–Co–Sr	0.01	87
Al–Ba–Sr	0.01	19

3.2. Indium sulphide molecular absorption

Indium sulphide has a molecular spectrum at 220–250 nm, containing a strong molecular band at 234.5 nm [2], which has been used previously for determinations by a continuum source method. Close to this band lie the emission lines of cobalt, iron, nickel, arsenic and tungsten. However, these emission lines did not overlap sufficiently with the absorption maximum of InS for measurements to give good results. Hence other lines of platinum, iron, cadmium and tungsten were tested in the area of the molecular spectra (Table 5). When using the platinum line at 234.0 nm, the absorptions measured were the highest,

Table 5
InS molecular absorption (A) measured by different atomic lines

Pt		Pt		W		Fe	
Wavelength (nm)	A	Wavelength (nm)	A	Wavelength (nm)	A	Wavelength (nm)	A
225.7	0.038	234.0	0.184	225.1	0.037	225.2	0.060
226.2	0.029	234.7	0.028	227.7	0.033	227.4	0.010
226.7	0.048	235.7	0.018	228.3	0.003	227.9	0.019
227.4	0.008	236.7	0.014	230.1	0.078	229.8	0.001
228.9	0.034	237.7	0.015	231.4	0.042	230.9	0.040
229.8	0.064	238.3	0.018	232.2	0.026	233.3	0.035
230.3	0.023	239.6	0.030	232.6	0.032	233.8	0.001
230.8	0.021	240.2	0.020	232.8	0.056		
231.3	0.030	241.8	0.058				
231.8	0.025	242.8	0.014				
232.6	0.026	243.7	0.093				
233.1	0.031	244.0	0.030				

Underlined values are moderate or high absorbances measured.

but the background absorption caused by In_2 molecular absorption [3] interfered seriously. The platinum hollow-cathode lamp was found to be the most suitable irradiation source for the measurements of indium sulphide molecular absorption when using the emission line at 243.7 and the weaker line at 241.8 nm. Iron, bismuth, barium, thallium, coper, chromium, lead, nickel and zinc were added to the indium solutions in order to find the most suitable chemical modifier and solution to bind the sulphur during the drying and ashing steps. Ba or Cr (0.01 M) containing indium solutions gave the best results when using a chemical modifier containing indium and one other metal. On the other hand, higher concentrations of indium in the solution gave higher absorbances on increasing the concentration from 0.01 to 0.1 M. Of the different combinations of metals in the chemical modifier, In–Ba–Co–Sr and In–Co–Sr solutions gave the best results. Higher concentrations of silver and strontium containing indium solution gave the highest absorptions but at the same time the background absorption became high and unstable. However, when measuring sulphur in organic compounds, 0.1 M indium solution was almost as good as the In–Co–Sr solution as a chemical modifier. The use of higher concentrations of indium solutions caused an increase in the background absorption. When measuring sulphur in organic compounds it is necessary to decrease the temperature of ashing in order to avoid the escape of sulphur because the metals added to indium solutions are not able to bind and effectively prevent the escape of sulphur during this step. The detection limit when measuring the sulphur as indium sulfide was 2–5 mg l^{-1}. The best results with the lowest detection limits were obtained when using uncoated graphite furnaces.

3.3. Tin sulphide molecular absorption

Tin sulfide has strong ($I = 10$) absorption bands between 271 and 316 nm and between 418 and 451 nm [3]. The molecular absorption was measured at each of those bands using hollow-cathode lamps of metallic elements. In Table 6 these bands and possible elements having emission lines near those wavelengths are presented. Weak absorptions were measured using the molybdenum line at 308.9 nm, the chromium line at 296.7 nm and the iron line at 316.4 nm. The best results with the strongest absorptions was measured using the emission lines of tungsten at 273.578 and 273.597 nm, so the tungsten hollow-cathode lamp was selected for the measurement of sulphur. In order to improve the sensitivity, drying and ashing steps were added to the furnace programme after the injection of the tin solution, before the injection of the sample solution. In this way the excess of chlorine is removed when using a chlorine-containing tin solution. Many metallic elements forming fairly stable molecules with sulphur. Sulphur was determined in solutions containing 1 g l^{-1} of some metallic elements in order to evaluate the possible interferences caused by these elements (Table 7).

Table 6
Strong molecular absorption bands of SnS and elements having emission lines close to them

Wavelength of SnS line (nm)	Elements having emission line at same wavelength
424.86	Cr, Cr, Fe
418.38	W
316.39	Fe, Mo
311.68	W
308.91	W, V, Mo
299.26	Fe
296.77	Cr
290.21	W, Ag
287.92	W, V
273.58	W, W, Mo

Table 7
Determination of sulphur in solutions containing 100 mg l^{-1} of sulphur and 1 g l^{-1} of interfering element

Interfering element	Amount of sulphur found (mg l^{-1})
Mn	49
Ba	49
Cu	75
Sr	81
Mg	82
Na	95
Ca	97

Table 8
Detection limits of SnS, AlS, InS and BaS by molecular absorption measurement

Molecule to be measured	Detection limit (mg l^{-1})
SnS	1
InS	2–5
AlS	6
BaS	10

These interferences are generally not very serious. The strongest interferences were caused by barium and manganese. However, all of these interferences of the different metals are usually negligible with real samples. The detection limit when measuring sulphur as tin sulphide is about 1 mg l^{-1}.

3.4. Barium sulphide molecular absorption

Barium sulphide has a molecular band at 370.20 nm [3] and the emission line of iron lies at the same wavelength. The absorption of possible BaS was measured at this wavelength using barium solutions containing cobalt, strontium and indium. The formation of BaS is most effective at higher temperatures than the formation of AlS and InS. Hence it can be concluded that thermally stable BaS is not formed at the temperatures where AlS and InS are formed. The determination of sulphur via the BaS molecular absorption is less sensitive than for the other sulphides tested (Table 8).

Table 9
Determination of sulphur in organic compounds using InS molecular absorption

Compound	Theoretical amount (%)	Measured (%)
Sodium toluene *p*-sulphonate ($CH_3C_6H_4SO_3 \cdot 2H_2O$)	13.9	14.1
Thiosalicylic acid (HSC_6H_4COOH)	20.8	20.0
Sodium 5-sulpho-3-hydroxy-benzoate ($C_7H_6O_6SNa$)	13.4	13.4
Sodium 3′,3′-dibromothymol-sulphonaphthalein ($C_{22}H_2O_5Br_22SNa$)	5.7	6.1

Table 10
Determination of sulphur via SnS molecular spectrometry absorption (MAS) and sulphate sulphur by turbidimetry in rain-water samples

Sample No.	Sulphur (mg l^{-1})	
	MAS	Turbidimetry
1	4.2	3.6
2	6.0	5.3

3.5. Determination of sulphur in real samples

The method for the determination of sulphur via the InS molecular absorption was tested by measuring sulphur in some organic compounds. Before the measurement, samples were dissolved in ethanol or water. Of the compounds tested, thiosalicylic acid was dissolved in ethanol and sodium toluene-*p*-sulphonate, sodium 5-sulpho-3-hydroxybenzoate and sodium 3′,3′-dibromothymolsulphonaphthalein in water. The measurements were made using a 0.01 M indium solution containing cobalt and strontium. The indium sulphide molecular absorption was measured using the platinum emission line at 243.67 nm. The results obtained in these measurements are in good agreement with theoretical amounts of sulphur in these samples (Table 9).

In order to test the method for the determination of sulphur via the SnS molecular absorption, sulphur was determined in two rain-water collector (NILU) samples (collection time 3 months) together with the determination of the sulphate sulphur by a turbidimetric method. The results obtained by molecular absorption, that is, measuring the total sulphur, agreed with the amounts of the sulphate sulphur measured (Table 10).

4. Conclusions

The methods for the determination of sulphur by molecular absorption using sharp line irradiation sources are sensitive and accurate. The sen-

sitivity when measuring sulphur as aluminium sulphide using an iron hollow-cathode lamp as the irradiation source is almost the same as that obtained by a continuum source method. The determination of sulphur as indium sulphide using a platinum hollow-cathode lamp is less sensitive than that using a continuum source method because no suitable lines of a metallic element lie at the InS absorption maximum. The measurements based on the barium sulphide molecular absorption gave moderate absorbances, but the determination of sulphur as barium sulphide was less sensitive than that for indium or aluminium sulphide.

The most useful methods for the determination of sulphur by molecular absorption using a sharp line irradiation source is to measure it as tin sulphide by the tungsten line at 273.5 nm or indium sulphide by the platinum line at 243.67 nm. A better detection limit was obtained with SnS. These measurement for the determination of sulphur are simple, no sample pretreatment is needed and they are easy to automate. The measurement of tin or indium sulphide by molecular absorption spectrometry may be useful for the practical determination of sulphur.

References

[1] K. Dittrich, B. Vorberg, J. Funk and V. Beyer, Spectrochim. Acta, Part B, 39 (1984) 349.
[2] K. Fuwa, Recent Advances in Analytical Spectroscopy, Pergamon Press, Oxford, 1981, p. 121.
[3] R.W.B. Pearse and A.G. Gaydon, The Identification of Molecular Spectra, Chapman and Hall, London and Wiley, New York, 4th edn., 1976, p. 68.
[4] G.R. Harrison, M.I.T. Wavelength Tables, M.I.T. Press, 1969.

ELSEVIER

Analytica Chimica Acta 295 (1994) 211–219

ANALYTICA CHIMICA ACTA

Improved catalytic photometric determination of iron(III) in cetylpyridinium premicellar aggregates

A. Alexiev [a,*], S. Rubio [b], M. Deyanova [a], A. Stoyanova [a], D. Sicilia [b], D. Pérez Bendito [b]

[a] *Department of Chemistry and Biochemistry, Medical University, 5800 Pleven, Bulgaria*
[b] *Department of Analytical Chemistry, Faculty of Sciences, University of Córdoba, Córdoba, Spain*

Received 29th March 1994

Abstract

Premicellar aggregates of the cationic surfactant cetylpyridinium chloride (CPC) enhance the catalytic activity of iron(III) on the oxidation of sulphanilic acid by potassium periodate in the presence of 1,10-phenanthroline as activator. The aggregates however have no effect on the uncatalysed reaction. The kinetic study presented in this paper shows that the effects of CPC on the iron(III)-catalysed reaction can be entirely attributed to increased reactant concentrations in the surfactant micelle subunits. The iron(III) effective concentration in the reaction medium is increased by formation of a transient catalyst–sulphanilic acid complex in the catalytic cycle which concentrates on the premicellar aggregates. Such an effect of CPC was exploited for the kinetic photometric determination of iron(III) over the linear range $0.1–4.0 \times 10^{-7}$ M with a detection limit of 3.37×10^{-9} M. (i.e., 7 times lower than that of the method using an aqueous medium). The relative precision for 2.0×10^{-7} M of iron(III) was 5%. The proposed method is highly sensitive and selective and was applied to the determination of iron in blood serum samples.

Key words: Catalytic methods; Iron; Cetylpyridinium premicellar aggregates

1. Introduction

Micellar catalysis has been used more frequently in the last few years to improve the sensitivity, rapidity, simplicity and, to a lesser extent, selectivity, of catalytic methods [1]. Since the primary source of the increased rates observed in most of the reactions concerned is the increased reactant concentration in the micellar pseudophase, the catalyst or reaction accelerator must concentrate in the pseudophase so that the sensitivity for its determination is improved relative to that obtained in an aqueous medium. Our experience in catalysed reactions tells us that direct concentration of the catalyst at the micellar surface is rendered unlikely by exclusion phenomena arising from substrates present in the reaction medium at concentrations which are fre-

* Corresponding author.

SSDI 0003-2670(94)00172-1

quently higher than that of the catalyst by a few orders of magnitude. For this reason, various alternative strategies have been developed to increase the sensitivity of catalytic kinetic methods in micellar media [1], namely: (a) formation of a stable catalyst–substrate complex that is concentrated on micelles [2,3], (b) use of multistep reactions [4,5] and (c) concentration of the monitored species within micelles [6].

In this work, strategy a was extended to reactions in which the catalytic cycle involves formation of a transient catalyst–substrate complex. This approach could theoretically be applied to many catalysed redox reactions where the catalyst (C) reacts with a substrate (A) to yield the product (P) and its own activated form (C*), from which it is regenerated on subsequent reaction with another substrate (B) to yield Y according to the following scheme:

$$A + C \leftrightarrow P + C^*$$

$$C^* + B \xrightarrow{\text{fast}} Y + C$$

Most catalytic methods are based on reactions of this type, where the formation of species C* involves a change in the oxidation state of the catalyst. When A is an organic substrate, interaction between A and C generally entails the prior formation of a charge-transfer complex between both species, which in turn requires that C be temporarily concentrated at the micellar surface if substrate A is concentrated by a group other than that via which the catalyst forms the complex. Since this step will be the rate determining step, the resulting local concentration of the catalyst can result in a more sensitive determination.

In order to test this approach, sulphanilic acid (SA), which has been used as a general substrate for catalytic determinations [7], was chosen as substrate A. The acid associates to cationic surfactant aggregates through electrostatic interactions with the sulphonic group, which faces the functional amine group. The oxidation of SA by periodate is reportedly catalysed by iron(III) in the presence of 1,10-phenanthroline as an activator, the reaction between SA and the unsaturated, positively charged, 1:1 Fe(III)–1,10-phenanthroline complex being the rate-determining step [8]. Inasmuch as four vacant coordination places in the inner coordination sphere of iron(III) exist, occurrence of an SA–Fe(III)–1,10-phenanthroline ternary complex transiently concentrated on the surfactant aggregate, is possible. The results obtained in relation to the influence of the cationic surfactant cetylpyridinium chloride (CPC) on the SA oxidation reaction demonstrate the advantages in terms of sensitivity and detection limit of using this surfactant for the kinetic determination of iron(III) at the nanomolar level; therefore, the proposed approach allows surfactant aggregates to be used in order to improve many other catalytic kinetic methods. On the other hand, because CPC is catalytically active in this reaction, even at submicellar concentrations, the true rate constant on the submicellar pseudophase can be calculated in order to determine whether the observed rate-enhancing effect of these aggregates is due to medium- or concentration-related effects [9].

2. Experimental

2.1. Apparatus

Kinetic measurements were made on both a Specol 11 and a Hitachi U-2000 spectrophotometer fitted with 5- and 1-cm cells, respectively. The spectrophotometer cell compartments were thermostated by means of circulating water. A conventional stalagmometer was used for surface tension measurements in order to determine the critical micelle concentration of the surfactant [10].

2.2. Reagents

Because of the high sensitivity of the reaction, special care was exercised as regards the purity of the materials and reagents used. All solutions were prepared from analytical-reagent grade chemicals and doubly-distilled water. Special attention was given to the iron assay of the reagents. The laboratory glassware was treated with an alkaline solution, and then kept in HCl (1:1) overnight, followed by rinsing with distilled and

doubly-distilled water. A stock Fe(III) solution ($\simeq 0.1$ M) was prepared by dissolving $\simeq 7$ g of $FeCl_3 \cdot 6H_2O$ (Reanal) in 250 ml of 2 M HCl (Merck). Its exact concentration was determined gravimetrically. Working strength solutions (7.5×10^{-6} M) were prepared daily by appropriate dilution with 0.01 M HCl. Aqueous solutions of sulphanilic acid (7.5×10^{-2} M, Fluka), potassium periodate (1.88×10^{-2} M, Fluka), 1,10-phenanthroline (7.5×10^{-3} M, Gliwice, Poland), sodium chloride (0.154 M, Merck) and cetylpyridinium chloride (3.75×10^{-3} M, Serva) were also prepared. Acetate buffers (1 M) of pH range 4.0–6.0 were prepared by mixing appropriate volumes of 1 M acetic acid and 1 M sodium hydroxide solutions. Finally, a protein precipitant solution was prepared by mixing 3 ml of thioglycolic acid and 97 ml of 0.6 M trichloroacetic acid in 2 M hydrochloric acid.

2.3. Recommended procedure for the kinetic determination of iron(III)

In a three-compartment reaction vessel was placed, 0.6 ml of sulphanilic acid (7.5×10^{-2} M) in the first; 0.8 ml of periodate (1.88×10^{-2} M) in the second and 0.0–0.4 ml of Fe(III) (7.5×10^{-6} M) plus 0.2 ml of CPC (3.75×10^{-3} M) and 0.1 ml of 1,10 – phenanthroline (7.5×10^{-3} M) in the third compartment. A volume of 5.8–5.4 ml of acetate buffer at pH 6.0 was divided into three approximately equal aliquots and added to each compartment, so the overall volume of the reaction mixture (7.5 ml) was roughly the same in each experiment. After the reaction ingredients were warmed to 40°C and mixed vigorously by shaking, the reaction mixture was transferred to a 5-cm cell and the absorbance at 360 nm recorded as a function of time. The reaction rate was calculated from the absorbance–time kinetic curves by using the tangent method. When the "fixed time" method was used the reaction vessel was returned to the thermostat after the reagents were mixed and the absorbance was measured at a fixed time of 10 min. The signal given by the blank solution was subtracted from those obtained for the samples.

2.4. Determination of iron(III) in human serum

A volume of 0.1 ml of blood serum was deproteinated by adding 0.1 ml of protein precipitant solution. After 5 min, the mixture was centrifuged at 3000 rpm (1000 *g*) for 15 min and 0.1 ml of the supernatant was diluted with 0.4 ml of 0.154 M sodium chloride solution. Aliquots of the diluted sample (0.1 ml) were analysed as described above.

2.5. Kinetics

Kinetic data for the oxidation reaction between sulphanilic acid and IO_4^-, catalysed by Fe(III)–1,10-phenanthroline in the presence of CPC, were obtained spectrophotometrically. In order to calculate the observed first-order rate constants, k_{obs} (s^{-1}), for this reaction, in a 10-ml volumetric flask were placed, in sequence, 4.0 ml of acetate buffer (2.0 M, pH 6), 1 ml of 6.0×10^{-2} M sulphanilic acid, 0.2 ml of 5.0×10^{-3} M 1,10-phenanthroline, 0.2 ml of 1.0×10^{-5} M Fe(III), appropriate volumes of CPC solution to give a final concentration between 0 and 1.0×10^{-4} M, and 0.2 ml of 8.0×10^{-4} M potassium periodate. An aliquot of the reaction mixture was transferred into a thermostated cell at 40 ± 0.1°C and the absorbance increase ($\lambda = 360$ nm) recorded as a function of time. Absorbance data were acquired and processed by the microcomputer using a rate-constant calculation program for obtaining the observed rate constants (k_{obs}). The constants were calculated from plots of $\ln(A_\infty - A_t)$ vs. time. The quoted k_{obs} values are the means of 5 measurements, so the accuracy of k_{obs} values was estimated to be better than $\pm 6\%$.

The model used to analyse kinetic data was essentially that developed by Berezin et al. [9], where the chemical reaction is assumed to take place in two pseudophases, one associated with the surfactant aggregates and the other with the bulk solvent. By using this model and the experimentally obtained k_{obs} values, the following parameters were estimated using the expressions shown below: second order rate constants (k_ψ, l mol^{-1} s^{-1}) as a function of the CPC concentration; the "true" second order rate constant for the reaction taking place in the CPC aggregates

(k_m, l mol^{-1} s^{-1}); and the association constant of sulphanilic acid to these aggregates (K_{SA}, M^{-1}).

The second-order rate constant for the reaction in an aqueous medium was determined from the kinetic curves obtained by using solutions prepared in a similar way but containing no CPC.

3. Results and discussion

The oxidation of sulphanilic acid by periodate under the catalytic action of iron(III) yields *o*-benzoquinone-4-sulphonic acid (BQS) as the main reaction product and small amounts of azobenzene-4,4′-disulphonic acid (ABDS), according to the following scheme [8]:

$$Fe(III) + SA \leftrightarrow Fe(II) + BQS$$

$$Fe(II) + IO_4^- \xrightarrow{fast} Fe(III) + IO_3^-$$

The role of 1,10-phenanthroline as activator involves the formation of a more stable complex with Fe(II) than with Fe(III).

In order to determine the influence of surfactant aggregates on the rate of this reaction, surfactants of different nature (cationic, anionic, non-ionic and zwitterionic) were tested at three concentration levels, namely below, close to, and above their critical micelle concentration (cmc). The only significant rate enhancement observed in the determination of Fe(III) was due to the cationic surfactant cetylpyridinium chloride (CPC), which was thus chosen for subsequent experiments. The profile of the absorption spectrum for the reaction products was identical in the presence and absence of CPC, which indicates that the nature of these was identical. Fig. 1 illustrates the effect of the surfactant on the uncatalysed and Fe(III)-catalysed sulphanilic acid–periodate systems. In the absence of the catalyst (curve 1), the reaction proceeded very slowly and was not influenced by the presence of CPC. On the other hand, the surfactant had a strong effect on the rate of the Fe(III)-catalysed reaction, as can be inferred by comparing curves 2 and 3; consequently, the kinetic determination of Fe(III) in the presence of CPC will be more sensitive. The time needed to obtain the final absorbance was considerably shortened by the presence of CPC (ca. 1 h) relative to an aqueous medium (ca. 48 h), the final absorbance value being identical for both media.

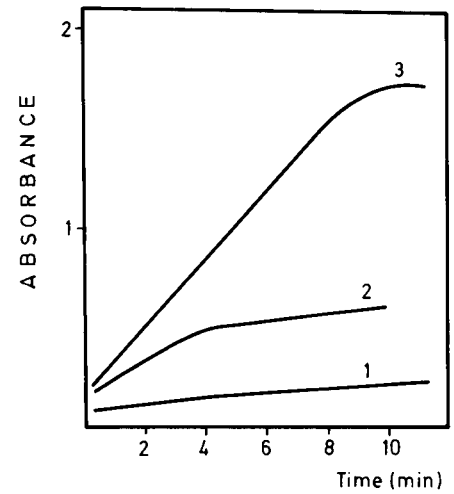

Fig. 1. Effect of CPC on both the uncatalysed and 2.0×10^{-7} M iron(III)-catalysed sulphanilic acid–periodate system in the presence of 2.0×10^{-4} M 1,10-phenanthroline. Kinetic curves: (1) uncatalysed and CPC-catalysed; (2) iron(III)-catalysed; (3) iron(III)–CPC-catalysed reaction. Solutions were prepared as described under Experimental.

3.1. Optimization of the reaction conditions

The influence of the concentration of CPC on the uncatalysed and Fe(III)-catalysed reaction was investigated over the range 0–4.0×10^{-4} M. CPC started to affect the rate of the catalysed reaction at concentrations above ca. 4.0×10^{-5} M. Taking into account that the surfactant cmc calculated from surface tension measurements under our reaction conditions was found to be 1.1×10^{-4} M, CPC micelles are clearly unnecessary for increasing the rate of this reaction. CPC did not modify the rate of the uncatalysed reaction, at least in the concentration range tested. We could not investigate the effect of the surfactant on the reactions considered at concentrations above ca. 1.3×10^{-4} M because a cetylpyridinium periodate was precipitated under such conditions.

The influence of other reaction variables (acidity of the medium and concentrations of the

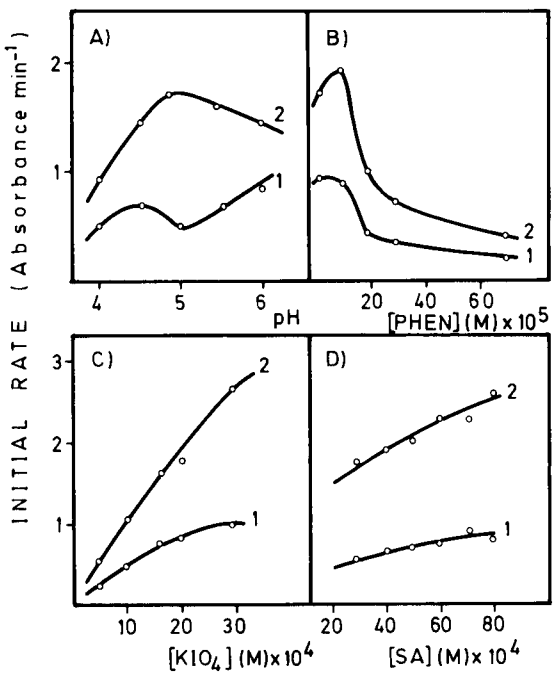

Fig. 2. Influence of (A) pH and (B) the 1,10-phenanthroline, (C) potassium periodate and (D) sulphanilic acid concentration on the rate of the iron(III)-catalysed (1) and iron(III)–CPC-catalysed (2) sulphanilic acid–periodate–1,10-phenanthroline system. $[Fe(III)] = 2.0 \times 10^{-7}$ M for curve (1) and 1.0×10^{-7} M for curve (2).

activator and reagents) on the rate of the catalysed reaction in the absence (curve 1) and presence (curve 2) of CPC is shown in Fig. 2. As can be seen from the results, the two profiles were identical or similar for every parameter, whether the surfactant was present or not.

The temperature was found not to affect the reaction rate of either CPC-accelerated or the non-accelerated reactions. Because this is rarely observed in chemical kinetics, it must be the result of equilibrium processes involving different states of periodate ion in solution [11]. In any case, it enhanced reproducibility of the analytical determination. Temperatures above 50°C were inadvisable for the determination of iron because of the low precision in the measurements.

3.2. Kinetic effects of CPC on the Fe(III)-catalysed sulphanilic acid–periodate system

As stated above, submicellar concentrations of CPC accelerate the reaction between sulphanilic acid and periodate in a Fe(III)–1,10-phenanthroline medium as catalyst. The effect cannot be attributed to solubilizate induced micellization since CPC started exerting its effect below the cmc obtained under the experimental reaction conditions (1.1×10^{-4} M).

Rate enhancements provided by premicellar aggregates can readily be rationalized in terms of the kinetic treatments derived for second-order reactions in aqueous micelles [9,12–14]. Based on such treatments, the reaction rate is determined by the reactant concentrations in the aggregates. Small premicellar aggregates contain more reactant molecules per aggregate than micelles at the same reagent concentrations [15]. Therefore, a more efficient reagent concentration in the smaller aggregates often results in higher second-order rate constants for reactions in premicellar aggregates than for those observed in micelles.

Scheme 1 outlines the reactions that take place in both the premicellar and the aqueous medium as regards the species involved in the rate determining-step only. In the scheme, CPC_m denotes the surfactant concentration of monomers or aggregates ineffective for catalysis and in equilibrium with the average concentration of catalytically effective CPC micelle subunits, $(CPC)_x$. Such an average concentration can be calculated from:

$$[CPC]_x = [CPC]_T - [CPC_m] \quad (1)$$

where $[CPC]_T$ is the overall surfactant concentration added to the reaction medium. Since $[CPC_m]$

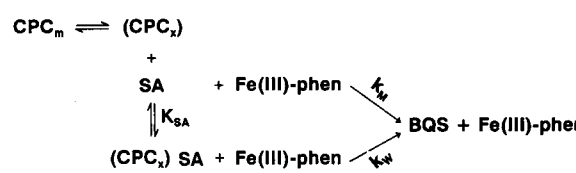

Scheme 1.

is not catalytically active, it can be estimated from the dependence of CPC-induced rate enhancements on the surfactant concentration. Parameter K_{SA} is the corresponding association constant of sulphanilic acid to micelle subunits, and k_w and k_m are the second-order rate constants for the redox reaction in the aqueous bulk solution and the micelle subunits, respectively.

Under pseudo-first-order conditions (e.g., sulphanilic acid in large excess), the observed first-order rate constant (k_{obs}) for the redox reaction in the presence of micellar subunits is given, according to the model developed by Berezin et al. [9] and implemented in the equations of Shiffman et al. [16], by

$$k_{obs} = \frac{[k_w + k_m K_{SA}[CPC]_x][SA]}{1 + K_{SA}[CPC]_x} \quad (2)$$

The observed second-order rate constants (k_ψ, l mol^{-1} s^{-1}) can be calculated from k_{obs}:

$$k_\psi = \frac{k_{obs}}{[SA]} \quad (3)$$

Fig. 3 shows the dependence of this parameter on the overall surfactant concentration. From this plot, [CPC_m] was estimated to be 4.0×10^{-5} M.

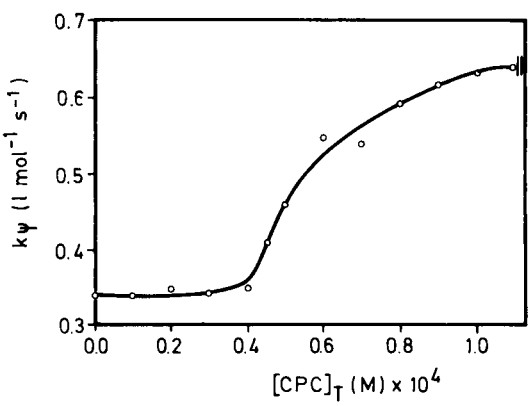

Fig. 3. Influence of the overall CPC concentration in the reaction medium on the second-order rate constant for the reaction between sulphanilic acid and periodate, catalysed by Fe(III)–1,10-phenanthroline. For conditions, see Experimental section, Kinetics.

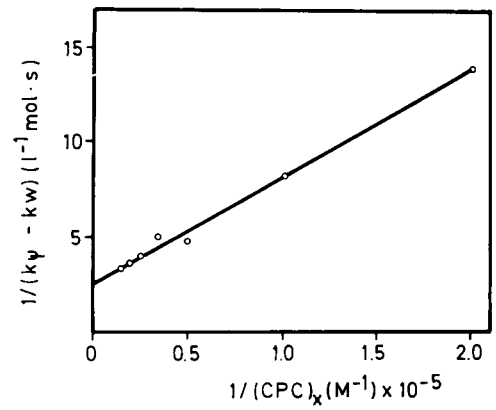

Fig. 4. Plot of $1/(k_\psi - k_w)$ against the reciprocal of the average concentration of effective micelle subunits, $(CPC)_x$.

Substituting k_{obs} by k_ψ in Eq. 2 and rearrangement yields:

$$\frac{1}{k_\psi - k_w} = \frac{1}{k_m - k_w} + \frac{1}{k_m - k_w}\frac{1}{K_{SA}[CPC]_x} \quad (4)$$

according to this equation predicted plots of $1/k_\psi - k_w$ against $1/[CPC]_x$ should be linear. The second-order rate constant for the reaction in an aqueous medium (k_w), calculated as described under Experimental, was (0.34 ± 0.03) l mol^{-1} s^{-1}. The results obtained for the reaction studied by plotting $1/k_\psi - k_w$ as a function of $1/[CPC]_x$ fitted Eq. 4 reasonably well (Fig. 4). From the intercept and slope of this linear plot, k_m (0.74 ± 0.09) l mol^{-1} s^{-1} and K_{SA} $(4.4 \times 0.7) \times 10^4$ l mol^{-1} were obtained.

The kinetic data provided by this treatment indicate that the observed premicelle-induced rate augmentation for the catalysed reaction can be entirely attributed to the increased reactant concentrations in the micellar subunits since no significant enhancement was observed for the "true" second-order rate constant in the premicellar pseudophase (k_m) relative to an aqueous medium (k_w).

The value for binding constant of sulphanilic acid to the submicellar aggregates (K_{SA}) suggests a strong substrate–aggregate interaction. How-

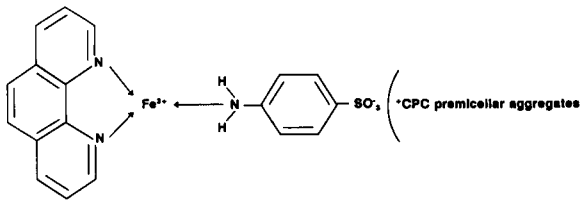

Scheme 2.

ever, this substrate concentration effect by itself cannot account for the premicelle induced augmentation observed in the catalysed reaction rate since no acceleration was found in the uncatalysed reaction. Inasmuch as the other reactant in the determining rate step is the Fe(III)–phenanthroline catalyst, which bears positive charge, a direct catalyst–micellar subunits association is impossible. This suggests indirect concentration of this catalyst on micellar subunits by formation of a transient phen–Fe(III)–SA ternary complex, a likely structure for which is depicted in Scheme 2.

3.3. Figures of merit of the analytical method

The absorbance–time kinetic curves obtained for the reaction in the presence of micellar subunits of CPC, run under the optimum experimental conditions, were processed by using two quantitation methods involving initial-rate and fixed-time measurements. The corresponding regression equations, correlation coefficients and detection limits are given in Table 1, which also includes the values for the same parameters obtained in the determination of Fe(III) in the absence of CPC for contrast. Based on the initial rate method, the catalytic activity of Fe(III) was apparently increased by a factor of ca. 5 in the presence of CPC according to the sensitivity obtained in the micellar subunits and the aqueous medium. The detection limit was improved about 7-fold in the presence of CPC based on the same measurement method. The precision of the proposed method, expressed as the relative standard deviation, was 5.0% [$n = 10$, for 2.0×10^{-7} M Fe(III)] and 6.2% [$n = 10$, for 4.0×10^{-7} M Fe(III)] in the presence and absence of CPC, respectively. No significant differences in this analytical parameter between the two media were observed.

In order to determine whether submicellar catalysis resulted in increased selectivity for the determination of Fe(III), the effect of various ions on the sulphanilic acid–periodate system in the presence and absence of CPC was studied.

Table 2
Effect of foreing ions on the determination of 2.0×10^{-8} M Fe(III)

Ion	Tolerated ion-to-Fe(III) mole ratio		Selectivity factor (with CPC/ without CPC)
	Without CPC	With CPC	
Co^{2+}	10	100	10
Ag^{+}	20	100	5
Ni^{2+}	200	200	1
Cu^{2+}	200	1000	5
Mn^{2+}	20	2	0.1
Zn^{2+}	200	200	1
Cr(VI)	200	2	0.01
Mo(VI)	200	2000	10
Fe^{2+}	20	20	1
Cl^{-}	20000	20000	1
PO_4^{3-}	20000	2000	0.1
CO_3^{2-}	20000	10000	0.5
SO_4^{2-}	20000	20000	1

Table 1
Analytical figures of merit of the proposed kinetic method

Measurement method	Concentration range (M)	(slope ± S.D.) × 10^{-2}	(intercept ± S.D.)	[a] r	Detection limit (M)
[b] Initial-rate	$0.5–4.0 \times 10^{-7}$	4.5 ± 0.2 U.A. s^{-1} M^{-1}	0.88 ± 0.03	0.9997	2.45×10^{-8}
[c] Initial-rate	$0.1–4.0 \times 10^{-7}$	22.2 ± 1.4 U.A. s^{-1} M^{-1}	1.1 ± 0.3	0.994	3.37×10^{-9}
[b] Fixed-time	$0.5–4.0 \times 10^{-7}$	1.3 ± 0.1 U.A. M^{-1}	0.25 ± 0.03	0.98	0.32×10^{-8}
[c] Fixed-time	$0.5–4.0 \times 10^{-7}$	4.3 ± 0.1 U.A. M^{-1}	0.42 ± 0.01	0.996	0.74×10^{-9}

[a] Correlation coefficient, $n = 5$. [b] In the absence and [c] presence of CPC.

Table 3
Determination of iron(III) in human serum samples

Iron(III) content (μM)	
Proposed method [a]	Merckotest [b]
8.25	8.06
9.75	8.84
9.75	8.36
9.75	8.73
10.75	13.13
11.25	13.65
13.88	13.85
14.25	13.43

[a] Average of three determinations.
[b] Average of two determinations.

The ions tested included those usually found in biological fluids owing to the potential use of this method for determining Fe(III) in this type of matrix. Table 2 summarizes the results obtained, as well as the selectivity factors, defined as the ratio between the tolerated concentration of foreign species in the presence and absence of CPC. The results demonstrate that the catalytic reaction studied is quite selective and scarcely affected by the presence of the surfactant in this respect.

The proposed method was applied to the determination of Fe(III) in blood serum. The method was found to be interference-free, so a calibration curve can be used for direct quantification. Use of a single external standard also gave consistent results. Table 3 shows the results obtained in the analysis of 8 serum samples by the proposed method and that based on the chromogen bathophenanthroline sulphonate. The reagents used in the latter are commercially available in kit form (Merckotest) and were obtained from Merck (Darmstadt, Cat. No 3307). The results provided by both methods were quite consistent.

4. Conclusion

This work opens up new prospects for improving the sensitivity of catalytic determinations based on redox reactions by using surfactant aggregates when no direct aggregate–catalyst interactions are involved. The proposed approach in which the catalytic cycle must include the formation of a transient substrate–catalyst complex, entails careful selection of a structurally appropriate substrate. Enhanced sensitivity for the catalyst determination can be achieved provided that the substrate concentrates in the surfactant aggregates via a group facing the functional group through which the catalyst forms the complex. This is the case in the reported determination of Fe(III) by using sulphanilic acid as substrate. Structurally similar compounds to sulphanilic acid were previously used for the determination of ions in micellar media by spectrophotometry of stable substrate–ion complexes provided that the ions bear charges of the same sign as the micelles [17]. Experiments aimed at investigating the effects of surfactant aggregates on other catalytic redox reactions involving structurally similar substrates to the one used in this work are in progress.

On the other hand, this work demonstrates that premicellar aggregates are effective means for enhancing the sensitivity of catalytic kinetic methods, thereby broadening the scope of application of surfactants in this area.

Acknowledgments

The authors gratefully acknowledge financial support from the Spanish CICyT (Project No. PB91-0840).

References

[1] D. Pérez-Bendito and S. Rubio, Trends Anal. Chem., 12 (1993) 9.
[2] D. Sicilia, S. Rubio and D. Pérez-Bendito, Anal. Chem., 64 (1992) 1490.
[3] D. Sicilia, S. Rubio and D. Pérez-Bendito, Anal. Chim. Acta, 266 (1992) 43.
[4] L. Lunar, S. Rubio and D. Pérez-Bendito, Anal. Chim. Acta, 237 (1990) 207.
[5] L. Lunar, S. Rubio and D. Pérez Bendito, Talanta, 39 (1992) 1163.
[6] D. Sicilia, S. Rubio and D. Pérez-Bendito, Fresenius' J. Anal. Chem., 342 (1992) 327.
[7] A. Alexiev and P.R. Bontchev, Mikrochim. Acta, (1970) 13.

[8] A. Alexiev and A.M. Stoyanova, Anal. Lett., 21 (1988) 1515.
[9] I.V. Berenzin, K. Martinek and A.K. Yatsimirskii, Russ. Chem. Rev., 42 (1973) 787.
[10] P. Mukerjee and K.J. Hysels, Critical Micelle Concentrations of Aqueous Surfactant Systems, NSRDS-NBS 36, U.S. Department of Commerce, Washington, DC, 1971.
[11] F.A. Cotton and G. Wilkinson, Advanced Inorganic Chemistry, Wiley, New York 1988, pp. 569.
[12] C.A. Bunton, Catal. Rev. Sci. Eng., 20 (1979) 1.
[13] K. Martinek, A.K. Yatsimirskii, A.V. Levashov and I.V. Berenzin, in K.L. Mittal (Ed.), Micellization, Solubilization and Microemulsions, Plenum Press, New York, 1977, pp. 489–508.
[14] L.S. Romsted, in K.L. Mittal (Ed.), Micellization, Solubilization and Microemulsions, Plenum Press, New York, 1977, pp. 509–530.
[15] J.H. Fendler, Membrane Mimetic Chemistry, Wiley, New York, 1982, pp. 6–47.
[16] R. Shiffman, Ch. Rav-Acha, M. Chevion, J. Katzhendler and S. Sarel, J. Org. Chem., 42 (1977) 3279.
[17] W.L. Hinze, in K.L. Mittal (Ed.), Solution Chemistry of Surfactants, Plenum, New York, 1979, pp. 85–99.

PUBLICATION SCHEDULE FOR 1994

	J	F	M	A	M	J	J	A	S	O	N	D
Anal. Chim. Acta	284/3 285/1–2 285/3	286/1 286/2 286/3	287/1–2 287/3 288/1–2	288/3 289/1 289/2	289/3 290/1–2 290/3	291/1–2 291/3 292/1–2	292/3 293/1–2 293/3	294/1 294/2 294/3	295/1–2 295/3 296/1	296/2 296/3 297/1–2	297/3 298/1 298/2	298/3 299/1 299/2
Vib. Spec.	6/2		6/3		7/1		7/2		7/3		8/1	

INFORMATION FOR AUTHORS

Detailed "Instructions to Authors" for *Analytica Chimica Acta* was published in Volume 289, No. 3, pp. 381–384. Free reprints of the "Instructions to Authors" of *Analytica Chimica Acta* and *Vibrational Spectroscopy* are available from the Editors or from: Elsevier Science B.V., P.O. Box 330, 1000 AH Amsterdam, The Netherlands. Telefax: (+31-20) 5862459.

Manuscripts. The language of the journal is English. English linguistic improvement is provided as part of the normal editorial processing. Authors should submit three copies of the manuscript in clear double-spaced typing on one side of the paper only. *Vibrational Spectroscopy* also accepts papers in English only.

Rapid publication letters. *Letters* are short papers that describe innovative research. Criteria for letters are novelty, quality, significance, urgency and brevity. Submission data: max. of 2 printed pages (incl. Figs., Tables, Abstr., Refs.); short abstract (e.g., 3 lines); *no* proofs will be sent to the authors; submission on floppy disc; *no* revision will be possible.

Abstract. All papers, reviews and letters begin with an Abstract (50–250 words) which should comprise a factual account of the contents of the paper, with emphasis on new information.

Figures. Figures should be suitable for direct reproduction and as rich in contrast as possible. One original (or sharp glossy print) and two photostat (or other) copies are required. Attention should be given to line thickness, lettering (which should be kept to a minimum) and spacing on axes of graphs, to ensure suitability for reduction in size on printing. Axes of a graph should be clearly labelled, along the axes, outside the graph itself.

All figures should be numbered with Arabic numerals, and require descriptive legends which should be typed on a separate sheet of paper. Simple straight-line graphs are not acceptable, because they can readily be described in the text by means of an equation or a sentence. Claims of linearity should be supported by regression data that include slope, intercept, standard deviations of the slope and intercept, standard error and the number of data points; correlation coefficients are optional.

Photographs should be glossy prints and be as rich in contrast as possible; colour photographs cannot be accepted. Line diagrams are generally preferred to photographs of equipment. Computer outputs for reproduction as figures must be good quality on blank paper, and should preferably be submitted as glossy prints.

Nomenclature, abbreviations and symbols. In general, the recommendations of IUPAC should be followed, and attention should be given to the recommendations of the Analytical Chemistry Division in the journal *Pure and Applied Chemistry* (see also *IUPAC Compendium of Analytical Nomenclature, Definitive Rules*, 1987).

References. The references should be collected at the end of the paper, numbered in the order of their appearance in the text (*not* alphabetically) and typed on a separate sheet.

Reprints. Fifty reprints will be supplied free of charge. Additional reprints (minimum 100) can be ordered. An order form containing price quotations will be sent to the authors together with the proofs of their article.

Papers dealing with vibrational spectroscopy should be sent to: Dr J.G. Grasselli, 150 Greentree Road, Chagrin Falls, OH 44022, U.S.A. Telefax: (+1-216) 2473360 (Americas, Canada, Australia and New Zealand) or Dr J.H. van der Maas, Department of Analytical Molecular Spectrometry, Faculty of Chemistry, University of Utrecht, P.O. Box 80083, 3508 TB Utrecht, The Netherlands. Telefax: (+31-30) 518219 (all other countries).

0003-2670/94/$07.00

Analytical Applications of Circular Dichroism

Edited by **N. Purdie** and **H.G. Brittain**

Techniques and Instrumentation in Analytical Chemistry Volume 14

Circular dichroism is a special technique which provides unique information on dissymmetric molecules. Such compounds are becoming increasingly important in a wide variety of fields, such as natural products chemistry, pharmaceutics, molecular biology, etc. The content of this book has been selected in order to feature the unique aspects of circular dichroism, and how these strengths can be of assistance to workers in the field.

Substantial discussions have been provided regarding the particular phenomena associated with dissymmetric compounds which give rise to the circular dichroism effect. Reviews are also given of the type of instrumentation available for the measurement of these effects. A number of chapters cover the wide range of applications illustrating the power of the method.

Owing to its broad appeal, the book will be of interest to workers in all areas of chemistry and pharmaceutical science.

Contents:

© 1994 360 pages Hardbound
Price: Dfl. 355.00 (US $ 202.75)
ISBN 0-444-89508-6

ORDER INFORMATION

For USA and Canada
ELSEVIER SCIENCE INC.
P.O. Box 945
Madison Square Station
New York, NY 10160-0757
Fax: (212) 633 3880

In all other countries
ELSEVIER SCIENCE B.V.
P.O. Box 330
1000 AH Amsterdam
The Netherlands
Fax: (+31-20) 5862 845

US$ prices are valid only for the USA & Canada and are subject to exchange rate fluctuations; in all other countries the Dutch guilder price (Dfl.) is definitive. Customers in the European Community should add the appropriate VAT rate applicable in their country to the price(s). Books are sent postfree if prepaid.

ELSEVIER SCIENCE B.V.

0003-2670(19940909)295:1/2;1-1